AGE, PROVENANCE AND TECTONIC IMPLICATIONS OF LATE PALEOZOIC

VOLCANIC TUFFS IN SOUTHWEST LAURENTIA

by

HEPENG TIAN

Presented to the Faculty of the Graduate School of

The University of Texas at Arlington in Partial Fulfillment

of the Requirements

for the Degree of

DOCTORAL OF PHILOSOPHY IN EARTH AND ENVIRONMENTAL SCIENCES

THE UNIVERSITY OF TEXAS AT ARLINGTON

August 2022

ACKNOWLEDGEMENTS

If you want to bet on someone, bet on yourself– Kobe Bryant

I would first like to express my deep gratitude to all those who have inspired, encouraged and supported me for years to complete this journey. Special appreciation goes to my supervisor, Prof. Majie Fan, for her professionalism, continual mentorship and extreme support during these years. I highly appreciate the great amount of time, patience, and guidance that Prof. Fan has provided teaching me theories, conducting lab procedures, writing proposals, presenting research and pursuing science. She is committed to conducting every aspect of science with the highest standards, from asking a question, writing a proposal, conducting experiments, data analysis, to presenting the results and wording a manuscript. She is passionate about research, science, her family, and life. Such attitude had a great impact on my performance, not just in academic pursuits, but also in daily life. She is open to learn new things and was very supportive when I proposed to about the application of machine learning to my data. She always tryed her best in helping me with my research, career endeavors, and life struggles. She is a true scientist, a mentor, and a wonderful role model.

I would also like to thank my committee members, including Mr. Lowell Waite, for his warm smiles and caring, endless support, continuous advice, and help through the entire journey and especially his contributions to chapters 2 and 3, Prof. Robert. J. Stern, for his academic challenges and professional guidance through my research and his contributions to chapters 2 and 3; Dr. Matthew Loocke, for analyzing the samples, processing the data and revising the manuscript on chapter 3; and Prof. Merlynd Nestell, for his time, comments, and guidance throughout the preparation and review of this dissertation.

I wish to thank the staff and management of Pioneer Natural Resources, Irving, Texas, for access to their subsurface core samples and for encouragement to carry out my research.

I would also like to note my appreciation to my parents and parents in-law. It was not easy for them to see us going to a different country and not be able to meet for many years. But they were very supportive through the entire time. They always do their best to help us through tough times and they never let us worry about them even when they struggle. Their commitment to their jobs, gratitudes to their lives and caring to their children inspired me to become a better person every single day. They are the best parents in the world, and I could not have come to this far without them.

I also like to thank my daughter Nora. It is a blessing to have her joining our family. She brought so much love and laughter to our home and inspired me every single day. She made me realize the beauty of inheritance, the meaning of life and the truth of love. She taught me to be more humble, patient, and caring, and every moment with her opens a new angle towards life. I truly appreciate what I already have, but at the same time I can not help wondering what exciting adventures we are about to embark upon.

ABSTRACT

AGE, PROVENANCE AND TECTONIC IMPLICATIONS OF LATE PALEOZOIC

VOLCANIC TUFFS IN SOUTHWEST LAURENTIA

Hepeng Tian, Ph.D.

The University of Texas at Arlington, 2022

Supervising Professor: Dr. Majie Fan

Assembly of the supercontinent Pangea is among the most important tectonic events in late Paleozoic Earth history. The diachronous Laurentia-Gondwana collision destroyed the intervening subduction zone(s) of the Rheic oceanic plate, ultimately leading to subduction of the Paleo-Pacific oceanic plate beneath western Pangea. However, details about the timing, nature, and geochemical signatures of the two arc systems during the transition from Rheic oceanic plate to Paleo-Pacific oceanic plate subduction are poorly understood. This lack of understanding, in part, reflects the fact that arc magmatic products (esp. granitic rocks) related to the Rheic ocean subduction are largely obscured by those related to the eastward subduction of the Paleo-Pacific oceanic plate beneath western Pangea together with the subsequent Pangea breakup, including deep burial, and erosion. Herein I study bulk tuff major and trace element geochemistry, and zircon U-Pb LA-ICP-MS and CA-ID-TIMS geochronology, Lu-Hf isotope and trace element compositions of ten well-preserved volcanic tuff units distributed in southwest Laurentia to reconstruct the tectonic sequence related to the final Pangea assembly. The tuff units include five Stanley tuffs from the Ouachita Mountains of southeastern Oklahoma and southwestern Arkansas, five tuffs from the subsurface of the Permian Basin in western Texas and eastern New Mexico, and three tuffs in the Glass Mountains in western Texas. The results show that the tuffs, ranging in age from Late Mississippian (327.8 ±0.8 Ma) to Guadalupian (266.5 ±0.1 Ma), originated from continental arcs with granitoid parent magma

composition. The Mississippian Barnett and Stanley tuffs have primitive zircon ƐHf values (0 to +5) similar to granitoids of the Maya block in northern Gondwana, suggesting that the tuffs were derived from volcanoes resulting from subduction of the Rheic oceanic plate. A rapid change of ƐHf signature occurred between the Cisuralian Wolfcamp B tuff (288.2 ±1.7 Ma), which has an average zircon ƐHf value (+5.5), similar to the Barnett and Stanley tuffs, and the Wolfcamp A tuff (287.2 ±0.5) that has an evolved average ƐHf value (-4.5). The rapid change within one Myr most likely reflects termination of the northern Gondwana arc following the assembly of Pangea and initiation of magmatism related to subduction of the paleo-Pacific oceanic plate beneath western Pangea. Results of this study show the arc signature became progressively more primitive from the late Cisuralian to Guadalupian between ca. 282 Ma and ca. 260 Ma.

Table of Contents

List of Illustrations

List of Tables

Chapter 1 INTRODUCTION

Plate reorganization associated with the assembly of the supercontinent Pangea is undoubtedly an important late Paleozoic tectonic event. Subduction of the Rheic plate beneath northern Gondwana may have started during the Early Mississippian, as early as ~348 Ma. The assembly of Pangea was marked by closure of the Rheic ocean, accretion of peri-Gondwanan terranes to Laurentia, and diachronous Laurentia-Gondwana collision to form the Appalachian-Ouachita-Marathon-Sonora orogenic belt. The collision destroyed the intervening subduction zone(s), ultimately leading to subduction of the Paleo-Pacific oceanic plate beneath western Pangea. However, details about the change from Rheic oceanic plate to Paleo-Pacific oceanic plate subduction remain poorly understood because the geologic record has been obscured by younger magmatism related to subduction of the paleo-Pacific oceanic plate, Pangea breakup, deep burial, and erosion. By studying age and geochemistry of ten well preserved late Paleozoic volcanic tuffs in southwestern Laurentia, this dissertation provides new data to propose a Late Mississippian northern Gondwana arc caused by the subduction of the Rheic oceanic plate under northern Gondwana and an early Permian western Pangea arc triggered by the subduction of the Paleo-Pacific oceanic plate beneath west Pangea. The transition between the two arc systems helps reconstruct the plate reorganization regarding to the final assembly of the super continent Pangea.

This dissertation includes two projects presented in Chapters 2 and 3. Chapter 2 is entitled *Mississippian southern Laurentia tuffs came from a northern Gondwana arc*. The study presents zircon trace element geochemistry, Lu-Hf isotope, and U-Pb geochronlogy data of the Late Mississippian Barnett and Stanley tuffs in southern Laurentia. The data suggest that these tuffs were sourced from a continental arc and provide evidence for the long inferred northern Gondwana arc formed by the subduction of the Rheic oceanic plate under northern Gondwana. This work was published in Geology in 2021. The citation is Tian, H., Fan, M., Valencia, V.A., Chamberlain, K., Stern, R.J., Waite, L., Mississippian southern Laurentia tuffs came from a northern Gondwana arc. Geology 2021; 50 (3): 266–271. doi: https://doi.org/10.1130/G49502.1. GSA states "An author has the right to use his or her

article or a portion of the article in a thesis or dissertation without requesting permission from GSA, provided the bibliographic citation and the GSA copyright credit line are given on the appropriate pages".

Chapter 3 is entitled *Rapid early Permian tectonic reorganization of Laurentia's plate margins: evidence from volcanic tuffs in the Permian Basin*. The study presents zircon trace element geochemistry, Lu-Hf isotopes, and U-Pb geochronlogy data of the Permian tuffs in and around the Permian Basin. The integration of the new data and those of the Mississippian tuff leads to the discovery that the primitive northern Gondwana arc terminated during the early Permian (~288 Ma), immediately followed by the initiation (~287 Ma) of the evolved west Pangea arc triggered by the subduction of the Paleo-Pacific oceanic plate beneath west Pangea. This chapter also has implications on the rate of plate reorganization and comparison between zircon LA-ICPMS and CA-ID-TIMS dates. This work was accepted to publish in Gondwana Research at the time of writing this dissertation. The citation is H. Tian, M. Fan, V. Valencia, K. Chamberlain, L. Waite, R.J. Stern, M. Locke, Rapid early Permian tectonic reorganization of Laurentia's plate margins: evidence from volcanic tuffs in the Permian Basin, USA, Gondwana Research (2022), doi: https://doi.org/10.1016/j.gr.2022.07.003. Gondwana Research states "Authors can include their articles in full or in part in a thesis or dissertation for non-commercial purposes."

Chapter 2 MISSISSIPPIAN SOUTHERN LAURENTIA TUFFS CAME FROM A NORTHERN GONDWANA ARC

Hepeng Tian[1], Majie Fan[1], Victor A. Valencia[2], Kevin Chamberlain[3], Robert J. Stern[4] and Lowell Waite[4]

[1]Department of Earth and Environmental Sciences, The University of Texas at Arlington, Arlington, Texas 76019, USA

[2]School of Environment, Washington State University, Pullman, Washington 99164, USA

[3]Department of Geology and Geophysics, University of Wyoming, Laramie, Wyoming 82071, USA

[4]Department of Geosciences, University of Texas at Dallas, Richardson, Texas 75083, USA

ABSTRACT

A Paleozoic arc that formed by southward subduction of the Rheic oceanic plate beneath northern Gondwana has long been inferred, but its history and geochemical signatures remain poorly understood. New U-Pb ages, juvenile εHf signatures, and trace-element composition data of young zircons from tuffs at two southern Laurentia sites indicate their derivation from a continental arc that was active from ca. 328 to ca. 317 Ma and permit correlation of sedimentary sequences 800 km apart in southern Laurentia. These include the Stanley tuffs in the Ouachita Mountains of southeastern Oklahoma and southwestern Arkansas and the newly discovered Barnett tuff in the subsurface of the Midland Basin in west Texas (USA). The Barnett tuff has a zircon chemical abrasion–isotope dilution–thermal ionization mass spectrometry U-Pb date of 327.8 ± 0.8 Ma, similar to the oldest Stanley tuff in the Ouachita Mountains. Zircon Hf isotope depleted mantle model ages further suggest that the source was a continental arc on basement with both Grenville and Pan-African affinities, pointing to northern Gondwana or peri-Gondwana terranes. The new data link the tuffs to granitoids (326 Ma) of the Maya block in southern Mexico, which was part of northern Gondwana. Correlation of the Stanley-Barnett tuffs across southern Laurentia suggests the likely presence of Mississippian tuffs over a broad region in southern Laurentia, and their usefulness for constraining absolute ages of basin fills and characterizing the Gondwanan arc.

2. 1 INTRODUCTION

Assembly of the supercontinent Pangea through Rheic Ocean closure and the subsequent Laurentia-Gondwana collision are among the most important tectonic events in late Paleozoic Earth history (e.g., Nance et al., 2014). It has long been inferred that the southward subduction of the Rheic oceanic plate formed an arc system in the peri-Gondwana realm, including the Carolina, Suwannee, Coahuila, and Maya blocks, originally located in northern Gondwana (e.g., Lopez, 1997; Lawton et al., 2021). However, the history and geochemical signatures of the arc system remain poorly understood because the geologic record has been obscured by younger magmatism related to subduction of the paleo-Pacific oceanic plate, Pangea breakup, deep burial, and erosion (e.g., Kirsch et al., 2012; Ortega-Obregón et al., 2013). The few studies of this arc and its geochemical signatures have also raised uncertainties about how to distinguish the inferred northern Gondwana arc from the Ordovician arc related to Iapetus Ocean closure (Alemán Gallardo et al., 2019) and the Permian–Triassic arc related to subduction of the paleo-Pacific oceanic plate (e.g., Torres et al., 1999). Studies of the arc system also have implications for understanding the Laurentia-Gondwana collision, for example, the geochemistry of Late Mississippian granitoids in the Maya block suggests breakoff of the Rheic oceanic slab accompanying collision along the Ouachita suture (Zhao et al., 2020), although Gondwana-derived sediments did not arrive in the Ouachita foreland during this time (Prines, 2020).

We describe a newly discovered Late Mississippian tuff in the Barnett Shale in the subsurface of the Midland Basin of west Texas, and use zircon geochemistry and geochronology to show that this tuff correlates with Late Mississippian Stanley tuffs exposed in the Ouachita Mountains (Shaulis et al., 2012). We infer that these tuffs were likely derived from volcanoes in the northern Gondwana arc, with the Ouachita Mountains being closer to the source than the Midland Basin. These tuffs are useful for chronostratigraphy and stratigraphic correlations, and their geochemical and isotopic attributes provide important insights into the Gondwana arc.

2. 2 GEOLOGICAL BACKGROUNDS

A diachronous collision between Laurentia and Gondwana formed the Ouachita-Marathon fold-and-thrust belt in southern Laurentia (Fig. 2-1A). Although the orogen has been eroded and mostly buried, the Ouachita Mountains in Oklahoma and Arkansas expose rocks deposited during Rheic Ocean closure (Fig. 2-1B). The Ouachita Mountains contain thick Carboniferous clastic rocks deposited in a deep-marine fan system, which was later deformed in an accretionary prism and incorporated into the orogen during collision (Morris, 1989). The Mississippian Stanley Group is ∼4 km thick and contains mostly shale and some interbedded sandstone. The group contains five major, widespread tuffs, including, from bottom to top, the Beavers Bend, Hatton, lower and upper Mud Creek, and Chickasaw Creek tuffs (Fig. S1 in the Supplemental Material1; Niem, 1977; Shaulis et al., 2012). The Stanley tuffs generally thin from south to north, with the lower four tuffs ranging up to 40 m thick in southern areas (Niem, 1977). The Midland Basin, which contains the newly discovered Barnett tuff described herein (See Appendix A, Fig.S1-1), is a major subbasin of the Permian Basin formed north of the Marathon salient, which is the western continuation of the Ouachita belt (Fig. 2-1A). The Permian Basin region was part of a passive margin from the Early Ordovician to Late Mississippian, and it achieved its current configuration during the Pennsylvanian–early Permian Laurentia-Gondwana collision and the Ancestral Rocky Mountain orogeny (Leary et al., 2017). The Mississippian, deep-marine Barnett Shale in the Midland Basin is ∼240 m thick (Mauck et al., 2018). The Barnett tuff, discovered in a core from the basin center (See Appendix A, Fig. S1-2), is the first reported tuff in the Midland Basin.
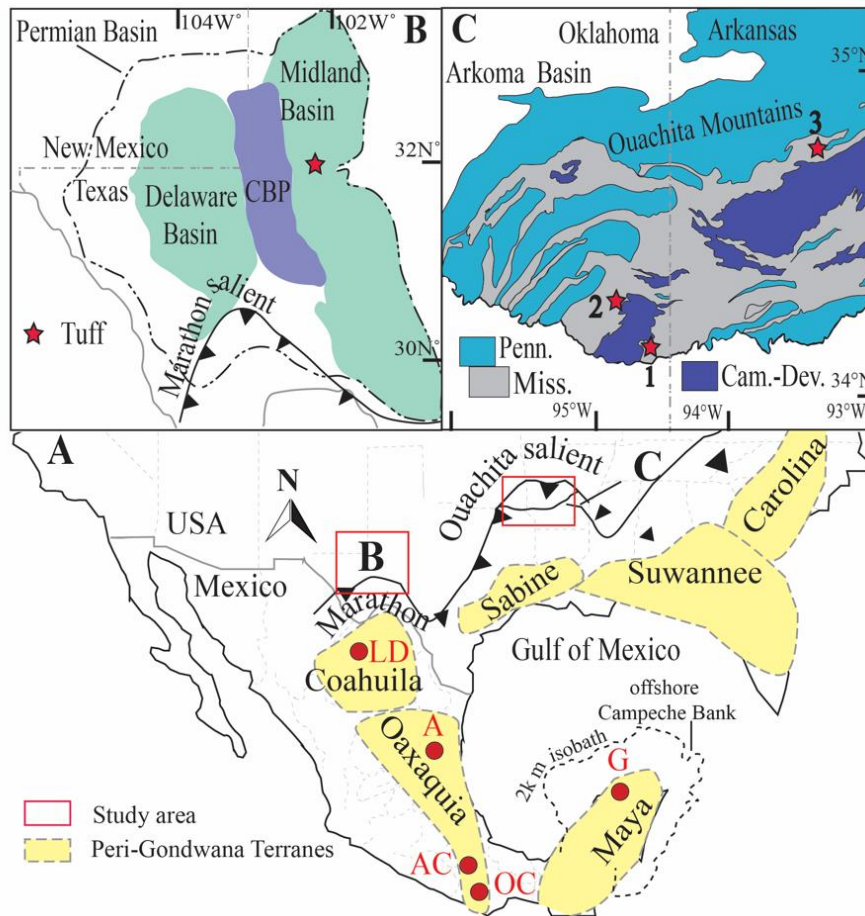
Figure 2-1. Simplified geologic maps of the study area. (A) Southern North America showing locations of peri-Gondwana terranes, the Ouachita-Marathon fold-and-thrust belt, and study areas. A— Aserradero Rhyolite; AC—Acatlan Complex; G—granitoids in Maya block; LD—Las Delicias arc; OC—Oaxacan Complex. Offshore Campeche Bank was modified after Dickinson and Lawton (2001). (B) Permian Basin showing location of the Midland Basin, which contains the Barnett tuff. CBP— Central Basin Platform. (C) Ouachita Mountains showing locations of five Stanley tuffs (modified after Shaulis et al., 2012): 1—Beavers Bend and Hatton tuffs; 2—Lower and Upper Mud Creek tuffs; 3— Chickasaw Creek tuff. Penn.—Pennsylvanian; Miss.—Mississippian; Cam-Dev.—Cambrian– Devonian.

22

Contractional tectonics during the late Paleozoic also reactivated rift-related faults of the southern Oklahoma aulacogen and formed the northwest-striking Red River and Muenster uplifts as part of the Amarillo–Wichita uplift (Walper, 1982; Keller et al., 1989; Montgomery et al., 2005; Elebiju et al., 2010; Alsalem et al., 2017). Reactivation of early Paleozoic normal faults also caused the initial rise of the basement-involved Llano uplift in southern Laurentia (Erlich and Coleman, 2005). Exhumation of the Llano uplift continued into the Late Pennsylvanian, which may have tilted the strata in the Fort Worth Basin westward (Thomas, 2003). The Fort Worth Basin may have experienced exhumation during the late Permian-Jurassic as a result of the opening of the Gulf of Mexico (Jarvie et al., 2005; Ewing, 2006; Stern and Dickinson, 2010).

2. 3 MATERIALS AND METHODS

Zircons were extracted from one Barnett tuff and five Stanley tuff beds. Scanning electron microscope (SEM) images of individual grains were taken to characterize roundness. Zircon U-Pb dates, Lu-Hf isotopes, and traceelement (TE) compositions were analyzed by laser ablation–inductively coupled plasma–mass spectrometry (LA-ICP-MS). Young grains of the Barnett tuff were plucked from the mount for chemical abrasion–isotope dilution–thermal ionization mass spectrometry (CA-ID-TIMS) dating following Mattinson (2005). Details about zircon separation, SEM imaging, analytical procedures, data reduction, and filtering are described in the Supplemental Material. In total, we report 741 zircon LA-ICP-MS and 7 TIMS U-Pb dates, and 65 Lu-Hf and 44 TE analyses (See Appendix A , Tables S1–S4). Zircon Hf isotope two-stage depleted mantle model ages (TDM2) were calculated using an average crustal value of 176Lu/177Hf = 0.0113 following Rudnick and Gao (2003). Errors of zircon U-Pb and Hf analyses and U-Pb ages are reported as 2σ standard deviation. The age of each tuff was calculated from the mode of the youngest dominant LA-ICPMS population in the kernel density estimation (KDE) plot (Fig. 2-2). The age was calculated as the weighted mean of more than three grains overlapping at 2σ, for which values had a mean square of weighted deviation (MSWD) near 1. See the Supplemental Material for more details.

2. 4 RESULTS

Zircons from four of the Stanley tuffs and the Barnett tuff were mostly elongated and euhedral and interpreted to be air-fall grains with minimal abrasion during transport (Figs. S2-3 and S2-4). The youngest mode date of the Barnett tuff was 326.6 ± 0.6 Ma (Fig. 2-2A), which matches well with the CA-ID-TIMS date of 327.8 ± 0.8 Ma (Fig. 2-2B; See Appendix A, Fig. S2-5), suggesting that our method of calculating tuff age from LA-ICP-MS dates was accurate. Four of five Stanley tuffs yielded dates of 327.1 ± 0.7, 320.7 ± 0.6, 320.4 ± 0.8, and 317.4 ± 0.5 Ma, respectively (Fig. 2-2A). The upper Mud Creek tuff did not have enough young grains for age determination. The Barnett tuff and the oldest Stanley tuff, Beavers Bend tuff, could be correlated based on overlapping ages.

In all tuffs, grains older than 500 Ma, which accounted for 16% of all grains, clustered at 850–500 Ma and 1300–900 Ma (Fig. 2-2C; See Appendix A, Fig. S6). The Hf isotope signatures of ca. 325 Ma zircons from all tuffs were juvenile, with most εHf values between 0 and 5 (Fig. 2-2D). These values are in the range of the Andean continental arc (e.g., Jones et al., 2015) but lower than those from intra-oceanic arcs and mid-oceanic ridge basalts (Workman and Hart, 2005; Dhuime et al., 2011). Zircon TDM2 ages ranged between ca. 700 and ca. 1400 Ma (Fig. 2-2D). Zircons from all units showed high total rare earth element (ΣREE) contents, enrichment of heavy (H) REEs, negative Eu anomalies, and positive Ce anomalies (Fig. 2-3; See Appendix A, Fig. S7). Discrimination diagrams following Belousova et al. (2002) and Grimes et al. (2015) project these tuffs to the granitoid parent rock composition and arc setting (Fig. 2-3).
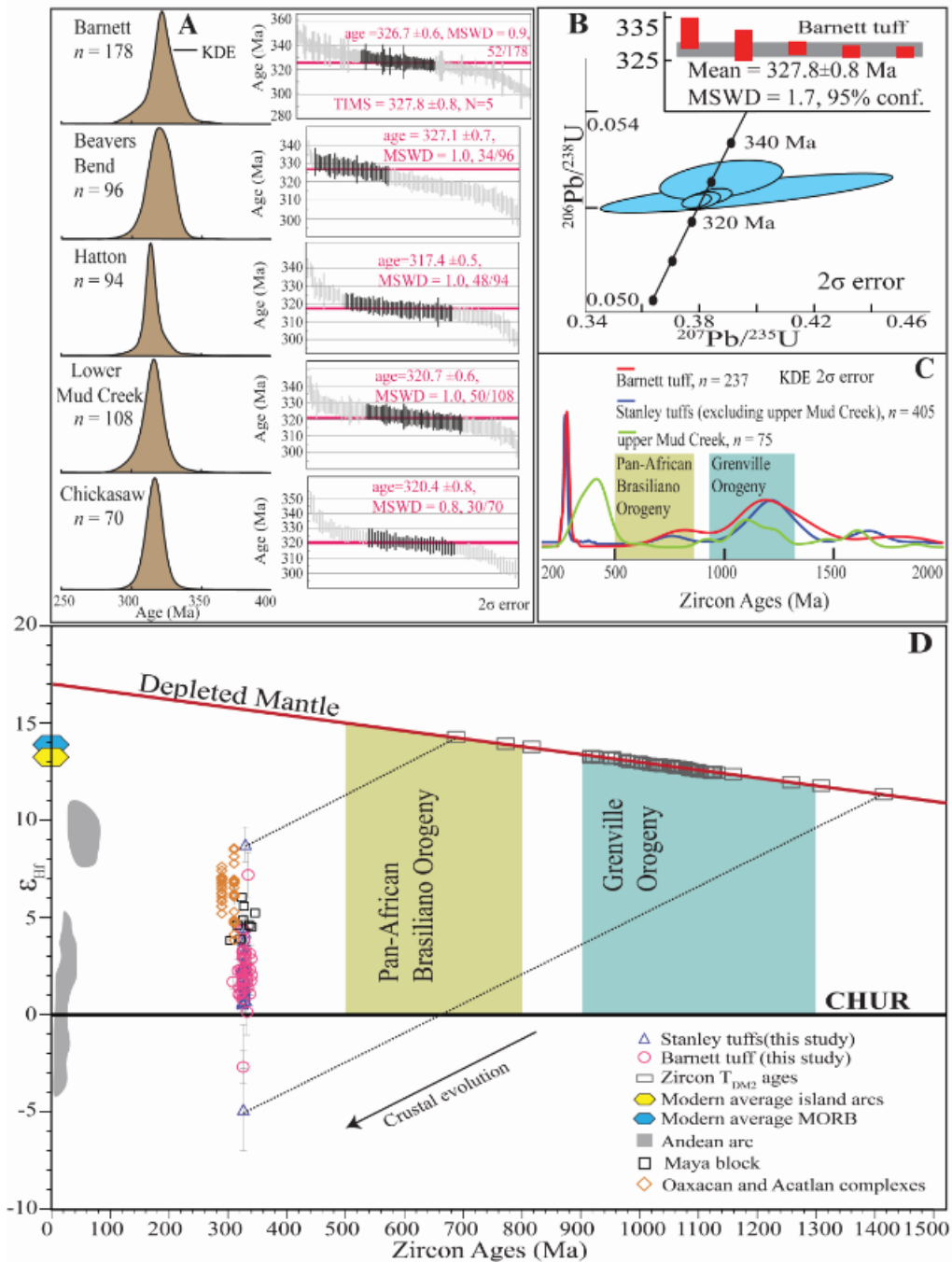
Figure 2-2. (A) Adaptive kernel density estimate (KDE) plots of the youngest statistical population

and ranked data plot showing the youngest mode date calculations for the Barnett and four Stanley

(Beavers Bend, Hatton, Lower Mud Creek, and Chicksaw) tuffs. Note that only grains shown in black were used for our calculations. Ages are given in Ma. MSWD—mean square of weighted deviates. (B) Concordia plot showing chemical abrasion–isotope dilution–thermal ionization mass spectrometry (CA-ID-TIMS) dates of the Barnett tuff. (C) KDE of all inductively coupled plasma–mass spectrometry (ICP-MS) dates. (D) Zircon U-Pb dates and εHf values of the Barnett and Stanley tuffs compared with those of Andean continental arc (Jones et al., 2015), average island arc (Dhuime et al., 2011), mid-oceanic ridge basalt (MORB; Workman and Hart, 2005), and Mississippian magmatic rocks in the Maya block (Zhao et al., 2020) and Oaxaquia block (Oaxacan and Acatlan complexes) (Ortega-Obregón et al., 2013) of Mexico. CHUR—chondritic uniform reservoir; TDM2—two-stage depleted mantle model ages.
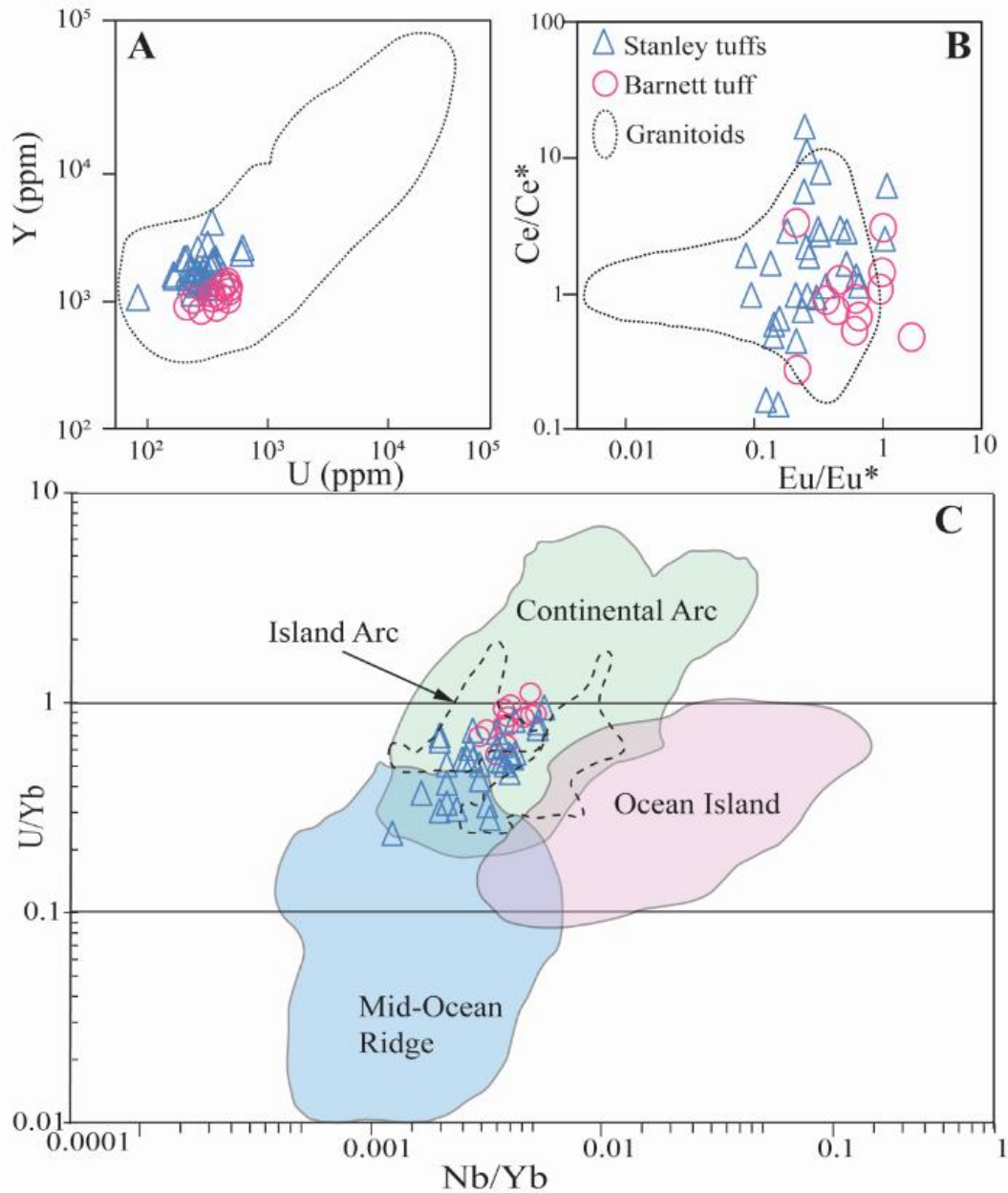
Figure 2-3. (A) Discrimination diagrams of (A) Y versus U abundances and (B) Ce/Ce* versus

Eu/Eu* ratios, where granitoid parent rock compositions follow Belousova et al. (2002) and Eu* and

Ce* were calculated as graphic and Nd_N2/Sm_N, respectively (where N indicates chondrite-

normalized abundances following McDonough and Sun [1995]). (C) U/Yb versus Nb/Yb, following

Grimes et al. (2015).

27

2. 5 CONTINENTAL ARC AFFINITY AND LOCATION

Our ages indicate that the Barnett and Beavers Bend tuffs resulted from the same or semi contemporary volcanic eruptions at ca. 328 Ma. Zircon TDM2 ages and TE signatures (Figs. 2-2 and 2-3; See Appendix A, Fig. S2-7) further suggest that both were sourced from a continental arc with felsic parent magma composition, consistent with the interpretation of whole-rock geochemistry of the Stanley tuffs (Loomis et al., 1994). Melts of continental crust have low positive or negative εHf values because continental crust has low Lu/ Hf and less radiogenic Hf than depleted mantle of similar ages (Kinny and Maas, 2003). However, zircons from a continental arc could yield a large range of εHf values where the melts have different degrees of mixing between mantlederived mafic melts and partial melts of old continental crust (Kemp et al., 2007). Zircon Hf model ages provide further constraints on the continental crust on which the arc was built (Dhuime et al., 2011). Our zircon TDM2 ages fall between the ages of the Grenville orogeny (1300–900 Ma) and the Pan-African orogeny (850–500 Ma) (Fig. 2-2D), suggesting that the parent melt was mostly derived from continental crust with both basement types, consistent with a northern Gondwana source. This interpretation is also supported by subordinate zircon U-Pb age modes at 850–500 Ma and 1300–900 Ma (Fig. 2-2C). These grains were most likely inherited from Gondwana Pan-African and Grenville basement.

Mississippian magmatism coeval with our reported Laurentia tuffs (ca. 328–317 Ma) has been reported from several Gondwanan or peri-Gondwanan blocks that lie in the Alleghanian-Ouachita hinterland. The magmatism includes, from east to west: Alleghanian granites (326–285 Ma) in the Carolina terrane of the southern Appalachians (Hibbard and Samson, 1995), granitoids (326 ± 5 Ma) in the Maya block (Zhao et al., 2020), Las Delicias arc (331–270 Ma) in the Coahuila block (Lopez, 1997), and the Aserradero Rhyolite (341 ± 4 Ma) (Ramírez-Fernández et al., 2021) in the Oaxaquia block of Mexico (Fig. 2-4A). All of these are Gondwanan or peri-Gondwanan terranes that accreted to southeastern and southern Laurentia during Rheic Ocean closure. The reconstructed distribution of these terranes suggests an elongated continental arc that developed on northern Gondwana caused by subduction of the Rheic oceanic plate (Fig. 2-4A). The Carolina terrane is predominantly composed of

Neoproterozoic to early Paleozoic rocks with juvenile bulk-rock εNd signatures, and the Alleghanian granites also contain inherited Grenvillian zircons (Mueller et al., 2011). However, it is generally agreed that the terrane was accreted to Laurentia during the Late Ordovician–Silurian (e.g., Hibbard et al., 2002), and reinterpretation of petrology and geochemistry data suggests that the granites were related to postcollision slab breakoff or delamination rather than continental arc magmatism (Zhao et al., 2020). In addition, the Carolina terrane is too distant to have provided proximal subaqueous pyroclastic flows to the Stanley tuffs.

The studied tuffs are most like Maya block granitoids, although a source in the poorly known Sabine terrane cannot be precluded. The Maya block lay south of the Ouachita Mountains, and the Coahuila block was adjacent to the Marathon thrust belt before the Gulf of Mexico opened in Jurassic time (Fig. 2-4). The Maya and Coahuila blocks both have Grenvillian and Pan-African basement, based on studies of igneous rocks and detrital zircons in their late Paleozoic strata (e.g., Martens et al., 2010; Lopez et al., 2001). Las Delicias arc volcanic rocks have juvenile εNd signatures (Lopez, 1997). However, zircons from these rocks have low Rb/Sr (<0.05) and La/Yb (<3.7) ratios and large ion lithophile elements (LILE) contents, including REEs, U, and Th, suggesting that the arc was developed on a thin continental crust with limited crustal contamination (Lopez, 1997). This signature is different from that of the bulk Stanley tuffs, which have high LILEs, Rb/Sr (average 3.2), and La/Yb (>10) (Loomis et al., 1994). The geochemical signatures, juvenile zircon εHf signatures (4–6), and TDM2 ages (1080–950 Ma) of Maya block granitoids (Zhao et al., 2020) are consistent with those of our studied tuffs (Fig. 2-2). The significantly older (ca. 341 Ma) Aserradero Rhyolite in the Oaxaquia block has an upper-crust source without evidence of mantle input, and the inherited zircons are all Grenvillian (Ramírez-Fernández et al., 2021). Carboniferous magmatism (ca. 311 Ma) documented in the Oaxacan and Acatlan metamorphic complexes in the Oaxaquia block are much younger than the Stanley and Barnett tuffs, and their oldest zircons have higher εHf values than those of our tuffs (Fig. 2-2D; Ortega-Obregón, 2013). In addition, the geochemical signatures of the complexes were interpreted to be related

to the subduction of the paleo-Pacific oceanic plate beneath western Gondwana (Ortega-Obregón, 2013).
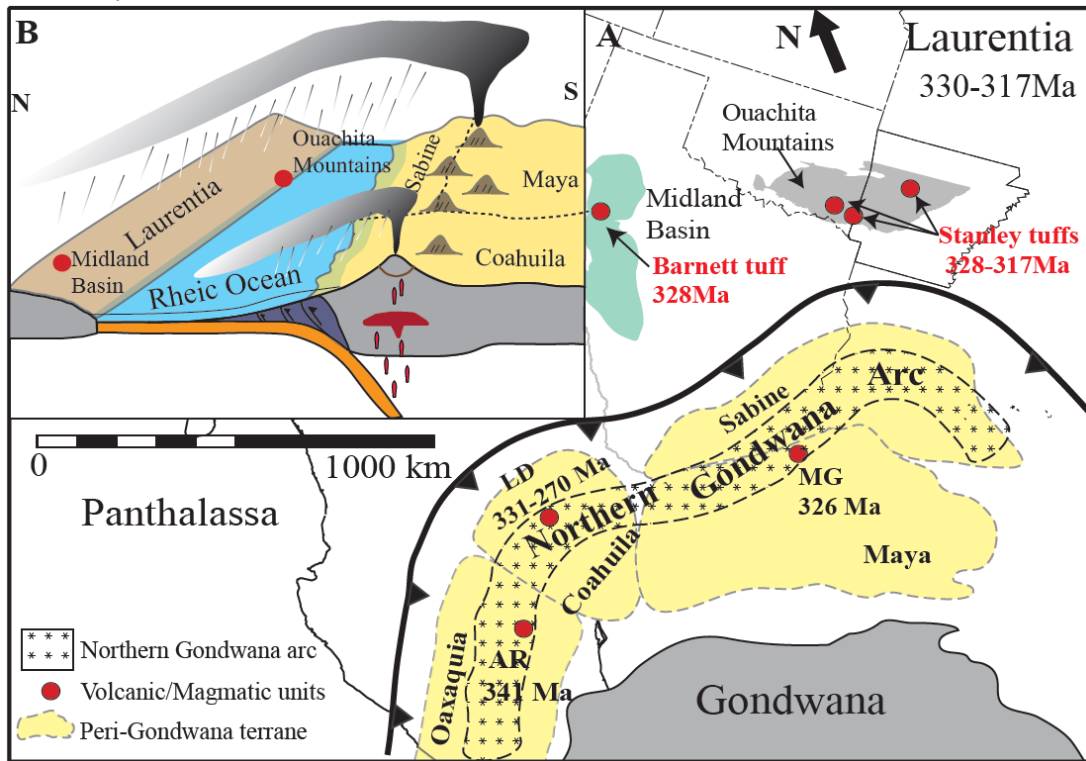
Figure 2-4. (A) Paleogeographic reconstruction at 330–317 Ma showing location of the Gondwana arc and rock units described in this paper, modified after Lawton et al. (2021). (B) Tectonic model for Late Mississippian magmatic activity in northern Gondwana. AR—Aserradero Rhyolite; LD—Las Delicias arc; MG—granitoids from the Chicxulub Scientific Drilling Project (https://www.icdp-online.org/projects/world/north-and-central-america/chicxulub-2-mexico/) in the Maya block.

2. 6 IMPLICATIONS

Our CA-ID-TIMS U-Pb zircon date of the Barnett tuff is the first absolute age of the Permian Basin sedimentary sequence. The previous apparent lack of datable tuff beds in the Permian Basin and diachronous nature of microfossil biozones raised uncertainty about the absolute ages of these important strata. In the Permian Basin, the lower part of the Barnett Shale was correlated to the international

Visean (346.7–330.9 Ma) Stage based on conodont biostratigraphy (Mauck et al., 2018). Our zircon U-Pb date (327.8 ± 0.8 Ma) of the Barnett tuff places some of the lower part of the Barnett Shale into the international Serpukhovian (330.9–323.2 Ma) Stage. The correlation between the Barnett and Beavers Bend tuffs across ∼800 km further suggests that tuffs of this age may be widespread along the southern Laurentia margin and might provide a means to constrain the absolute ages of other basin fill, such as that in the Fort Worth Basin.

Our results suggest that Gondwana-Laurentia collision did not occur until after the youngest arc magmatism at ca. 317 Ma, which is consistent with the results of sediment provenance studies (See Appendix A , Fig. S2-6). Neoproterozoic zircons sourced from the Pan-African orogen of Gondwana did not arrive in Laurentia during the Late Mississippian deposition of the Stanley Group (Prines, 2020), but they are present in Pennsylvanian strata of the Fort Worth Basin (Alsalem et al., 2018; See Appendix A, Fig. S2-6), indicating that the collision in the Ouachita salient happened during the Pennsylvanian.

2. 7 CONCLUSIONS

Our new zircon U-Pb dates, εHf signatures, and trace-element compositions of tuffs from the Ouachita Mountains and the Midland Basin imply that a continental arc was active from ca. 328 to ca. 317 Ma due to subduction of the Rheic oceanic plate beneath northern Gondwana. During the Late Mississippian, eruptions of arc volcanoes delivered tuffs northward into the adjacent deep-water basin between the arc and Laurentia and further north to southern Laurentia. The deep-water deposits were then incorporated in the Ouachita orogen during the subsequent Laurentia-Gondwana collision. Our results have implications for chronostratigraphy in southern Laurentia as well as the timing of Laurentia-Gondwana collision.

2. 8 ACKNOWLEDGMENTS

2. 9 REFERENCES CITED

Alemán-Gallardo, E.A., Ramírez-Fernández, J.A., Rodríguez-Díaz, A.A., Velasco-Tapia, F., Jenchen,U., Cruz-Gámez, E.M., De León-Barragán, L., and Navarro-De León, I., 2019, Evidence for an Ordovician continental arc in the pre-Mesozoic basement of the Huizachal-Peregrina anticlinorium, Sierra Madre Oriental, Mexico: Peregrina Tonalite: Mineralogy and Petrology, v. 113, p. 505–525, https://doi.org/10.1007/s00710-019-00660-4.

Alsalem, O.B., Fan, M., Zamora, J., Xie, X., and Griffin, W.R., 2018, Paleozoic sediment dispersal before and during the collision between Laurentia and Gondwana in the Fort Worth Basin, USA: Geosphere, v. 14, p. 325–342, https://doi.org/10.1130/GES01480.1.

Belousova, E.A., Griffin, W.L., O'Reilly, S.Y., and Fisher, N.I., 2002, Igneous zircon: Trace element composition as an indicator of source rock type: Contributions to Mineralogy and Petrology, v. 143, p. 602–622, https://doi.org/10.1007/s00410-002-0364-7.

Dhuime, B., Hawkesworth, C., and Cawood, P., 2011, When continents formed: Science, v. 331, p. 154–155, https://doi.org/10.1126/science.1201245.

Dickinson, W.R., and Lawton, T.F., 2001, Carboniferous to Cretaceous assembly and fragmentation of Mexico: Geological Society of America Bulletin, v. 113, p. 1142–1160, https://doi.org/10.1130/0016-7606(2001)113<1142:CTCAAF>2.0.CO;2.

Grimes, C.B., Wooden, J.L., Cheadle, M.J., and John, B.E., 2015, "Fingerprinting" tectono-magmatic provenance using trace elements in igneous zircon: Contributions to Mineralogy and Petrology, v. 170, 46, https://doi.org/10.1007/s00410-015-1199-3.

Hibbard, J.P., and Samson, S., 1995, Orogenesis exotic to the Iapetan cycle in the southern Appalachians, in Hibbard, J.P., et al., eds., Current Perspectives in the Appalachian-Caledonian Orogen: Geological Society of Canada Special Paper 41, p. 191–205.

Hibbard, J.P., Stoddard, E.F., Secor, D.T., and Dennis, A.J., 2002, The Carolina zone: Overview of Neoproterozoic to early Paleozoic peri-Gondwanan terranes along the eastern flank of the southern Appalachians: Earth-Science Reviews, v. 57, p. 299–339, https://doi.org/10.1016/S0012-8252(01)00079-4.

Jones, R.E., Kirstein, L.A., Kasemann, S.A., Dhuime, B., Elliott, T., Litvak, V.D., Alonso, R., and Hinton, R., 2015, Geodynamic controls on the contamination of Cenozoic arc magmas in the southern Central Andes: Insights from the O and Hf isotopic composition of zircon: Geochimica et Cosmochimica Acta, v. 164, p. 386–402, https://doi.org/10.1016/j.gca.2015.05.007.

Kemp, A.I.S., Hawkesworth, C.J., Foster, G.L., Paterson, B.A., Woodhead, J.D., Hergt, J.M., Gray, C.M., and Whitehouse, M.J., 2007, Magmatic and crustal differentiation history of granitic rocks from Hf-O isotopes in zircon: Science, v. 315, p. 980–983, https://doi.org/10.1126/science.1136154.

Kinny, P.D., and Maas, R., 2003, Lu-Hf and Sm-Nd isotope systems in zircon: Reviews in Mineralogy and Geochemistry, v. 53, p. 327–341, https://doi.org/10.2113/0530327.

Kirsch, M., Keppie, J.D., Murphy, J.B., and Solari, L., 2012, Permian–Carboniferous arc magmatism and basin evolution along the western margin of Pangea: Geochemical and geochronological evidence from the eastern Acatlán Complex, southern Mexico: Geological Society of America Bulletin, v. 124, p. 1607–1628, https://doi .org/10.1130/B30649.1.

Lawton, T.F., Blakey, R.C., Stockli, D.F., and Liu, L., 2021, Late Paleozoic (Late Mississippian–Middle Permian) sediment provenance and dispersal in western equatorial Pangea: Palaeogeography, Palaeoclimatology, Palaeoecology, v. 572, p. 1–35, https://doi.org/10.1016/j.palaeo. 2021.110386.

Leary, R.J., Umhoefer, P., Smith, M.E., and Riggs, N., 2017, A three-sided orogen: A new tectonic model for Ancestral Rocky Mountain uplift and basin development: Geology, v. 45, p. 735–738, https://doi.org/10.1130/G39041.1.

Loomis, J., Weaver, B., and Blatt, H., 1994, Geochemistry of Mississippian tuffs from the Ouachita Mountains, and implications for the tectonics of the Ouachita orogen, Oklahoma and Arkansas: Geological Society of America Bulletin, v. 106, p. 1158–1171, https://doi.org/10.1130/0016-7606(1994)106<1158:GOMTFT>2.3.CO;2.

Lopez, R., 1997, The Pre-Jurassic Geotectonic Evolution of the Coahuila Terrane, Northwestern Mexico: Grenville Basement, a Late Paleozoic Arc: Triassic Plutonism, and the Events South of the Ouachita Suture [Ph.D. thesis]: Santa Cruz, California, University of California, p. 55–147.

Lopez, R., Cameron, K.L., and Jones, N.W., 2001, Evidence for Paleoproterozoic, Grenvillian, and Pan-African age Gondwanan crust beneath northeastern Mexico: Precambrian Research, v. 107. p. 195–214, https://doi.org/10.1016/S0301-9268(00)00140-6.

Martens, U., Weber, B., and Valencia, V.A., 2010, U/Pb geochronology of Devonian and older Paleozoic beds in the southeastern Maya block, Central America: Its affinity with peri-Gondwana terranes: Geological Society of America Bulletin, v. 122, p. 815–829, https://doi.org/10.1130/B26405.1.

Mattinson, J.M., 2005, Zircon U-Pb chemical abrasion ("CA-TIMS") method: Combined annealing and multi-step partial dissolution analysis for improved precision and accuracy of zircon ages: Chemical Geology, v. 220, p. 47–66, https://doi.org/10.1016/j.chemgeo.2005.03.011.

Mauck, J.V., Loucks, R.G., and Entzminger, D.J., 2018, Stratigraphic architecture, depositional systems, and lithofacies of the Mississippian Upper Barnett Two Finger Sand Interval, Midland, Basin, Texas: Gulf Coast Association of Geological Societies Journal, v. 7, p. 21–45, http://www .gcags.org/Journal/2018.GCAGS. Journal/2018 .GCAGS.Journal.v7.02.p21-45.Mauck.et.al.pdf.

McDonough, W.F., and Sun, S.S., 1995, The composition of the Earth: Chemical Geology, v. 120, p. 223–253, https://doi.org/10.1016/0009-2541(94)00140-4.

Morris, R.C., 1989, Stratigraphy and sedimentary history of post-Arkansas Novaculite Carboniferous rocks of the Ouachita Mountains, in Hatcher, R.D., Jr., et al., eds., The Appalachian-Ouachita Orogen in the United States: Boulder, Colorado, Geological Society of America, The Geology of North America, v. F-2, p. 591–602, https://doi.org/10.1130/DNAG-GNA-F2.591.

Mueller, P., Heatherington, A., and Foster, D., 2011, Alleghanian granites of the southern Appalachian orogen: Keys to Pangean reconstructions, in Huebner, M.T., and Hatcher, R.D., Jr., eds., The Geology of the Inner Piedmont at the Northeast End of the Pine Mountain Window: Georgia Geological Society Guidebook 31, p. 39–48.

Nance, R.D., Murphy, J.B., and Santosh, M., 2014, The supercontinent cycle: A retrospective essay: Gondwana Research, v. 25, p. 4–29, https://doi.org/10.1016/j.gr.2012.12.026.

Niem, A.R., 1977, Mississippian pyroclastic flow and ash-fall deposits in the deep-marine Ouachita flysch basin, Oklahoma and Arkansas: Geological Society of America Bulletin, v. 88, p. 49–61, https://doi.org/10.1130/0016-7606(1977)88<49:MPFAAD>2.0.CO;2.

Ortega-Obregón, C., Solari, L., Gómez-Tuena, A., Elías-Herrera, M., Ortega-Gutiérrez, F., and Macías-Romo, C., 2013, Permian–Carboniferous arc magmatism in southern Mexico: U-Pb dating, trace element and Hf isotopic evidence on zircons of earliest subduction beneath the western margin of Gondwana: International Journal of Earth Sciences, v. 103, p. 1287–1300, https://doi.org/10.1007/s00531-013-0933-1.

Prines, S.T., 2020, U-Pb Detrital Zircons of the Synorogenic Carboniferous Deep-Water Clastic Deposits in the Ouachita Mountains, Arkansas, United States [M.S. thesis]: Fort Worth, Texas, Texas Christian University, 80 p.

Ramírez-Fernández, J.A., Alemán-Gallardo, E.A., Cruz-Castillo, D., Velasco-Tapia, F., Jenchen, U., Becchio, R., León-Barragán, L.D., and Casas-Peña, J.M., 2021, Early Mississippian precollisional, peri-Gondwanan volcanic arc in NE-Mexico: Aserradero Rhyolite from Ciudad Victoria, Tamaulipas: International Journal of Earth Sciences, v. 110, p. 2435–2463, https://doi.org/10.1007/s00531-021-01992-3.

Rudnick, R.L., and Gao, S., 2003, Composition of the continental crust, in Rudnick, R.L., ed., Treatise on Geochemistry Volume 3: The Crust: Oxford, UK, Elsevier, p. 1–64, https://doi . org/10.1016/B0-08-043751-6/03016-4.

Shaulis, B.J., Lapen, T.J., Casey, J.F., and Reid, D.R., 2012, Timing and rates of flysch sedimentation in the Stanley Group, Ouachita Mountains, Oklahoma and Arkansas, U.S.A.: Constraints from U-Pb zircon ages of subaqueous ash-flow tuffs: Journal of Sedimentary Research, v. 82, p. 833–840, https://doi.org/10.2110/jsr.2012.68.

Torres, R., Ruiz, J., Patchett, P.J., and Grajales, J.M., 1999, Permo-Triassic continental arc in eastern México: Tectonic implications for reconstructions of southern North America, in Bartollini, C., Wilson, J.L., and Lawton, T.F., eds., Mesozoic Sedimentary and Tectonic History of North-Central Mexico: Geological Society of America Special Paper 340, p. 191–196, https://doi.org/10.1130/0-8137-2340-X.191.

Workman, R., and Hart, S.R., 2005, Major and trace element composition of depleted mantle: Earth and Planetary Science Letters, v. 231, p. 53–72, https://doi.org/10.1016/j.epsl.2004.12.005.

Zhao, J., et al., 2020, Geochemistry, geochronology and petrogenesis of Maya block granitoids and dykes from the Chicxulub impact crater, Gulf of México: Implications for the assembly of Pangea: Gondwana Research, v. 82, p. 128–150, https://doi.org/10.1016/j.gr.2019.12.003.

Chapter 3 RAPID EARLY PERMIAN TECTONIC REORGANIZATION OF LAURENTIA'S

PLATE MARGINS: EVIDENCE FROM VOLCANIC TUFFS IN THE PERMIAN BASIN, USA

Hepeng Tian[1], Majie Fan[1], Victor A. Valencia[2], Kevin Chamberlain[3], Robert J. Stern[4] and Lowell Waite[4]

[1]Department of Earth and Environmental Sciences, The University of Texas at Arlington, Arlington, Texas 76019, USA

[2]School of Environment, Washington State University, Pullman, Washington 99164, USA

[3]Department of Geology and Geophysics, University of Wyoming, Laramie, Wyoming 82071, USA

[4]Department of Geosciences, University of Texas at Dallas, Richardson, Texas 75083, USA

ABSTRACT

Early Permian arc magmatism is critical to understanding the final assembly of the supercontinent Pangea and subsequent plate reorganization. Herein we report the geochronology and geochemistry of Cisuralian and Guadalupian volcanic tuffs in southwestern Laurentia and infer the magmatic sources and plate reorganization related to Laurentia-Gondwana collision. Zircon CA-ID-TIMS U-Pb dates of tuffs in the Wolfcamp B, Wolfcamp A and lower Spraberry units in the Permian Basin provide the first set of absolute ages of Cisuralian deposits in this basin. Zircon geochemistry data further show that the parent melts of these tuffs were granitic melts that formed in continental arcs. Syn-depositional zircons from the Wolfcamp B tuff beds (288.2 ±1.7 Ma) have an average εHf value of +5.5 and TDM2 model ages between 675-1207 Ma, reflecting a mixture of juvenile mantle melts and Precambrian crust. The isotopic signature is consistent with Mississippian Laurentian tuffs derived from a northern Gondwana arc formed by the subduction of the Rheic oceanic plate. However, zircons from a Wolfcamp A tuff bed (287.2 ±0.5 Ma) show an average εHf value of -4.5, much more evolved than the inferred northern Gondwana arc, but consistent with granitoids of similar or younger age in the Oaxaquia terrane. This change in εHf most likely reflects magmatism related to subduction of a paleo-Pacific oceanic plate beneath western Pangea. Our interpretation suggests a late Cisuralian plate

reorganization that was caused by plate reorganization following Pangea assembly led to rapid (~ 1 Myr) initiation of subduction beneath western Pangea. This study also compares tuff dates from LA-ICPMS and CA-ID-TIMS U-Pb dating and concludes that the weighted mean date of the youngest dominant KDE mode (WMYDM) is the best way to approximate LA-ICPMS dates to true depositional ages.

3. 1 INTRODUCTION

3.1.1 Late Paleozoic tectonics

Plate reorganizations, as natural consequences of plate tectonics, are difficult to recognize in the pre-Jurassic geologic record. The driving forces of plate reorganization are derived principally from mantle convection or plates with dynamic feedback between the two (e.g., Anderson et al., 2001; King et al., 2002; Matthews et al., 2012; Mallard et al., 2016). Major plate reorganizations that took as short as less than a few million years are thought to be less likely caused by mantle buoyance forces due to oceanic slab subduction, ocean plate thickening, or upwelling of mantle plume. They are more likely caused by changes in plate motion due to creation of new or destruction of old plate margins (Richards and Lithgow-Bertelloni, 1996). The rates of plate reorganization in the last 200 Myr, with less uncertainty for the last 100 Myr, are traditionally determined from analysis of ocean-floor magnetic lineations (e.g., Morra et al., 2013); this approach is not possible before the Jurassic because older seafloor has been subducted. The sparsity of geologic evidence for the rate of plate reorganization >200 Myr limits our understanding of plate tectonic history and assessment of the geodynamic drivers of plate reorganizations.

Plate reorganization associated with assembly of the supercontinent Pangea is undoubtedly an important late Paleozoic tectonic event. Subduction of the Rheic plate beneath northern Gondwana may have started during the Early Mississippian (e.g., Estrada-Carmona et al., 2006; Tian et al., 2022; Zhao

et al., 2020), as early as ~348 Ma (Ramirez-Fernandez et al., 2021). The assembly of Pangea was marked by closure of the Rheic ocean, accretion of peri-Gondwanan terranes to Laurentia, and diachronous Laurentia-Gondwana collision to form the Appalachian-Ouachita-Marathon-Sonora orogenic belt (e.g., Nance and Linnemann, 2008; Domeier and Torsvik, 2014). The collision destroyed the intervening subduction zone(s), ultimately leading to subduction of the Paleo-Pacific oceanic plate beneath western Pangea. However, details about the change from Rheic oceanic plate to Paleo-Pacific oceanic plate subduction are poorly understood. The lack of understanding, in part, reflects the fact that arc magmatic products (esp. granitic rocks) related to Rheic ocean subduction may have been overprinted by those related to the eastward subduction of the Paleo-Pacific oceanic plate beneath western Pangea. Torres et al. (1999) proposed that a Permian-Triassic (287-232 Ma) continental arc in eastern Mexico (the East Mexico arc) was likely caused by eastward subduction of the Paleo-Pacific oceanic plate beneath western Gondwana and claimed that this arc may have extended into California, USA. This inference is supported by arc magmatism that initiated as early as early Permian (275 Ma) in the Mojave Desert, southern California, USA (Cecil et al., 2019) as well as the dominant ~274 Ma zircon age cluster in the Permian Monos Formation deposited in a forearc setting in northwestern Sonora, Mexico (Dobbs et al., 2021). Moreover, Kirsch et al. (2012) and Ortega-Obregón et al. (2014) suggested that the Permian-Triassic arc, related to subduction of the Paleo-Pacific oceanic plate, may have started during the Pennsylvanian (311 Ma) in southern Mexico. An alternative model is that the early Permian plutonic and volcanic rocks in southern, central and northern Mexico represent the southwestern extension of Rheic oceanic plate subduction beneath western Gondwana due to the preservation of Rheic ocean vestiges and lack of Triassic magmatic units related to subduction of the Paleo-Pacific oceanic plate in the region (e.g., Elías-Herrera and Ortega-Gutiérrez, 2002; Vega-Granillo et al., 2007, 2009; Ortega-Gutiérrez et al., 2018; Zúñiga et al., 2020). Consequently, Permian magmatic units in Mexico south of the Marathon-Sonora belt are interpreted as either products of Paleo-Pacific or Rheic oceanic plate subduction (e.g., Keppie et al., 2008; Nance et al., 2010; Ortega-Obregón et al.,

2014; Rosales-Lagarde et al., 2005; Coombs et al., 2020). Therefore, studies of early Permian magmatic units near the west terminus of the Laurentia-Gondwana collisional belt are important for understanding the change from one subduction system to the other and the evolution of magmatism related to Pangea assembly.

3.1.2 Permian Basin chronostratigraphy

The Permian Basin of western Texas and southeastern New Mexico contains thick Paleozoic sedimentary rocks that record the last stages in the late Paleozoic assembly of Pangea (e.g., Ross, 1986; Yang and Dorobek, 1995; Liu and Stockli, 2020). Despite many decades of study by especially industry geoscientists, the ages of basin-fills are poorly constrained because of the lack of isotopic dates and the scarcity of paleontological studies. Age constraints for Early and Middle Permian (Cisuralian and Guadalupian) series in the subsurface of the basin are mostly based on subsurface correlations to the outcrop type sections in the Glass and Guadalupe Mountains, western Texas, respectively (e.g., Silver and Todd, 1969; Handford, 1981; Mazzullo and Reid, 1989; Hamlin and Baumgardner, 2012; Baumgardner et al., 2016). The chronostratigraphy of Cisuralian type sections are based on the correlation of microfossils to the sections with Global Boundary Stratotype Section and Point (GSSP) where absolute ages are constrained by isotopic dating of tuffs (Behnken, 1984; Wardlaw and Davydov, 2000; Ross and Ross, 2003; 2009; Wahlman, 2013; Wardlaw and Nestell, 2014). Few microfossil studies have been conducted in the Cisuralian series of the Permian Basin and are focused on deep-water deposits in the northern part of the basin (Wahlman et al., 2016; Kohn et al., 2019). These sites are unsuitable for basin-wide stratigraphic correlation, which is a common practice of chronostratigraphic correlation to constrain the depositional ages of other sites, because these deposits were disturbed by episodic debris flows (Baumgardner et al., 2016) and fossils at shallow depth may have been later mixed into deep-water deposits. Additionally, microfossil studies in western Texas have mostly followed the North America Permian regional time scale defined by fusulinids whereas the International Time Scale for the Permian Period was defined by conodonts and isotopic dates (Chernykh

and Ritter, 1997; Davydov et al., 1998; Chuvashov et al., 2002; Chernykh et al., 2006; Chuvashov et al., 2013). The use of different microfossils makes difficult a direct correlation between the North America Permian regional time scale with the International Permian Scale.

Herein we report whole rock geochemistry, zircon U-Pb geochronology using both CA-ID-TIMS and LA-ICPMS, and zircon hafnium isotope and trace element geochemistry of 11 late Paleozoic volcanic tuffs (~288 to ~280 Ma) preserved in the Permian Basin and the Guadalupe Mountains north of the Marathon orogenic belt (Fig.3-1). These data are used to 1) constrain tuff ages and refine the chronostratigraphy of lower Permian strata in the Permian Basin; 2) understand the magmatic affinity and sources of these tuffs; and 3) unravel tectonic processes during the final collision of Laurentia and Gondwana near the western edge of the central Pangea suture. Our results have implications for best practices in statistical analysis of LA-ICPMS dates for age determination and the rate of plate reorganization.

3. 2 GEOLOGICAL BACKGROUNDS

The Permian Basin is located in western Texas and southeastern New Mexico, USA. It is over 400 km across and is one of the largest sedimentary basins in North America. It is bounded by the Marathon-Ouachita fold-and-thrust belt to the south, the Diablo Platform to the west, the Northwestern Shelf to the northwest, the Northern Shelf to the north and the Eastern Shelf to the east (Fig.3-1). The Basin is subdivided into the Delaware Basin in the west and the Midland Basin in the east, separated by the Central Basin Platform. The region was part of a broad continental basin on the southern Laurentian passive margin from Early Ordovician to Late Mississippian time, known as the Tobosa Basin, and was reshaped and structurally differentiated during the Carboniferous-Early Permian by NNW-SSE trending Ancestral Rocky Mountain structures to the north (Leary et al., 2017) and the Laurentia-Gondwana collision to the south (Ross, 1986). It is generally thought that the collision began in the Appalachians during the Late Mississippian and propagated westward to the Ouachita Mountains

41

in Arkansas and Oklahoma in the Early Pennsylvanian and ended in the Marathon region in western Texas and Sonora by the Early Permian (Poole et al., 2005).
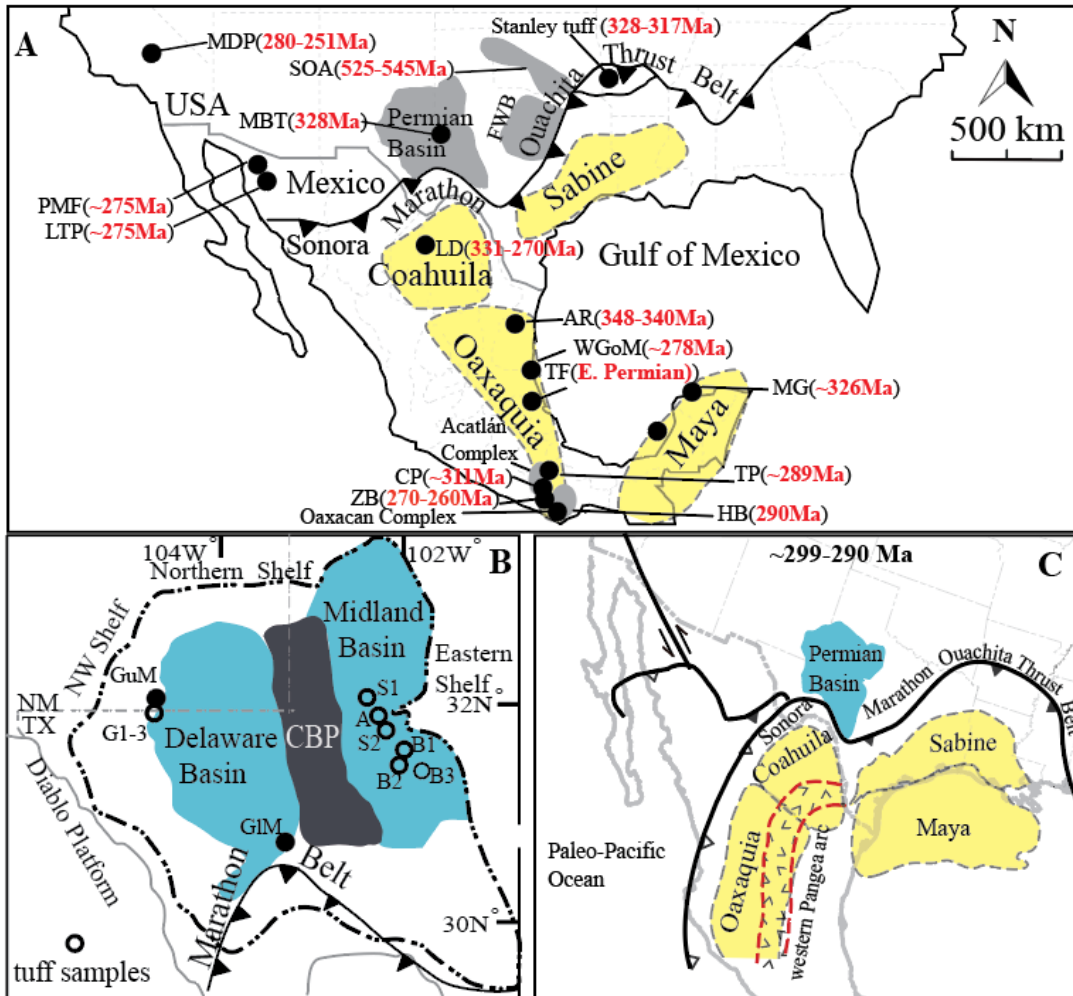
Figure 3-1. Simplified geologic map of A) southern North America showing the locations of Peri-Gondwana terranes, the Ouachita-Marathon-Sonora fold and thrust belt, the Permian Basin, and the tuff sources discussed in the paper. AR: Aserradero Rhyolite (Ramírez-Fernánde et al., 2021); CP: Cuanana pluton (zircon εHf between +3 and +9; Ortega-Obregón et al., 2014); FWB: Fort Worth Basin; HP: Honduras batholith (zircon εHf values between +5 and +8; Ortega-Obregón et al., 2014); LD: Las Delicias arc (whole rock εNd between +2.6 and +5.3; Lopez, 1997); LTP: Los Tanques

pluton (zircon εHf signature of ~-7.5; Riggs et al., 2016); MDP: Mojave Desert pluton (zircon εHf between -5 and +10 for 280-260 Ma zircon grains; Cecil et al., 2019); MT: Mississippian Barnett tuff in the Midland Basin (zircon εHf of between 0 and +5; Tian et al., 2022); PMF: Permian Monos Formation (Dobbs et al., 2021); MG: Early Mississippian granitoids (zircon εHf between +3.8 and +6.0; Zhao et al., 2020); SOA: Southern Oklahoma Aulacogen (Thomas et al., 2016); TP: Totoltepec pluton (whole rock εNd between -0.8 and +2.6; Kirsch et al., 2012); TF: lower Permian Tuzancoa Formation (whole rock εNd of +4.4; Rosales-Lagarde et al., 2005); WGoM: western Gulf of Mexico (zircon εHf of -6.0; Coombs et al., 2020); ZB: Zaniza batholith (zircon εHf between -14 and -1; Ortega-Obregón et al., 2014). B) Map showing the Permian Basin the studied volcanic tuffs in the basin. CBP: Central basin platform; GlM: Glass Mountains; GuM: Guadalupian Mountains. C) Paleogeographic map of southern Laurentia and northern Gondwana at ~299-290 Ma. The figure is modified after Lawton et al. (2021). Black triangles represent orogenic front and white triangles represent convergent plate margin. To the northwest of Sonora, arc magmatism in the Caborca Block was approximately coeval with the Sonora orogeny, suggesting the onset of subduction of paleo-Pacific plate beneath Caborca during this time may have caused the inception of Cordilleran arc (Lawton et al., 2021).

During the passive margin stage, the Tobosa Basin was in a marine depositional environment and accommodated nearly 1 km of siliciclastic and carbonate rocks with minor carbonate turbidites. The sequence includes Lower Ordovician sandstones and shales, overlain by Middle-Upper Ordovician, Silurian, Middle Devonian, and Mississippian carbonates with subordinate siliciclastic rocks, and the Upper Devonian and Lower Mississippian Woodford Shale (e.g., Adams, 1965; Ross, 1986; Dutton et al., 2005). The pre-collision Upper Mississippian to Middle Pennsylvanian sedimentary rocks in the Permian Basin are characterized by thinly bedded limestone, shale and sandstone that were deposited in a shallow-marine environment (Ross, 1986). During the Late Pennsylvanian to early Permian

collision, the Basin experienced rapid flexural subsidence, thrust faulting, and major glacioeustactic sea-level changes (Crowell, 1978), and accommodated a thick section (~4.2 km) of deep-marine shale and turbidite deposits that overlie the Lower Ordovician-Middle Pennsylvanian marine siliciclastic and carbonate rocks (Ross, 1986). The deepwater depositional environment persisted until the end of Guadalupian before the Basin was blanketed by upper Permian evaporites (Silver and Todd, 1969).

Nine Cisuralian volcanic tuffs were collected from subsurface cores in the Midland Basin where the total thickness of Permian strata is about 1.5-2.0 km (Hill, 1996). Adams (1939) first divided the Permian strata in the Permian Basin into four North America stages based on biostratigraphy and lithology, including the Wolfcampian, Leonardian, Guadalupian and Ochoan (Fig. 3-2). Permian strata in the Glass Mountains, to the south of the Delaware Basin (Fig. 3-1), is a continuous and complete succession from the base of the Wolfcampian stage to the top of the Guadalupian stage and is considered as the type section of Permian strata in North America (Hill, 1996). Stratigraphic correlations of Permian strata between the subsurface of the Midland Basin and Glass Mountains exposures are mainly by lithology (Ross, 1986; Yang and Dorobek, 1995; Hill, 1996) with a few biostratigraphic constraints from Kohn et al. (2019). In the Glass Mountains, Wolfcampian sedimentary rocks mainly consist of shale and limestone; Leonardian rocks are shale with thin beds of limestone; Guadalupian rocks are mainly limestone; and Ochoan rocks are massive evaporites (Adams, 1965).

The subsurface lithostratigraphic nomenclature in the Permian Basin is not synonymous with the formal chronostratigraphic intervals from Glass Mountains type sections but evolved to serve hydrocarbon exploration purposes. Early Permian Wolfcampian operational units include the Wolfcamp Shale, which is subdivided into A, B, C and D units, from top to bottom (Fig. 3-2). Microfossil studies and stratigraphic correlations have shown that the Wolfcamp D unit is Late Pennsylvanian (Baumgardner et al, 2016) while the Wolfcamp A is early Leonardian (Wilde, 1975; Mazzullo, 1982; Mazzullo et al., 1987; Mazzullo and Reid, 1989; Wilde, 1990). Kohn et al. (2019) studied conodonts from core samples in the northern Midland Basin and proposed that the upper

boundary of the Wolfcampian stage should be placed in the uppermost Wolfcamp B unit and the bases of the International Asselian, Sakmarian and Kungurian Stages should be placed in the lowermost Wolfcamp C, Wolfcamp C and Wolfcamp A units, respectively (Fig. 3-2). The Leonardian stage in the Midland Basin contains the Dean and Spraberry Formations. The Dean Formation is mainly sandstone, and the Spraberry Formation consists of calcareous and silica-rich mudstone interbedded with siltstone and sandstone. The Spraberry Formation is further divided by oil industry geologists into several informal units, including the Leonard shale, Jo Mill sand, and lower, middle, and upper Spraberry (Handford, 1981; Hamlin and Baumgardner, 2012).

Three volcanic tuffs were collected from Guadalupian exposures in the Guadalupe Mountains, which is located on the northwestern margin of the Delaware Basin (Fig. 3-1) and is the site of GSSPs of the Guadalupian Roadian, Wordian and Capitanian epochs in ascending order (e.g., Glenister et al., 1992, 1999; Lucas and Shen, 2018). The Guadalupian Series consists of the Cutoff Formation, Cherry Canyon Formation, and the Bell Canyon Formation in ascending order (Fig. 3-2). The formations are dominated by siliciclastic rocks with some typical shelf carbonate facies proximal to shelf margins (Adams, 1965).

Period	Series/Epoch	ICS Stage/Age (Ma)	North America Regional Stage	Biostratigraphic constraints		Lithostratigraphic nomenclature	
				Fusulinids	Conodonts	Formation/Unit	Lithology
Permian	Guadalupian	260 — Capitanian	Capitanian	N/A	*J.shannoni*	Bell Canyon	
					J.postserrata		
		265 — Wordian	Wordian		*J.aserrata*	Cherry Canyon	
		270 — Roadian	Roadian		*Jinogondolella nankingensis*	Brushy Canyon	
						Cutoff	
	Cisuralian	275 — Kungurian	Leonardian	*Parafusulina*		Sprab. upper / middle / lower / Jo Mill / Leonard shale / Dean	
		280 —					
		283.5 — Artinskian		*Schwagerina*	*N.exscuptus*	Wolfcamp Shale A	
		285 —					
			?				
		290 — 290.1 — Sakmarian	Wolfcampian	*Monodiexodina*		Wolfcamp Shale B	
				Pseudoschwagerina			
		295 — 295.5 — Asselian		*Schwagerina Triticites*	*S.barskovi*	Wolfcamp Shale C	
		298.9 —					

Shaly sandstone   Shale   Shaly carbonate   ▬ Tuff

Figure 3-2. Lower Permian stratigraphy in the Midland Basin and its correlation with the International Time Scale (International Commission of Stratigraphy, 2020). The lithostratigraphy and conodont zones of the Guadalupian Series are modified after Wu et al., (2019). The lithostratigraphic column of the Permian Series are modified after Heckel and Clayton (2006) and Henderson et al. (2012). Note that *Streptognathodus barskovi* and *Neostreptognathodus exsculptus* are conodonts that used to define the boundary between the Asselian Stage and Sakmarian Stage, and the Artinskian Stage and Kungurian Stage, respectively. Kohn et al. (2019) reported *S. barskovi* and *N. exsculptus* in the Wolfcamp A and Wolfcamp C units in northern Midland Basin.

3. 3 MATERIALS AND METHODS

3.3.1 Samples

Nine tuff horizons were identified from six Midland Basin subsurface cores (Fig. 3-1B) donated by Pioneer Natural Resources *(https://www.pxd.com).* These tuffs include six samples from the Wolfcamp B unit, one sample from the Wolfcamp A unit, and two samples from the Spraberry Formation (Figs. S3-1 and S3-2, Table S3-1 in the supplementary document). The six Wolfcamp B tuffs are from three cores and are correlated based on petrophysical data. Five of the Wolfcamp B samples have insufficient grains of Permian age for statistical analysis, thus all six samples were combined as the Wolfcamp B tuff and the data is mostly from Wolfcamp B5 sample.

The stratigraphic intervals of the tuffs were determined by petrophysical correlations following Hamlin and Baumgardner (2012) and Baumgardner et al. (2016). The base of the Wolfcamp A unit is characterized by an abrupt increase of gamma-ray signal referred as the "hot shale" marker, the base of the Wolfcamp B unit is marked by the middle Wolfcampian unconformity, the lower Wolfcamp C is marked by relatively low resistivity, and the Wolfcamp D unit has high gamma and high resistivity (Baumgardner et al., 2016). Our Wolfcamp A tuff is located about 45 m above the "hot shale" marker and our Wolfcamp B tuffs are located 20-60 m below the "hot shale" marker. The two Spraberry tuffs (Spraberry 1 and Spraberry 2) were collected from the lower Spraberry unit above the Jo Mill sand.

Oil industry geologists commonly identify tuffs based on fluorescence under ultraviolet light. The tuffs are greenish gray and show bright orange to dark brown fluorescence, and the interbedded shales are dark grey and do not show fluorescence (Fig. S3-2). Wolfcamp B tuffs are 3-12 cm thick, and the other tuffs are 2.5-5 cm thick. Some Wolfcamp B tuffs show erosional bases and wavy interbeds with shale (Fig. S3-2), suggesting erosion and transport. Tuffs in the other units show sharp lower and diffusive upper boundaries indicating gradual settling without major perturbation during deposition. The physical appearance and major element compositions of these tuffs differ from those of the interbedded shales. The tuffs also contain abundant zircons most and zircons in this study are unrounded,

unusual for deepwater shale. Although the abundance of detritus in these tuffs cannot be determined, following the definition that tuffs contain greater than 75% ash (Schmid, 1981), it is appropriate to classify the Wolfcamp A and Spraberry samples we studied as tuffs. The Wolfcamp B samples are most likely reworked tuffs (see our discussion).

Three tuff samples were collected from the Bell Canyon and Cherry Canyon Formations in the Guadalupe Mountains, at the same locations as sample BR040915-1B (our G1), NippleHill-2 (our G2), and MC053117-3 (our G3; Fig. S3-1) in Wu et al. (2020) (Table S3-1 in the supplementary document). All three tuffs are less than 20 cm thick and have grayish green color. The morphology and geochemistry of these tuffs have been described by Nicklen et al. (2015), and their ages have been determined using zircon U-Pb geochronology by Ramezani and Bowring (2018) and Wu et al. (2020).

3.3.2 Bulk tuff geochemistry

Bulk tuff major and trace elements were analyzed in the Shimadzu Center for Environmental, Forensics, and Material Science at the University of Texas at Arlington. Representative shale samples from the Wolfcamp B, Wolfcamp A and Spraberry units were also analyzed for comparison. Major element compositions were determined by a Shimadzu XRF-1800 wavelength dispersive X-ray fluorescence spectrometer. Trace element compositions were measured using a Shimadzu ICPMS2030 inductively coupled plasma mass spectrometer. See supplementary document under the section "Analytical Methods" for details.

3.3.3 Zircon morphology

Zircons were extracted from eleven tuff beds following standard procedures, including disc mill crushing, ultrasonic shaking to remove attached clays, pan washing, magnetic separation, and heavy liquid separation. All zircons from the tuffs were handpicked using a binocular microscope. Before mounting zircon grains in epoxy resin discs, a portion of the Wolfcamp A, Wolfcamp B, and Spraberry

grains were randomly selected and imaged using a Hitachi S3000N scanning electronic microscope (SEM) to characterize grain morphology. These grains were classified into five classes of roundness following Gärtner et al. (2013). The classes include completely unrounded, poorly rounded, rounded, well rounded, and completely rounded following our study of the Mississippian Barnett tuff in the Permian Basin (Fig. S3-4 in Tian et al., 2022). After mounting and polishing, representative grains were imaged using a SEM and cathodoluminescence (CL) to observe internal zoning structures and inclusions to determine spots for U-Pb dating, Hf isotope analysis and rare earth element composition. Zircon grains primarily with volcanic textures such as muted, broad zonation under cathodoluminescence and morphologies with elongate tips, longitudinal gas tracks and transverse channels were primarily targeted for Laser Ablation-Inductively Coupled Plasma Mass Spectrometry (LA-ICPMS) and Chemical Abrasion-Isotope Dilution-Thermal Ionization Mass Spectrometry (CA-ID-TIMS) analyses. All zircon U-Pb dates, Lu-Hf isotope and trace element (TE) composition analysis by LA-ICP-MS were conducted at the Radiogenic Isotope and Geochronology Lab at Washington State University. After LA-ICPMS analyses, representative young zircon grains from Wolfcamp and Spraberry tuffs were plucked from the mount and analyzed at University of Wyoming by chemical abrasion, isotope dilution, thermal ionization mass spectrometry (CA-ID-TIMS) following Mattinson (2005). Analytical procedures, data reduction and filtering are described in the supplementary document under the section "Analytical Methods". For LA-ICPMS results, $^{207}Pb/^{206}Pb$ dates were used for grains older than 1300 Ma and $^{206}Pb/^{238}U$ dates were used for grains younger than 1300 Ma. Filters of 15% discordance (calculated as the ratio of $^{206}Pb/^{238}U$ and $^{207}Pb/^{206}Pb$ dates) and a 5% reverse discordance were applied to zircons older than 500 Ma to exclude grains that may have been influenced by Pb loss or poor matrix match between samples and standards leading to differential laser induced elemental fractionation (Allen and Campbell, 2012; Schaltegger et al., 2015). Discordance could not be used as a filter for grains less than 500 Ma because young ICPMS dates have large $^{207}Pb/^{206}Pb$ uncertainties, and many analyses appear to be disconcordant.

3. 4 RESULTS

3.4.1 Whole rock geochemistry for Midland Basin tuffs

All tuff whole-rock samples had a loss on ignition (LOI) >10%. After LOI normalization, the samples contain 59 to 70 wt.% SiO_2, 21 to 31 wt.% Al_2O_3, 0.3 to 0.5 wt.% TiO_2, 2.2 to 3.9 wt.% Fe_2O_3, 1.1 to 2.4 wt.% MgO, 0.6 to 1.9 wt.% CaO, 0 to 1.2 wt.% P_2O_5 and 4.5 to 6.6 wt.% K_2O + Na_2O (Tables S2 and S3). On a K_2O-SiO_2 diagram, Spraberry tuffs plot as shoshonitic series and Wolfcamp tuffs plot as high-K calc-alkaline series (Fig. 3-3). In general, the tuffs show high Si, Al, and alkalis but low Ti content. Chemical index of alteration (CIA) of the samples was calculated using Al_2O_3/ (Al_2O_3 + CaO + K_2O + Na_2O). The CIA index of the tuff samples are between 0.73-0.82, higher than that of the shale samples (0.61-0.69).
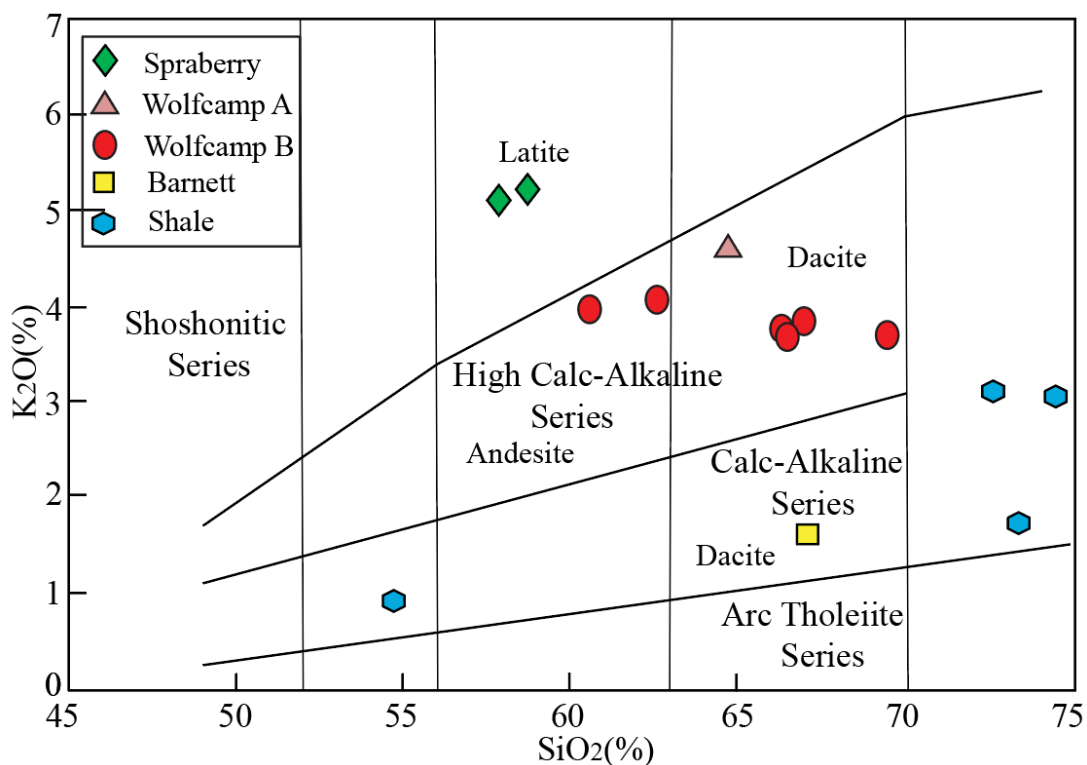
Figure 3-3. K2O vs. SiO2 classification diagram showing whole rock major element compositions of the volcanic tuffs and shale, modified from Peccerillo and Taylor (1976).

On a Zr/TiO2-Nb/Y diagram following Winchester and Floyd (1977), whole-rock trace element data place the tuffs into the dacite or andesite category, consistent with the TAS diagram (Fig. 3-4A). The tuffs are strongly enriched in large ion lithophile elements (LILE), such as Cs, Rb and Ba, and depleted in high field strength elements (HFSE), such as Nb, P and Ti (Fig. 3-4B). The samples plot in volcanic arc granite or within-plate granite settings in a Rb/(Y+Nb) plot (Pearce et al., 1984) (Fig. 3-4C). Chondrite-normalized rare earth element (REE) patterns are enriched in light REEs, show flat to slightly positive heavy REE slopes and moderate to no negative Eu anomalies with Eu/Eu* between 0.33-1.04 (Fig. 3-4D). All these features are typical of upper continental crust (Rudnick and Gao, 2003).
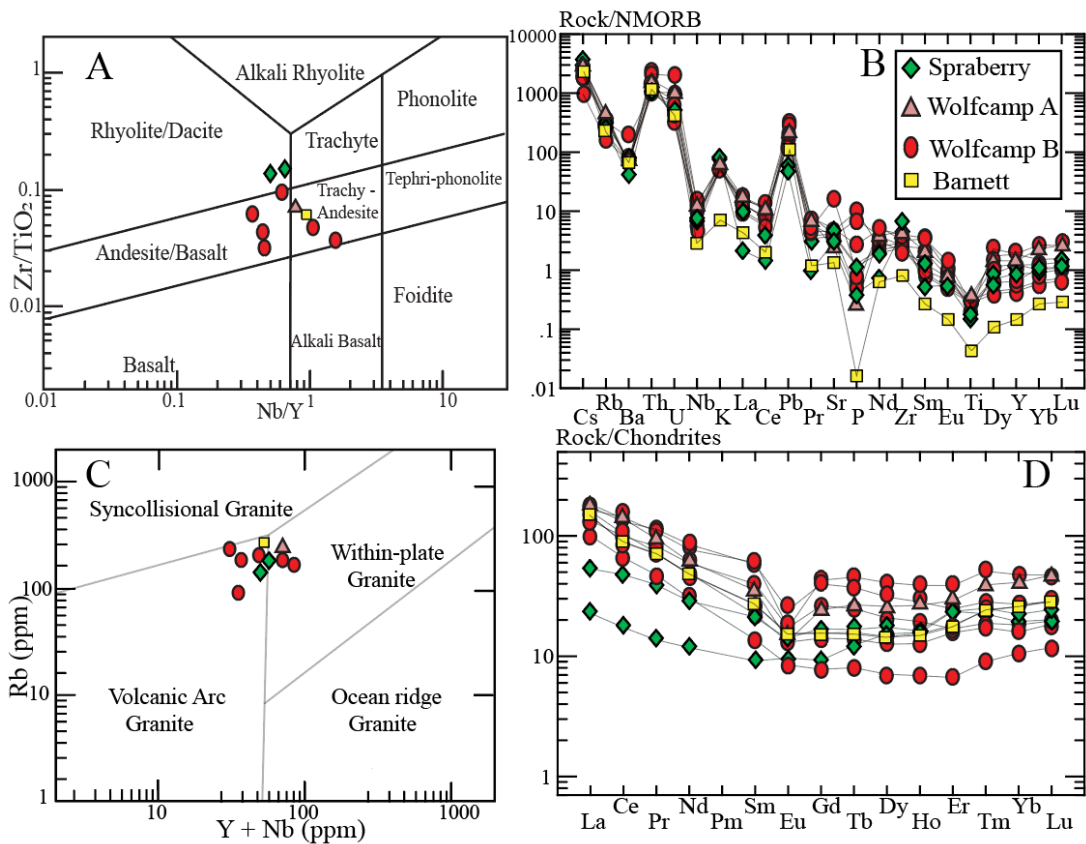
Figure 3-4. Whole rock trace element diagrams of all the volcanic tuffs. A) Zr/TiO2 vs. Nb/Y discrimination diagram, modified from Winchester and Floyd (1977). B) Mid-Ocean Ridge Basalt-

normalized incompatible element diagram after Sun and McDonough (1989). C) Rb vs. Y+Nb discrimination diagram after Pearce et al. (1984). D) Chondrite-normalized REE diagram after Sun and McDonough (1989).

The shale samples have LOI from 7.4 to 21.7 %. After LOI normalization, the shale samples contain 55 to 75 wt.% SiO_2, 5 to 16 wt.% Al_2O_3, 0.1 to 0.8 wt.% TiO_2, 2.27 to 4.3 wt.% Fe_2O_3, 1.2 to 2.1 wt.% MgO, 0.6 to 32.8 wt.% CaO, 0 to 0.5 wt.% P_2O_5 and 1.6 to 4.5 wt.% $K_2O + Na_2O$ (Table S3). Wolfcamp A and Wolfcamp B are carbonate-rich and have high LOI and CaO values. In general, the shale samples have higher SiO_2, much higher CaO and much lower Al_2O_3 than the tuffs.

3.4.2 Zircon morphology and geochronology

Zircon roundness data show that about 73% of Wolfcamp B grains are rounded to completely rounded, while the percentage of roundness for the Wolfcamp A and lower Spraberry grains are 28% and 0%, respectively (Fig. 3-5). In addition, around 60% of the Wolfcamp B grains, but less than 30% grains from other units show fractures or collision marks.
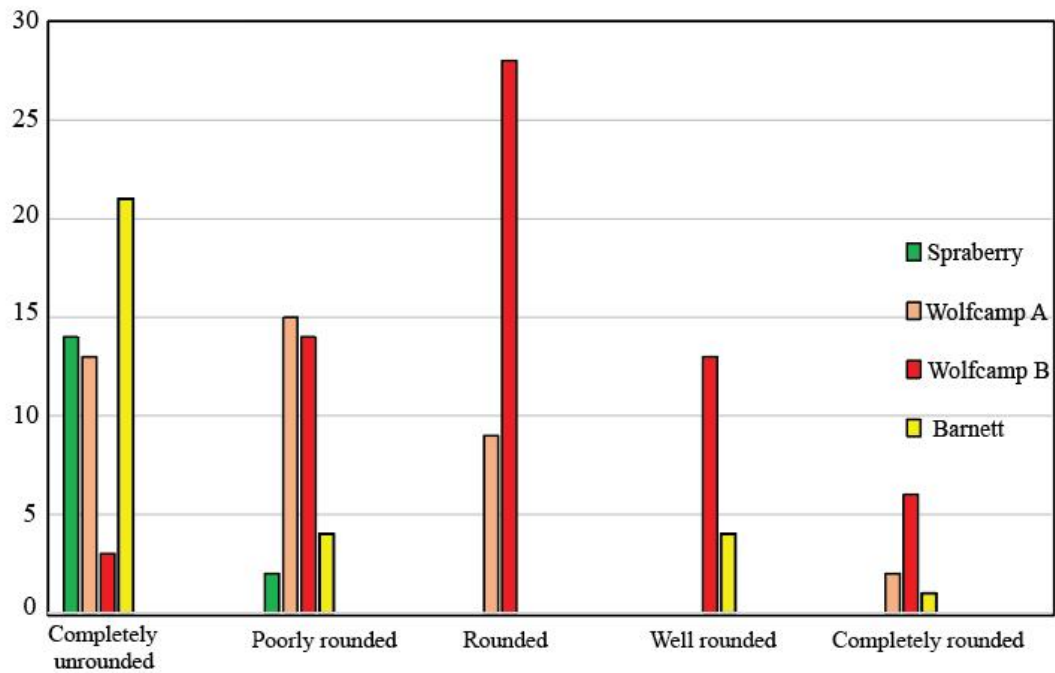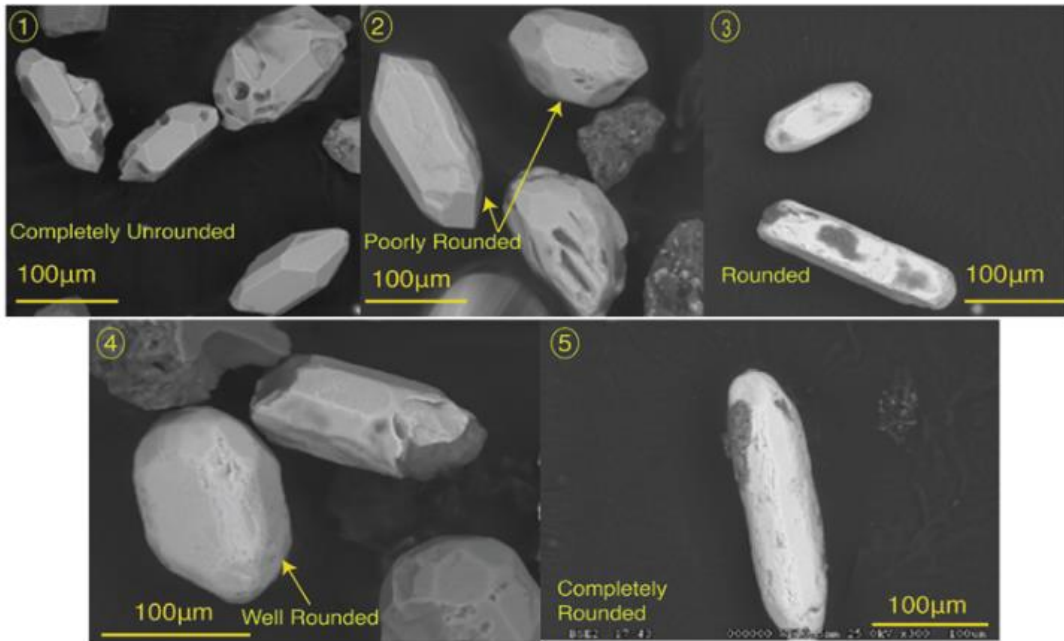
Figure 3-5. Counts for each zircon roundness category for the Midland Basin tuffs. Pictures of different zircon morphology of the Mississippian Barnett tuff are published in Tian et al. (2022).

3.4.3 Zircon U-Pb dates

After filtering, a total of 631 zircon LA-ICPMS U-Pb dates are reported in this study, including 439 for Midland Basin tuffs and 192 for Guadalupian tuffs (Fig. 3-6). Twenty-eight dates are > 25 Ma younger than biostratigraphic ages and our CA-ID-TIMS dates, likely caused by lead loss or matrix mismatch between zircon reference and unknowns (Allen and Campbell, 2012; Schoene, 2014; Schaltegger et al., 2015; Coutts et al., 2019), and were excluded for age determination. A total of 29 CA-ID-TIMS dates are reported for Midland Basin tuffs. The depositional age of each tuff is interpreted as the weighted mean of the youngest CA-ID-TIMS dates (WMTIMS) (Fig. 3-7). The distribution of the LA-ICPMS dates for each sample is shown by both probability distribution plot (PDP) and kernel density estimation (KDE) (Fig. 3-8). The LA-ICPMS dates were interpreted using different statistical methods and the results were compared with the WMTIMS dates to determine the most appropriate method for interpreting LA-ICPMS dates. Statistical methods include the youngest single grain date (YSG; Dickinson and Gehrels, 2009), weighted mean date of the youngest cluster of three or more grains overlap at 2σ error (YSP-youngest statistical population) with a mean square weighted deviation (MSWD) near 1 (Coutts et al., 2019), youngest mode date from the KDE (YMKDE) plot (cf. YPP of Dickinson and Gehrels, 2009), and TuffZirc date (TZ) on the youngest age group. TuffZirc uses a Monte Carlo model to generate a statistical youngest age from a group of genetically related grains (Ludwig and Mundil, 2002; Ludwig, 2008). A new statistical approach, weighted mean date of the youngest dominant KDE mode (WMYDM, Tian et al., 2022) with a MSWD near 1, is also used here for comparison. This method modifies the YSP approach from Coutts et al. (2019). We note that the dataset for YSP is much larger in Coutts et al. (2019) than in this study, but our dataset still permits useful comparisons between calculated dates. The youngest dominant population, which is the YSP, is assumed to be from a single eruptive event for volcanic tuffs. We use the KDE method described in Vermeesch (2012), which uses adaptative kernel density estimates. Adaptive kernel density estimates vary the bandwidth according to the local density, which means that where data density is sparse, a

54

large bandwidth is used, and the density estimate is smooth. To remove the influence of mode skewness, dates along both sides of the mode date are included progressively to derive a date with MSWD near 1. The WMYDM method excludes ICPMS dates at both tails of the distribution that do not overlap at 2σ with the mode. These scattered dates typically reflect Pb loss, matrix effect-related bias, and inheritance of grains from the magma source (e.g., Schaltegger et al., 2015). The youngest mode date from the PDP plot of each tuff is also calculated, but not reported here as PDP oversmooths date distribution of all our samples (see details in discussion).

A total of 114 zircon Hf isotopic values were analyzed with 24 for the middle Permian G3 tuff, 16 for the Spraberry 1 tuff, 10 for the Spraberry 2 tuff, 26 for the Wolfcamp A tuff, and 38 for the Wolfcamp B tuff. Most Hf analyses were conducted on grains with dates close to their CA-ID-TIMS dates.
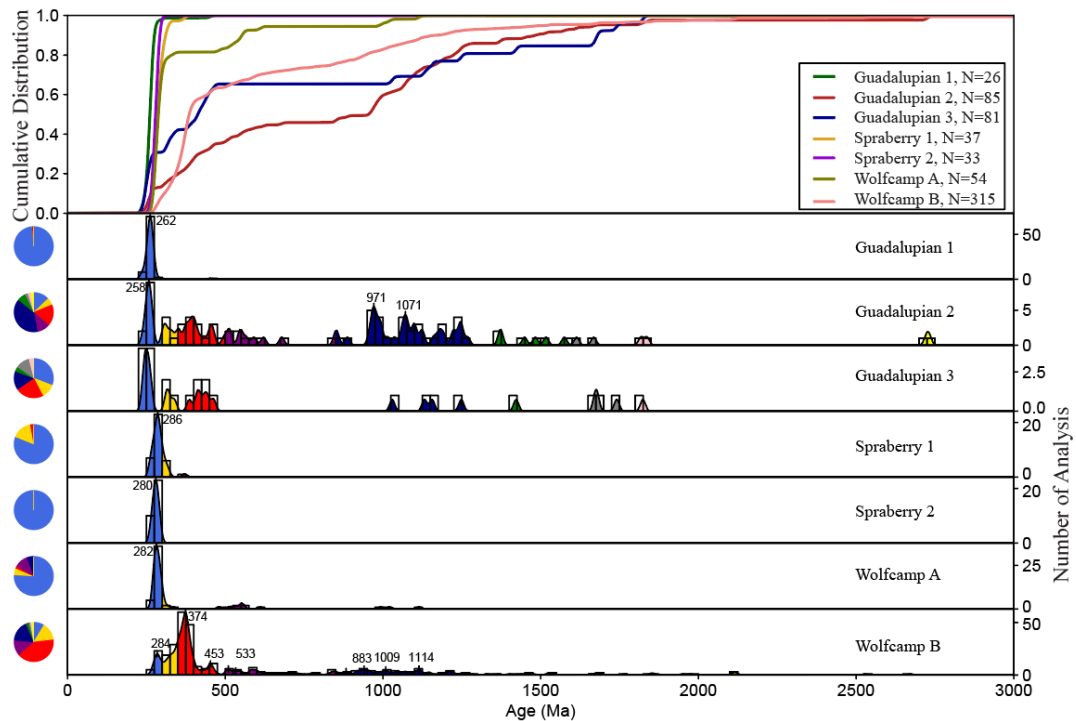
Figure 3-6. Zircon LA-ICPMS U-Pb date distribution for all the volcanic tuffs. The plot is shown as kernel density estimation. The numbers on the plot are peak modes.
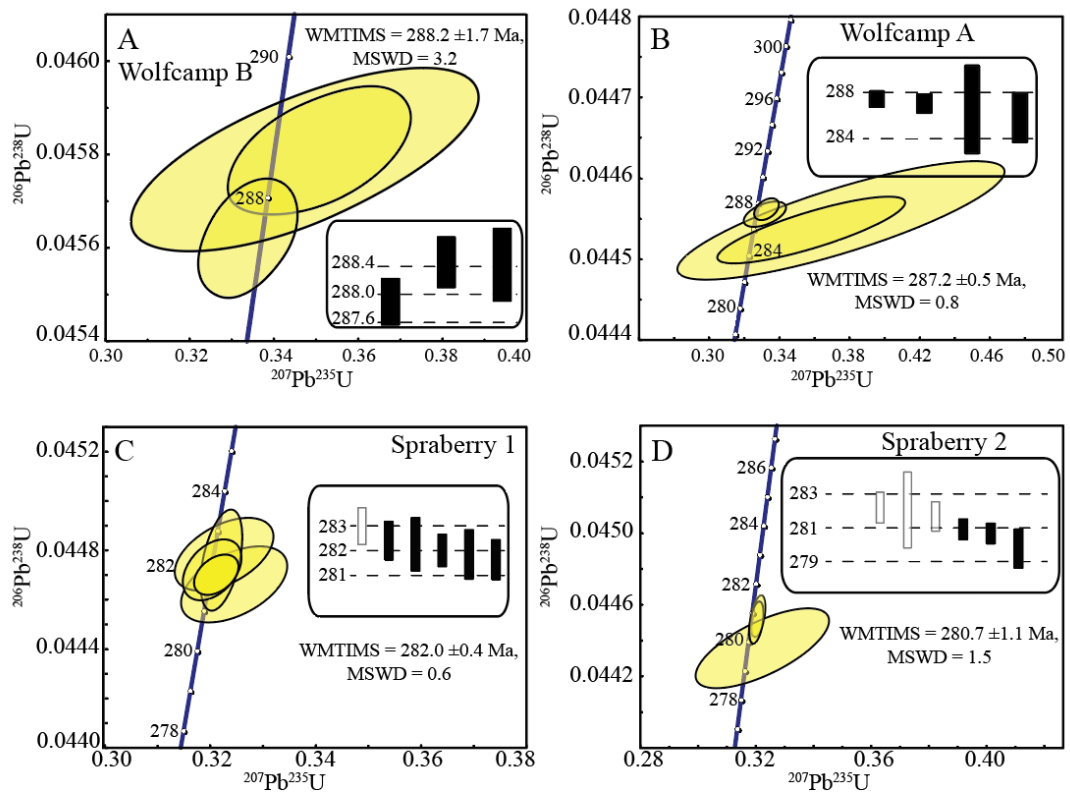
Figure 3-7. Concordia plots (206Pb/238U vs. 207Pb/235U) and weighted mean of the CA-ID-TIMS dates for the Wolfcamp B (A), Wolfcamp A (B), Spraberry 1(C) and Spraberry 2 (D) tuffs. Zircon dates marked by black bars are used to calculate the true depositional ages. The reported CA-ID-TIMS uncertainties are 2σ.
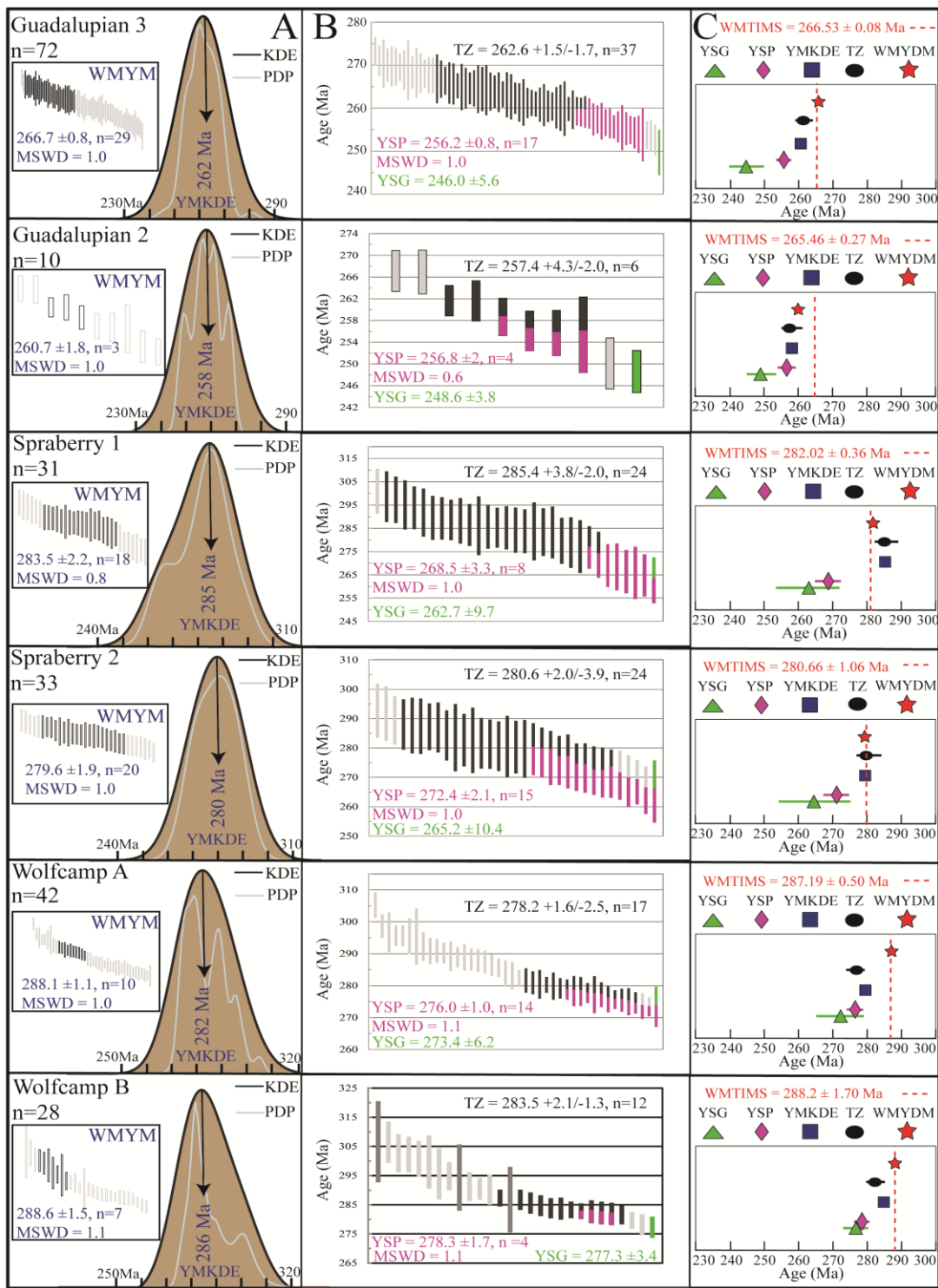
Figure 3-8. Comparison of statistical LA-ICPMS dates and the true depositional ages determined by CA-ID-TIMS dating. Column A is the distribution of the youngest peak mode with both probability density plot (PDP) and kernel density estimation (KDE). Zircon dates marked in black lines are used for the mode. Column B is the age distribution and statistical results of the youngest single grain date (YSG, dates marked in green color), weighted mean of the youngest cluster date (YSP, dates marked in purple color) and TuffZirc date (TZ, dates marked in black color). MSWD (mean square weighted deviation), weighted mean age of the youngest dominant KDE mode (WMYDM) with MSWD near 1 is the preferred statistical LA-ICPMS date. Column C compares weighted mean CA-ID-TIMS dates (WMTIMS) with calculated dates from LA-ICPMS data alone.

3.4.3.1 Wolfcamp B tuff

A total of 315 LA-ICPMS and 7 CA-ID-TIMS zircon U-Pb dates were interpreted for the Wolfcamp B tuff. LA-ICPMS dates range from 2673 ±39 to 270 ±7 Ma (YSG) with 9% < 300 Ma, 58% between 300-500 Ma, 11% between 500-850 Ma, 15% between 900-1300 Ma, 5% between 1300-2000 Ma, and 2% > 2000 Ma (Fig.3-6). The WMTIMS was calculated to be 288.2 ±1.7 Ma from three of the young CA-ID-TIMS dates (Fig. 3-7A). Although the tuff is most likely reworked and the date is potentially a maximum age, this date is the true depositional age (TDA) for it cannot be younger than the Wolfcamp A tuff at a higher stratigraphic level. A total of 27 LA-ICPMS dates ranging from 277.3 ±3.4 to 306.6 ±13.6 Ma were used for statistical calculations (Fig. 3-8). The YMKDE date is 286 Ma, the WMYDM date calculated from 7 dates is 288.6 ±1.5 Ma (MSWD =1.1), the YSP date calculated from 4 grains is 278.3 ±1.7 Ma (MSWD= 1.1), and the TZ date calculated from 12 grains is 283.5 +2.1/-1.3 Ma.

Hf isotope analysis of Wolfcamp B zircons was conducted on both the <300 Ma cluster representing the volcanic zircons, and >300 Ma zircons interpreted as being detrital or inherited from the upper crustal source. All large grains in the volcanic group were analyzed for Hf isotopes, yielding

seven analyses. The seven grains, with LA-ICPMS dates between 284.7±3.3 Ma and 291.3 ±4.7 Ma, have εHf values between +0.5 and +8.8 with an average of +5.5. A total of 29 Hf data points is from detrital/inherited grains. In the 300-500 Ma group, 24 grains, with LA-ICPMS dates ranging from 345.3 ±3.7 Ma to 465.8 ±15.1 Ma, have εHf values between -5.2 and +6.3 with an average of +2.8. Only two grains have negative Hf values. In the 500-850 Ma group, four grains, with LA-ICPMS dates between 525 ±19 Ma and 639.2 ±8.9 Ma, have εHf values ranging from -2.7 to +12.7 with an average of +7.2. The TDM2 age ranges from 675 Ma to 1207 Ma for volcanic grains and from 550 to 1652 Ma for detrital grains.

3.4.3.2 Wolfcamp A tuff

A total of 54 LA-ICPMS and six CA-ID-TIMS zircon U-Pb dates were measured from the Wolfcamp A tuff. LA-ICPMS dates range from 1114 ±16 to 273.4 ±6.2 Ma (YSG) with 76% < 300 Ma, 7% between 300-500 Ma, 11% between 500-850 Ma, and 6% between 900-1300 Ma (Fig. 3-6). The WMTIMS is 287.2 ±0.5 Ma based on the four youngest CA-ID-TIMS dates (Fig. 3-7B). A total of 41 LA-ICPMS dates ranging from 273.4 ±6.2 to 317.4±5.6 Ma were used for statistical calculations (Fig. 3-8). The YMKDE is 282 Ma, the WMYDM date calculated from 10 dates is 288.1 ±1.1 Ma (MSWD=1), the YSP date calculated from 14 dates is 276.0 ±1.0 Ma (MSWD=1.1), and the TZ date calculated from 17 dates is 278.2 +1.6/-2.5 Ma.

Among the 26 Wolfcamp A Hf analyses, 19 grains with LA-ICPMS dates ranging from 280.9 ±3.5 Ma to 298.6 ±3.6 Ma show εHf values varying from -2.2 to -6.0 with an average of -4.5. The TDM2 ages of all grains are between 1381 to 1616 Ma.

3.4.3.3 Spraberry tuff

A total of 37 LA-ICPMS and 8 CA-ID-TIMS U-Pb dates was interpreted for the Spraberry tuff. LA-ICPMS dates range from 371.2 ±13.9 to 262.7 ±9.7 Ma (YSG) with 81% <300 Ma and 19%

between 300-500 Ma (Fig. 3-6). The WMTIMS was calculated to be 282.0 ±0.4 Ma from the youngest five dates (Fig. 3-7C). A total of 31 Spraberry dates ranging from 262.7±9.7 Ma to 300.9 ±9.5 Ma was used for statistical calculations (Fig. 3-8). The YMKDE is 285 Ma, the WMYDM calculated from 18 dates is 283.5 ±2.2 Ma (MSWD=0.8), the YSP calculated from 8 dates is 268.5 ±3.3 Ma (MSWD =1.0), and the TZ date calculated from 24 dates is 285.4 +3.8/-2.1 Ma.

A total of 33 LA-ICPMS and 8 CA-ID-TIMS U-Pb dates was interpreted for the Spraberry 2 tuff. The LA-ICPMS dates range from 292.7±9.1 to 265.2 ±10.4 Ma (YSG) (Fig. 3-6). The WMTIMS was calculated to be 280.7 ±1.1 Ma from the three youngest dates (Fig. 3-7D). All LA-ICPMS dates were used for statistical calculations (Fig. 3-8). The YMKDE is 280 Ma, the WMYDM date calculated from 20 dates is 279.6 ±1.9 Ma (MSWD=1), the YSP date calculated from 15 dates is 272.4 ±2.1 Ma (MSWD=1.0), and the TZ calculated from 24 dates is 280.6 +2.1/-3.9 Ma.

Among the 16 Spraberry 1 Hf analyses, 9 zircons with LA-ICPMS dates between 272.9 ±5.6 and 288.0 ±8.6 Ma are considered volcanic, and these have ƐHf values between +0.5 and -6.0 with an average of -2.3. Among the 10 Spraberry 2 Hf analyses, 9 zircons with LA-ICPMS dates between 271.2 ±8.1 and 297.9 ±9.1 Ma are considered volcanic and their ƐHf values range from -0.4 to -5.1 with an average of -3.5. The TDM2 ages of all Spraberry zircons are between 1197 and 1649 Ma.

3.4.3.4 Guadalupe Mountain tuff

A total of 26 LA-ICPMS zircon U-Pb dates was obtained for the G1 tuff. A CA-ID-TIMS date of 262.1 ± 0.1 Ma was reported by Wu et al. (2020) for this tuff. The LA-ICPMS dates range from 1824 ±49 to 241.6 ±3.1 Ma (YSG) with 31% <270 Ma, 35% between 300-500Ma, 8% between 900-1300 Ma, and 27% between 1300-2000 Ma (Fig. 3-6). The available young dates are not sufficient to generate PDP or KDE plots or calculate a TZ date. The YSP was calculated to be 260.4 ±6.7 Ma (MSWD= 2.6) from three dates.

A total of 85 LA-ICPMS zircon U-Pb dates was obtained for the G2 sample. A CA-ID-TIMS date of 265.5 ± 0.3 Ma was reported by Wu et al. (2020). The LA-ICPMS dates range from 2732 ±20 to 240.0 ±3.0 Ma (YSG) with 13% < 300 Ma, 24% between 300-500 Ma, 12% between 500-850 Ma, 36% between 900-1300 Ma, 13% between 1300-2000 Ma, and 2% > 2000 Ma (Fig. 3-6). A total of 10 LA-ICPMS dates ranging from 246.8 ±3.8 to 267.1 ±3.8 Ma (YSG) were used for statistical calculations (Fig. 3-8). The YMKDE is 258 Ma, the WMYDM calculated from three dates is 260.7 ±1.8 Ma (MSWD=1.0), the YSP calculated from four dates is 256.8 ±2.0 Ma (MSWD =0.6), and the TZ calculated from six dates is 257.4 +4.3/-2.0 Ma.

A total of 81 LA-ICPMS zircon U-Pb dates was reported for the G3 sample. A CA-ID-TIMS date of 266.5 ± 0.1 Ma was reported by Wu et al. (2020). The LA-ICPMS dates range from 1824 ±49 to 235.5 ±5.6 Ma (YSG) with 98% < 300 Ma and 2% > 300 Ma (Fig. 3-6). Seventy-three LA-ICPMS dates ranging from 246.0 ±5.6 Ma to 281.4 ±4.9 Ma were used for statistical calculations (Fig. 3-8). The YMKDE is 262 Ma, the WMYDM calculated from 29 dates is 266.7 ±0.8 Ma (MSWD=1.0), the YSP calculated from 17 grains is 256.2 ±0.8 Ma (MSWD=1), and the TZ calculated from 37 dates is 262.6 +1.5/-1.6 Ma. The ƐHf values of 24 grains with LA-ICPMS dates between 263.1 ±5.2 and 270.3 ±5.5 Ma ranges from +1.9 to -2.8 with an average of -0.1. The TDM2 of all the grains are between 1102 and 1401 Ma.

3.4.3.5 Mississippian tuff

As a comparison, data reported for the Mississippian Barnett tuff in the Midland Basin and five Mississippian tuffs in the Stanley Group in the Ouachita Mountains (Tian et al., 2022) are summarized here. The Barnett tuff in the Midland Basin has LA-ICPMS zircon dates from 339.9 ±4.3Ma to 300.4 ±4.4 Ma (YSP), a WMTIMS of 327.8 ±0.8 Ma, YSP of 304.0 ±1.2 Ma, YMKDE of 325 Ma, WMYDM of 326.7 ±0.6 Ma, and TZ of 326.2 +1.0/-0.6 Ma. Zircons between 340-308 Ma

have ƐHf values mostly between 0 and +5 with an average of +2. The TDM2 ranges between 682 and 1432 Ma.

3.4.3.6 Summary

Nearly all statistical approaches for interpreting LA-ICPMS data yield U-Pb dates somewhat younger than the corresponding WMTIMS dates in this study (Fig. 3-8C). The YSPs are 10 to 20 Myr younger than the corresponding WMTIMS dates, but the other statistical treatments of LA-ICPMS ages are within 96% of the WMTIMS dates. Among the statistical approaches, the WMYDM best approximates WMTIMS dates even though the Wolfcamp A and Wolfcamp B distributions are skewed toward younger dates and the Spraberry 1 distribution is slightly negatively skewed toward old dates (Fig. 3-8A).

Hf isotopes distinguishes older and younger tuffs. Mississippian tuffs (average ƐHf = +2) and Wolfcamp B tuffs (average ƐHf = + 5.5) have younger TDM2 model ages (675 and 1432 Ma). The Wolfcamp A and Spraberry tuffs have an average ƐHf < -2.2 and older TDM2 model ages (1197 - 1649 Ma). The middle Permian G3 tuff shows an intermediate Hf signature with an average ƐHf close to 0 and TDM2 model ages between 1102-1401 Ma.
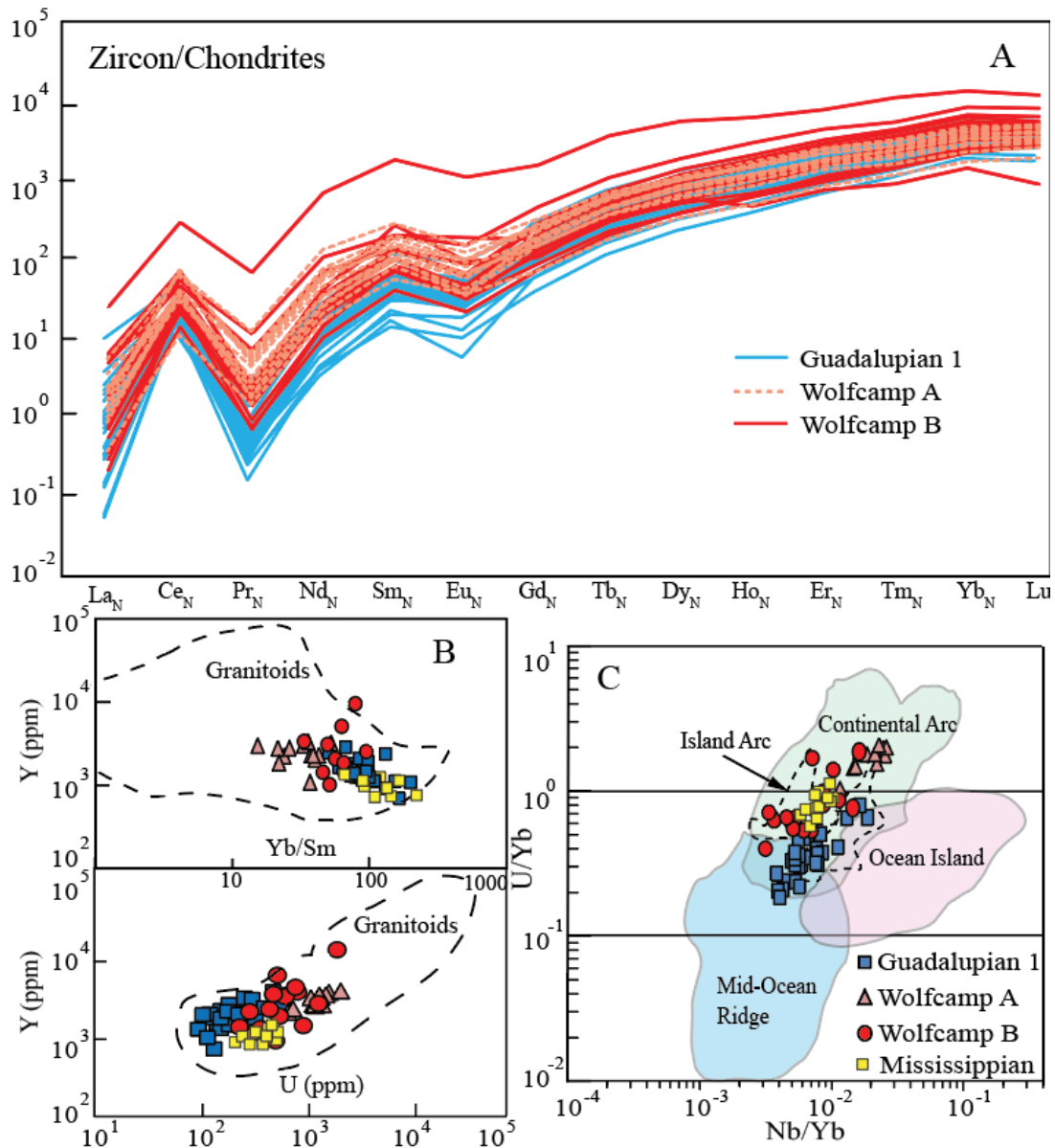
Figure 3-9. A) Zircon rare earth element compositions normalized to chondrites following
McDonough and Sun (1995). B) Zircon trace element composition discrimination diagram following
Belousova et al. (2002). C) Zircon trace element composition discrimination diagram following
Grimes et al. (2015).

3. 5 DISCUSSIONS

Below we use our new data to discuss four topics: 1) how well do LA-ICPMS and CA-ID-TIMS U-Pb zircon ages agree; 2) the implications for Permian Basin chronostratigraphy; 3) where was the volcano(es) that ejected the ashes? and 4) the implications for understanding the Late Paleozoic tectonic evolution of southern Laurentia.

3. 5.1 Comparison of LA-ICPMS and CA-ID-TIMS dates

Constraining TDA of tuffs from zircon U-Pb dates is limited by analytical precision and by potential inaccuracies introduced by Pb loss and matrix mismatches from LA-ICPMS methods. LA-ICPMS is the most used zircon U-Pb dating technique given its low cost and rapid data acquisition, but has low analytical precision (>1%; Gehrels, 2014). Systematic offsets by laser ablation, likely reflecting matrix effects caused by mismatch of standards and unknowns, are commonly observed (Allen and Campbell, 2012; Schoene, 2014; Schaltegger et al., 2015; Coutts et al., 2019). These uncertainties do not affect CA-ID-TIMS dates, which have typical analytical precisions of ~0.1% (Gehrels, 2014). Results derived from statistical treatment of LA-ICPMS dates are frequently used to approximate TDA, but all these statistical approaches could be biased by lead loss, statistical defects, and matrix effects, and the influence of each of these three factors on statistical dates is variable (Coutts et al., 2019). Our dataset adds to the few studies that identify the best statistical approaches for interpretating LA-ICPMS dates to match CA-ID-TIMS dates (e.g., Spencer et al., 2016; Herriott et al., 2019).

In this study, the WMTIMS date is taken as the TDA for each tuff and is compared with other LA-ICPMS statistical dates. All the YSGs are 10-20 Myr younger than the TDAs, which may be mainly attributed to lead loss (Coutts et al., 2019). Half of the grains dated by both LA-ICPMS and CA-ID-TIMS have LA-ICPMS dates older than WMTIMS dates (Fig.S3-3), which is most likely caused by matrix effect (Allen and Campbell, 2012) for the LA-ICPMS data or may reflect antecrystic, pre-eruptive or inherited zircons for the CA-ID-TIMS data. Although inheritance of older cores may cause

LA-ICPMS dates older than TDAs, such grains have been excluded based on CL image screening before analysis. Our comparison further shows that nearly all the statistical dates from LA-ICPMS data are somewhat younger than the TDAs, agreeing with the results of previous studies (Coutts et al., 2019; Herriott et al., 2019). Because of the influence of lead loss, YSP and YC2σ (mean date of the youngest cluster at 2σ error, Dickinson and Gehrels, 2009) dates that selectively sample grains from the negative tail (young date) of the distribution will likely result in an erroneously younger interpreted TDA.

Our results also show that the YMKDE, TZ, and WMYDM dates (Fig. 3-8C) are within 96% of the TDAs although often biased toward younger dates, suggesting that all these dates can be used to approximate TDAs if CA-ID-TIMS dates are not available. Among these approaches, the WMYDM dates are consistently the closest to the TDA dates. This result is different from those of previous studies, which showed that the YSP dates best approximate detrital zircon maximum depositional ages because of their high coincidence with CA-ID-TIMS dates (Herriot et al., 2019). This difference with our results might reflect the fact that ours are dominantly syn-depositional volcanic zircons with a single mode from a single eruption (cf., Cawood et al., 2012; Spencer et al., 2016). The PDP distribution is widely used to display zircon dates and recognize modes (Ludwig, 2008). The PDP was designed to reduce the importance of imprecise measurements and emphasize more precise measurements by taking the individual analytical precision as the bandwidth, which, however, can produce noisy results when applied to high-precision data and yield oversmoothed density estimations when dataset is large and/or analytical precision is low (Vermeesch, 2012). The PDP overfits all of our LA-ICPMS analyses (Fig. 3-8A) because of low analytical precision. The KDE deploys the Gaussian distribution by adapting the bandwidth according to local density without considering individual analytical precision (Vermeesch, 2012). The Wolfcamp A and Wolfcamp B LA-ICPMS age distributions are positively skewed (to young dates) and the Spraberry 1 distribution is negatively skewed (to old dates) (Fig. 3-8A), which result in younger and older YMKDE dates than the TDAs, respectively. The comparison shows that the skewness of LA-ICPMS dates should be carefully evaluated before the YMKDE approach is used. Our

study confirms that WMYDM approach compensates for skewness by calculating the mean of the mode dates with MSWD near 1 and better approximates the TDAs.

If the accuracy of TDA needs to be better than ±4% for a given application, our results suggest that it is important to pair LA-ICPMS data with CA-ID-TIMS analyses. Chemical abrasion removes the effects of Pb loss and isotope dilution minimizes the dependence on standard analyses for measuring dates thereby avoiding potential matrix-induced inaccuracies from LA-ICPMS derived TDAs (Schoene, 2014; Schaltegger et al., 2015). An alternative strategy of annealing zircons and standards prior to LA-ICPMS analysis has been championed by Allen and Campbell (2012) as it seems to minimize matrix effects and yield LA-ICPMS dates that are within 0.5% of CA-ID-TIMS dates. Merely annealing zircons prior to analysis would not require the sophisticated labs and methods needed for complete chemical abrasion and could be more widely applied.

3. 5.2 Implimentations for Permian Chronostratigraphy

The development of the oil industry in the Permian Basin resulted in complicated lithostratigraphic nomenclature (e.g., Montgomery, 1996). The early Permian North American regional stages were mainly studied in the well-exposed Permian section in the Glass Mountains to the southwest of the Delaware Basin (e.g., Behnken, 1984; Wardlaw and Davydov, 2000; Ross and Ross, 2003; 2009; Wahlman, 2013; Wardlaw and Nestell, 2014). The subsurface stratigraphic architecture of the Midland Basin was primarily constrained by petrophysical log signatures referenced to the type sections in the Glass Mountains (e.g., Mazzullo and Reid, 1988; Hamlin and Baumgardner, 2012; Baumgardner et al., 2016). Ages presented in this study improves the chronostratigraphy.

Recent biostratigraphy studies in the Permian Basin suggest that the Pennsylvanian-Permian boundary is in the lowermost Wolfcamp C unit and that the Wolfcampian-Leonardian boundary should be placed in the uppermost Wolfcamp B unit (e.g., Wahlman et al., 2016; Kohn et al., 2019). These studies also suggest that the boundaries of the Asselian, Sakmarian, Artinskian and Kungurian stages

are in the uppermost Wolfcamp C, middle Wolfcamp B, and Wolfcamp A units, respectively (Fig. 3-2). Assuming the Pioneer proprietary stratigraphic correlations are correct, our new dates have implications for the absolute ages of the Wolfcamp Shale. Our Wolfcamp A and Wolfcamp B tuffs have WMTIMS dates of 287.2 ±0.5 Ma and 288.2 ±1.7 Ma, respectively, consistent with biostratigraphic results that correlate the Wolfcamp B unit to the late Sakmarian and early Artinskian stages and the Wolfcamp A unit to the late Artinskian stage. Based on the stratigraphic thickness between the two tuffs (Pioneer proprietary information), assuming a stable sedimentation rate, the data yield an average sedimentation rate of ~65 m/Myr (0.065mm/y) for the upper Wolfcamp B and lower Wolfcamp A unit. The base of the Wolfcamp C unit is about 396 m below the Wolfcamp B tuff. If the base of Wolfcamp C is considered the beginning of the Permian Period (298.9 Ma), the average sedimentation rate in the Wolfcamp C and lower Wolfcamp B unit is ~37 m/Myr (0.037mm/y). Given these rocks have experienced compaction, the estimated sedimentation rates are higher than modern average global ocean pelagic sedimentation rate which is less than 35 m/Myr (0.035mm/y) (e.g., Davies et al., 1977). The sedimentation rate almost doubled from the Wolfcamp C-lower Wolfcamp B unit to the upper Wolfcamp B-lower Wolfcamp A unit, which likely reflects an increase in turbidite sedimentation in the Wolfcamp B unit given turbidites are well documented in lower Permian strata in the Permian Basin (Hamlin and Baumgardner; 2012; Baumgardner et al., 2016).

The two Spraberry samples reside in the same lithostratigraphic interval based on well logs. Studies of fusulinid microfossils show that the Spraberry Formation is of Leonardian age (e.g., Silver and Todd, 1969; Handford, 1981). The two Spraberry tuffs have WMTIMS dates of 282.0 ±0.4 and 280.7 ±1.1 Ma, overlapping within uncertainty. The Spraberry tuffs are ~365 m above the Wolfcamp A tuff. If the mean WMTIMS date (281.4 Ma) of the two tuffs is used, the sedimentation rate between the upper Wolfcamp A unit and the lower Spraberry Formation is ~49 m /Myr (0.049mm/y), lower than that of the upper Wolfcamp B-Wolfcamp A unit.

3. 5.3 Magmatic affinity and source of the tuffs

Alteration of the late Paleozoic tuffs makes the whole rock geochemistry data less reliable. The whole rock major and trace element data show dacite or andesite compositions (Figs. 3-3 and 3-4) while zircon trace element data show granitic composition (Fig. 3-9), most likely because of diagenesis of the tuffs. It has been suggested that the formation of zeolites by altering volcanic glass in tuffs is accompanied by increases in Mg and Al contents and decrease in Si content (e.g., Marantos et al., 2008). Alteration of the bulk tuffs is further supported by the high CIA index. Alteration of tuffs also causes rare earth element fractionation (e.g., Murakami and Ishihara, 2008). Therefore, the whole rock geochemistry data are not used to interpret the source of the tuffs.

Our zircon trace element data suggest that all the tuffs came from continental arcs with granitoid parent magma compositions (Fig. 3-9). The εHf dropped from an average of +5.5 to -4.5 between the Wolfcamp B and Wolfcamp A volcanic zircons within 1 Myr. Zircon Hf signature of magmatic units that were adjacent to the Permian Basin during the late Paleozoic are plotted together with our data for discussing parent magma affinity and sources of different tuffs (Fig. 3-10).
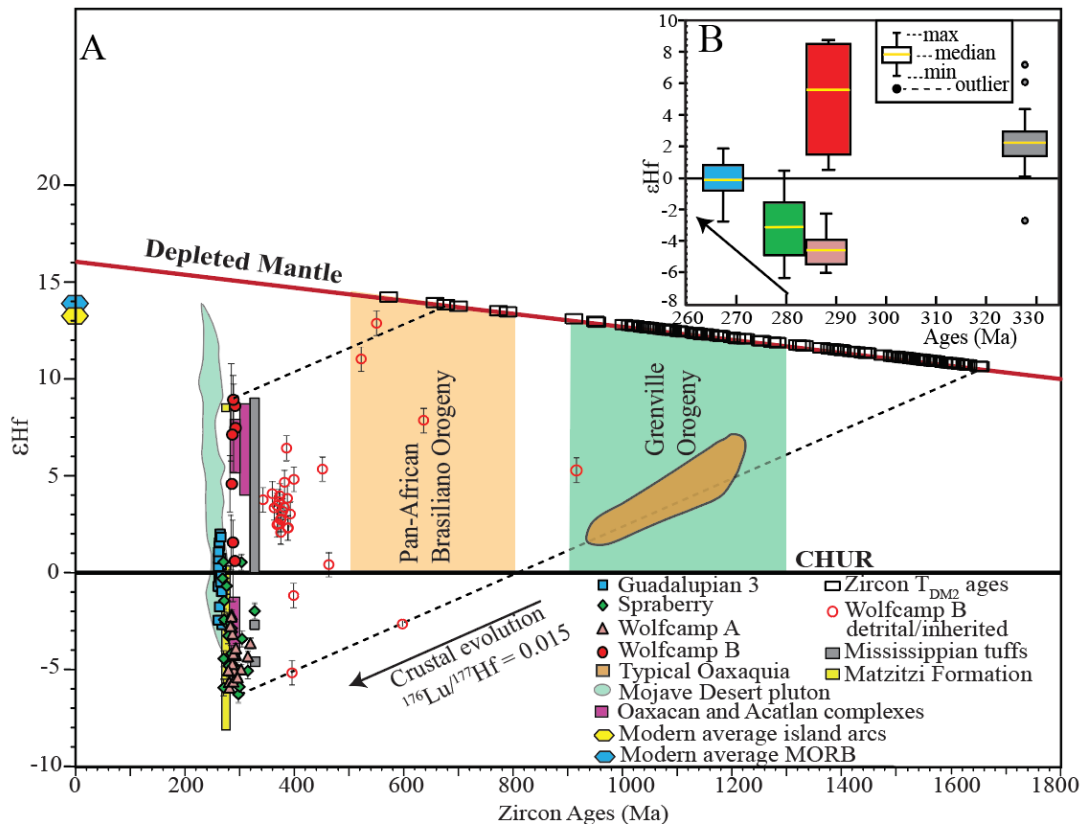
Figure 3-10. A) Zircon U-Pb dates, ƐHf values and TDM2 ages of the volcanic tuffs are compared with those of the Andean continental arc (Jones et al., 2015), average island arc (Dhuime et al., 2011), mid ocean ridge basalt (MORB, Workman and Hart, 2005), and Late Paleozoic magmatic rocks in the Ouachita-Marathon region and Mexico. TDM2 ages were calculated using an average crustal value of 176Lu/177Hf = 0.015 following Griffin et al. (2002). Oaxacan and Acatlán complexes data are from Ortega-Obregón et al. (2014). Matzitizi Formation data are from Zúñiga et al. (2020). Mississippian tuff data are from Tian et al. (2022). Mojave Desert pluton data are from Cecil et al. (2019). "Typical Oaxaquia" data are from Weber et al. (2010). CHUR means chondritic uniform reservoir. Note that the ƐHf values become more juvenile from the Wolfcamp A and Spraberry tuffs to Guadalupian tuffs and the trend is consistent with that in the Mojave Desert pluton data (Cecil et al., 2019). B) Box plot of zircon U-Pb dates, ƐHf values of volcanic tuffs for the sample G3 (266.5Ma), Spraberry (279.8 Ma),

Wolfcamp A (287.2 Ma) and Wolfcamp B (288.2 Ma), the legends are the same with A. The ages of the tuffs in the box plot are the interpreted true depositional ages for these tuffs. The width of the box plot does not represent the uncertainty of the age.

3. 5.3.1 Mississippian tuffs

Tian et al. (2022) compared the geochemical signature of Mississippian tuffs (328-317 Ma) in the Midland Basin and Ouachita Mountains with other magmatic units and suggested that these tuffs were most likely from a northern Gondwana arc. The study further suggested that the arc was developed on the Maya or Sabine block by southward subduction of the Rheic ocean beneath the peri-Gondwana realm in northern Gondwana (Fig. 3-1C). The TDM2 ages are between 682 and 1432 Ma, suggesting that the arc developed on crust with both Grenville and Pan-African affinities (Tian et al., 2022). The Aserradero Rhyolite near Ciudad Victoria, Mexico, has continental arc geochemical signature with zircon crystallization ages of 348-340 Ma (Ramírez-Fernánde et al., 2021), suggesting that the northern Gondwana arc may have started as early as the Early Mississippian.

3. 5.3.2 Wolfcamp B tuffs

Some Wolfcamp B tuffs were reworked because they have erosional contacts with the underlying shale and wavy bedding (Figs. S3-1 and S3-2). The tuffs have abundant old (>300 Ma) and rounded grains (Fig. 3-5), indicating that some or all of the tuffs were redeposited and/or mixed with detrital sediments. Nevertheless, there are sufficient angular, magmatic grains to obtain a WMTIMS age of 288.2 ±1.7 Ma. Magmatic units of similar age and geochemical compositions include 1) plutonic rocks in the Honduras batholith of the Oaxacan and Acatlán metamorphic complexes (Oaxaquia terrane) in southern Mexico, which are tonalite to quartz diorite with a zircon LA-ICPMS date of 290 ±2 Ma, ƐHf values between +5 and +8, and TDM2 model ages between 795 and 948 Ma (Ortega-Obregón et al., 2014); 2) quartz diorites in the Totoltepec pluton of the Acatlán metamorphic complex, which has

a zircon LA-ICPMS date of 289 ±2 Ma, whole rock ℰNd values between -0.8 and +2.6, and TDM model ages between 930 and 1160 Ma (Kirsch et al., 2012); 3) granitoids with zircon LA-ICPMS dates of 294±3 Ma in the Oaxaquia terrane on the western margin of Gulf of Mexico (Coombs et al., 2020); and 4) Las Delicias volcanic series of northern Mexico, with zircon LA-ICPMS dates mostly clustered at 331 Ma and 270 Ma and a plutonic sample near Sierra El Granizo of 285±3 Ma, whole rock ℰNd values between +2.6 and +5.3, and TDM model ages between 691 and 1502 Ma (Lopez, 1997). Early Permian volcaniclastic rocks in sedimentary successions deposited in forearc or intra-arc settings are well documented in several places in Mexico (e.g., Lopez, 1997; McKee et al., 1998; Rosales-Lagarde et al., 2005). One of the examples is the lower Permian Tuzancoa Formation of east-central Mexico, which has a whole rock ℰNd value of +4.4 and TDM model age of 672 Ma and was suggested to be derived from a submarine continental arc (Rosales-Lagarde et al., 2005). Plutonic rocks in the Oaxaquia terrane were suggested to be continental arcs, caused by subduction of the Paleo-Pacific plate beneath western Pangea (e.g., Keppie et al., 2008; Nance et al., 2010; Kirsch et al., 2012) or Rheic plate beneath northern Gondwana (e.g., Elías-Herrera and Ortega-Gutiérrez, 2002; Vega-Granillo et al., 2007, 2009; Ortega-Obregón et al., 2014; Ortega-Gutiérrez et al., 2018; Coombs et al., 2020). The Las Delicias arc is also a continental arc formed by the subduction of the Laurentia plate beneath the Coahuila terrane (Lopez, 1997).

The ℰHf signature supports that the Wolfcamp B tuffs ultimately sourced from the continental arc in the Peri-Gondwana realm. Zircons younger than 300 Ma in Wolfcamp B tuffs have an average ℰHf value of +5.5 and TDM2 model ages between 675 and 1207 Ma, slightly different from those of the Mississippian tuffs with an average ℰHf value of +2, and TDM2 between 682 and 1432 Ma. The isotopic signatures can be explained by mixing mantle-derived magmas and older continental crust (Arndt and Goldstein, 1987), similar to Mississippian tuffs that show the influence of Pan-African/Brasiliano and Grenville sources (Tian et al., 2022). The ℰHf signature is also similar to the Cuanana pluton of the Acatlán metamorphic complex, which has a zircon ICP-MS date of 311 ±2 Ma,

ɛHf values between +3 and +9, and TDM2 model ages between 795 and 948 Ma (Ortega-Obregón et al., 2014).

The interpretation that Wolfcamp B tuffs were ultimately sourced from a northern Gondwana arc is also supported because these tuffs contain 14% zircons between 500-850 Ma, which were ultimately sourced from Pan-African/Brasiliano basement, and 15% between 900-1300 Ma ultimately sourced from Grenville basement (Fig. 3-6). The 500-850 Ma group has ɛHf values ranging between -2.7 and +12.7, consistent with the signature of detrital Pan-African/Brasiliano zircons in Paleozoic sedimentary rocks on the Laurentian margin (e.g., Thomas et al., 2017; Waite et al., 2020). However, the two youngest zircons (525 ±19 Ma and 553 ±6 Ma) of this group could also be recycled from the Southern Oklahoma Aulacogen (SOA) related to the Iapetan rifting, because the ages and ɛHf values are similar to those of SOA magmatic units (Thomas et al., 2016). Both the Oaxaquia and Coahuila terranes have Pan-African/Brasiliano and Grenville basement (Weber et al., 2010; Lopez et al., 2001). These peri-Gondwana terranes were close or attached to the southern Laurentia margin during the late Paleozoic because of Gondwana-Laurentia collision. Therefore, Wolfcamp B tuffs were most likely sourced from a continental arc on the Oaxaquia and Coahuila terranes.

The interpretation that Wolfcamp B tuffs were ultimately sourced from a northern Gondwana arc is further supported because the tuffs contain 50% zircons between 300-500 Ma with a peak at ~375 Ma (Fig. 3-10). The mode is not present in the detrital record of Laurentia before deposition of the Wolfcamp B unit (Fig. 3-11), and it is not reported in the Mississippian Stanley Group in the Ouachita Mountains (McGuire, 2017), Pennsylvanian sandstones in the Fort Worth Basin (Alsalem et al., 2017) and the Wolfcamp C unit in the Midland Basin (Liu and Stockli, 2020), suggesting that the zircon source of this age was not close to the Laurentia margin before Wolfcamp B deposition. Even though the Taconic, Acadian, and Alleghenian orogenesis in the Appalachians produced Paleozoic zircons, these only make a small portion in the lower Permian sedimentary rocks in the Appalachian foreland (e.g., Thomas et al., 2017), thus the Appalachians cannot be the ultimate source of Wolcamp B tuffs.

However, Paleozoic zircons are common in the lower part of the Mississippian Santa Rosa Formation in southeastern Mexico (Weber et al., 2009). In addition to the Aserradero Rhyolite (348-340 Ma) near Ciudad Victoria, Mexico (Ramírez-Fernánde et al., 2021), granitoids of 380-410 Ma and 371 ±34 Ma were reported from the Acatlán Complex, southern Mexico (Yañez et al., 1991). Zircons of this age were also found in Pennsylvanian sedimentary rocks in the Arbuckle uplift in southern Oklahoma (Thomas et al., 2016) and the Marathon foreland in western Texas (Thomas et al., 2019); both were suggested to be derived from the Coahuila terrane (Fig. 3-1A). These ~375 Ma zircons have TDM2 model ages that mostly overlap with the Grenville Orogeny (900-1300 Ma), suggesting that the source was igneous material built on Grenville basement in the Peri-Gondwana realm. These zircons have an average εHf value of +2.8, similar to that of the Mississippian tuffs (Tian et al., 2021). Therefore, magmatism of ~375 Ma likely reflects early arc formation associated with subduction of the Rheic oceanic plate, and the dominance of 300-500 Ma zircons in Wolfcamp B tuffs suggests that these are most likely reworked tuffs and/or arc materials. If this interpretation is correct, the arrival of arc material by ~288 Ma, likely in the form of reworked tuffs delivered by rivers and deepwater gravity flows from northern Gondwana, may record the final stage of Gondwana-Laurentia collision and headwater erosion or catchment integration of northward-flowing rivers from highlands in northern Gondwana.
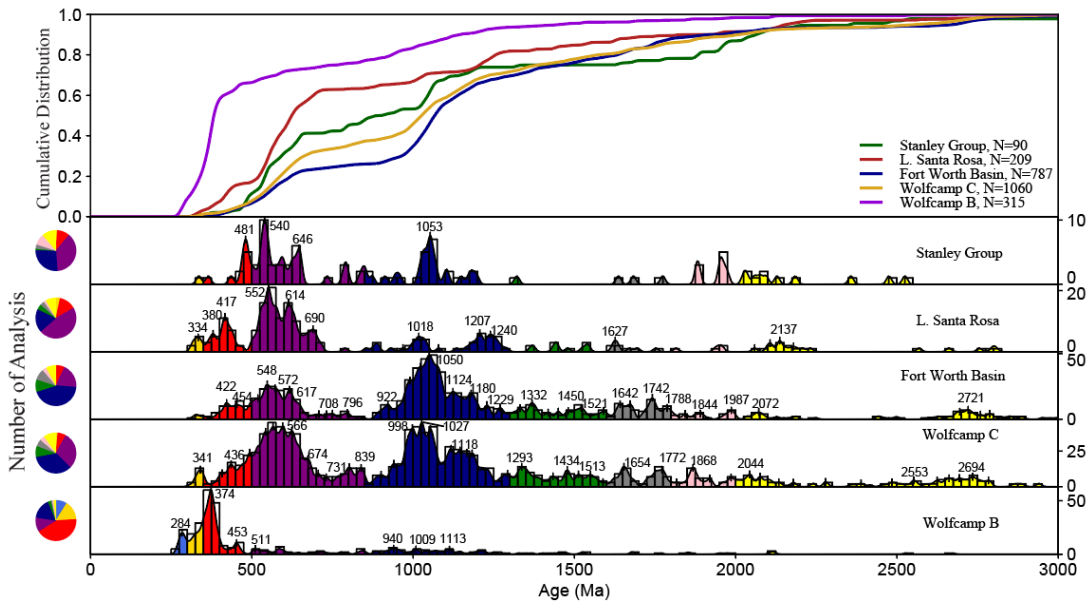
Figure 3-11. LA-ICPMS U-Pb date distributions of detrital zircons near the study area. Data of the Late Mississippian Stanley Group are from McGuire (2017), the lower part of the Late Mississippian Santa Rosa Formation are from Weber et al. (2009), the Middle–Late Pennsylvanian strata in the Fort Worth Basin are from Alsalem et al. (2017), the Cisuralian Wolfcamp C unit are from Liu and Stockli (2020). The plot was shown as kernel density estimation. The numbers on the plot are peak modes. Data from strata of the lower part of the Santa Rosa have 1σ uncertainty and all other data have 2σ uncertainty.

3. 5.3.3 Wolfcamp A and Spraberry tuffs

Abundant unrounded zircons in the Wolfcamp A and Spraberry tuffs (Fig. 3-5) suggest that these tuffs have little detrital or inherited component. They also have similar εHf signature (Fig. 3-10), suggesting that they may come from the same arc system. Magmatic units of similar age are also reported in the Oaxaquia terrane in southern Mexico. The best match for the Wolfcamp A tuff is the 287 ±2 Ma Zanita Batholith, which has εHf values between -4 and -1, and TDM2 ages between 1330 and 1550 Ma (Ortega-Obregón et al., 2014). Zúñiga et al. (2020) reported two groups of volcanic clasts in the Matzitzi Formation, southern Mexico. The intermediate group has zircon LA-ICPMS dates

between 282 and 271 Ma, ƐHf values between -8.1 and +0.2 and TDM2 ages between 1470 and 1520 Ma. This signature matches well with that of our Spraberry tuffs. The second group is ~281 Ma and has ƐHf values between -3.6 and +8.4 (1 grain) and TDM2 ages between 1280 and 1320 Ma. The geochemical variability of these zircons suggests a heterogeneous parent melt caused by different mixtures of mantle-derived melts and Grenville basement. In southern Mexico, the Oaxaquia peri-Gondwana basement is 1200-1400 Ma, with ƐHf values between +5 and +7 (Weber et al., 2010) (Fig. 3-10). Melting this basement decreases the ƐHf values of parent magma. Therefore, Wolfcamp A and Spraberry tuffs were also most likely sourced from a continental arc on the Oaxaquia terrane.

3. 5.3.4 Guadalupe Mountains tuffs

Magmatic units between 275 and 260 Ma are documented in southern Mexico (e.g., Ortega-Obregón et al., 2014), eastern Mexico (Coombs et al., 2020); northwestern Mexico (Riggs et al., 2016; Dobbs et al., 2021), and the Mojave Desert of California, USA (Cecil et al., 2019). These units may represent an ~N-S volcanic arc system formed by the eastward subduction of the Paleo-Pacific oceanic plate beneath the northwestern Gondwana (western Pangea arc) and southwestern Laurentia (Cordillera arc) (Fig. 3-1C). The arc system may have initiated at different times at different latitudes and the zircon ƐHf signature of these arc magmas may have varied because different segments were built on crust of different ages and compositions. Zircon grains of 270-260 Ma on the Oaxaquia terrane in southern and eastern Mexico, including the Zaniza batholith and subsurface granitoids along the western Gulf of Mexico, have ƐHf values between -16 and +0.2 (Ortega-Obregón et al., 2014; Coombs et al., 2020), more evolved than those from the Mojave Desert (ƐHf values between -1.3 and +11.5) and our Guadalupian tuffs. Zircon grains of ~275 Ma in the Los Tanques pluton in Sonora, Mexico, also have more evolved ƐHf signatures (average is -7.5) (Riggs et al., 2016) than our Guadalupian tuffs. Therefore, arc magmatism in southern and northwestern Mexico was not likely to be the source of the Guadalupian tuffs. Mojave Desert pluton zircons show a significant increase of ƐHf values through time between

280-200 Ma, with the ƐHf values of 280-260 Ma zircons between -5 and +10 (Cecil et al., 2019). The trend was suggested to reflect decreasing crustal contamination of mantle-derived melts through time because of extension and crustal thinning (Cecil et al., 2019). Therefore, it seems that the source of the Guadalupian tuffs is the Cordillera arc, most likely related to Mojave Desert plutons. Ash transport from volcano(es) about 1500 km to the west of the Texas may be facilitated by westerly winds at the low latitude of western equatorial Pangea (Tabor and Poulsen, 2007).

3. 5.4 Implications for the late Paleozoic tectonics of southern Laurentia

It is debated whether late Cisuralian magmatisms discussed above reflect the final pulse of the northern Gondwana arc system formed by subduction of the Rheic oceanic plate (e.g., Elías-Herrera and Ortega-Gutiérrez, 2002; Vega-Granillo et al., 2007, 2009; Ortega-Gutiérrez et al., 2018) or the initiation of eastward subduction of the Paleo-Pacific oceanic plate beneath southwestern Pangea (e.g., Keppie et al., 2008; Nance et al., 2010). Our geochemical records show an abrupt change of mean zircon ƐHf signature from +5.5 to - 4.5 between Wolfcamp B and A tuffs that occurred near or within 1 Myr (between 288.2 and 287.2 Ma). A similar abrupt shift to evolved ƐHf signature has been documented in Oaxaquia terrane magmatic rocks (Ortega-Obregón et al., 2014; Coombs et al., 2020). While Ortega-Obregón et al. (2014) attributed this to a change to more crustal contamination, Coombs et al. (2020) suggested that the juvenile signature was related to Rheic plate subduction that may have ended by ~286 Ma and the evolved signature (ƐHf between -16 and -4), initiated by ~274 Ma, reflects late- or post-collisional magmatism influenced by Paleo-Pacific plate subduction. Furthermore, Zhao et al. (2020) suggested that magmatism in the Marathon segment ended by 270 Ma, as part of the late Paleozoic magmatism that ended diachronously from west to east along the Appalachian-Ouachita-Marathon belt, with the youngest magmatism was sourced from juvenile lower crust during post-orogenic slab break-off.

The geochemical similarity between magmatic zircons in the Wolfcamp B tuffs and the Mississippian Barnett tuff in the Midland Basin suggests that arc volcanism related to the subduction of the Rheic oceanic plate may have lasted until at least ~288 Ma (CA-ID-TIMS in this study) (Fig. 3-12). This is consistent with the inferred age of ~286 Ma (ICP-MS) from granitoid εHf signatures in eastern Mexico (Coombs et al., 2020). This abrupt change of geochemical signature reflects a change of parent magma to a much more evolved composition that could have been caused by increased contribution from old continental crust, which can be achieved in four ways: 1) crustal thickening associated with subduction; 2) involvement of crust of different age and composition; 3) changing depth of magma evolution; and 4) formation of a new magmatic plumbing system for a new arc. Whereas crustal thickening and underthrusting of lower crust into the melt source region are common in orogenic systems, crustal assimilation is a gradual process and it takes at least 5 Myr to cause a major decrease in arc εHf signature (e.g., DeCelles et al., 2009). Changing crustal composition of the northern Gondwana arc magmas also seems unlikely to be a cause of the abrupt isotope shift. Grains older than 500 Ma in the Wolfcamp A and B tuffs are mostly between 500-850 Ma and 900-1300 Ma, suggesting the sources of both tuffs have Pan-African/Brasiliano and Grenville basement. The sources should be peri-Gondwana terranes (i.e., Oaxaquia terrane) that have both Pan-African/Brasiliano and Grenville basement (Weber et al., 2010; Lopez et al., 2001). Zhao et al. (2020) suggested that magmatism in northern Gondwana may have lasted until ~270 Ma with the youngest magma derived from lower crust (Pan-African Orogeny materials) because of Rheic oceanic slab break-off. Changing from synorogenic to post-orogenic slab break-off magmatism cannot explain the observed abrupt isotopic shift because the εHf signatures of Wolfcamp A-Spraberry zircons are more evolved than those of the ~326 Ma granitoids (+3.8 to +6.0) on the Maya peri-Gondwana terrane, which is suggested to reflect post-orogenic magmatism in the Ouachita segment (Zhao et al., 2020).
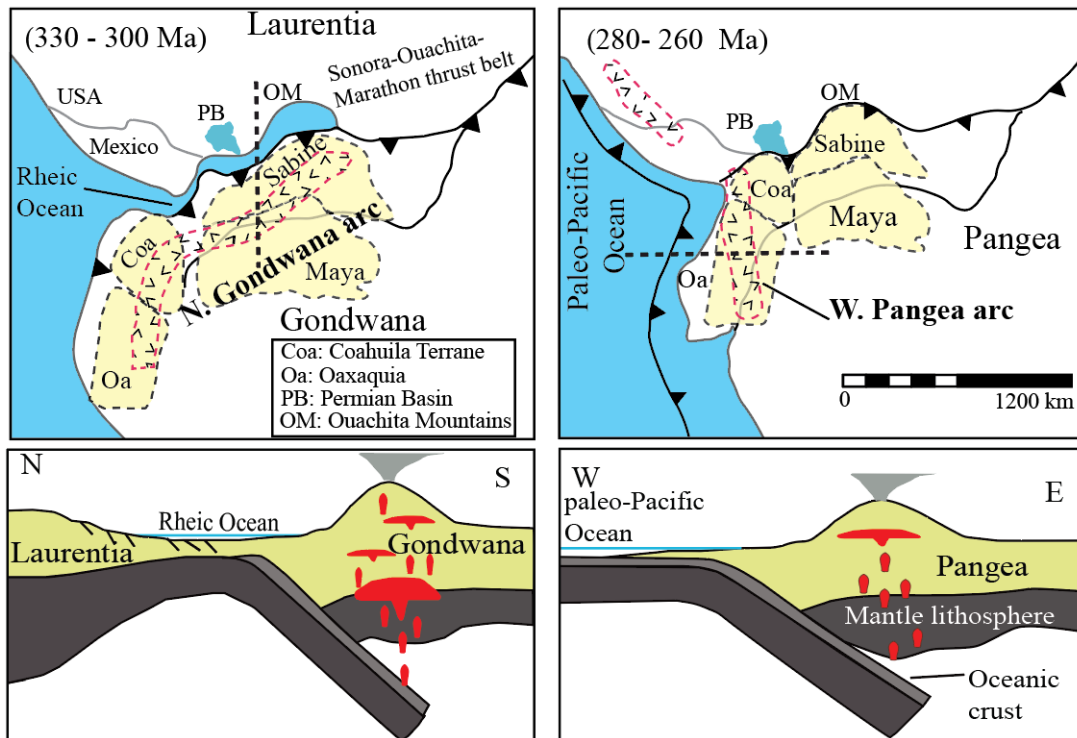
Figure 3-12. Paleogeography reconstructions for two time periods after Ortega-Obregón et al. (2014) and Lawton et al. (2021). Thick black dash lines represent the locations of cross sections shown in the lower panel.

The abrupt isotopic change can be best explained by the termination of the northern Gondwana arc system and initiation of a new convergent margin along western Pangea associated with a new Paleo-Pacific plate subduction system (Fig. 3-12). The gradual increase of εHf values from Wolfcamp A to Spraberry and Guadalupian tuffs (Fig. 3-10) is similar to the trend observed in the Mojave Desert pluton that was interpreted to be caused by diminishing sediment input as subduction of the Paleo-Pacific plate proceeded (Cecil et al., 2019). This similarity in εHf trend, but difference in time between the magmatism in Mexico (~287 Ma) and Mojave Desert (~275 Ma) suggests that subduction of the Paleo-Pacific plate initiated at different times along the Laurentian margin. This age does not match well with the interpretation of Coombs et al. (2020), who suggested that the western Pangea arc, with

negative εHf values similar to those of our Wolfcamp A and Spraberry tuffs, initiated in Mexico by ~274 Ma. That study has a sampling gap for ~286-274 Ma, thus it could have missed the early initiation of the west Pangea arc.

Our results show that the late Cisuralian (~288 Ma) plate reorganization occurred very rapidly, near or less than 1 Myr. This reorganization was marked by the cessation of Laurentia-Gondwana collision that partly subducted the southern Laurentia margin beneath Gondwana, and the initiation of a new subduction zone along the southwestern Pangean margin. Our study thus confirms the inference that major plate reorganizations taking as little time as less than a few million years are more likely caused by changes in plate motion due to plate margin creation or destruction (Richards and Lithgow-Bertelloni, 1996). Subduction of the Paleo-Pacific beneath western Gondwana may have caused the Permian-Triassic continental arc in eastern Mexico (e.g., Torres et al., 1990; Rosales-Lagarde et al., 2005; Coombs et al., 2020) and magmatic rocks of the Oaxacan and Acatlán metamorphic complexes in southwestern Mexico (Ortega-Obregón et al., 2014). The cessation of Pangea assembly changed the plate motion and promoted the northward propagation of the subduction system along western Pangea.

3. 6 CONCLUSIONS

This study reports the first group of isotopic ages for early Permian tuffs in the Permian Basin and examines the geochemical and isotopic signatures of these tuffs and the Mississippian and Guadalupian tuffs in southern Laurentia to understand their magmatic affinities and tectonic significance. Our zircon CA-ID-TIMS dates show that the boundary between the Wolfcamp B and Wolfcamp A unit in the Midland Basin is ~287 Ma, which complements recent biostratigraphy results that correlate the Wolfcamp B unit to the late Sakmarian and early Artinskian stages, and the Wolfcamp A to the late Artinskian stage. Geochemical data of all these Mississippian-Permian tuffs and their zircons show continental arc signatures. Comparison of the geochemical data of these tuffs and magmatic units in Mexico and California further establishes the potential source of the tuffs on peri-

Gondwana terranes in Mexico. The εHf values abruptly change at ~287 Ma from higher, more juvenile signatures in the Mississippian and early Cisuralian Wolfcamp B tuffs to consistently negative εHf values in the Cisuralian Wolfcamp A and Spraberry tuffs. At the same time, a higher proportion of more angular zircons appear in the tuffs and the proportion of detrital zircons decreases. The ~288 Ma zircon signature shift between 288.2-287.2 Ma is best explained by the termination of the northern Gondwana arc system related to subduction of the Rheic oceanic plate and initiation of a western Pangea arc system related to subduction of the Paleo-Pacific oceanic plate.

In addition to the chronostratigraphy and tectonic significance, the comparison of LA-ICPMS dates derived from different statistical approaches and the true depositional ages of the tuffs determined by CA-ID-TIMS zircon dating offers important new insights to better understand the limitation of LA-ICPMS zircon ages. Several commonly used statistical approachs, including the weighted mean date of the youngest cluster of three or more grains overlapping at 2σ error (YSP), weighted mean date of the youngest mode from KDE (WMKDE), and TuffZirc date all are too young, but within 96% of the true depositional ages, thus can be used to approximate true depositional age if CA-ID-TIMS ages are not available. The newly defined, weighted mean date of the youngest dominant KDE mode (WMYDM) is closest to the true depositional age, and the small difference between this date and true depositional age may reflect the skewness of the LA-ICPMS zircon age distribution. Chemical abrasion pre-treatment or simply annealing zircons prior to LA-ICPMS analysis may greatly improve the accuracy of the LA-ICPMS method in assessing true depositional ages from tuffs.

3. 7 ACKNOWLEDGMENTS

3. 8 REFERENCES CITED

Adams, J.E., Cheney, M.G., Deford, R.K., Dickey, R.I., Dunbar, C.O., Hills, J.M., King, R.E., Lloyd, E.R., Miller, A.K., and Needham, C.E., 1939. Standard Permian Section of North America. AAPG Bull. 23, 1673–1678. doi.org/10.1306/3D933136-16B1-11D7-8645000102C1865D

Adams, J.E., 1965. Stratigraphic-tectonic development of Delaware Basin, West Texas and southeastern New Mexico. AAPG Bull. 49, 2140-2148.

Allen, C.M., and Campbell, I.H., 2012. Identification and elimination of a matrix-induced systematic error in LA-ICP-MS 206P /238U dating of zircon. Chem. Geol. 333, 157–165.

Anderson, D.L., 2001. Top-Down Tectonics? Science 293, 2016–2018.

Alsalem, O.B., Fan, M., Zamora, J., Xie, X., and Griffin, W.R., 2018. Paleozoic sediment dispersal before and during the collision between Laurentia and Gondwana in the Fort Worth Basin, USA. Geosphere 14, 1–18.

Arndt, N.T., and Goldstein, S.L. 1987. Use and abuse of crust-formation ages. Geology 15, 893-895. doi.org/10.1130/0091-7613(1987)15<893:UAAOCA>2.0.CO;2.

Baumgardner, R.W., Hamlin, H.S., and Rowe, H., 2016. Lithofacies of the Wolfcamp and lower Leonard intervals, southern Midland Basin, Texas. The University of Texas at Austin, Bureau of Economic Geology, Report of Investigations 281, 67.

Behnken, F.H., 1984. Conodont biostratigraphy of the Wolfcampian Series Standard Section (Lower Permian, Sakmarian) Wolfcamp Hills, west Texas. Geological Society of America - Abstracts with Programs 16, 124.

Belousova, E., Griffin, W., O'Reilly, S.Y., Fisher, N., 2002. Igneous zircon: trace element composition as an indicator of source rock type. Contrib. to Mineral. Petrol. 143, 602-622. doi.org/10.1007/s00410-002-0364-7

Cawood P.A., Hawkesworth C.J., and Dhuime B., 2012. Detrital zircon record and tectonic setting. Geology 40, 875–878. doi:10.1130/G32945.1.

Cecil, M.R., Ferrer, M.A., Riggs, N.R., Marsaglia, K.M., Kyland-er-Clark, A., Ducea, M.N., and Stone, P., 2019. Early arc development recorded in Permian–Triassic plutons of the northern Mojave Desert region, California, USA. Geol. Soc. Am. Bull. 131, 749–765. doi .org /10 .1130 /B31963.1.

Chernykh, V.V., and Ritter, S.M., 1997. Streptognathodus (Conodonta) Succession at the Proposed Carboniferous-Permian Boundary Stratotype Section, Aidaralash Creek, Northern Kazakhstan. J. Paleontol.71, 459-474.

Chernykh, V.V., Chuvashov, B.I., Davydov, V.I., Schmitz, M., and Snyder, W.S., 2006. Usolka section (southern Urals, Russia): A potential candidate for GSSP to define the base of the GzhelianStage in the global chronostratigraphic scale. Geologija 49, 205-217.

Chuvashov, B.I., Chernykh, V.V., Leven, E.Y., Davydov, V.I., Bowring, S., Ramezani, J., Glenister B.F., Henderson C., Schiappa T.A., Northrup C.J., Snyder W.S., Spinosa C., and Wardlaw, B.R., 2002. Progress report on the base of the Artinskian and base of the Kungurian by the Cisuralian Working Group. Permophiles 41, 13-16.

Chuvashov, BI., Chernykh, V.V., Shen, S., and Henderson, C.M., 2013. Proposal for the Global Stratotype Section and Point (GSSP) for the base-Artinskian Stage (Lower Permian). Permophiles 58, 26-34.

Coombs, H.E., Kerr, A.C., Pindell, J., Buchs, D., Weber, B., and Solari, L., 2020. Petrogenesis of the crystalline basement along the western Gulf of Mexico: Post-collisional magmatism during the formation of Pangea. In: Martens, U., Molina Garza, R.S. (Eds.), Southern and Central Mexico: Basement Framework, Tectonic Evolution, and Provenance of Mesozoic–Cenozoic Basins: Geological Society of America Special Paper 546, p. 29–52.

Coutts, D.S., Matthews, W.A., and Hubbard, S.M., 2019. Assessment of widely used methods to derive depositional ages from detrital zircon populations. Geosci. Front. 10, 1421–1435. doi: https://doi.org/10.1016/j.gsf.2018.11.002.

Crowell, J.C., 1978. Gondwanan glaciation, cyclothems, continental positioning and climate change. Am. J. Sci. 278, 1345-1372.

Davies, T.A., Hay, W.W., Southam, J.R., and Worsley, T.R., 1977. Estimates of Cenozoic Oceanic Sedimentation Rates. Science 197, 53-55. doi: 10.1126/science.197.4298.53

Davydov, V.I., Glenister, B.F., Spinosa, C., Ritter, S.M., Chernykh, V.V., Wardlaw, B.R., and Synder, W.S., 1998. Proposal of Aidaralash as Global Stratotype Section and Point (GSSP) for base of the Permian System: Episodes 21, 11-18.

DeCelles, P.G., Ducea, M.N., Kapp, P., and Zandt, G., 2009. Cyclicity in Cordilleran orogenic systems. Nat. Geosci. 2, 251-257.

Dhuime, B., Hawkesworth, C.J., and Cawood, P., 2011. When Continents Formed. Science 331, 154-155. doi: 10.1126/science.1201245

Dickinson, W.R., and Gehrels, G.E., 2009. Use of U – Pb ages of detrital zircons to infer maximum depositional ages of strata : A test against a Colorado Plateau Mesozoic database. Earth Planet. Sci. Lett. 288, 115–125. doi: 10.1016/j.epsl.2009.09.013.

Dobbs, S.C., Riggs, N.R., Marsaglia, K.M., González-León, G.M., Cecil, M.R., and Smith, M.E., 2021. The Permian Monos Formation: Stratigraphic and detrital zircon evidence for Permian Cordilleran arc development along the southwestern margin of Laurentia (northwestern Sonora, Mexico). Geosphere 17, 520-537.

Domeier, M., Torsvik, T.H., 2014. Plate tectonics in the late Paleozoic. Geosci. Front. 5, 303-350. doi.org/10.1016/j.gsf.2014.01.002.

Dutton, S.P., Kim, E.M., Broadhead, R.F., Raatz, W.D., Breton, C.L., Ruppel, S.C., and Kerans, C., 2005. Play analysis and leading-edge oil-reservoir development methods in the Permian Basin:

Increased recovery through advanced technologies. AAPG Bull. 89, 553–576, doi .org /10 .1306 /12070404093.

Elías-Herrera, M., and Ortega-Gutiérrez, F., 2002. Caltepec fault zone: an early Permian dextral transpressional boundary between the Proterozoic Oaxacan and Paleozoic Acatlán complexes, southern Mexico, and regional tectonic implications. Tectonics 21, 1–18. doi.org/10.1029/2000TC001278

Estrada-Carmona, J., Weber, B., Scherer, E.E., Martens, U., and Elías-Herrera, M., 2016. Lu-Hf geochronology of Mississippian high-pressure metamorphism in the Acatlán Complex, southern México. Gondwana Res. 34, 174-186.

Gärtner, A., Linnemann, U., Sagawe, A., Hofmann, M., Ullrich, B., and Kleber, A., 2013. Morphology of zircon crystal grains in sediments – characteristics, classifications, definitions. Cent. Eur. Geol. 59, 65–73.

Gehrels, G., 2014. Detrital Zircon U-Pb Geochronology Applied to Tectonics. Annu. Rev. Earth Planet. Sci. 42, 127–149. doi: 10.1146/annurev-earth-050212-124012.

Glenister, B.F., Boyd, D.W., Furnish, W.M., Grant, R.E., Harris, M.T., Kozur, h., Lambert, L.L., Nassichuk, W.W., Newell, N.D., Pray, L.C., Spinosa, C., Wardlaw, B.R., Wilde, G.J., Yanceytm T.E., 1992. The Guadalupian: proposed international standard for a middle Permian series: Int. Geol. Rev. 34, 857–888.

Glenister, B. F., Wardlaw, B.R., Lambert, L.L., Spinosa, C., Bowring, S. A., Erwin, D.H., Menning, M., and Wilde, G.L., 1999. Proposal of Guadalupian and component Roadian, Wordian, and Capitanian Stages as international standards for the middle Permian Series: Permophiles 34, 3-11.

Grimes, C.B., Wooden, J.L., Cheadle, M.J., and John, B., 2015. "Fingerprinting" tectono-magmatic provenance using trace elements in igneous zircon. Contrib. to Mineral. Petrol. 170, 1-26.

Griffin, W.L., Wang, X., Jackson, S.E., Pearson, N.J., O'Reilly, S.Y., Xu, X., Zhou, X., 2002. Zircon chemistry and magma mixing, SE China: in-situ analysis of Hf isotopes, Pingtan and Tonglu igneous complexes. Lithos 61, 237–269.

Gursky, H.J., and Michalzik, D., 1989. Lower Permian turbidites in the northern Sierra Madre Oriental, Mexico. Zentralblatt für Geologie und Paläontologie 1, 821–838.

Hamlin, H.S., and Baumgardner, R.W., 2012. Wolfberry (Wolfcampian-Leonardian) Deep-water Depositional Systems in the Midland Basin: Stratigraphy, Lithofacies, Reservoirs, and Source Rocks. the University of Texas at Austin, Bureau of Economic Geology, Report of Investigations 277, 1-61.

Handford, C., 1981. Sedimentology and Genetic Stratigraphy of Dean and Spraberry Formations (Permian), Midland Basin, Texas. AAPG Bull. 65, 1602-1616. 10.1306/03B5962A-16D1-11D7-8645000102C1865D.

Heckel, P.H., and Clayton, G., 2006. The Carboniferous System. Use of the new official names for the subsystems, series, and stages. Geol. Acta 4, 403–407. doi: 10.1016/S0016-7878(06)80045-3.

Henderson, C.M., Wardlaw, B.R., Davydov, V.I., Schmitz, M.D., Schiappa, T.A., Tierney, K.E., and Shen, S., 2012. Proposal for base-Kungurian GSSP. Permophiles 56, 8-21.

Herriott, T.M., Crowley, J.L., Schmitz, M.D., Wartes, M.A., and Gillis, R.J., 2019. Exploring the law of detrital zircon : LA-ICP-MS and CA-TIMS geochronology of Jurassic forearc strata. Geology 47, 1044–1048.

Hill, C.A., 1996. Geology of the Delaware Basin, Guadalupe, Apache and Glass Mountains, New Mexico and West Texas. Society of Economic Mineralogists and Paleontologists, Permian Basin Section 96-39, 1-480.

Jones, R.E., Kirstein, L.A., Kasemann, S.A., Dhuime, B., Elliott, T., Litvak V.D., Alonso, R., and Hinton, R., 2015. Geodynamic controls on the contamination of Cenozoic arc magmas in the

southern Central Andes: Insights from the O and Hf isotopic composition of zircon. Geochim. Cosmochim. Acta 164, 386-402,

Keppie, J., Dostal, J., Murphy, J., and Nance, R., 2008. Synthesis and tectonic interpretation of the westernmost Paleozoic Variscan orogen in southern Mexico: from rifted Rheic margin to active Pacific margin. Tectonophysics 461, 277–290. https://doi.org/10.1016/j. tecto.2008.01.012

King, S.D., Lowman, J.P., and Gable, C.W., 2002. Episodic tectonic plate reorganizations driven by mantle convection. Earth Planet. Sci. Lett. 203, 83–91.

Kirsch, M., Keppie, J.D., Murphy, J.B., and Solari, L.A, 2012. Permian–Carboniferous arc magmatism and basin evolution along the western margin of Pangea: geochemical and geochronological evidence from the eastern Acatlán Complex, southern Mexico. Geol. Soc. Am. Bull. 124, 1607–1628. doi.org/10.1130/B30649.1

Kohn, J., Barrick, J.E., Wahlman, G.P., and Baumgardner, R., 2019. Late Pennsylvanian (Virgilian) to early Permian (Leonardian) conodont biostratigraphy of the "Wolfcamp Shale," northern Midland Basin, Texas. In: Denne, R.A., Kahn, A. (Eds.), Geologic Problem Solving with Microfossils IV. SEPM Special Publication 111, 245–261.

Le Maitre, R.W.,1989. A Classification of Igneous Rocks and Glossary of Terms, Recommendations of the IUGS Commission on the Systematics of Igneous Rocks. Oxford: Blackwell.

Lawton, T.F., Blakey, R.C., Stockli, D.F., and Liu, L., 2021. Late Paleozoic (Late Mississippian-middle Permian) sediment provenance and dispersal in western equatorial Pangea. Palaeogeogr. Palaeoclimatol. Palaeoecol. 572, 1-35. doi.org/10.1016/j.palaeo.2021.110386

Leary, R.J., Umhoefer, P., Smith, M.E., and Riggs, N., 2017. A three-sided orogen: A new tectonic model for Ancestral Rocky Mountain uplift and basin development. Geology 45, 735–738. doi: 10.1130/G39041.1.

Liu, L., and Stockli, D.F., 2020. U-Pb ages of detrital zircons in lower Permian sandstone and siltstone of the Permian basin, west Texas, USA: Evidence of dominant Gondwanan and peri-Gondwanand sediment input to Laurentia. Geol. Soc. Am. Bull. 132, 245–262. doi10.1130/B35119.1.

Lopez, R., 1997. The pre-Jurassic geotectonic evolution of the Coahuila terrane, northwestern Mexico: Grenville basement, a late Paleozoic arc: Triassic plutonism, and the events south of the Ouachita suture. Ph.D. thesis, University of California.

Lopez, R., Cameron, K.L., and Jones, N.W., 2001. Evidence for Paleoproterozoic, Grenvillian, and Pan-African age Gondwanan crust beneath northeastern Mexico. Precambrian Res. 107, 195–214.

Lucas, S.G., and Shen, S.Z., 2018. The Permian timescale: an introduction. Geol. Soc. Lond. Spec. Publ. 450, 1-19. doi.org/10.1144/SP450.1

Ludwig, K.R., and Mundil, R., 2002. Extracting reliable U-Pb ages and errors from complex populations of zircons from Phanerozoic tuffs. Geochim. Cosmochim. Acta 66 (15A), 463.

Ludwig, K.R., 2008. User's Manual for Isoplot 3.70. Berkeley Geochronology Center Special Publication, 76.

Mallard, C., Coltice, N., Seton, M., Müller, R.D., Tackley, P.J., 2016. Subduction controls the distribution and fragmentation of Earth's tectonic plates. Nature 535, 140–143.

Marantos, I., Markopoulos, Th., Christidis, G. E., Perdikatsis, V. Geochemical characteristics of the alteration of volcanic and volcaniclastic rocks in the Feres Basin, Thrace, NE Greece. Clay Miner. 43, 575–595.

Matthews, K.J., Seton, M., Müller, R.D., 2012. A global-scale plate reorganization event at 105-100 Ma. Earth Planet. Sci. Lett. 355-356, 283–298.

Mattinson, J.M., 2005. Zircon U-Pb chemical abrasion ("CA-TIMS") method: Combined annealing and multi-step partial dissolution analysis for improved precision and accuracy of zircon ages. Chem. Geol. 220, 47–66. doi .org/10.1016/j.chemgeo.2005.03.011.

Mazzullo, S.J., 1982. Stratigraphy and Depositional Mosaics of Lower Clear Fork and Wichita Groups (Permian), Northern Midland Basin, Texas. AAPG Bull. 66, 210-227.

Mazzullo, S.J., Reid, A.M., and Mazzullo, L.J., 1987. Basinal Lower Permian Facies, Permian Basin: Part I - Stratigraphy of the Wolfcampian-Leonardian Boundary. West Texas Geological Society Bulletin 26, 5-9.

Mazzullo, S.J., and Reid, A.M., 1989. Lower Permian Platform And Basin Depositional Systems, Northern Midland Basin, Texas. In: Crevello, P.D., Wilson, J.L., Sarg, J.F., Read, J. F. (Eds.), Controls on Carbonate Platforms and Basin Development, SEPM Society for Sedimentary Geology 44, 305-320.

McGuire, P.R., 2017. U-Pb detrital zircon signature of the Ouachita orogenic belt. M.S. thesis, Texas Christian University.

Mckee, J.W., Jones, N.W., and Anderson, T.H. 1988. La Delicias basin: a record of late Paleozoic arc volcanism in northeastern Mexico. Geology 16, 37–40. doi.org/10.1130/0091-7613(1988)016,0037:LDBARO.2.3.CO;2.

Morra, G., Seton, M., Quevedo, L., and Müller, R.D., 2013. Organization of the tectonic plates in the last 200 Myr. Earth Planet. Sci. Lett. 373, 93–101.

Montgomery, S.L., 1996. Permian "Wolfcamp" Limestone Reservoirs: Powell Ranch Field, Eastern Midland Basin. AAPG Bull. 80, 1349-1365. doi.org/10.1306/64ED9A38-1724-11D7-8645000102C1865D

Murakami, H., Ishihara, S., 2008, REE Mineralization of Weathered Crust and Clay Sediment on Granitic Rocks in the Sanyo Belt, SW Japan and the Southern Jiangxi Province, China. Resour. Geol. 58, 373-401.

Nance, R.D., Gutierrez-Alonso, G., Keppie, J.D., Linnemann, U., Murphy, J.B., Quesada, C., Strachan, R.A., and Woodcock N.H., 2010. Evolution of the Rheic Ocean. Gondwana Res. 17, 194–222. doi:10.1016/j.gr.2009.08.001

Nicklen, B., Gorden, J., Lance, L., Warren, H., 2015. Tephrochronology of the Manzanita Limestone in the Middle Permian (Guadalupian) Type Area, West Texas and southeastern New Mexico, USA. Stratigraphy 12, 123-147.

Ortega-Gutiérrez, F., Elías-Herrera, M., Morán-Zenteno, D.J., Solari, L., Weber, B., and Luna-González, L., 2018. The pre-Mesozoic metamorphic basement of Mexico, 1.5 billion years of crustal evolution: Earth Sci. Rev. 183, 2–37. doi.org/10. 1016/j.earscirev.2018.03.006

Ortega-Obregón, C., Solari, L., Gómez-Tuena, A., Elías-Herrera, M., Ortega-Gutiérrez, F., and Macías-Romo, C., 2014. Permian–Carboniferous arc magmatism in southern Mexico: U–Pb dating, trace element and Hf isotopic evidence on zircons of earliest subduction beneath the western margin of Gondwana. Int. J. Earth Sci. 103, 1287–1300. doi.org/10.1007/s00531-013-0933-1.

Pearce, J.A., Harris, N.B.W., and Tindle, A.G., 1984. Trace Element Discrimination Diagrams for the Tectonic Interpretation of Granitic Rocks. J. Petrol. 25, 956–983. doi.org/10.1093/petrology/25.4.956.

Peccerillo, A., and Taylor, S.R., 1976. Geochemistry of Eocene calc-alkaline volcanic rocks from the Kastamonu area, Northern Turkey. Contrib. to Mineral. Petrol. 58, 63-81.

Poole, F.G., Perry William J., J., Madrid, R.J., and Amaya-Martínez, R., 2005. Tectonic synthesis of the Ouachita-Marathon-Sonora orogenic margin of southern Laurentia. In: Anderson, T.H., Nourse, J.A. McKee, J.W., Steiner, M.B. (Eds.), Stratigraphic and structural implications for timing of deformational events and plate-tectonic model. Geol. Soc. Am. Spec. Pap. 393, 543–596. doi.org/10.1130/0-8137-2393-0.543.

Ramírez-Fernández, J.A., Alemán-Gallardo, E.A., Cruz-Castillo, D., Velasco-Tapia, F., Jenchen, U., Becchio, R., León-Barragán, L.D., and Casas-Peña, J.M., 2021. Early Mississippian precollisional, peri-Gondwanan volcanic arc in NE-Mexico: Aserradero Rhyolite from Ciudad Victoria, Tamaulipas. Int. J. Earth Sci. 110, 2435–2463,

Ramezani, J., and Bowring, S.A., 2018. Advances in numerical calibration of the Permian timescale based on radioisotopic geochronology. In: Lucas, S.G., Shen, S. (Eds.), The Permian Times. Geol. Soc. Lond. Spec. Publ. 450, 51–60. doi.org/10.1144/SP450.17.

Richards, M.A., and Lithgow-Bertelloni, C., 1996. Plate motion changes, the Hawaiian-Emperor bend, and the apparent success and failure of geodynamic models. Earth Planet. Sci. Lett. 137, 19–27.

Riggs, N.R., Barth, A.P., Walker, J.D., Lindner, P., Gonzalez- Leon, C., Cecil, M. Robinson, and Marsaglia, K.M., 2016, Implications of Permian magmatism in south-west Laurentia for tectonic reconstructions: Geological Society of America Abstracts with Programs, v. 48, no. 7, http://doi.org/10.1130/abs/2016AM-279985.

Rosales-Lagarde, L., Centeno-García, E., Dostal, J., Sourtovar, F., Ochoa-Camarillo, H., Quiroz-Barroso, S., 2005. The Tuzancoa Formation: evidence of an Early Permian submarine continental arc in east-central Mexico. Int. Geol. Rev. 47, 901–919. doi.org/10.2747/0020-6814.47.9.901

Ross, C.A., 1986, Paleozoic evolution of southern margin of Permian Basin. Geol. Soc. Am. Bull. 97, 536–554. doi: 10.1130/0016-7606(1986)97<536.

Ross, C.A., and Ross, J.R.P., 2003. Fusulinid sequence evolution and sequence extinction in Wolfcampian and Leonardian Series (Lower Permian), Glass Mountains, West Texas. Rivista Italiana di Paleontologia e Stratigrafia 109, 281-306.

Ross, C.A., and Ross, J.R.P., 2009. Paleontology, a tool to resolve late Paleozoic structural and depositional histories. SEPM Special Publication 93, 93–110.

Rudnick, R.L., and Gao, S., 2003. Composition of the continental crust. In: Rudnick, R.L., (Ed.), Treatise on Geochemistry, Volume 4: The Crust: Oxford, UK, Elsevier, 1–64. doi .org/10.1016/B0-08-043751-6/03016-4.

Schaltegger, U., Schmitt, A.K., and Horstwood, M,S.A., 2015. U-Th-Pb zircon geochronology by ID-TIMS , SIMS, and laser ablation ICP-MS: recipes, interpretations, and opportunities. Chem. Geol. 402, 89–110. doi: https:// doi .org/10.1016/ j.chemgeo.2015.02.028.

Schoene, B., 2014, U–Th–Pb Geochronology. In: Rudnick, R.L., (Ed.), Treatise on Geochemistry (second edition), Volume 4: The Crust: Oxford, UK, Elsevier, 341–378. doi .org/10.1016/B978-0-08-095975-7.00310-7.

Schmid, R. 1981. Descriptive nomenclature and classification of pyroclastic deposits and fragments: Recommendations of the IUGS Subcommission on the Systematics of Igneous Rocks. Geology 9: 41–43.

Sharman, G.R., Sharman, J.P., Sylvester, Z., 2018. detritalPy: A Python-based toolset for visualizing and analysing detrital geo-thermochronologic data. Depos. Rec. 4, 202–215. https://doi.org/10.1002/dep2.45

Silver, B.A., and Todd, R.G., 1969. Permian Cyclic Strata, Northern Midland and Delaware Basins, West Texas and Southeastern New Mexico. AAPG Bull. 53, 2223-2251. doi:10.1306/5d25c94d-16c1-11d7-8645000102c1865d.

Spencer, C.J., Kirkland, C.L., and Taylor, R.J.M., 2016. Strategies towards statistically robust interpretations of in situ U e Pb zircon geochronology. Geosci. Front. 7, 581–589. doi: 10.1016/j.gsf.2015.11.006.

Sun, W., and McDonough, W.F., 1989. Chemical and isotopic systematics of oceanic basalts: Implications for mantle composition and processes. Geol. Soc. Lond. Spec. Publ. 42, 313-345. doi:10.1144/GSL.SP.1989.042.01.19.

Tabor N.J., and Poulsen, C.J., 2008, Palaeoclimate across the Late Pennsylvanian–Early Permian tropical palaeolatitudes: A review of climate indicators, their distribution, and relation to palaeophysiographic climate factors. Palaeogeogr. Palaeoclimatol. Palaeoecol. 268, 293–310.

Thomas, W.A., Gehrels, G.E., and Romero, M.C., 2016. Detrital zircons from crystalline rocks along the Southern Oklahoma fault system, Wichita and Arbuckle Mountains, USA. Geosphere 12, 1224–1234. doi10.1130/GES01316.1.

Thomas, W.A., Gehrels, G.E., Greb, S.F., Nadon, G.C., Satkoski, A.M., Romero, M.C., 2017. Detrital zircons and sediment dispersal in the Appalachian foreland. Geosphere 13, 2206-2230. doi.org/10.1130/GES01525.1.

Thomas, W.A., Gehrels, G.E., Lawton, T.F., Satterfield, J.I., Romero, M.C., and Sundell, K.E., 2019. Detrital zircons and sediment dispersal from the Coahuila terrane of northern Mexico into the Marathon foreland of the southern Mid-continent. Geosphere 15, 1102–1127. doi .org /10 .1130 /GES02033.1.

Tian, H., Fan, M., Valencia, V., Chamberlain, K., Waite, L., and Stern, R.J., 2022. Mississippian Laurentian tuffs came from a northern Gondwana arc. Geology. doi.org/10.1130/G49502.1.

Torres, R., Ruiz, J., Patchett, P.J., and Grajales-Nishimura, J.M., 1999. Permo-Triassic continental arc in eastern Mexico; tectonic implications for reconstructions of southern North America. In: Bartolini, C., Wilson, J.L., Lawton, T.F. (Eds.), Mesozoic Sedimentary and Tectonic History of North-Central Mexico. Geol. Soc. Am. Spec. Pap. 340, 191–196.

Vega-Granillo, R., Talavera-Mendoza, O., Meza-Figueroa, D., Ruiz, J., Gehrels, G.E., López-Martínez, M., and de La Cruz-Vargas, J.C., 2007. Pressure–temperature–time evolution of Paleozoic high-pressure rocks of the Acatlán Complex (southern Mexico): implications for the evolution of the Iapetus and Rheic Oceans. Geol. Soc. Am. Bull. 119, 1249–1264. doi.org/10.1130/B226031.1

Vega-Granillo, R., Calmus, T., Meza-Figueroa, D., Ruiz, J., Talavera-Mendoza, O., and López-Martínez, M., 2009. Structural and tectonic evolution of the Acatlán Complex, southern Mexico: its role in the collisional history of Laurentia and Gondwana. Tectonics 28, TC4008, doi.org/10.1029/2007TC002159.

Vermeesch, P., 2012. On the visualisation of detrital age distributions. Chem. Geol. 312, 190–194. doi.org/10.1016/j.chemgeo.2012.04.021.

Wahlman, G.P., 2013. Pennsylvanian to Lower Permian (Desmoinesian – Wolfcampian) fusulinid biostratigraphy of Midcontinent North America Stratigraphy 10, 73-104.

Wahlman, G.P., Barrick, J., and Baumgardner, W., 2016. Fusulinid and conodont biostratigraphy of the "Wolfcamp Shale" in the Midland Basin, West Texas: a progress report. West Texas Geological Society 2016 Fall Symposium, WTGS Special Publication 16-32.

Waite, L., Fan, M., Collins, D., Gehrels, G., and Stern, R. J., 2020. Detrital zircon provenance evidence for an early Permian longitudi-nal river flowing into the Midland Basin of west Texas: Int. Geol. Rev. 62, 1–21. doi.org/10.1080/00206814.2020.1756930.

Wardlaw, B.R., and Davydov, V.I., 2000. Preliminary Placement of the International Lower Permian working Standard to the Glass Mountains, Texas. Permophiles 36, 11-14.

Wardlaw, B.R., and Nestell, M.K., 2014. The first appearance of Streptognathodus isolatus in the Permian of Texas. Permophiles 59, 17-19.

Weber, B., Valencia, V.A., Schaaf, P., and Ortega-Gutiérrez, F., 2009. Detrital zircon ages from the Lower Santa Rosa Formation, Chiapas: Implications on regional Paleozoic stratigraphy. Revista Mexicana de Ciencias Geológicas 26, 260–276.

Weber, B, Scherer, E.E., Schulze, C, Valencia, V.A., Montecinos, P, Mezger, K, and Ruiz, J., 2010. U–Pb and Lu–Hf isotope systematics of lower crust from central–southern Mexico– geodynamic significance of Oaxaquia in a Rodinia realm: Precambrian Res. 182, 149–162.

Wilde, G.L., 1975. Fusulinid-defined Permian stages. Permian Exploration Boundaries and

Stratigraphy. West Texas Geological Society and Permian Basin Section, Publication, 65-75.

Wilde, G.L., 1990. Practical fusulinid zonation: the species concept; with Permian Basin emphasis. West Texas Geological Society Bulletin 44, 5-34.

Winchester, J.A., and Floyd, P.A., 1977. Geochemical discrimination of different magma series and their differentiation products using immobile elements. Chem. Geol. 20, 325-343. doi.org/10.1016/0009-2541(77)90057-2

Workman, R.K., and Hart, S.R., 2005. Major and trace element composition of the depleted MORB mantle (DMM). Earth Planet. Sci. Lett. 231, 53-72.

Wu, Q., Ramezani, J., Zhang, H., Yuan, D.X., Erwin, D.H., Henderson, C.M., Lambert, L.L., Zhang, Y.C., and Shen, S.Z., 2020. High-precision U-Pb zircon age constraints on the Guadalupian in West Texas, USA. Palaeogeogr. Palaeoclimatol. Palaeoecol. 548, 109668.

Yañez, P., Patchett, P.J., Ortega-Gutiérrez, F., and Gehrels, G.E., 1991. Isotopic studies of the Acatlán Complex, southern Mexico: Implications for Paleozoic North American tectonics. Geol. Soc. Am. Bull. 103, 817–828. doi:10.1130/0016-7606 (1991)103<0817:ISOTAC>2.3.CO;2.

Yang, K.M., and Dorobek, S., 1995. The Permian Basin of West Texas and New Mexico: Flexural Modeling and Evidence for Lithospheric Heterogeneity across the Marathon Foreland. In: Dorobek, S.L., Ross, G.M. (Eds.), Stratigraphic Evolution of Foreland Basins. doi:10.2110/pec.95.52.0037.

Zhao, J., Xiao, L., Gulick, S.P.S., Morgan, J.V., Kring, D., Fucugauchi, J.U., Schmieder, M., de Graaf, S.J., Wittmann, A., Ross, C.H., Claeys, P., Pickersgill, A., Kaskes, P., Goderis, S., Rasmussen, C., Vajda, V., Ferrière, L., Feignon, J., Chenot, E., Perez-Cruz, L., Sato, H., Yamaguchi, K., IODP-ICDP Expedition 364 scientists, 2020. Geochemistry, geochronology and petrogenesis

of Maya block granitoids and dykes from the Chicxulub impact crater, Gulf of México: Implications for the assembly of Pangea. Gondwana Res. 82, 128–150.

Zúñiga, S.J., Solari, L.A., and Ortega-Obregón, C., 2020. Permian igneous clasts from the Matzitzi Formation, southern Mexico: isotopic constraints on the final amalgamation of Pangea. Geol. Soc. Lond. Spec. Publ. 503, 481-496. doi.org/10.1144/SP503-2019-238.

Chapter 4 CONCLUSIONS

This dissertation helps reconstruct the plate reorganization regarding to the assembly of the super continent Pangea. In chapter 2, I utilized zircon trace element geochemistry, Lu-Hf isotopes and U-Pb geochronology to propose the presence of a primitive Late Mississippian northern Gondwana arc caused by the subduction of the Rheic oceanic plate under northern Gondwana. In chapter 3, I studied bulk tuff geochemistry, zircon trace element geochemistry, Lu-Hf isotopes and U-Pb geochronology of ten volcanic tuff units in southwest Laurentia to propose the extension of the northern Gondwana arc into early Permian at about 288 Ma, the initiation of a western Pangea arc at about 287 Ma triggered by the subduction of the Paleo-Pacific oceanic plate beneath west Pangea and the extension of the western Pangea arc into late Permian at 260 Ma. In addition to tectonic significance, this chapter also compares tuff dates from LA-ICPMS and CA-ID-TIMS U-Pb dating and concludes that the weighted mean date of the youngest dominant KDE mode (WMYDM) is the best way to approximate LA-ICPMS dates to true depositional ages. In chapter 4, I applied machine learning algorithms to claasify volcanic tuffs into tectonics backgrounds and showed how machine learning algorithms can help solve high dimensional and large dataset problems in the geoscience domain.

Chapter 5 PERSPECTIVES ON FUTURE WORKS

5.1 FINDING MORE LATE PALEOZOIC TUFFS IN SOUTHERN LAURENTIA

Before this study, there was no volcanic tuff absolute dating of the upper Paleozoic strata in the Permian Basin. The newly discovered Mississippian Barnett volcanic tuff in the Permian Basin and its correlation to tuffs in the Ouachita Mountains and igneous rocks in southern Mexico suggest that late Paleozoic tuffs maybe widespread in southern Laurentia (Tian et al., 2022a). Therefore, it is very likely that many late Paleozoic tuffs are preserved in the subsurface of the Midland Basin and other petroleum-bearing basins (e.g,, the Delaware, Fort Worth, and Anadarko basins) in southern Laurentia. Strong collaboration between industry and academy is needed to discover these tuffs in cores. Similar studies, once conducted to these tuffs, will not only improve regional stratigraphic correlation and absolute dating of the basin fills, but also test my conclusion about the rapid switch from termination of the northern Gondwana arc to initiation of the western Pangea arc (Tian et al., 2022b).

5.2 INTEGRATING BIOSTRATIGRAPHY STUDY AND TUFF ABSOLUTE DATING

The Permian International Time Scale and North America regional time scale are based on conodonts and fusulinids microfossils, respectively. The Global Boundary Stratotype Section and Point (GSSPs) of the Cisuralian epoch of the Permian Period are in Russia and Kazakhstan, where microfossils and absolute dating of tuffs are integrated to determine the fossil assemblages and/or first and last appearances of specific index fossils in the GSSP (Chernykh and Ritter, 1997; Davydov et al., 1998; Chuvashov et al., 2002; Chernykh et al., 2006). In the Permian Basin and several other basins in southern Laurentia, ages of basin fills were previously determined based on microfossil studies and lithostratigraphic correlation between a study site with the site with microfossil age constraints (Adams 1939; Ross 1986; Hill 1996; Wardlaw and Davydov, 2000; Wardlaw, 2004; Ross

and Ross, 2009; Wahlman, 2013; Wardlaw and Nestell, 2014). A major problem of this practice is that some of the microfossils may show diachronous first/last appearance because of changes in regional environmental factors. Therefore, it will be critical to test previous age interpretation by integrating microfossil studies and tuff absolute dating from a specific core in the Permian Basin. Such a study is also helpful to determine the relationship between the late Paleozoic North America regional time scale and the International Time Scale for they use different microfossils.

5.3 CONDUCTING PLUTONIC ROCKS STUDY IN THE SOURCE TERRANES

Although the geochemical similarity between the Late Mississippian Barnett tuff and granitoid rock in the peri-Gondwana Maya block offers convincing evidence that the tuff was from a volcano that formed the granitoid (Tian et al., 2022a). More studies of plutonic rocks of similar age in the Maya terrane and potentially Sabine terrane should be conducted to further test this conclusion and better characterize the northern Gondwana arc. Previous studies also suggested that the subduction of the Rheic oceanic plate became younger southwestward, implying that the late Paleozoic northern Gondwana arc became younger from the Maya/Sabin terranes to the Oaxaquia terrane. Study to plutonic rocks in these terranes can further test this long-perceived tectonic process (e.g., Elías-Herrera and Ortega-Gutiérrez, 2002; Vega-Granillo et al., 2007, 2009; Ortega-Gutiérrez et al., 2018; Zúñiga et al., 2020). This study also suggests that the Wolfcamp A and Spraberry tuffs were from volcanoes in Oaxaquia terrane in southern Mexico, caused by subduction of the Paleo-Pacific oceanic plate (Tian et al., 2022b). Geochemical signatures of these potential source rocks have not been well studied, and current studies debated on whether the plutonic rocks in the Oaxaquia terrane reflects late subduction of the Rheic plate or early subduction of the Paleo-Pacific plate (Zúñiga et al., 2020). Therefore, late Paleozoic plutonic rocks in the peri-Gondwana terranes in Mexico should be better studied to understand the geochemical signatures and time durations of the two arc systems.

5.4 APPLYING MACHINE LEARNING ON TUFF SOURCE IDENTIFICATION

The traditional way of interpreting zircon isotopic and trace element compositions is to compare such data with discrimination diagrams established from studies of zircons from three tectonic settings (Mid Ocean Ridge Basalt, Oceanic Island, and Continental Arc). A major limitation of this approach is that the binary or ternary correlations used in the discrimination diagrams depend only on two or three variables, and the low dimensionality ignores the usefulness of many other trace element and isotopic data. In addition, zircon chemical compositions are very sensitive to their crystallization conditions, such as temperature, pressure, oxygen fugacity (e.g., Prowatke and Klemme, 2005; Rubatto and Hermann, 2007; Trail et al., 2011; Miller et al., 2015) and fractionation between zircon and other minerals (e.g., Kirkland et al., 2015). Therefore, two or three variables may be not effective enough to reduce the influences of crystallization environments, especially for zircons without their parent petrological information. A supervised ML algorithm, Support Vector Machines, is very useful in dealing with high-dimensional datasets to classify unknown samples into labeled categories (e.g., Cortes and Vapnik 1995). The algorithm has been tested in similar subjects (e.g., Petrelli and Perugini, 2016; Petrelli et al., 2016). Once the geochemical signatures, particularly zircon trace element and Hf isotope data, of the potential parent rocks are better studied, SVM algorithm can be applied into these data to better classify the zircons into different tectonic settings and link the data with potential sources to further test the two arc systems and the rapid switch between them.

5.5 REFERENCE CITED

Adams, J.E., Cheney, M.G., Deford, R.K., Dickey, R.I., Dunbar, C.O., Hills, J.M., King, R.E., Lloyd, E.R., Miller, A.K., and Needham, C.E., 1939. Standard Permian Section of North America. AAPG Bull. 23, 1673–1678. doi.org/10.1306/3D933136-16B1-11D7-8645000102C1865D

Belousova, E., Griffin, W., O'Reilly, S.Y., Fisher, N., 2002. Igneous zircon: trace element composition as an indicator of source rock type. Contrib. to Mineral. Petrol. 143, 602-622. doi.org/10.1007/s00410-002-0364-7

Belousova E.A, Jiménez J.M.G, Graham I, Griffin W.L, O'Reilly S.Y, Pearson N, Martin L, Craven S, Talavera C., 2015. The enigma of crustal zircons in upper-mantle rocks: clues from the Tumut ophiolite, southeast Australia. Geology 43:119–222. doi:10.1130/G36231.1

Bishop, C., 2007. Pattern recognition and machine learning. Springer Verlag, New York.

Carley T.L, Miller C.F, Wooden J.L, Padilla A.J, Schmitt A.K, Economos R.C, Bindeman I.N, Jordan B.T., 2014. Iceland is not a magmatic analog for the Hadean: evidence from the zircon record. Earth Planet Sci Lett 405:85–97. doi:10.1016/j.epsl.2014.08.015

Chernykh, V.V., & Ritter, S.M., 1997, Streptognathodus (Conodonta) Succession at the Proposed Carboniferous-Permian Boundary Stratotype Section, Aidaralash Creek, Northern Kazakhstan. Journal of Paleontology, v.71, p. 459-474.

Chernykh, V.V., Chuvashov, B.I., Davydov, V.I., Schmitz, M., & Snyder, W.S., 2006, Usolka section (southern Urals, Russia): A potential candidate for GSSP to define the base of the Gzhelian Stage in the global chronostratigraphic scale: Geologija, v. 49, p. 205-217.

Chuvashov, B. I., Chernykh, V.V., Leven, E.Y., Davydov, V.I., Bowring, S., Ramezani, J., Glenister B. F., Henderson C., Schiappa T.A., Northrup C.J., Snyder W. S., Spinosa C., Wardlaw, B. R., 2002, Progress report on the base of the Artinskian and base of the Kungurian by the Cisuralian Working Group. Permophiles, v. 41, p. 13-16.

Chuvashov, B.I., Chernykh, V.V., Shen, S., & Henderson, C.M., 2013, Proposal for the Global Stratotype Section and Point (GSSP) for the base-Artinskian Stage (Lower Permian): Permophiles, v. 58, p. 26-34.

Davydov, V.I., Glenister, B.F., Spinosa, C., Ritter, S.M., Chernykh, V.V., Wardlaw, B.R., & Synder, W.S., 1998, Proposal of Aidaralash as Global Stratotype Section and Point (GSSP) for base of the Permian System. Episodes, v. 21, p. 11-18.

Elías-Herrera, M., and Ortega-Gutiérrez, F., 2002. Caltepec fault zone: an early Permian dextral transpressional boundary between the Proterozoic Oaxacan and Paleozoic Acatlán complexes, southern Mexico, and regional tectonic implications. Tectonics 21, 1–18. doi.org/10.1029/2000TC001278

Grimes C.B, John B.E, Kelemen P.B, Mazdab F, Wooden J.L, Cheadle M.J, Hanghøj K, Schwartz J.J., 2007. The trace element chemis- try of zircons from oceanic crust: a method for distinguishing detrital zircon provenance. Geology 35:643–646. doi:10.1130/ G23603A.1

Grimes C.B, John B.E, Cheadle M.J, Mazdab F.K, Wooden J.L, Swapp S, Schwartz J.J,2009. On the occurrence, trace element geo- chemistry, and crystallization history of zircon from in situ ocean lithosphere. Contrib Miner Petrol 158:757–783

Grimes, C.B., Wooden, J.L., Cheadle, M.J., and John, B., 2015. "Fingerprinting" tectono-magmatic provenance using trace elements in igneous zircon. Contrib. to Mineral. Petrol. 170, 1-26.

Hill, C.A., 1996. Geology of the Delaware Basin, Guadalupe, Apache and Glass Mountains, New Mexico and West Texas. Society of Economic Mineralogists and Paleontologists, Permian Basin Section 96-39, 1-480.

Kirkland C.L, Smithies R.H, Taylor R.J.M, Evans N, McDonald B., 2015. Zircon Th/U ratios in magmatic environs. Lithos 212–215:397–414

Lin, X., Chang, H., Wang, K., Zhang, G., and Meng, G., 2020. Machine learning for source identification of dust on the Chinese Loess Plateau. Geophysical Research Letters, 47, e2020GL088950. https://doi.org/10.1029/2020GL088950

Miller C.F, Claiborne L.L, Gualda G.A.R, Padilla A.D, Thomas D, Carley T.L, Covey A.K., 2015. Improved partition coefficients for zircon/melt from in situ analysis of glass and crystal rims:

coherent behavior, strong temperature dependence. Geol Soc Am Abstracts with Programs. 47(7):278

Murphy, K.P., Machine Learning: A Probabilistic Perspective, 2012.The MIT Press, Cambridge, MA.

Ortega-Gutiérrez, F., Elías-Herrera, M., Morán-Zenteno, D.J., Solari, L., Weber, B., and Luna-González, L., 2018. The pre-Mesozoic metamorphic basement of Mexico, 1.5 billion years of crustal evolution: Earth Sci. Rev. 183, 2–37. doi.org/10. 1016/j.earscirev.2018.03.006

Ortega-Obregón, C., Solari, L., Gómez-Tuena, A., Elías-Herrera, M., Ortega-Gutiérrez, F., and Macías-Romo, C., 2014. Permian–Carboniferous arc magmatism in southern Mexico: U–Pb dating, trace element and Hf isotopic evidence on zircons of earliest subduction beneath the western margin of Gondwana. Int. J. Earth Sci. 103, 1287–1300. doi.org/10.1007/s00531-013-0933-1.

Petrelli, M., Bizzarri, R., Morgavi, D., Baldanza, A., Perugini, D., 2017. Combining machine learning techniques, microanalyses and large geochemical datasets for tephrochronological studies in complex volcanic areas: New age constraints for the Pleistocene magmatism of central Italy, Quaternary Geochronology, V40, P 33-44.

Petrelli, M., Perugini, D., 2016. Solving petrological problems through machine learning: the study case of tectonic discrimination using geochemical and isotopic data 171. doi:10.1007/s00410-016-1292-2

Prowatke S, Klemme S., 2005. Effect of melt composition on the partitioning of trace elements between titanite and silicate melt. Geochim Cosmochim Acta 69:695–709. doi:10.1016/j. gca.2004.06.037

Ross, C.A., 1986, Geological Society of America Bulletin Paleozoic evolution of southern margin of Permian basin: Geological Society of America Bulltin, v. 97, p. 536–554, doi: 10.1130/0016-7606(1986)97<536.

Ross, C., and Ross, J.R.P., 2009, Paleontology, a Tool To Resolve Late Paleozoic Structural and Depositional Histories: SEPM Special Publication, v.93, p. 93–110.

Rubatto D, Hermann J., 2007. Experimental zircon/melt and zircon/ garnet trace element partitioning and implication for the geochro- nology of crustal rocks. Chem Geol 241:38–61. doi:10.1016/j. chemgeo.2007.01.027

Tian, H., Fan, M., Valencia, V., Chamberlain, K., Waite, L., and Stern, R.J., 2022a. Mississippian Laurentian tuffs came from a northern Gondwana arc. Geology. doi.org/10.1130/G49502.1.

Tian, H., Fan, M., Victor, V., Chamberlain, K., Waite, L., Stern, R.J., Loocke, M.,2022b. Rapid early Permian tectonic reorganization of Laurentia's plate margins: Evidence from volcanic tuffs in the Permian Basin, USA, Gondwana Research, V.111, P. 76-94, https://doi.org/10.1016/j.gr.2022.07.003.

Trail D, Watson E.B, Tailby N.D., 2011. The oxidation state of Hadean magmas and implications for early Earth's atmosphere. Nature 480:79–82. doi:10.1038/nature10655

Vega-Granillo, R., Talavera-Mendoza, O., Meza-Figueroa, D., Ruiz, J., Gehrels, G.E., López-Martínez, M., and de La Cruz-Vargas, J.C., 2007. Pressure–temperature–time evolution of Paleozoic high-pressure rocks of the Acatlán Complex (southern Mexico): implications for the evolution of the Iapetus and Rheic Oceans. Geol. Soc. Am. Bull. 119, 1249–1264. doi.org/10.1130/B226031.1

Vega-Granillo, R., Calmus, T., Meza-Figueroa, D., Ruiz, J., Talavera-Mendoza, O., and López-Martínez, M., 2009. Structural and tectonic evolution of the Acatlán Complex, southern Mexico: its role in the collisional history of Laurentia and Gondwana. Tectonics 28, TC4008, doi.org/10.1029/2007TC002159.

Wahlman, G.P. 2013., Pennsylvanian to Lower Permian (Desmoinesian – Wolfcampian) fusulinid biostratigraphy of Midcontinent North America. Stratigraphy, v.10, p. 73-104.

Wardlaw, B.R., & Davydov, V.I., 2000, Preliminary Placement of the International Lower Permian

working Standard to the Glass Mountains, Texas. Permophiles, 36, 11-14.

Wardlaw, B.R., 2004, Correlation of the Cisuralian Stages to the North American Regional
Standard. Permophiles, 44, 13.

Wardlaw, B.R., & Nestell, M.K., 2014, The first appearance of Streptognathodus isolatus in the
Permian of Texas. Permophiles, v. 59, p. 17-19.

Zhao, J., Xiao, L., Gulick, S.P.S., Morgan, J.V., Kring, D., Fucugauchi, J.U., Schmieder, M., de Graaf,
S.J., Wittmann, A., Ross, C.H., Claeys, P., Pickersgill, A., Kaskes, P., Goderis, S., Rasmussen,
C., Vajda, V., Ferrière, L., Feignon, J., Chenot, E., Perez-Cruz, L., Sato, H., Yamaguchi, K.,
IODP-ICDP Expedition 364 scientists, 2020. Geochemistry, geochronology and petrogenesis
of Maya block granitoids and dykes from the Chicxulub impact crater, Gulf of México:
Implications for the assembly of Pangea. Gondwana Res. 82, 128–150.

Zúñiga, S.J., Solari, L.A., and Ortega-Obregón, C., 2020. Permian igneous clasts from the Matzitzi
Formation, southern Mexico: isotopic constraints on the final amalgamation of Pangea. Geol.
Soc. Lond. Spec. Publ. 503, 481-496. doi.org/10.1144/SP503-2019-238.

Appendix A

Supplemental Materials for Chapter 1

THE TUFFS

The Stanley tuffs are distributed in the Stanley Group (Fig. S1) and have been well described by Hill (1967), Niem (1977), Loomis et al. (1994), and Shaulis et al. (2012). The Beavers Bend and Hatton tuffs are in the same stratigraphic section; the lower and upper Mud Creek tuffs are in the same section; and the Chikasaw tuff is from a different section.

The Stanley tuffs have sharp lower and sharp or gradational upper contacts with shale (Niem, 1977). The lower four tuffs contain three main gradational lithologies, including a lower massive, pumiceous vitric-crystal tuff with a thin crystal-rich base, a middle bedded, pumiceous tuff, and an upper massive or bedded, fine-grained vitric tuff; the Chickasaw tuff contains only bedded vitric tuff (Niem, 1977). Phenocrysts of coarse sand-size and rip-up mud clasts up to cobble-size in the two lower units suggest these tuffs were deposited from submarine pyroclastic flows downslope from the volcano that erupted them, and the better-sorted upper unit suggests gradual setting of ashfall (Niem, 1977).

The Barnett tuff in the Permian Basin is thin, about 4-cm-thick, fine-grained, and shows sharp lower and diffusive upper contacts with shale, indicating settling of ashfall without major perturbations in the sedimentary system. The Barnett tuff was collected from a core in the center of Martin County in west Texas (Fig. S2A). The tuff resides in the lower Barnett Shale (Fig. DR 2B) based on correlation of gamma ray logs of the core and a type well (API: 42317345670000) adjacent to the core (Mauck et al., 2018). The Barnett tuff is about 4 cm thick and is orange under ultraviolet light (Fig. S2B).

ANALYTICAL METHODS AND RESULTS

Zircon separation and morphology

Zircon grains were separated following standard procedures, including disc mill crushing, ultrasonic shaking to remove attached clays on grains, pan washing, magnetic separation, and heavy

liquid concentration. All the zircon grains in the tuffs were handpicked under a binocular microscope for analysis. The grains are less than 250 □m, and generally euhedral and elongated (Fig. S3). Before mounting zircon grains in epoxy resin discs for geochemical analysis, over 30 grains of each sample were randomly selected and imaged using a Hitachi S3000N scanning electronic microscope (SEM) to characterize grain morphology. These grains were classified into five classes of roundness following Gärtner et al., (2013). The five classes include completely unrounded, poorly rounded, rounded, well rounded and completely rounded (Fig. S4A). Except for the upper Mud Creek tuff in the Stanley Group, more than 90% of the zircons in the other five tuffs are poorly rounded or unrounded, suggesting limited physical abrasions (Fig. S4B). The upper Mud Creek tuff has 22% of grains in the rounded and well-rounded categories.

All the zircon grains were then mounted in epoxy resin discs and polished. Representative grains were imaged using a SEM and cathodoluminescence (CL) to observe internal zoning structures and inclusions to determine spots for U-Pb age, Hf isotope analysis and rare earth element composition. Only euhedral grains were selected for analysis. Prismatic shape and internal oscillatory zoning suggest magmatic origin of grains, and small grains without oscillatory zoning likely resulted from rapid eruptive growth.

Zircon U-Pb dates and Hf isotopes by LA-ICPMS

Zircon U-Pb dates of the five Stanley tuffs and a portion of the Barnett tuff sample were measured at the Radiogenic Isotope and Geochronology Lab (RIGL) at Washington State University using an Analyte G2 193 excimer laser ablation system coupled with a Thermo-Finnigan Element 2 single-collector, inductively coupled, plasma mass spectrometer. The laser parameters were 25-35 µm in diameter spot size (depending on the size of the zircon grains), 10HZ repetition rate and ~5.5 J/cm^2. For the U-Pb measurement, we mostly followed the method of Chang et al. (2006), except for the use of the 193nm laser system instead of the 213nm laser. A 10-second blank measurement of the He and

Ar carrier gasses (Laser off) before each analysis followed by 250 scans across masses ^{202}Hg, ^{204}Pb+Hg, ^{206}Pb, ^{207}Pb, ^{208}Pb, ^{232}Th, ^{235}U and ^{238}U during ~30 second laser ablation period. Analyses of zircon unknowns and quality control zircon grains were interspersed with analyses of external calibration standards, typically with 10-12 unknowns bracketed by multiple analyses of two different zircon standards (Plešovice and FC-1). The Plešovice standard (337 Ma; Sláma et al., 2008) was used to calibrate the ^{206}Pb/^{238}U and ^{207}Pb/^{235}U dates, and the FC-1 standard (1099 Ma; Paces and Miller, 1993) was used for calibration of ^{207}Pb/^{206}Pb dates owing to its high-count rate for ^{207}Pb (~2-4 times higher than that of Plešovice). Zircon 91500 (1065 Ma; Wiedenbeck et al., 1995) and Temora2 (417 Ma; Black et al., 2004) were used as quality control standards. Data were processed offline using the Iolite software (Paton et al., 2011). Common Pb correction was performed using the ^{207}Pb method (Williams, 1998). Plots were calculated using Isoplot 4.16 (Ludwig, 2012). Zircon U-Pb data are reported in Table S   1   .

After the U-Pb analysis, Lu-Hf isotope compositions of selected zircon grains of the five tuffs were analyzed at the Washington State University using an Analyte G2 193nm excimer laser ablation system coupled with a Thermo-Finnigan Neptune multi-collector mass spectrometer. Because the laser beam used for this analysis was 35-40 μm in diameter, only larger zircon grains were selected for this analysis. The laser system parameters used were laser fluence of ~5.5 J/cm2 and repetition rate of 10 Hz. This study used the same instrument configuration, operating parameters and data reduction methods discussed by Fisher et al. (2014), with the exception that U-Pb dates were not simultaneously determined. In this "dedicated Hf" method, the output from the ablation cell was mixed with N_2 gas and delivered directly to the Neptune MC-ICPMS. To reduce inter-laboratory bias, the Plešovice zircon standard (^{176}Hf/^{177}Hf = 0.282482 ± 13, Sláma et al., 2008) was regularly analyzed between sample blocks and used to correct the measured ^{176}Hf/^{177}Hf of unknowns. Given the potentially large range of (Lu+Yb)/Hf in zircon samples, accurate correction for the isobaric interference of ^{176}Yb and ^{176}Lu on ^{176}Hf is imperative and should be assessed using quality control zircons interspersed with samples

(Fisher et al., 2014b). Over the course of this session, five analyses of the FC-1 zircon (^{176}Hf/^{177}Hf = 0.282184 ± 16, Woodhead and Hergt, 2005) yielded a ^{176}Hf/^{177}Hf of 0.282186 ± 44 (2SD), ten analyses of the Temora-2 zircon (^{176}Hf/^{177}Hf = 0.282686 ± 8, Woodhead and Hergt, 2005) yielded a ^{176}Hf/^{177}Hf of 0.282694 ± 38(2SD), and fourteen analyses of the 91500 zircons (S-MC-ICPMS ^{176}Hf/^{17}7Hf = 0.282306 ± 8, Blichert-Toft, 2008) yielded a ^{176}Hf/^{177}Hf of 0.282305 ± 40 (2SD). Analyses of these quality control zircons agree well with published MC-ICPMS isotope compositions of purified Hf from these zircons, attesting to the accuracy of the interference correction methods employed.

Internal 2-sigma precision was typically ~1.1 εHf. Analyses with less than 25 ratios, and/or internal 2-sigma uncertainty over 2 εHf units were discarded and not presented here. Present day εHf values were calculated using the CHUR parameters reported by Bouvier et al. (2008). Zircon Lu-Hf data are reported in Table S2.

The U-Pb dates and Lu-Hf isotopic compositions of the remaining Barnett tuff zircons were analyzed using a laser ablation split stream (LASS) approach in which U-Pb dates and Lu-Hf isotopic compositions were determined simultaneously by coupling the single New Wave 213nm laser ablation system with the two mass spectrometers. The ablated particles were evacuated from the sample cell in a single piece of tubing, which was then split downstream into two separate paths using a ''Y'' connection. Each tube was attached to an individual mass spectrometer and the separated components were analyzed for different compositions concurrently. Zircon grains with fractures or small grains (less than 40 μm) were excluded from analysis. The experimental procedures follow Fisher et al. (2014). The U-Pb and Lu-Hf data of the Barnett tuff are reported in Tables S1&2.

Errors of zircon U-Pb dates and εHf values are both reported as 2σ standard deviation. ^{207}Pb/^{206}Pb dates were interpreted for grains older than 1200 Ma and ^{206}Pb/^{238}U dates were interpreted for grains younger than 1200 Ma. Filters of 10% discordance and a 5% reverse discordance were applied to zircons over 500 Ma to exclude grains that may have been influenced by Pb loss or poor matrix match between samples and standards (Fig. S5). Grains less than 500 Ma were not filtered by

discordance because young ICPMS dates have large $^{207}Pb/^{235}U$ uncertainty. Age plots were conducted using the Isoplot software (Ludwig, 2008) and the DZstat software (Saylor and Sundell, 2016).

Zircon U-Pb date of the Barnett tuff by CA-ID-TIMS

After the U-Pb and Lu-Hf analyses, seven zircons in the youngest group of the Barnett tuff were analyzed by chemical abrasion, isotope dilution, thermal ionization mass spectrometry (CA-ID-TIMS) at the University of Wyoming. These grains were plucked from the epoxy mount after LA-ICP analysis and selected to test whether the range of dates from LA-ICP was robust or was an artifact of Pb loss and matrix mismatch. Zircon dissolution and chemistry were adapted from methods developed by Parrish et al. (1987) and Mattinson (2005). Zircon grains were chemically abraded by annealing them for 50 hours at 850°C and partially dissolving them in HF and HNO_3 acids for 12 hours at 180°C. Single zircon grains were then spiked with a mixed $^{205}Pb/^{233}U/^{235}U$ tracer (ET535), dissolved in HF and HNO_3 at 235 °C for 30 hours, and converted to chlorides at 180 °C for 16 hours. Dissolved zircon samples were loaded onto single rhenium filaments with silica gel and H_3PO_4 without any further chemical processing. Isotopic compositions were measured on a Micromass Sector 54 mass spectrometer in single-collector, peak-switching mode using the Daly-photomultiplier collector for all isotopes. Mass discrimination of 0.25 ± 0.10 %/amu for Pb was determined by replicate analyses of NIST SRM 981. UO_2 fractionation was determined internally and corrected for oxide interference. Pb blank averaged <1 pg for zircons. Isotopic composition of the Pb blank was measured as 18.572±0.39, 15.731±0.43, and 38.380±0.97 for $^{206}Pb/^{204}Pb$, $^{207}Pb/^{204}Pb$ and $^{208}Pb/^{204}Pb$, respectively. U blanks were consistently less than 0.01 pg. Concordia coordinates, intercepts, and uncertainties were calculated using PBMacDAT and ISOPLOT programs (based on Ludwig 1988, 1991); initial Pb isotopic compositions were estimated from the Stacey and Kramers (1975) model. $^{206}Pb/^{238}U$ and $^{207}Pb/^{206}Pb$ ratios and dates were corrected for Th-disequilibrium after Schärer (1984) assuming a magma Th/U of 2.2. The decay constants used by PBMacDAT and ISOPLOT are those recommended by the I.U.G.S.

Subcommission on Geochronology (Steiger and Jäger, 1977), including 0.155125 x 10^{-9}/yr for ^{238}U, 0.98485 x 10^{-9}/yr for ^{235}U and 137.88 for present-day ^{238}U/^{235}U ratio. Precision of the weighted mean ^{206}Pb/^{238}U date is reported in the ±X/Y/Z format of Schoene et al., (2006), with X as the analytical uncertainty (95% confidence), Y includes tracer calibration uncertainties for comparisons to other U-Pb dates, and Z includes U decay uncertainties for comparison to dates from other systems as long as the uncertainties of those dates have been fully propagated. Zircon U-Pb data of the CA-ID-TIMS analyses are reported in Table S3.

Youngest mode weighted mean date

Many detrital zircon studies have been conducted to evaluate methods of the maximum depositional ages using LA-ICPMS dates (e.g., Spencer et al., 2016; Coutts et al., 2019; Herriot et al., 2019). We modified the youngest statistical population (YSP) approach from Coutts et al. (2019) which selects the negative tail of the youngest population of LA-ICPMS dates (>= 2) and calculates the weighted mean of their dates with a mean square weighted deviation (MSWD) near 1. A recent study of Jurassic volcaniclastic strata in Alaska shows that the YSP approach yields the best coincidence with CA-ID-TIMS dates (Herriot et al., 2019). Because our samples are volcanic tuffs, the youngest dominant population, which is the YSP, should be from a single eruptive event. We calculate the age of each tuff using the mode of YSP in the kernel density estimation (KDE) plot (Fig. 2A). The age was calculated as the weighted mean of more than three grains overlapping at 2σ and has a mean square weighted deviation (MSWD) near 1. This method excludes ICPMS dates at both tails of the distribution that do not overlap at 2σ with the mode. These scattered dates typically reflect Pb loss, matrix effect-related bias, and inheritance of grains from the magma source (e.g., Schaltegger et al., 2015).

Our youngest mode weighted mean date of the Barnett tuff matches the CA-ID-TIMS date well, indicating that this approach yields accurate tuff ages. Our youngest mode dates of the Beavers Bend, Lower Mud Creek, and Chickasaw tuffs are consistent with the results from Shaulis et al., (2012)

using the same statistical approach, but produced higher precision (Table DR5). Our method dates the Hatton tuff to 317.4 ±0.5 Ma (n = 48), which is younger than the date (324.8 ±2.5 Ma; n = 9) reported in Shaulis et al. (2012). The Hatton tuff date is also younger than the lower Mud Creek and Chickasaw tuff dates. These differences suggest either that the earlier stratigraphy is incorrect and the Hatton tuff is the youngest Stanley tuff, or that there are minor unresolved age biases in some of these data sets.

Dates older than 350 Ma

In all tuffs, grains older than 350 Ma are mostly clustered at 350-500 Ma, 500-850 Ma, 900-1300 Ma, and 1300-1600 Ma (Fig. S6). The zircon ICPMS dates of the upper Mud Creek tuff cluster at <330 Ma (4%), 350-500 Ma (49%), 500-850 Ma (7%), 900-1300 Ma (27%) and 1300-1600 Ma (13%). The composite U-Pb data of the other four Stanley tuffs are mostly <350 Ma (91%) with a few grains in the other clusters, including 350-500 Ma (3%), 500-850 Ma (2%), and 900-1300 Ma (4%). The Barnett tuff also has abundant grains <350 Ma (68%), with other grains in the clusters of 350-500 Ma (6%), 500-850 Ma (6%), 900-1300 Ma (15%) and 1300-1600 Ma (2%).

Zircon Rare Earth Element Analyses

Zircons large enough to accommodate another laser ablation spot were selected for rare earth element analysis at the Washington State University using the same LA-ICP-MS instrument used for Lu-Hf isotope analysis. New laser spots were placed within the same zone for U-Pb and Lu-Hf isotope analyses. Each analysis consists of two cleaning pulses, followed by 10 seconds of washout, 18 seconds of gas blank, and 40 seconds ablation time followed by 15 seconds of waiting time before moving the stage. Three standards, including NIST610 and NIST612 (both are synthetic glass standards) and zircon reference 91500, were dispersed every 15 analyses. Correction and data reduction were carried out using the Iolite Software (Woodhead et al, 2007). The trace element analytical data are summarized in Figure S7 and reported in Table S4.

DISCUSSION OF OLD GRAINS

The upper Mud Creek tuff has 22% of grains in the rounded and well-rounded categories (Fig. DR4), suggesting physical abrasion through sediment transport. The sample has only three grains < 330 Ma suggesting that the tuff contains detrital grains in the depositional system and possibly inherited grains from the magma source. About 50% of the grains are in the 350-500 Ma group, which is significantly more than those in sandstone of the Stanley Group (Fig, DR6; Prine, 2020). Grains of these ages are both abundant in upper Paleozoic in the Appalachian foreland on Laurentia, representing the Acadia and Taconic orogenies (e.g., Thomas et al., 2017), and in Mexico that was on Gondwana during the late Paleozoic, such as the part of the Mississippian Santa Rosa Formation in southeastern Mexico (Weber et al., 2009) and magmatism of 410-370 Ma in the Acatlan Complex, southern Mexico (Yañez et al., 1991). Although Paleozoic grains have been suggested to be transported from the Appalachians into the Arkoma shelf by a large transcontinental river (e.g., Wang and Bidgoli, 2019), the age distribution of the upper Mud Creek tuff is very different from that of the Stanley sandstone that is representative to the zircon age signature of the deep-water depositional environment in Laurentia margin. Therefore, Paleozoic grains in the upper Mud Creek tuff were most likely recycled from the approaching peri-Gondwana terranes and/or inherited from the inferred Gondwana arc. The other four Stanly tuffs, including the Beavers Bend, Hatton, lower Mud Creek and Chickasaw tuffs, have only <10% grains older than 350 Ma that are detrital and/or inherited.

Both the Barnett and four Stanley tuffs have old grains clustered at 350-500 Ma, 500-850 Ma, and 900-1300 Ma. The 900-1300 Ma zircons were ultimately from the Grenville basement that was distributed in the Appalachians and western Texas on Laurentia, and in Peri-Gondwana terranes (e.g., Lopez et al., 2001; Thomas et al., 2017). The 500-850 Ma zircons are characteristic of Peri-Gondwana or Gondwana source as these grains were ultimately from the Pan-African and Brasiliano orogeny on Gondwana (e.g., Weber et al., 2009). Given that Laurentia-Gondwana collision had not extended to

Texas during the Mississippian, the presence of 500-850 Ma age group in these tuffs suggests that some, if not all, of the old grains in the tuffs were most likely inherited from the inferred Gondwana arc.
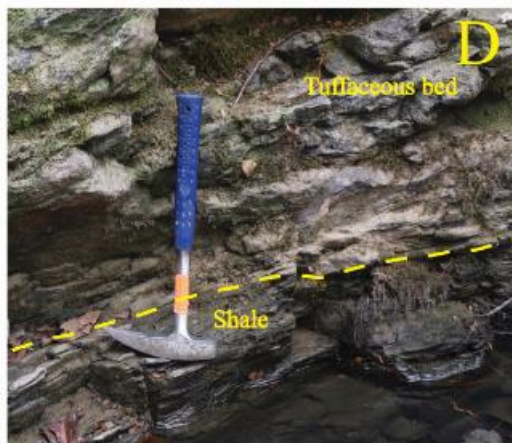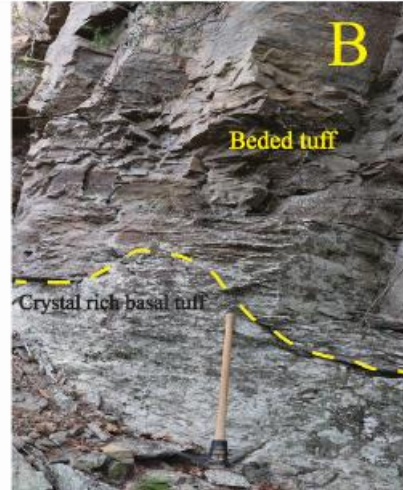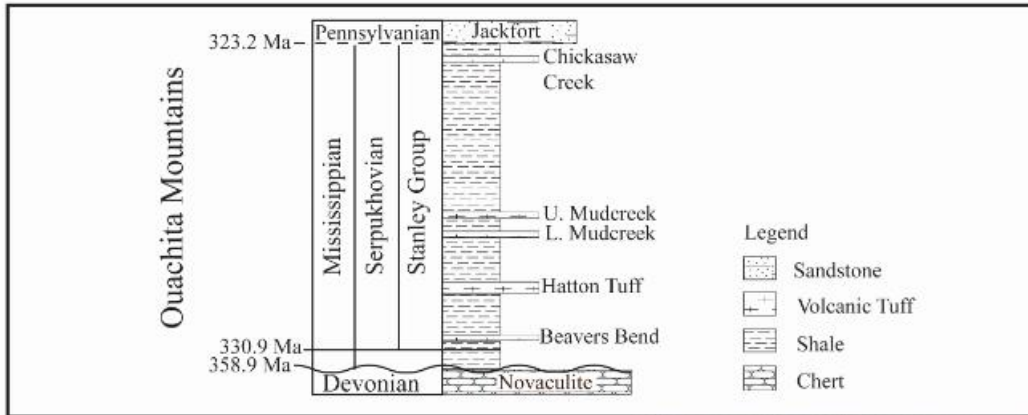
Figure S2-1. Stratigraphic column of the Stanley Group in the Ouachita Mountains showing the stratigraphic levels of the five studied tuffs (modified after Shaulis et al., 2012) and field photos of the tuffs. A). The Beavers Bend tuff (34.135064, -94.676459); B). The Hatton tuff (34.135056, -94.676472); C). The lower Mud Creek tuff (34.313572, -94.820431); and D). The Chickasaw Creek tuff (34.73169, -93.35568). Note that the upper Mud Creek tuff was collected at the same location as the lower Mud Creek tuff.

A

Permian Basin
● Type Well
★ Well with Barnett tuff

B

Gamma Ray

Upper Barnett Shale

Lower Two Finger Sand

Lower Barnett Shale

Barnett tuff
11700 feet

Type log
Studied Log with the Barnett tuff

Barnett tuff under UV light

4 cm
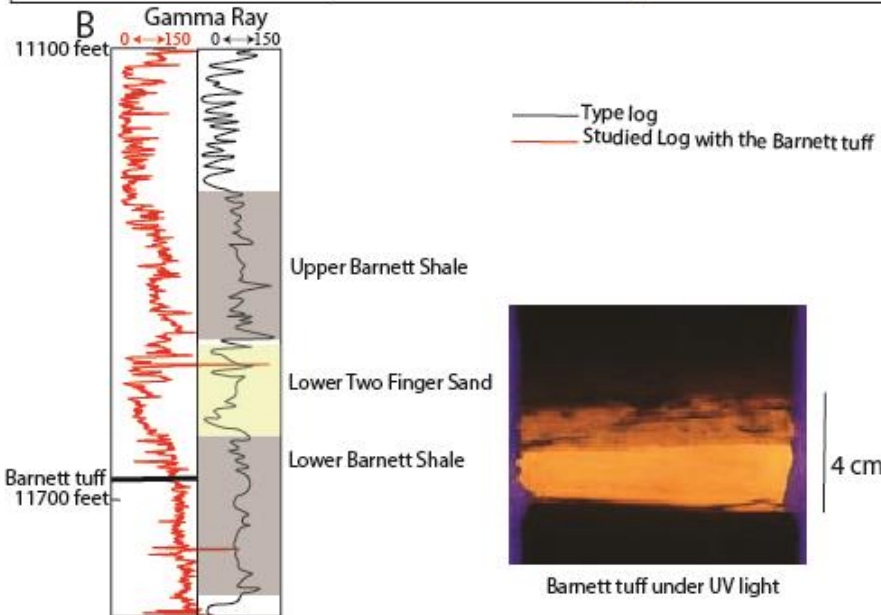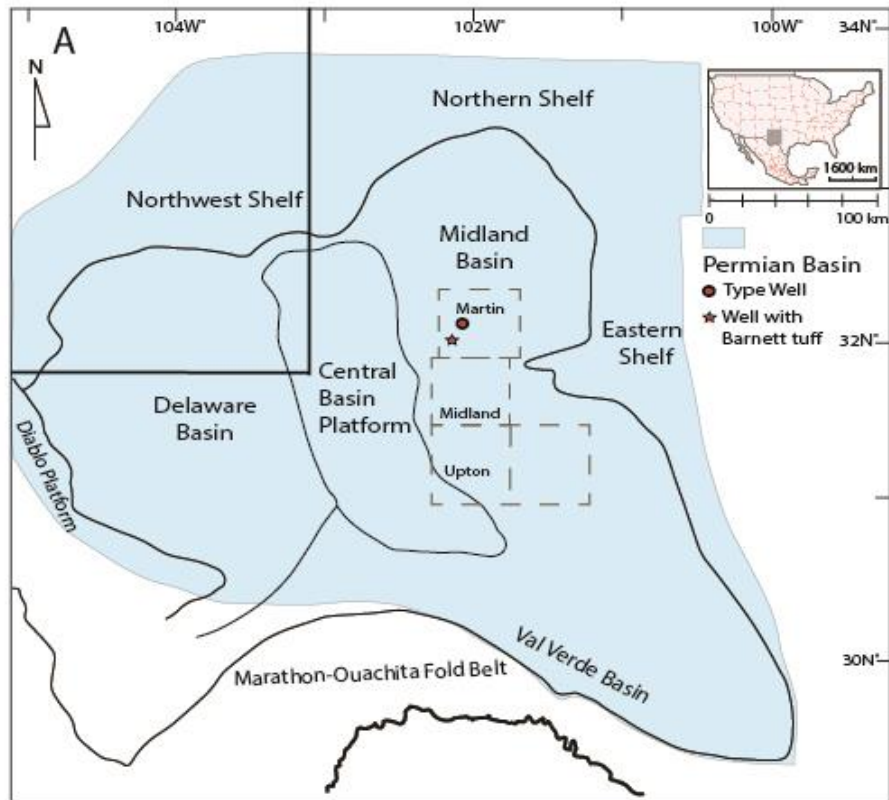
Figure S2-2. A) Locations of the Midland Basin in west Texas and our studied core and the type log in Martin County. B) Gamma ray log correlation of our studied core containing the Barnett tuff and the type log in Mauck et al. (2018). Note that the sharp lower boundary and diffusive upper boundary of the Barnett tuff in our studied core. The tuff is not recognized in the type log.
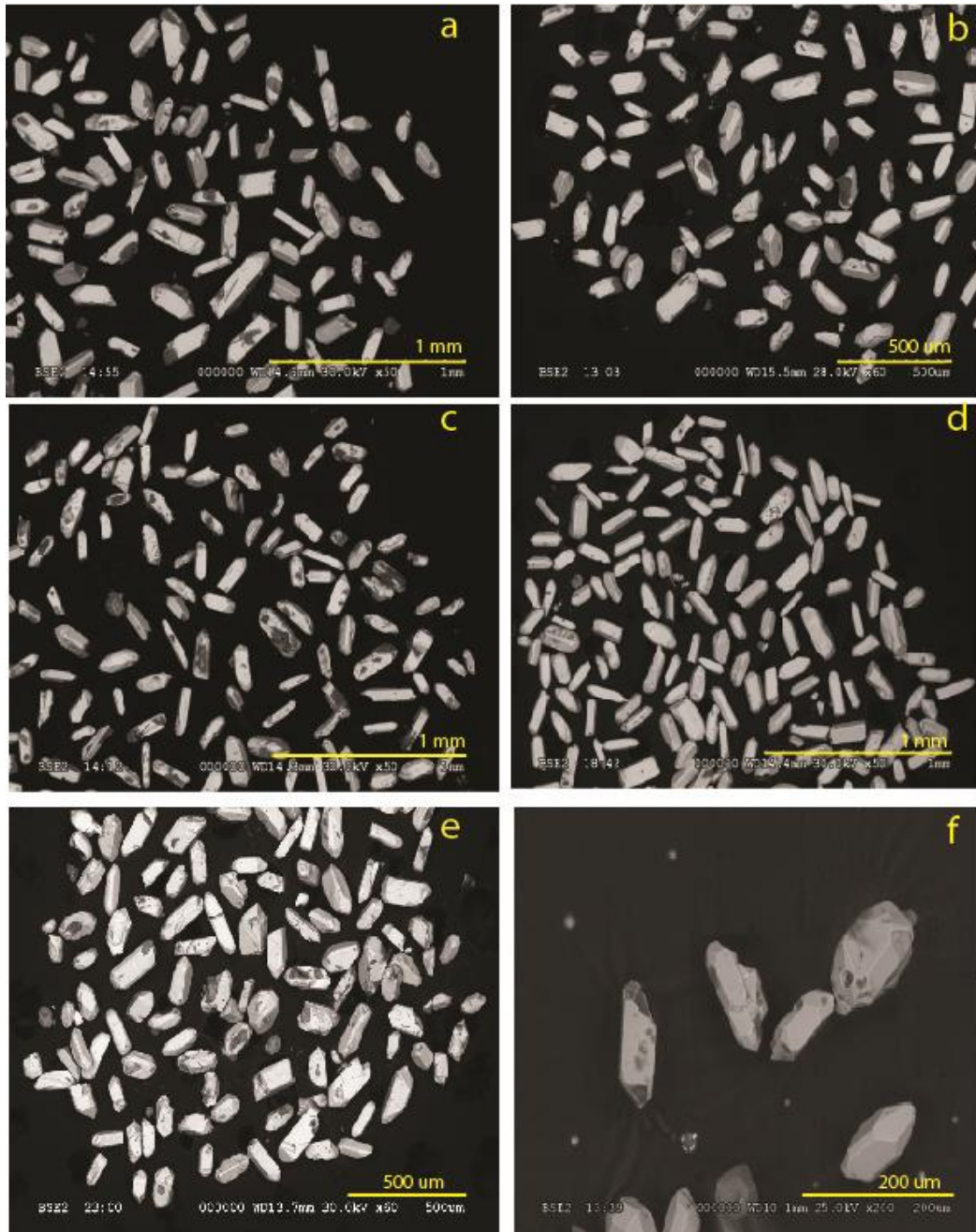
Figure S2-3. Scanning Electron Microscope images of the zircons from the Stanley tuffs and the Barnett tuff. A. Beavers Bend tuff; B) Hatton tuff, C) Lower Mud Creek tuff; D) Upper Mud Creek tuff; E) Chickasaw Creek tuff; and F) Barnett tuff.
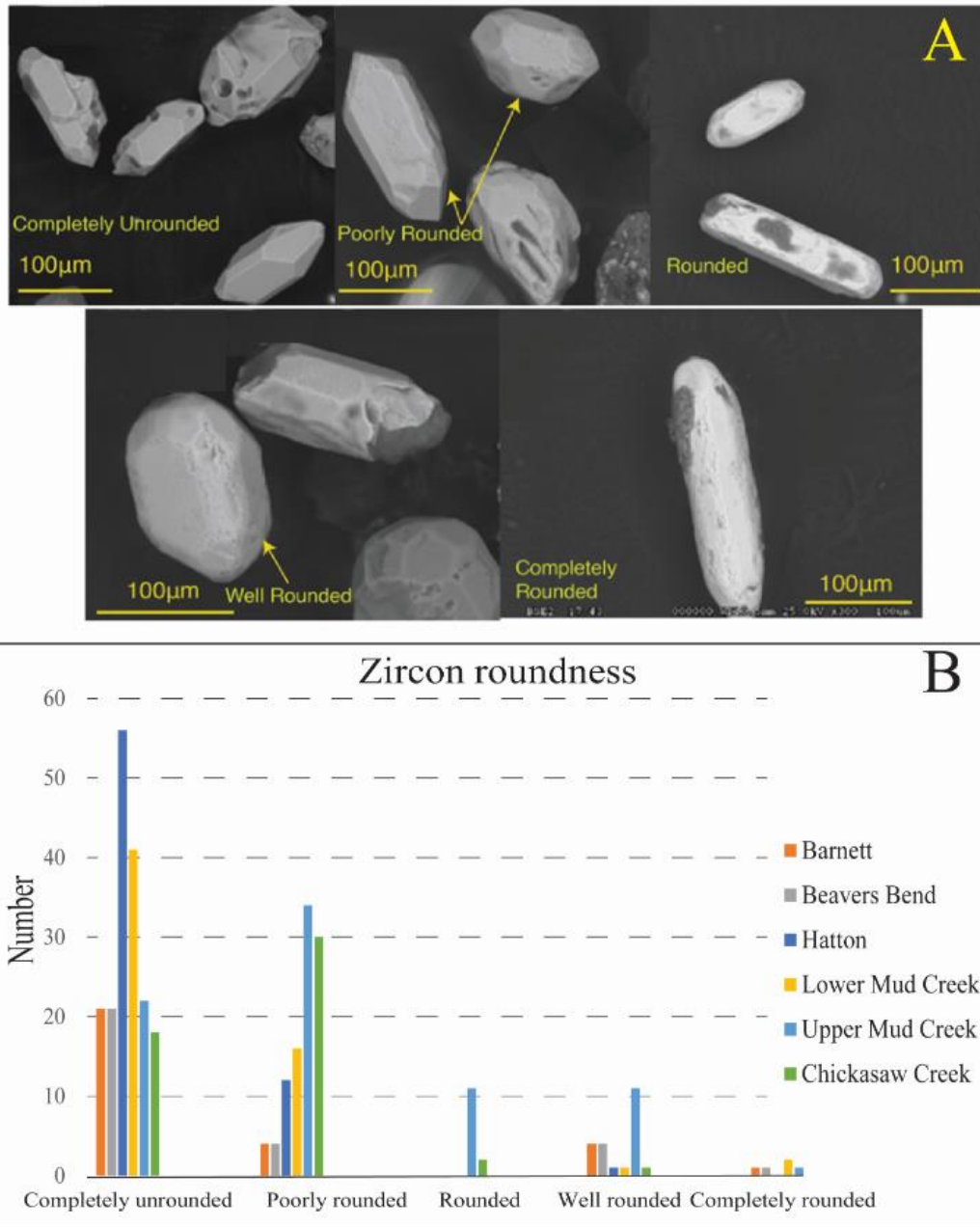
Figure S2-4. A) Pictures of representative grains for five roundness categories. B) Plot shows roundness data for zircons from all the tuffs. Note that zircons that are rounded, well rounded and completely rounded were filtered out for dating.

119
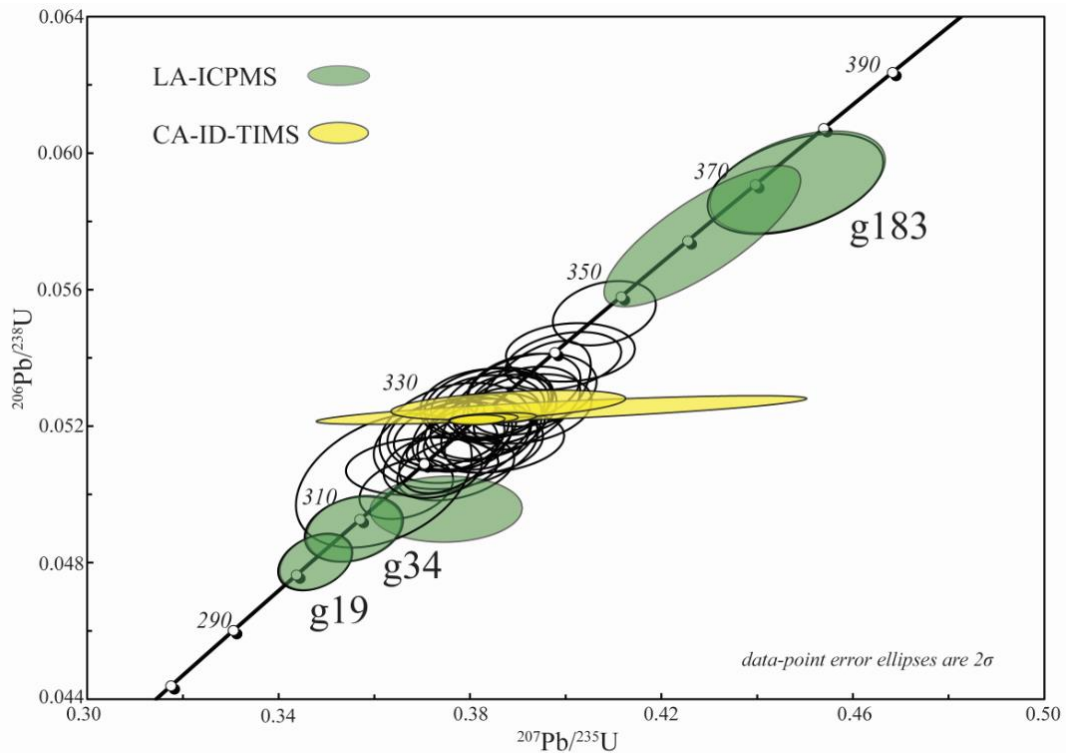
Figure S2-5. Concordia plot for LA-ICPMS dates vs. CA-ID-TIMS dates for the Barnett tuff. Grains that produced the green-filled ellipses were plucked from the ICP mount and analyzed by CA-ID-TIMS (yellow ellipses), thereby directly comparing the two dating methods. The observation that all the CA-ID-TIMS dates form a single tight cluster strengthens our confidence that the ages of the zircons are ca. 328 Ma and that the variation within the LA-ICPMS dates is due to either Pb loss (g19, g34, and all others that are younger than the TIMS dates) or matrix mismatch, which can produce dates that are anomalously old (e.g., Schaltegger et al., 2015; g183 and the others that are older than the TIMS dates). The YSP of the LA-ICPMS date is 327 Ma despite the large overall variation. The agreement between YSP from the LA-ICPMS date and the CA-ID-TIMS date in this sample adds to evidence from other direct comparative studies of the two methods (e.g., Herriott et al., 2019; Coutts et al., 2019) and supports interpreting the YSPs as the best estimates for MDAs from LA-ICPMS data.
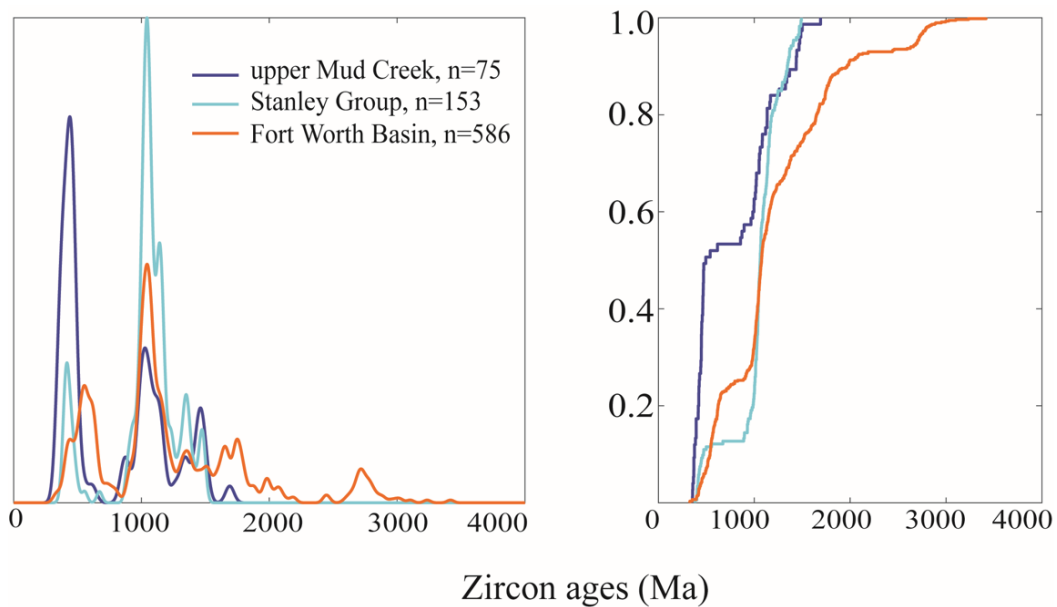
Figure S2-6. Zircon age KDE plots and cumulative distribution function plots for the upper Mud Creek tuff, Late Mississippian sandstone in the Stanley Group (Prine, 2020) and Middle Pennsylvanian sandstone in the Fort Worth Basin in northern Texas (Alsalem et al., 2018).
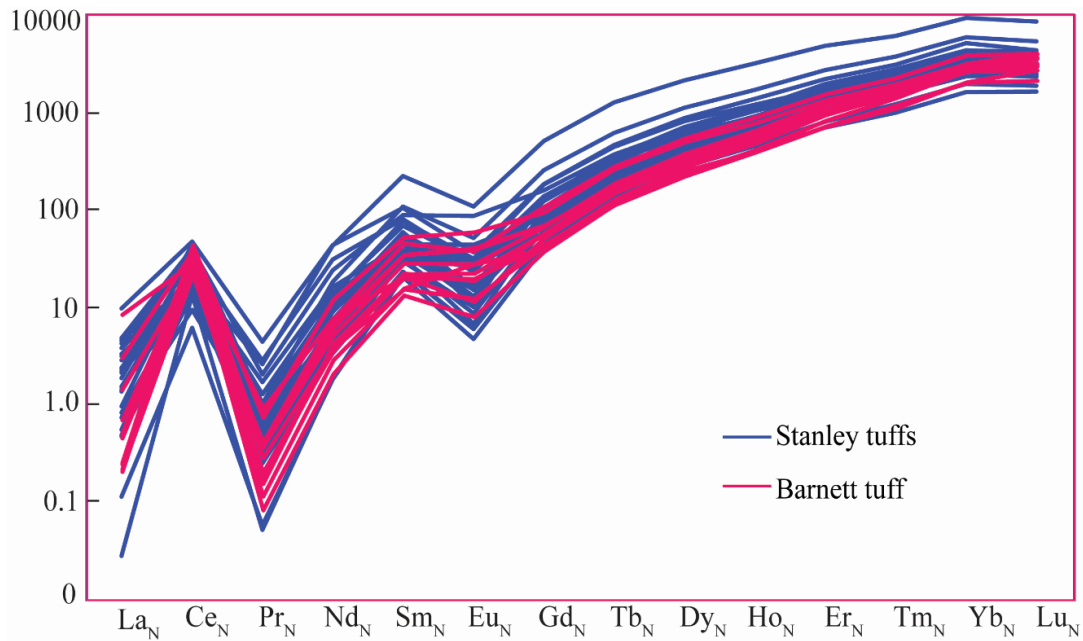
Figure S2-7. Zircon REE patterns normalized to Chondrite after McDonough and Sun (1995).

References

Alsalem, O.B., Fan, M., Zamora, J., Xie, X. and Griffin, W.R., 2018, Paleozoic sediment dispersal before and during the collision between Laurentia and Gondwana in the Fort Worth Basin, USA: Geosphere, v. 14, p. 325–342.

Black, L.P., Kamo, S.L., Allen, C.M., Davis, D.W., Aleinikoff, J.N., Valley, J.W., Mundil, R., Campbell, I.H., Korsch, R.J., Williams, I.S., and Foudoulis, C., 2004, Improved Pb-206/U-218 microprobe geochronology by the monitoring of a trace-element-related matrix effect; SHRIMP, ID-TIMS, ELA-ICP-MS and oxygen isotope documentation for a series of zircon standards: Chemical Geology, v. 205, p. 115-140.

Blichert-Toft, J., 2008, The Hf isotopic composition of zircon reference material 91500: Chemical Geology, v. 253, p. 252-257.

Bouvier, A., Vervoort, J.D., Patchett, P.J., 2007, The Lu-Hf and Sm-Nd isotopic composition of

      CHUR: constraints from unequilibrated chondrites and implications for the bulk composition

      of terrestrial planets: Earth and Planetary Science Letters, v 219, p. 311.

Chang, Z., Vervoort, J.D., McClelland, W.C., and Knaack, C., 2006, U-Pb dating of zircon by LA-

      ICP-MS: Geochemistry, Geophysics, Geosystems, v.7, p.1-14, doi: 10.1029/2005GC001100.

Coutts, D.S., Matthews, W.A., and Hubbard, S.M., 2019, Assessment of widely used methods to

      derive depositional ages from detrital zircon populations: Geosci-ence Frontiers, v.10, no. 4,

      p.1421–1435, https://doi .org/10.1016/ j.gsf.2018.11.002.

Fisher, C.M., Hanchar, J.M., Samson, S.D., Dhuime, B., Blichert-Toft, J., Vervoort, J.D., and Lam,

      R., 2011, Synthetic zircon doped with hafnium and rare earth elements_ A reference material

      for in situ hafnium isotope analysis _ Elsevier Enhanced Reader.pdf: chemica, v. 286, p.32–

      47.

Fisher, C.M., Vervoort, J.D., and Dufrane, S.A., 2014, Accurate Hf isotope determinations of

      complex zircons using the "laser ablation split stream" method: Geochemistry, Geophysics,

      Geosystems, v. 15, p.121–139, doi: 10.1002/2013GC004962.

Herriott, T. M., Crowley, J. L., Schmitz, M. D., Wartes, M. A., & Gillis, R. J. (2019). Exploring the

      law of detrital zircon: LA-ICP-MS and CA-TIMS geochronology of Jurassic forearc strata,

      Cook Inlet, Alaska, USA: Geology, v. 47, p.1044–1048, https://doi.org/10.1130/G46312.1

Hill, J.G., 1967, Sandstone petrology and stratigraphy of the Stanley Group (Mississippian), southern

      Ouachita Moutains, Oklahoma [PhD thesis]: Madison, University of Wisconsin, 106 p.

Loomis, J., Weaver, B., and Blatt, H., 1994, Geochemistry of Mississippian tuffs from the Ouachita

      Mountains, and implications for the tectonics of the Ouachita Orogen, Oklahoma and

      Arkansas: Geological Society of America Bulletin, v. 106, p. 1158–1171, doi: 10.1130/0016-

7606(1994)106<1158:GOMTFT>2.3.CO;2.

Lopez, R., Cameron, K.L., Jones, N.W., 2001, Evidence for Paleoproterozoic, Grenvillian, and Pan-African age Gondwanan crust beneath northeastern Mexico, Precambrian Research, v. 107, p.195-214, https://doi.org/10.1016/S0301-9268(00)00140-6.

Ludwig, K.R., 2008, User's Manual for Isoplot 3.70: Berkeley Geochronology Center Special Publication, p.76.

Ludwig, K.R., 1988, PBDAT for MS-DOS, a computer program for IBM-PC compatibles for processing raw Pb-U-Th isotope data, version 1.24: U.S. Geological Survey, Open-File Report 88-542, 32 pp.

Ludwig, K.R., 1991, ISOPLOT for MS-DOS, a plotting and regression program for radiogenic-isotope data, for IBM-PC compatible computers, version 2.75: U.S. Geological Survey, Open-File Report 91-445, 45 pp.

Mauck, J.V., Loucks, R.G., Entzminger, D.J., 2018, Stratigraphic Architecture, Depositional Systems, and Lithofacies of the Mississippian Upper Barnett Two Finger Sand Interval, Midland, Basin, Texas: Gulf Coast Association of Geological Societies. v.7, p.21-45, doi: 10.26153/tsw/9455.

McDonough, William & Sun, S.S., 1995, The composition of the Earth: Chemical Geology,v.67, p.1050- 1056.

Mattinson, J.M, 2005, Zircon U-Pb chemical abrasion ("CA-TIMS") method: combined annealing and multi-step partial dissolution analysis for improved precision and accuracy of zircon ages: Chemical Geology, v.220, p.47-66.

Niem, A.R., 1977, Mississippian pyroclastic flow and ash-fall deposits in the deep-marine Ouachita flysch basin, Oklahoma and Arkansas: Geological Society of America Bulletin, v.88, p.49–

61.

Paces, J.B., and Miller Jr, J.D., 1993, Precise U-Pb ages of Duluth Complex and related mafic
intrusions, northeastern Minnesota: Geochronological insights to physical, petrogenetic,
paleomagnetic, and tectonomagmatic processes associated with the 1.1 Ga Midcontinent Rift
System: Journal of Geophysical Research, v. 98, p. 13997-14013.

Paton, C., Hellstrom, J., Paul, B., Woodhead, J. and Hergt, J., 2011. Iolite: Freeware for the
visualisation and processing of mass spectrometric data: Journal of Analytical Atomic
Spectrometry, v.26, p. 2508-2518.

Parrish, R.R., Roddick, J.C., Loveridge, W.D., and Sullivan, R.D., l987, Uranium-lead analytical
techniques at the geochronology laboratory, Geological Survey of Canada, in Radiogenic age
and isotopic studies, Report 1: Geological Survey of Canada Paper 87-2, p.3–7.

Prines, S.T., 2020, U-Pb Detrital Zircons of the Syn-orogenic Carboniferous Deep-water Clastic
Deposits in the Ouachita Mountains, Arkansas, United States [M.S. Thesis]: Texas Christian
University, 80 p.

Saylor, J.E. and Sundell, K.E., 2016, Quantifying comparison of large detrital geochronology data
sets: Geosphere, v.12, p.203-220.

Schaltegger, U., Schmitt, A.K., Sciences, S., Angeles, L., Survey, B.G., and Schaltegger, U.,
2015, U-Th-Pb zircon geochronology by ID-TIMS , SIMS , and laser ablation ICP-MS :
recipes , interpretations , and opportunities: Chemical Geology, v. 402, p. 89–110,
doi: https:// doi .org/10.1016/ j.chemgeo.2015.02.028.

Schoene, B., Crowley, J.L., Condon, D.J., Schmitz, M.D. and Bowring, S.A., 2006. Reassessing the
uranium decay constants for geochronology using ID-TIMS U–Pb data: Geochimica et
Cosmochimica Acta, *70*(2), pp.426-445.

Sláma, J., Košler, J., Condon, D.J., Crowley, J.L., Gerdes, A., Hanchar, J.M., Horstwood, M.S.A., Morris, G.A., Nasdala, L., Norberg, N., Schaltegger, U., Schoene, B., Tubrett, M.N., and Whitehouse, M.J., 2008, Plešovice zircon — A new natural reference material for U–Pb and Hf isotopicmicroanalysis: Chemical Geology v. 249, p. 1-35.

Stacey, J.S. and Kramers, J.D., 1975, Approximation of terrestrial lead isotope evolution by a two-stage model: Earth and Planetary Science Letters, v. 26, p.207–221.

Steiger, R.H. and Jäger, E., 1977, Subcommission on geochronology: convention on the use of decay constants in geo- and cosmochronology: Earth and Planetary Science Letters, v. 36, p.359-362.

Thomas, W.A., Gehrels, G.E., Greb, S.F., Nadon, G.C., Satkoski, A.M., and Romero, M.C., 2017, Detrital zircons and sediment dispersal in the Appalachian foreland: Geosphere, v. 13, no. 6, p. 2206–2230, doi:10.1130/GES01525.1.

Wang, W., and Bidgoli, T., 2019, Detrital Zircon Geochronologic Constraints on Patterns and Drivers of Continental-Scale Sediment Dispersal in the Late Mississippian: Geochemistry, Geophysics, Geosystems. v.20, p. 5522-5543, 10.1029/2019GC008469.

Weber, B., Valencia, V.A., Schaaf, P., and Ortega-Gutiérrez, F., 2009, Detrital zircon ages from the Lower Santa Rosa Formation, Chiapas: Implications on regional Paleozoic stratigraphy: Revista Mexicana de Ciencias Geológicas, v. 26, no. 1, p. 260–276.

Wiedenbeck, M., Allé, P., Corfu, F., Griffin, W.L., Meier, M., Oberli, F., Von Quadt, A., Roddick, J.C., and Spiegel, W., 1995, Three natural zircon standards for U-Th-Pb, Lu-Hf, trace element and REE analyses: Geostandards Newsletters, v. 19, p. 1-23.

Williams, I.S., 1998, U-Th-Pb geochronology by ion microprobe: M.A. McKibben, W.C. Shanks III,

      W.I. Ridley (Eds.), Applications of Microanalytical Techniques to Understanding

      Mineralizing Processes: Reviews in Economic Geology, v. 7, p. 1-35.

Woodhead, J. and Hergt, J., 2007, A Preliminary Appraisal of Seven Natural Zircon Reference

      Materials for In Situ Hf Isotope Determination: Geostandards and Geoanalytical Research,

      v.29, p.183-195.

Table S2-1. Zircon U-Pb geochronologic analyses by Laser-Ablation Multicollector Inductively Coupled Plasma Mass Spectrometry

Sample ID	U ppm	U/Th	Pb 207 Corrected $^{207}Pb/^{235}U$	2s Abs Error	$^{206}Pb/^{238}U$	2s Abs Error	Corr. Coef.	Non Corrected $^{238}U/^{206}Pb$	2s Abs Error	$^{207}Pb/^{206}Pb$	2s Abs Error
Beavers Bend											
Beavers Bend-1	251	2.0	0.3780	0.0190	0.0494	0.0010	0.188	20.1613	0.4065	0.0555	0.0026
Beavers Bend-2	381	1.7	0.3750	0.0081	0.0495	0.0008	0.351	20.1491	0.3288	0.0550	0.0012
Beavers Bend-3	164	2.7	0.4215	0.0160	0.0518	0.0009	0.215	19.1424	0.3151	0.0590	0.0022
Beavers Bend-4	204	1.7	0.3923	0.0084	0.0531	0.0007	0.325	18.8182	0.2337	0.0536	0.0011
Beavers Bend-5	279	1.6	0.3764	0.0063	0.0482	0.0005	0.331	20.6313	0.2299	0.0567	0.0010
Beavers Bend-6	98	4.7	1.8373	0.0360	0.1740	0.0019	0.251	5.7241	0.0623	0.0766	0.0015
Beavers Bend-7	651	1.9	0.5812	0.0075	0.0741	0.0009	0.495	13.4825	0.1545	0.0569	0.0007
Beavers Bend-8	144	2.6	0.4046	0.0097	0.0521	0.0007	0.571	19.0949	0.2589	0.0563	0.0011
Beavers Bend-9	153	1.8	0.3998	0.0110	0.0521	0.0006	0.102	19.1351	0.2050	0.0557	0.0017
Beavers Bend-10	263	1.2	0.3979	0.0110	0.0522	0.0008	0.189	19.0949	0.2990	0.0553	0.0016
Beavers Bend-11	239	2.2	0.3917	0.0130	0.0526	0.0012	0.224	18.9753	0.4321	0.0540	0.0019
Beavers Bend-12	68	1.6	1.8125	0.0390	0.1772	0.0024	0.344	5.6433	0.0764	0.0742	0.0016
Beavers Bend-13	357	4.7	0.5662	0.0089	0.0736	0.0009	0.341	13.5962	0.1627	0.0558	0.0009
Beavers Bend-14	242	1.3	0.3792	0.0093	0.0498	0.0008	0.219	19.9960	0.3199	0.0552	0.0014
Beavers Bend-15	320	1.1	0.4570	0.0088	0.0487	0.0007	0.407	20.1248	0.2673	0.0681	0.0012
Beavers Bend-16	242	1.8	0.3983	0.0091	0.0507	0.0005	0.135	19.6155	0.2078	0.0570	0.0014
Beavers Bend-17	285	1.3	0.3993	0.0080	0.0525	0.0007	0.455	19.0006	0.2491	0.0552	0.0010
Beavers Bend-18	180	1.2	0.3978	0.0110	0.0488	0.0009	0.260	20.3335	0.3597	0.0592	0.0017
Beavers Bend-19	1108	0.6	0.4007	0.0085	0.0519	0.0006	0.224	19.1865	0.2061	0.0560	0.0012
Beavers Bend-20	476	1.1	0.3752	0.0064	0.0500	0.0005	0.334	19.9362	0.1868	0.0544	0.0009
Beavers Bend-21	535	1.0	0.3943	0.0130	0.0479	0.0009	0.102	20.6697	0.3931	0.0597	0.0023

128

Beavers Bend-22	657	5.5	1.6661	0.0240	0.1661	0.0027	0.686	6.0168	0.0977	0.0728	0.0011
Beavers Bend-23	337	1.3	0.3799	0.0070	0.0514	0.0005	0.311	19.4477	0.1967	0.0537	0.0010
Beavers Bend-24	434	1.2	0.3989	0.0091	0.0522	0.0008	0.251	19.0803	0.2767	0.0554	0.0013
Beavers Bend-25	489	0.8	0.3738	0.0110	0.0498	0.0007	0.267	20.0441	0.2772	0.0545	0.0017
Beavers Bend-26	453	1.2	0.3839	0.0110	0.0512	0.0007	0.082	19.4894	0.2735	0.0544	0.0016
Beavers Bend-27	273	1.0	0.4343	0.0140	0.0486	0.0009	0.375	20.2388	0.3564	0.0648	0.0020
Beavers Bend-28	831	0.8	0.3843	0.0067	0.0497	0.0006	0.421	20.0401	0.2369	0.0561	0.0010
Beavers Bend-29	375	1.5	0.3761	0.0090	0.0504	0.0006	0.051	19.8216	0.2240	0.0542	0.0014
Beavers Bend-30	2294	1.0	0.3952	0.0075	0.0522	0.0006	0.250	19.0986	0.2189	0.0549	0.0011
Beavers Bend-31	100	1.1	2.1466	0.0480	0.1940	0.0031	0.349	5.1387	0.0819	0.0803	0.0018
Beavers Bend-32	392	1.5	0.3803	0.0090	0.0511	0.0005	0.179	19.5389	0.1947	0.0540	0.0013
Beavers Bend-33	610	0.9	0.3804	0.0073	0.0496	0.0005	0.318	20.0682	0.1973	0.0556	0.0010
Beavers Bend-34	414	1.1	0.3937	0.0110	0.0507	0.0007	0.246	19.6194	0.2579	0.0563	0.0015
Beavers Bend-35	576	1.2	0.3679	0.0098	0.0503	0.0006	0.328	19.8807	0.2451	0.0531	0.0014
Beavers Bend-36	850	1.0	0.3734	0.0070	0.0503	0.0006	0.302	19.8610	0.2170	0.0539	0.0010
Beavers Bend-37	702	1.0	0.4805	0.0180	0.0490	0.0006	0.147	19.9322	0.2463	0.0712	0.0027
Beavers Bend-38	223	1.7	1.9238	0.0540	0.1769	0.0023	0.336	5.6180	0.0726	0.0789	0.0020
Beavers Bend-39	556	0.9	0.4022	0.0087	0.0523	0.0006	0.238	19.0513	0.2250	0.0558	0.0013
Beavers Bend-40	827	0.7	0.4171	0.0150	0.0496	0.0006	0.015	19.9402	0.2465	0.0610	0.0025
Beavers Bend-41	834	0.8	0.3904	0.0071	0.0502	0.0006	0.355	19.8138	0.2277	0.0564	0.0010
Beavers Bend-42	877	1.0	0.3819	0.0075	0.0503	0.0006	0.316	19.8255	0.2516	0.0551	0.0011
Beavers Bend-43	910	3.3	0.4917	0.0100	0.0635	0.0008	0.391	15.7208	0.2051	0.0562	0.0012
Beavers Bend-44	506	1.1	0.3817	0.0079	0.0504	0.0006	0.293	19.7668	0.2344	0.0549	0.0012
Beavers Bend-45	536	1.4	0.3819	0.0083	0.0508	0.0006	0.187	19.6580	0.2473	0.0546	0.0013
Beavers Bend-46	777	0.8	0.3749	0.0073	0.0496	0.0005	0.359	20.0884	0.2139	0.0548	0.0010
Beavers Bend-47	586	1.3	0.3997	0.0110	0.0509	0.0010	0.012	19.5465	0.3744	0.0570	0.0019

Beavers Bend-48	591	1.0	0.4034	0.0100	0.0518	0.0008	0.437	19.2160	0.2917	0.0565	0.0013
Beavers Bend-49	947	1.1	0.3817	0.0068	0.0518	0.0008	0.126	19.3050	0.2870	0.0535	0.0012
Beavers Bend-50	1240	1.1	0.4674	0.0310	0.0606	0.0029	0.627	16.4745	0.7871	0.0560	0.0027
Beavers Bend-51	556	6.0	0.5626	0.0120	0.0704	0.0010	0.140	14.1643	0.2006	0.0580	0.0014
Beavers Bend-52	403	1.4	0.3745	0.0084	0.0501	0.0006	0.210	19.9084	0.2220	0.0542	0.0012
Beavers Bend-53	595	1.2	0.3814	0.0094	0.0504	0.0008	0.351	19.7824	0.3248	0.0549	0.0014
Beavers Bend-54	169	0.9	0.7608	0.0180	0.0911	0.0012	0.184	10.9529	0.1440	0.0606	0.0015
Beavers Bend-55	584	1.1	0.3963	0.0080	0.0518	0.0006	0.300	19.2382	0.2073	0.0555	0.0011
Beavers Bend-56	399	0.7	0.3795	0.0110	0.0501	0.0008	0.350	19.9164	0.2975	0.0550	0.0015
Beavers Bend-57	620	1.1	0.3922	0.0069	0.0525	0.0006	0.200	19.0150	0.2169	0.0542	0.0011
Beavers Bend-58	567	1.2	0.3774	0.0082	0.0502	0.0009	0.278	19.8886	0.3679	0.0546	0.0013
Beavers Bend-59	539	1.1	0.3716	0.0072	0.0503	0.0005	0.257	19.8570	0.1972	0.0536	0.0011
Beavers Bend-60	725	0.9	0.3957	0.0140	0.0518	0.0008	0.449	19.2345	0.2812	0.0554	0.0018
Beavers Bend-61	568	1.1	0.3968	0.0067	0.0525	0.0006	0.310	18.9898	0.1983	0.0548	0.0009
Beavers Bend-62	473	1.2	0.3716	0.0088	0.0510	0.0008	0.390	19.6155	0.2963	0.0529	0.0012
Beavers Bend-63	545	1.0	0.3809	0.0075	0.0505	0.0006	0.128	19.7394	0.2338	0.0547	0.0012
Beavers Bend-64	532	1.0	0.3751	0.0088	0.0511	0.0005	0.085	19.5733	0.1992	0.0533	0.0013
Beavers Bend-65	342	1.2	0.3759	0.0069	0.0512	0.0006	0.196	19.5274	0.2174	0.0533	0.0010
Beavers Bend-66	427	1.2	0.3988	0.0077	0.0516	0.0005	0.160	19.3050	0.1789	0.0561	0.0012
Beavers Bend-67	423	1.1	0.4068	0.0084	0.0520	0.0005	0.093	19.1461	0.1943	0.0568	0.0013
Beavers Bend-68	787	0.6	0.4629	0.0200	0.0505	0.0006	0.027	19.4477	0.2156	0.0665	0.0030
Beavers Bend-69	549	0.7	0.4102	0.0097	0.0490	0.0009	0.467	20.1816	0.3747	0.0607	0.0013
Beavers Bend-70	420	1.3	0.3755	0.0070	0.0503	0.0005	0.223	19.8531	0.2089	0.0542	0.0011
Beavers Bend-71	443	1.1	0.3903	0.0084	0.0525	0.0007	0.304	19.0114	0.2494	0.0539	0.0012
Beavers Bend-72	563	1.2	0.3811	0.0068	0.0507	0.0006	0.301	19.6657	0.2166	0.0545	0.0010
Beavers Bend-73	705	1.0	0.3823	0.0079	0.0508	0.0006	0.299	19.6387	0.2314	0.0546	0.0011

Beavers Bend-74	349	1.3	0.3923	0.0078	0.0517	0.0006	0.262	19.3013	0.2235	0.0551	0.0011
Beavers Bend-75	327	1.6	0.3986	0.0092	0.0528	0.0006	0.196	18.9072	0.2288	0.0548	0.0013
Beavers Bend-76	344	1.6	0.3955	0.0130	0.0523	0.0011	0.136	19.0840	0.4006	0.0549	0.0020
Beavers Bend-77	669	1.1	0.3942	0.0100	0.0522	0.0006	0.343	19.1132	0.2338	0.0548	0.0014
Beavers Bend-78	596	1.1	0.3987	0.0110	0.0517	0.0007	0.452	19.2827	0.2417	0.0560	0.0013
Beavers Bend-79	392	1.4	0.4031	0.0130	0.0514	0.0008	0.339	19.3536	0.3146	0.0569	0.0018
Beavers Bend-80	260	1.6	0.4031	0.0120	0.0522	0.0007	0.196	19.0731	0.2692	0.0560	0.0017
Beavers Bend-81	677	0.8	0.4094	0.0180	0.0482	0.0011	0.504	20.4918	0.4619	0.0616	0.0023
Beavers Bend-82	490	1.5	0.3834	0.0110	0.0513	0.0007	0.251	19.4477	0.2799	0.0542	0.0016
Beavers Bend-83	149	1.7	0.5898	0.0150	0.0733	0.0010	0.360	13.6054	0.1814	0.0584	0.0014
Beavers Bend-84	378	1.8	0.5627	0.0130	0.0656	0.0007	0.196	15.0921	0.1617	0.0622	0.0015
Beavers Bend-85	298	1.2	0.3997	0.0110	0.0521	0.0007	0.246	19.1388	0.2564	0.0557	0.0014
Beavers Bend-86	811	1.1	0.3995	0.0110	0.0490	0.0008	0.209	20.2184	0.3229	0.0591	0.0016
Beavers Bend-87	515	1.1	0.4103	0.0170	0.0500	0.0010	0.313	19.8413	0.3937	0.0596	0.0024
Beavers Bend-88	971	1.2	0.4030	0.0100	0.0515	0.0007	0.407	19.3274	0.2764	0.0568	0.0013
Beavers Bend-89	385	1.3	0.4107	0.0110	0.0520	0.0012	0.241	19.1205	0.4387	0.0573	0.0018
Beavers Bend-90	546	1.1	0.3730	0.0073	0.0501	0.0005	0.349	19.9164	0.2023	0.0540	0.0010
Beavers Bend-91	229	1.1	1.6156	0.0580	0.1551	0.0028	0.090	6.4020	0.1148	0.0756	0.0029
Beavers Bend-92	399	1.5	0.3715	0.0091	0.0507	0.0008	0.294	19.7239	0.2996	0.0532	0.0013
Beavers Bend-93	162	1.9	0.3772	0.0099	0.0511	0.0006	0.185	19.5656	0.2412	0.0536	0.0015
Beavers Bend-94	312	1.6	0.3955	0.0110	0.0522	0.0008	0.411	19.1168	0.2777	0.0550	0.0014
Beavers Bend-95	501	1.0	0.4156	0.0076	0.0539	0.0007	0.487	18.5014	0.2396	0.0560	0.0009
Beavers Bend-96	178	0.9	0.4345	0.0100	0.0524	0.0009	0.369	18.9179	0.3257	0.0602	0.0014
Beavers Bend-97	385	1.2	0.3733	0.0070	0.0506	0.0005	0.289	19.7278	0.2102	0.0535	0.0010
Beavers Bend-98	446	1.1	0.3779	0.0069	0.0506	0.0007	0.346	19.7317	0.2531	0.0542	0.0010
Beavers Bend-99	587	0.9	0.3688	0.0055	0.0503	0.0005	0.331	19.8728	0.2014	0.0532	0.0008

Beavers Bend-100	488	1.0	0.4129	0.0120	0.0516	0.0006	0.319	19.2641	0.2301	0.0581	0.0015
Beavers Bend-101	394	1.7	0.3759	0.0081	0.0514	0.0007	0.111	19.4628	0.2689	0.0531	0.0013
Beavers Bend-102	355	1.3	0.3654	0.0088	0.0507	0.0007	0.200	19.7394	0.2844	0.0523	0.0013
Beavers Bend-103	166	2.2	1.8008	0.0360	0.1747	0.0031	0.658	5.7176	0.1013	0.0748	0.0012
Beavers Bend-104	289	1.4	0.4003	0.0120	0.0523	0.0010	0.492	19.0476	0.3628	0.0555	0.0015
Beavers Bend-105	61	2.7	1.7005	0.0360	0.1676	0.0022	0.284	5.9559	0.0780	0.0736	0.0016
Beavers Bend-106	379	1.3	0.3727	0.0070	0.0493	0.0005	0.284	20.2388	0.2130	0.0549	0.0010
Beavers Bend-107	612	1.0	0.3780	0.0069	0.0510	0.0006	0.234	19.5925	0.2111	0.0538	0.0010
Beavers Bend-108	633	1.3	0.3819	0.0083	0.0500	0.0006	0.196	19.9203	0.2381	0.0554	0.0013
Beavers Bend-109	674	1.5	0.3847	0.0078	0.0504	0.0007	0.244	19.7785	0.2777	0.0554	0.0012
Beavers Bend-110	363	1.5	0.3965	0.0095	0.0518	0.0007	0.460	19.2271	0.2625	0.0555	0.0012
Beavers Bend-111	980	3.0	0.3998	0.0100	0.0497	0.0009	0.445	19.9800	0.3633	0.0584	0.0016
Beavers Bend-112	434	1.6	0.3880	0.0086	0.0526	0.0007	0.330	18.9934	0.2489	0.0535	0.0012
Hatton											
Hatton Tuff_1	69	2.3	0.3989	0.0180	0.0523	0.0010	0.0001	19.0476	0.3447	0.0553	0.0026
Hatton Tuff_2	152	2.5	0.3797	0.0091	0.0502	0.0006	0.1603	19.8689	0.2211	0.0549	0.0014
Hatton Tuff_3	864	1.3	0.3770	0.0085	0.0503	0.0008	0.3147	19.8452	0.2954	0.0544	0.0012
Hatton Tuff_4	202	1.8	0.3806	0.0072	0.0502	0.0005	0.2331	19.8570	0.1893	0.0550	0.0011
Hatton Tuff_5	23	3.6	1.6518	0.0520	0.1607	0.0030	0.2660	6.1958	0.1152	0.0746	0.0023
Hatton Tuff_6	91	2.5	0.3912	0.0120	0.0502	0.0009	0.1477	19.8098	0.3375	0.0565	0.0018
Hatton Tuff_7	135	2.2	0.4041	0.0190	0.0521	0.0016	0.3347	19.1205	0.5849	0.0563	0.0026
Hatton Tuff_8	144	2.4	0.3721	0.0079	0.0505	0.0005	0.0001	19.7981	0.2117	0.0535	0.0013
Hatton Tuff_9	158	1.8	0.3787	0.0100	0.0499	0.0008	0.2351	19.9880	0.3036	0.0551	0.0016
Hatton Tuff_10	288	1.7	0.3860	0.0076	0.0480	0.0006	0.1542	20.6569	0.2432	0.0583	0.0012
Hatton Tuff_11	437	1.1	0.4443	0.0130	0.0478	0.0008	0.3173	20.5297	0.3372	0.0675	0.0018
Hatton Tuff_12	167	2.3	0.3787	0.0086	0.0488	0.0006	0.1670	20.3915	0.2370	0.0563	0.0013

Hatton Tuff_13	164	2.2	0.3769	0.0095	0.0498	0.0007	0.3354	20.0160	0.2885	0.0549	0.0013
Hatton Tuff_14	117	1.9	0.3874	0.0100	0.0492	0.0007	0.2374	20.1939	0.2651	0.0571	0.0016
Hatton Tuff_15	145	2.1	0.3807	0.0086	0.0500	0.0006	0.2643	19.9521	0.2548	0.0553	0.0013
Hatton Tuff_16	184	2.6	0.3720	0.0093	0.0506	0.0008	0.3594	19.7317	0.2998	0.0533	0.0014
Hatton Tuff_17	156	2.3	0.3897	0.0130	0.0511	0.0007	0.3284	19.4970	0.2775	0.0553	0.0017
Hatton Tuff_18	334	1.3	0.3791	0.0061	0.0502	0.0005	0.2911	19.8728	0.2133	0.0548	0.0009
Hatton Tuff_19	136	2.1	0.3789	0.0084	0.0508	0.0005	0.1976	19.6425	0.2083	0.0541	0.0012
Hatton Tuff_20	165	1.9	0.3783	0.0079	0.0500	0.0005	0.2533	19.9442	0.2029	0.0549	0.0012
Hatton Tuff_21	144	2.5	0.3761	0.0080	0.0504	0.0006	0.1637	19.7902	0.2350	0.0541	0.0012
Hatton Tuff_22	140	2.4	0.3728	0.0091	0.0502	0.0005	0.0524	19.8965	0.2098	0.0539	0.0014
Hatton Tuff_23	111	2.1	0.3780	0.0100	0.0507	0.0007	0.1779	19.6889	0.2597	0.0541	0.0015
Hatton Tuff_24	253	1.4	0.3742	0.0084	0.0496	0.0006	0.3132	20.0924	0.2543	0.0547	0.0013
Hatton Tuff_25	204	1.7	0.3695	0.0073	0.0501	0.0006	0.2545	19.9362	0.2424	0.0535	0.0011
Hatton Tuff_26	49	2.6	1.4754	0.0320	0.1499	0.0024	0.4810	6.6489	0.1061	0.0714	0.0013
Hatton Tuff_27	204	1.9	0.3783	0.0087	0.0501	0.0006	0.2554	19.9084	0.2299	0.0548	0.0013
Hatton Tuff_28	169	2.1	0.3754	0.0083	0.0502	0.0008	0.3014	19.8926	0.3087	0.0543	0.0012
Hatton Tuff_29	155	2.1	0.3985	0.0084	0.0513	0.0005	0.0809	19.4175	0.1923	0.0564	0.0013
Hatton Tuff_30	187	1.8	0.3777	0.0073	0.0499	0.0006	0.3323	19.9760	0.2434	0.0549	0.0010
Hatton Tuff_31	144	2.2	0.3662	0.0091	0.0499	0.0007	0.1065	20.0080	0.2602	0.0532	0.0014
Hatton Tuff_32	135	2.4	0.3999	0.0085	0.0522	0.0007	0.2696	19.0949	0.2443	0.0556	0.0012
Hatton Tuff_33	129	1.9	0.4021	0.0110	0.0500	0.0006	0.3878	19.8689	0.2408	0.0584	0.0015
Hatton Tuff_34	104	2.9	0.3741	0.0120	0.0501	0.0007	0.0840	19.9283	0.2859	0.0542	0.0019
Hatton Tuff_35	163	1.4	0.3828	0.0120	0.0502	0.0007	0.2706	19.8413	0.2598	0.0553	0.0016
Hatton Tuff_36	179	1.9	0.3693	0.0060	0.0499	0.0005	0.2456	20.0280	0.1925	0.0537	0.0009
Hatton Tuff_37	147	2.2	0.3777	0.0089	0.0505	0.0006	0.2396	19.7746	0.2151	0.0543	0.0013
Hatton Tuff_38	119	2.4	0.3799	0.0087	0.0509	0.0006	0.0130	19.6271	0.2119	0.0542	0.0013

Hatton Tuff_39	271	1.5	0.4217	0.0120	0.0487	0.0008	0.1388	20.2799	0.3290	0.0629	0.0017
Hatton Tuff_40	235	1.3	0.3722	0.0093	0.0496	0.0006	0.0575	20.0965	0.2423	0.0544	0.0015
Hatton Tuff_41	116	2.3	0.3769	0.0088	0.0507	0.0006	0.0799	19.6812	0.2363	0.0539	0.0014
Hatton Tuff_42	179	1.6	0.4365	0.0120	0.0496	0.0006	0.0585	19.8807	0.2213	0.0639	0.0018
Hatton Tuff_43	147	1.5	0.3743	0.0075	0.0505	0.0006	0.3323	19.7824	0.2309	0.0538	0.0010
Hatton Tuff_44	121	2.1	0.4036	0.0091	0.0540	0.0006	0.4448	18.4843	0.2153	0.0542	0.0011
Hatton Tuff_45	62	2.7	0.3624	0.0099	0.0493	0.0006	0.0284	20.2511	0.2297	0.0533	0.0016
Hatton Tuff_46	202	1.5	0.3706	0.0120	0.0497	0.0007	0.2369	20.0803	0.2984	0.0541	0.0017
Hatton Tuff_47	230	1.8	0.3859	0.0100	0.0519	0.0007	0.2953	19.2567	0.2559	0.0540	0.0014
Hatton Tuff_48	113	3.1	0.3840	0.0180	0.0501	0.0013	0.3090	19.8807	0.5138	0.0556	0.0022
Hatton Tuff_49	162	1.4	0.3651	0.0096	0.0474	0.0007	0.2374	21.0040	0.3088	0.0559	0.0016
Hatton Tuff_50	70	1.4	1.3443	0.0450	0.1430	0.0030	0.2288	6.9881	0.1465	0.0682	0.0024
Hatton Tuff_51	61	1.9	0.3958	0.0120	0.0518	0.0006	0.2064	19.2271	0.2255	0.0554	0.0016
Hatton Tuff_52	380	1.8	0.4293	0.0120	0.0496	0.0008	0.1060	19.8965	0.3009	0.0628	0.0019
Hatton Tuff_53	146	2.3	0.3678	0.0093	0.0500	0.0005	0.1134	19.9920	0.1998	0.0534	0.0014
Hatton Tuff_54	226	2.1	0.3778	0.0092	0.0504	0.0007	0.3266	19.8020	0.2862	0.0544	0.0013
Hatton Tuff_55	59	1.8	0.7397	0.0290	0.0866	0.0014	0.2551	11.4943	0.1850	0.0620	0.0022
Hatton Tuff_56	148	2.4	0.3668	0.0094	0.0477	0.0006	0.1496	20.8725	0.2614	0.0558	0.0015
Hatton Tuff_57	144	2.0	0.3681	0.0086	0.0497	0.0006	0.2492	20.0803	0.2258	0.0537	0.0012
Hatton Tuff_58	143	1.5	0.3911	0.0095	0.0517	0.0006	0.0775	19.2976	0.2346	0.0549	0.0014
Hatton Tuff_59	180	2.3	0.3804	0.0100	0.0510	0.0008	0.4816	19.5656	0.2986	0.0541	0.0013
Hatton Tuff_60	164	2.3	0.3718	0.0078	0.0505	0.0005	0.0947	19.7785	0.1839	0.0534	0.0012
Hatton Tuff_61	138	1.9	0.4176	0.0120	0.0498	0.0005	0.5340	19.8847	0.2096	0.0609	0.0014
Hatton Tuff_62	271	1.8	0.3894	0.0170	0.0490	0.0011	0.2662	20.2840	0.4526	0.0577	0.0026
Hatton Tuff_63	190	2.2	0.3709	0.0100	0.0500	0.0007	0.3004	19.9601	0.2829	0.0538	0.0015
Hatton Tuff_64	175	2.6	0.3720	0.0100	0.0496	0.0007	0.5288	20.1086	0.2750	0.0544	0.0013

Hatton Tuff_65	181	1.9	0.4631	0.0160	0.0503	0.0008	0.4675	19.5198	0.2972	0.0668	0.0020
Hatton Tuff_66	24	2.1	2.0640	0.0530	0.1901	0.0024	0.2409	5.2493	0.0661	0.0788	0.0019
Hatton Tuff_67	130	3.3	0.4155	0.0130	0.0518	0.0008	0.3515	19.1755	0.3015	0.0582	0.0019
Hatton Tuff_68	157	1.6	0.3833	0.0110	0.0500	0.0007	0.0271	19.9164	0.2578	0.0556	0.0017
Hatton Tuff_69	191	1.8	0.3952	0.0150	0.0494	0.0006	0.4421	20.0844	0.2461	0.0580	0.0021
Hatton Tuff_70	216	2.4	0.3764	0.0096	0.0508	0.0007	0.1651	19.6734	0.2864	0.0538	0.0015
Hatton Tuff_71	265	2.7	0.3831	0.0130	0.0504	0.0007	0.1256	19.7941	0.2899	0.0552	0.0019
Hatton Tuff_72	454	1.3	0.3718	0.0058	0.0503	0.0005	0.2731	19.8689	0.1816	0.0537	0.0009
Hatton Tuff_73	84	4.0	0.4144	0.0260	0.0534	0.0010	0.2348	18.6463	0.3303	0.0563	0.0029
Hatton Tuff_74	157	2.7	0.3748	0.0091	0.0506	0.0006	0.0904	19.7550	0.2146	0.0538	0.0014
Hatton Tuff_75	121	2.4	0.3702	0.0140	0.0472	0.0009	0.1431	21.0571	0.4079	0.0569	0.0023
Hatton Tuff_76	212	2.2	0.3842	0.0082	0.0517	0.0006	0.1923	19.3125	0.2089	0.0539	0.0013
Hatton Tuff_77	233	1.9	0.3729	0.0067	0.0509	0.0006	0.2297	19.6541	0.2125	0.0532	0.0010
Hatton Tuff_78	126	2.1	0.3761	0.0091	0.0505	0.0007	0.1425	19.7550	0.2537	0.0540	0.0014
Hatton Tuff_79	275	1.5	0.3882	0.0085	0.0519	0.0006	0.2850	19.2419	0.2110	0.0543	0.0011
Hatton Tuff_80	219	2.3	0.3747	0.0068	0.0509	0.0005	0.2178	19.6155	0.1885	0.0534	0.0010
Hatton Tuff_81	248	2.0	0.3811	0.0120	0.0503	0.0007	0.2264	19.8295	0.2713	0.0550	0.0018
Hatton Tuff_82	184	2.1	0.3749	0.0097	0.0495	0.0008	0.1360	20.1572	0.3210	0.0550	0.0016
Hatton Tuff_83	263	6.4	0.5961	0.0110	0.0760	0.0007	0.1836	13.1475	0.1158	0.0569	0.0011
Hatton Tuff_84	162	2.3	0.3729	0.0130	0.0509	0.0006	0.1226	19.6502	0.2471	0.0532	0.0019
Hatton Tuff_85	162	2.6	0.3863	0.0091	0.0522	0.0006	0.1406	19.1388	0.2015	0.0537	0.0013
Hatton Tuff_86	206	2.1	0.3833	0.0078	0.0517	0.0005	0.2409	19.3199	0.1792	0.0538	0.0011
Hatton Tuff_87	150	2.1	0.3795	0.0095	0.0503	0.0006	0.3525	19.8452	0.2402	0.0548	0.0013
Hatton Tuff_88	147	1.6	0.3810	0.0130	0.0511	0.0006	0.0001	19.5351	0.2328	0.0541	0.0019
Hatton Tuff_89	256	2.1	0.3769	0.0084	0.0507	0.0009	0.4983	19.6812	0.3292	0.0539	0.0011
Hatton Tuff_90	88	2.8	0.4195	0.0100	0.0543	0.0008	0.1359	18.3621	0.2529	0.0561	0.0014

Hatton Tuff_91	209	2.0	0.3782	0.0120	0.0506	0.0009	0.3299	19.7122	0.3342	0.0542	0.0017
Hatton Tuff_92	84	2.0	0.3874	0.0140	0.0483	0.0010	0.2768	20.5508	0.4097	0.0582	0.0021
Hatton Tuff_93	199	2.9	0.3864	0.0110	0.0509	0.0006	0.2598	19.5925	0.2457	0.0551	0.0015
Hatton Tuff_94	166	1.6	0.3879	0.0079	0.0504	0.0005	0.1539	19.7785	0.1917	0.0559	0.0011
Hatton Tuff_95	214	2.2	0.3826	0.0086	0.0502	0.0006	0.1353	19.8531	0.2325	0.0553	0.0013
Hatton Tuff_96	114	4.6	1.4350	0.0260	0.1500	0.0013	0.2924	6.6622	0.0577	0.0694	0.0012
Hatton Tuff_97	404	1.4	0.5381	0.0190	0.0522	0.0010	0.0756	18.6220	0.3468	0.0748	0.0029
Hatton Tuff_98	175	2.5	0.3864	0.0094	0.0507	0.0005	0.1820	19.6580	0.2048	0.0553	0.0013
Hatton Tuff_99	210	2.9	0.3942	0.0170	0.0490	0.0008	0.4816	20.2634	0.3080	0.0584	0.0024
Hatton Tuff_100	71	3.5	0.3892	0.0110	0.0503	0.0007	0.1319	19.7785	0.2699	0.0561	0.0017
Hatton Tuff_101	205	2.0	0.3765	0.0085	0.0512	0.0005	0.2939	19.5351	0.2023	0.0534	0.0012
Hatton Tuff_102	198	2.4	0.3720	0.0081	0.0501	0.0004	0.1858	19.9362	0.1749	0.0539	0.0012
Hatton Tuff_103	183	1.7	0.3842	0.0100	0.0511	0.0007	0.1621	19.5389	0.2711	0.0546	0.0015
L Mud Creek											
Lower Mud Creek-1	495	1.0	0.4294	0.0200	0.0518	0.0007	0.2027	19.1424	0.2675	0.0602	0.0029
Lower Mud Creek-2	739	1.8	0.3976	0.0140	0.0515	0.0007	0.0001	19.3349	0.2542	0.0560	0.0022
Lower Mud Creek-3	301	1.7	0.3788	0.0130	0.0505	0.0006	0.0145	19.7511	0.2419	0.0544	0.0020
Lower Mud Creek-4	208	1.4	0.4087	0.0150	0.0543	0.0008	0.2962	18.3790	0.2635	0.0546	0.0019
Lower Mud Creek-5	446	1.1	0.3714	0.0120	0.0503	0.0008	0.1457	19.8649	0.2999	0.0536	0.0017
Lower Mud Creek-6	176	1.5	0.3747	0.0130	0.0498	0.0006	0.1073	20.0321	0.2528	0.0546	0.0019
Lower Mud Creek-7	364	1.6	0.4331	0.0150	0.0500	0.0007	0.0001	19.7239	0.2645	0.0628	0.0024
Lower Mud Creek-8	51	2.0	0.4070	0.0200	0.0539	0.0012	0.2737	18.5185	0.4115	0.0548	0.0025
Lower Mud Creek-9	176	1.6	0.3777	0.0140	0.0517	0.0006	0.0129	19.3386	0.2393	0.0530	0.0021
Lower Mud Creek-10	437	1.0	0.4089	0.0180	0.0511	0.0007	0.0271	19.4515	0.2459	0.0581	0.0025

Lower Mud Creek-11	186	1.3	0.4699	0.0260	0.0507	0.0008	0.0487	19.3686	0.2964	0.0673	0.0037
Lower Mud Creek-12	208	1.5	0.3800	0.0130	0.0514	0.0007	0.2239	19.4213	0.2452	0.0536	0.0019
Lower Mud Creek-13	507	2.5	0.4297	0.0130	0.0531	0.0012	0.3754	18.6916	0.4193	0.0587	0.0019
Lower Mud Creek-14	384	1.1	0.3867	0.0110	0.0524	0.0008	0.3867	19.0549	0.3014	0.0535	0.0015
Lower Mud Creek-15	672	1.1	0.3875	0.0150	0.0513	0.0008	0.3302	19.4439	0.3100	0.0548	0.0020
Lower Mud Creek-16	172	1.6	0.3786	0.0110	0.0500	0.0006	0.1990	19.9283	0.2303	0.0549	0.0017
Lower Mud Creek-17	257	1.9	0.3856	0.0130	0.0508	0.0006	0.1851	19.6348	0.2429	0.0551	0.0019
Lower Mud Creek-18	233	1.5	0.3926	0.0130	0.0517	0.0005	0.2093	19.2864	0.2009	0.0551	0.0019
Lower Mud Creek-19	383	1.2	0.4131	0.0140	0.0506	0.0007	0.2890	19.5848	0.2762	0.0592	0.0019
Lower Mud Creek-20	239	1.6	0.3960	0.0180	0.0489	0.0008	0.2376	20.2963	0.3337	0.0588	0.0027
Lower Mud Creek-21	490	1.0	0.3931	0.0120	0.0521	0.0007	0.1143	19.1351	0.2526	0.0547	0.0017
Lower Mud Creek-22	344	1.0	0.3882	0.0130	0.0493	0.0008	0.2688	20.1532	0.3046	0.0571	0.0018
Lower Mud Creek-23	303	1.3	0.3880	0.0120	0.0516	0.0007	0.1892	19.3499	0.2696	0.0546	0.0017
Lower Mud Creek-24	341	1.2	0.3916	0.0130	0.0517	0.0012	0.3553	19.3050	0.4472	0.0550	0.0018
Lower Mud Creek-25	196	1.6	0.3982	0.0130	0.0502	0.0006	0.0330	19.7785	0.2308	0.0575	0.0020
Lower Mud Creek-26	461	1.1	0.4115	0.0130	0.0492	0.0008	0.1724	20.1167	0.3237	0.0607	0.0020
Lower Mud Creek-27	209	1.5	0.3968	0.0099	0.0510	0.0006	0.2398	19.5313	0.2174	0.0565	0.0014
Lower Mud Creek-28	319	0.9	0.3908	0.0130	0.0506	0.0007	0.1891	19.6657	0.2630	0.0560	0.0019
Lower Mud Creek-29	186	1.8	0.3779	0.0140	0.0510	0.0008	0.1458	19.5963	0.2957	0.0538	0.0021
Lower Mud Creek-30	390	1.2	0.3939	0.0120	0.0519	0.0007	0.1468	19.2234	0.2587	0.0551	0.0017
Lower Mud Creek-31	890	0.6	0.3928	0.0110	0.0509	0.0005	0.0838	19.5695	0.2030	0.0560	0.0016
Lower Mud Creek-32	227	1.4	0.3866	0.0120	0.0523	0.0008	0.1071	19.0949	0.2735	0.0536	0.0017

Lower Mud Creek-33	527	1.9	0.3757	0.0110	0.0493	0.0007	0.1300	20.2143	0.2697	0.0553	0.0017
Lower Mud Creek-34	181	1.6	0.3752	0.0120	0.0513	0.0006	0.0923	19.4970	0.2281	0.0531	0.0018
Lower Mud Creek-35	260	1.6	0.3879	0.0140	0.0513	0.0007	0.1090	19.4553	0.2801	0.0549	0.0020
Lower Mud Creek-36	184	1.7	0.3993	0.0140	0.0516	0.0007	0.2011	19.2827	0.2566	0.0561	0.0019
Lower Mud Creek-37	186	1.7	0.3842	0.0130	0.0512	0.0005	0.2533	19.4742	0.2048	0.0544	0.0017
Lower Mud Creek-38	155	2.0	0.4309	0.0240	0.0513	0.0009	0.2695	19.2790	0.3159	0.0609	0.0032
Lower Mud Creek-39	428	1.3	0.3802	0.0089	0.0519	0.0005	0.0603	19.2456	0.1963	0.0531	0.0013
Lower Mud Creek-40	180	1.2	0.3806	0.0170	0.0506	0.0009	0.2612	19.7239	0.3579	0.0546	0.0024
Lower Mud Creek-41	312	1.4	0.3957	0.0110	0.0530	0.0007	0.1404	18.8501	0.2629	0.0542	0.0015
Lower Mud Creek-42	210	1.6	0.3734	0.0097	0.0506	0.0006	0.1394	19.7589	0.2499	0.0536	0.0015
Lower Mud Creek-43	861	1.0	0.4011	0.0110	0.0508	0.0007	0.1042	19.5733	0.2490	0.0573	0.0016
Lower Mud Creek-44	274	1.5	0.4079	0.0130	0.0516	0.0007	0.1133	19.2530	0.2595	0.0573	0.0020
Lower Mud Creek-45	216	1.5	0.3771	0.0100	0.0515	0.0006	0.1106	19.4024	0.2221	0.0531	0.0014
Lower Mud Creek-46	168	1.6	0.3785	0.0140	0.0511	0.0012	0.0769	19.5313	0.4578	0.0537	0.0021
Lower Mud Creek-47	398	1.3	0.3822	0.0096	0.0521	0.0007	0.1959	19.1755	0.2427	0.0532	0.0014
Lower Mud Creek-48	359	1.1	0.3880	0.0120	0.0504	0.0006	0.1683	19.7746	0.2464	0.0559	0.0016
Lower Mud Creek-49	204	1.7	0.3820	0.0140	0.0513	0.0007	0.2254	19.4553	0.2687	0.0540	0.0019
Lower Mud Creek-50	282	1.2	0.3864	0.0097	0.0502	0.0007	0.1350	19.8255	0.2869	0.0558	0.0015
Lower Mud Creek-51	164	1.8	0.3745	0.0120	0.0512	0.0007	0.0663	19.5351	0.2595	0.0531	0.0018
Lower Mud Creek-52	373	1.6	0.3794	0.0110	0.0493	0.0009	0.4819	20.1857	0.3504	0.0558	0.0012
Lower Mud Creek-53	291	1.4	0.4011	0.0120	0.0501	0.0007	0.3489	19.8255	0.2791	0.0581	0.0017
Lower Mud Creek-54	454	1.3	0.3914	0.0110	0.0492	0.0008	0.0831	20.1816	0.3218	0.0577	0.0018

Lower Mud Creek-55	399	0.9	0.3836	0.0071	0.0512	0.0006	0.2713	19.5046	0.2130	0.0544	0.0011
Lower Mud Creek-56	230	1.4	0.3866	0.0120	0.0522	0.0008	0.0506	19.1278	0.2854	0.0537	0.0019
Lower Mud Creek-57	225	1.5	0.3815	0.0100	0.0516	0.0006	0.1141	19.3461	0.2096	0.0536	0.0015
Lower Mud Creek-58	328	1.1	0.3841	0.0110	0.0508	0.0009	0.0001	19.6464	0.3628	0.0549	0.0019
Lower Mud Creek-59	170	1.8	0.3977	0.0120	0.0520	0.0007	0.0001	19.1718	0.2610	0.0555	0.0019
Lower Mud Creek-60	184	1.7	0.3883	0.0130	0.0511	0.0010	0.1168	19.4970	0.3649	0.0551	0.0019
Lower Mud Creek-61	324	0.9	0.3703	0.0140	0.0500	0.0008	0.3514	19.9601	0.3307	0.0537	0.0019
Lower Mud Creek-62	178	1.4	0.4006	0.0110	0.0515	0.0007	0.2042	19.3162	0.2574	0.0564	0.0016
Lower Mud Creek-63	210	1.7	0.3849	0.0120	0.0506	0.0007	0.3713	19.7044	0.2679	0.0552	0.0016
Lower Mud Creek-64	151	1.8	0.3829	0.0130	0.0516	0.0007	0.0001	19.3424	0.2694	0.0538	0.0020
Lower Mud Creek-65	197	1.6	0.3758	0.0110	0.0511	0.0008	0.1625	19.5695	0.2949	0.0534	0.0017
Lower Mud Creek-66	225	1.5	0.3905	0.0120	0.0522	0.0007	0.1543	19.1314	0.2416	0.0543	0.0017
Lower Mud Creek-67	351	1.4	0.3891	0.0200	0.0500	0.0010	0.0001	19.9124	0.3886	0.0565	0.0057
Lower Mud Creek-68	354	1.3	0.3907	0.0150	0.0509	0.0009	0.2707	19.5733	0.3448	0.0557	0.0019
Lower Mud Creek-69	371	1.5	0.3804	0.0160	0.0519	0.0012	0.4039	19.2678	0.4455	0.0532	0.0020
Lower Mud Creek-70	335	1.5	0.3827	0.0110	0.0511	0.0006	0.0801	19.5160	0.2247	0.0543	0.0016
Lower Mud Creek-71	198	1.4	0.4310	0.0190	0.0470	0.0009	0.5347	20.9030	0.3889	0.0666	0.0026
Lower Mud Creek-72	309	2.0	0.3724	0.0120	0.0502	0.0008	0.1717	19.8847	0.3124	0.0538	0.0018
Lower Mud Creek-73	251	1.6	0.3874	0.0100	0.0524	0.0007	0.1364	19.0549	0.2396	0.0536	0.0015
Lower Mud Creek-74	195	1.8	0.3921	0.0120	0.0514	0.0006	0.0470	19.3761	0.2365	0.0553	0.0018
Lower Mud Creek-75	200	1.5	0.3884	0.0120	0.0501	0.0007	0.1611	19.8847	0.2728	0.0563	0.0018
Lower Mud Creek-76	214	1.6	0.3753	0.0120	0.0507	0.0006	0.1669	19.6967	0.2405	0.0537	0.0017

Lower Mud Creek-77	184	2.1	1.5565	0.0610	0.1518	0.0027	0.2931	6.5445	0.1156	0.0744	0.0026
Lower Mud Creek-78	228	1.5	0.3927	0.0140	0.0514	0.0008	0.1465	19.3798	0.2892	0.0554	0.0020
Lower Mud Creek-79	385	3.4	0.6273	0.0270	0.0779	0.0021	0.6152	12.8041	0.3443	0.0584	0.0019
Lower Mud Creek-80	82	1.0	1.1445	0.0400	0.1254	0.0026	0.5117	7.9554	0.1646	0.0662	0.0020
Lower Mud Creek-81	270	1.8	0.3984	0.0130	0.0504	0.0009	0.4848	19.7394	0.3429	0.0574	0.0016
Lower Mud Creek-82	317	1.5	0.3901	0.0120	0.0505	0.0007	0.2074	19.7006	0.2794	0.0560	0.0016
Lower Mud Creek-83	234	1.7	0.4365	0.0170	0.0526	0.0011	0.3822	18.8324	0.3901	0.0602	0.0022
Lower Mud Creek-84	281	1.2	0.3786	0.0120	0.0505	0.0007	0.2659	19.7589	0.2577	0.0544	0.0016
Lower Mud Creek-85	510	0.8	0.3791	0.0120	0.0500	0.0008	0.2831	19.9362	0.3060	0.0550	0.0017
Lower Mud Creek-86	263	1.4	0.3863	0.0120	0.0519	0.0007	0.1355	19.2382	0.2628	0.0540	0.0018
Lower Mud Creek-87	212	1.6	0.3822	0.0150	0.0500	0.0008	0.1661	19.9402	0.3181	0.0555	0.0022
Lower Mud Creek-88	183	1.9	0.3926	0.0160	0.0513	0.0010	0.2439	19.4175	0.3770	0.0555	0.0021
Lower Mud Creek-89	154	2.3	0.3800	0.0120	0.0509	0.0008	0.1096	19.6194	0.2925	0.0542	0.0018
Lower Mud Creek-90	189	1.7	0.3836	0.0130	0.0515	0.0007	0.0001	19.3723	0.2439	0.0540	0.0020
Lower Mud Creek-91	265	1.2	0.3750	0.0140	0.0504	0.0009	0.1406	19.8138	0.3651	0.0540	0.0022
Lower Mud Creek-92	305	1.2	0.4151	0.0170	0.0517	0.0014	0.0001	19.1939	0.5158	0.0582	0.0030
Lower Mud Creek-93	296	1.6	0.3882	0.0150	0.0517	0.0009	0.2789	19.3088	0.3318	0.0545	0.0021
Lower Mud Creek-94	430	1.2	0.4076	0.0180	0.0499	0.0011	0.0321	19.8807	0.4348	0.0593	0.0029
Lower Mud Creek-95	234	1.9	0.3821	0.0130	0.0506	0.0007	0.2692	19.7122	0.2875	0.0548	0.0019
Lower Mud Creek-96	194	1.9	0.3782	0.0220	0.0496	0.0013	0.3618	20.0803	0.5242	0.0553	0.0028
Lower Mud Creek-97	192	2.1	0.4169	0.0270	0.0527	0.0017	0.3526	18.8679	0.6052	0.0574	0.0036
Lower Mud Creek-98	311	1.3	0.4036	0.0120	0.0510	0.0007	0.2973	19.4856	0.2696	0.0574	0.0017

Lower Mud Creek-99	312	1.5	0.4050	0.0230	0.0517	0.0011	0.5691	19.2308	0.4068	0.0568	0.0026
Lower Mud Creek-100	309	1.2	0.4054	0.0170	0.0480	0.0008	0.0020	20.6016	0.3438	0.0613	0.0028
Lower Mud Creek-101	303	1.7	0.3910	0.0170	0.0464	0.0011	0.3700	21.3220	0.5001	0.0612	0.0026
Lower Mud Creek-102	226	1.5	0.4000	0.0140	0.0489	0.0008	0.1081	20.2840	0.3415	0.0594	0.0022
Lower Mud Creek-103	212	1.8	0.3794	0.0200	0.0498	0.0008	0.2709	20.0200	0.3327	0.0553	0.0028
Lower Mud Creek-104	315	1.6	0.3821	0.0140	0.0511	0.0008	0.1057	19.5503	0.3096	0.0543	0.0021
Lower Mud Creek-105	133	2.1	0.3918	0.0170	0.0523	0.0009	0.0212	19.1022	0.3175	0.0544	0.0025
Lower Mud Creek-106	418	1.6	0.4317	0.0180	0.0561	0.0012	0.0418	17.7620	0.3786	0.0558	0.0027
Lower Mud Creek-107	228	1.7	0.3798	0.0130	0.0507	0.0008	0.1948	19.7006	0.3105	0.0544	0.0018
Lower Mud Creek-108	190	1.9	0.3887	0.0160	0.0518	0.0008	0.0799	19.2827	0.2900	0.0545	0.0024
Lower Mud Creek-109	397	1.3	0.3678	0.0150	0.0469	0.0007	0.1275	21.1909	0.3054	0.0569	0.0024
Lower Mud Creek-110	286	1.4	0.3803	0.0130	0.0506	0.0006	0.2108	19.7083	0.2369	0.0545	0.0018
Lower Mud Creek-111	264	1.6	0.3877	0.0160	0.0509	0.0008	0.0643	19.5925	0.3148	0.0553	0.0024
Lower Mud Creek-112	171	1.6	0.3849	0.0130	0.0503	0.0007	0.0633	19.8020	0.2745	0.0555	0.0019
Lower Mud Creek-113	196	1.7	0.3950	0.0140	0.0501	0.0007	0.2537	19.8413	0.2638	0.0572	0.0020
Lower Mud Creek-114	367	1.2	0.3896	0.0110	0.0510	0.0006	0.0402	19.5313	0.2403	0.0554	0.0017
Lower Mud Creek-115	224	1.4	0.3802	0.0092	0.0501	0.0006	0.1683	19.9124	0.2339	0.0551	0.0014
Upper Mud Creek											
Upper Mud Creek-1	94	2.6	1.5804	0.0280	0.1597	0.0015	0.2565	6.2539	0.0587	0.0718	0.0013
Upper Mud Creek-2	138	1.6	1.8210	0.0420	0.1732	0.0024	0.2382	5.7537	0.0795	0.0763	0.0019
Upper Mud Creek-3	43	1.2	1.9525	0.0530	0.1807	0.0026	0.2635	5.5096	0.0789	0.0784	0.0021
Upper Mud Creek-4	285	1.2	0.5910	0.0140	0.0734	0.0010	0.2795	13.5777	0.1770	0.0584	0.0014

141

Upper Mud Creek-5	714	3.9	0.5408	0.0092	0.0667	0.0009	0.1395	14.9142	0.1913	0.0588	0.0012
Upper Mud Creek-6	54	1.8	2.1631	0.0490	0.1982	0.0027	0.3616	5.0429	0.0687	0.0792	0.0017
Upper Mud Creek-7	377	1.6	0.6301	0.0180	0.0758	0.0013	0.3158	13.1234	0.2239	0.0603	0.0016
Upper Mud Creek-8	917	5.6	0.5021	0.0170	0.0630	0.0014	0.4461	15.7978	0.3494	0.0578	0.0017
Upper Mud Creek-9	561	1.5	0.4496	0.0071	0.0602	0.0006	0.3458	16.6058	0.1710	0.0542	0.0009
Upper Mud Creek-10	90	0.7	0.8717	0.0230	0.1002	0.0014	0.2497	9.9404	0.1383	0.0631	0.0017
Upper Mud Creek-11	90	1.8	1.6543	0.0400	0.1640	0.0019	0.2278	6.0864	0.0704	0.0732	0.0018
Upper Mud Creek-12	151	0.9	4.0720	0.0770	0.2836	0.0038	0.4855	3.5026	0.0466	0.1042	0.0018
Upper Mud Creek-13	168	1.3	1.8245	0.0370	0.1772	0.0020	0.4574	5.6402	0.0636	0.0747	0.0014
Upper Mud Creek-14	151	2.7	1.6952	0.0290	0.1669	0.0019	0.4511	5.9809	0.0680	0.0737	0.0012
Upper Mud Creek-15	77	2.9	2.9645	0.0800	0.2348	0.0047	0.3796	4.2319	0.0842	0.0916	0.0024
Upper Mud Creek-16	1110	5.2	0.5251	0.0130	0.0619	0.0008	0.2040	16.0179	0.1950	0.0616	0.0015
Upper Mud Creek-17	119	1.6	0.5951	0.0150	0.0763	0.0010	0.2955	13.1062	0.1718	0.0566	0.0014
Upper Mud Creek-18	144	3.3	1.7573	0.0380	0.1691	0.0023	0.3070	5.8928	0.0799	0.0754	0.0017
Upper Mud Creek-19	63	3.1	3.1215	0.0580	0.2420	0.0031	0.3530	4.1051	0.0522	0.0936	0.0017
Upper Mud Creek-20	459	7.8	0.4289	0.0082	0.0573	0.0008	0.3827	17.4368	0.2493	0.0543	0.0010
Upper Mud Creek-21	292	1.2	0.6003	0.0160	0.0665	0.0010	0.3027	14.8368	0.2201	0.0655	0.0015
Upper Mud Creek-22	377	0.8	0.5607	0.0110	0.0719	0.0007	0.2101	13.8985	0.1294	0.0566	0.0011
Upper Mud Creek-23	115	1.9	3.2537	0.0640	0.2547	0.0030	0.3071	3.9216	0.0461	0.0927	0.0018
Upper Mud Creek-24	495	1.9	0.5346	0.0110	0.0677	0.0008	0.5273	14.7341	0.1672	0.0573	0.0011
Upper Mud Creek-25	177	3.6	1.7334	0.0330	0.1702	0.0017	0.4034	5.8685	0.0585	0.0739	0.0013
Upper Mud Creek-26	939	1.8	0.5852	0.0150	0.0721	0.0009	0.1777	13.8179	0.1680	0.0589	0.0015

Upper Mud Creek-27	523	0.9	0.5987	0.0110	0.0591	0.0009	0.2805	16.4935	0.2340	0.0735	0.0014
Upper Mud Creek-28	728	2.8	0.5664	0.0130	0.0721	0.0008	0.1928	13.8504	0.1554	0.0570	0.0014
Upper Mud Creek-29	62	1.6	0.5820	0.0200	0.0719	0.0011	0.2366	13.8504	0.2110	0.0587	0.0021
Upper Mud Creek-30	970	2.1	0.6867	0.0190	0.0591	0.0016	0.0009	16.2602	0.4230	0.0843	0.0034
Upper Mud Creek-31	407	2.1	2.0904	0.0410	0.1920	0.0032	0.6075	5.1975	0.0864	0.0790	0.0013
Upper Mud Creek-32	639	1.6	0.5577	0.0110	0.0709	0.0008	0.2185	14.0865	0.1548	0.0571	0.0011
Upper Mud Creek-33	928	5.3	0.5040	0.0160	0.0583	0.0012	0.0001	16.9492	0.3447	0.0627	0.0023
Upper Mud Creek-34	286	1.6	0.5726	0.0140	0.0728	0.0009	0.0510	13.7231	0.1657	0.0571	0.0016
Upper Mud Creek-35	74	2.9	1.6633	0.0420	0.1633	0.0023	0.3310	6.1050	0.0857	0.0739	0.0018
Upper Mud Creek-36	509	6.1	0.5367	0.0130	0.0676	0.0008	0.1513	14.7449	0.1652	0.0576	0.0015
Upper Mud Creek-37	122	2.5	2.1092	0.0450	0.1957	0.0023	0.2922	5.1099	0.0601	0.0782	0.0016
Upper Mud Creek-38	344	6.6	0.5331	0.0098	0.0684	0.0008	0.3081	14.5900	0.1746	0.0565	0.0010
Upper Mud Creek-39	323	1.1	0.3883	0.0090	0.0496	0.0006	0.2241	20.0521	0.2332	0.0568	0.0013
Upper Mud Creek-40	178	1.7	0.5951	0.0140	0.0751	0.0009	0.2486	13.2961	0.1626	0.0575	0.0014
Upper Mud Creek-41	601	4.6	1.8372	0.0370	0.1598	0.0020	0.3151	6.1538	0.0757	0.0834	0.0017
Upper Mud Creek-42	133	24.4	3.3259	0.1200	0.2540	0.0043	0.1371	3.9185	0.0660	0.0950	0.0037
Upper Mud Creek-43	665	6.9	0.6396	0.0160	0.0747	0.0013	0.6856	13.2802	0.2293	0.0621	0.0011
Upper Mud Creek-44	251	1.0	1.9167	0.0410	0.1788	0.0019	0.3385	5.5710	0.0590	0.0778	0.0016
Upper Mud Creek-45	631	5.1	0.7713	0.0340	0.0797	0.0024	0.4622	12.3305	0.3649	0.0702	0.0021
Upper Mud Creek-46	858	2.2	0.5075	0.0096	0.0631	0.0008	0.2919	15.7803	0.1868	0.0584	0.0011
Upper Mud Creek-47	404	57.0	1.3845	0.0320	0.1448	0.0016	0.2938	6.8966	0.0761	0.0694	0.0016
Upper Mud Creek-48	168	0.8	0.5793	0.0160	0.0712	0.0009	0.1650	13.9782	0.1759	0.0590	0.0016

Upper Mud Creek-49	312	2.3	0.5893	0.0130	0.0746	0.0009	0.3455	13.3833	0.1594	0.0573	0.0012
Upper Mud Creek-50	237	1.9	0.5809	0.0140	0.0726	0.0010	0.4226	13.7457	0.1833	0.0581	0.0013
Upper Mud Creek-51	765	4.8	0.4284	0.0098	0.0568	0.0007	0.2159	17.5747	0.2069	0.0547	0.0013
Upper Mud Creek-52	121	2.2	3.2441	0.0690	0.2567	0.0026	0.1879	3.8986	0.0395	0.0917	0.0020
Upper Mud Creek-53	146	1.3	3.2879	0.0570	0.2619	0.0036	0.2921	3.8314	0.0528	0.0911	0.0017
Upper Mud Creek-54	106	5.2	1.7049	0.0300	0.1692	0.0018	0.3134	5.9067	0.0628	0.0731	0.0013
Upper Mud Creek-55	247	2.0	0.5927	0.0200	0.0754	0.0014	0.4137	13.2450	0.2456	0.0570	0.0014
Upper Mud Creek-56	394	2.2	0.5405	0.0250	0.0602	0.0013	0.0089	16.3666	0.3482	0.0651	0.0029
Upper Mud Creek-57	94	0.5	1.4197	0.0480	0.1421	0.0023	0.4167	6.9930	0.1125	0.0725	0.0021
Upper Mud Creek-58	67	1.2	1.7154	0.0690	0.1625	0.0033	0.3210	6.1125	0.1233	0.0766	0.0029
Upper Mud Creek-59	483	1.1	0.5845	0.0130	0.0743	0.0010	0.2652	13.4481	0.1736	0.0571	0.0013
Upper Mud Creek-60	153	1.0	2.8068	0.0510	0.2314	0.0028	0.5087	4.3103	0.0520	0.0880	0.0015
Upper Mud Creek-61	141	2.4	1.9525	0.0470	0.1879	0.0022	0.3063	5.3305	0.0625	0.0754	0.0017
Upper Mud Creek-62	466	9.7	0.4406	0.0087	0.0589	0.0006	0.1810	16.9779	0.1758	0.0543	0.0011
Upper Mud Creek-63	809	0.6	0.9487	0.0300	0.0568	0.0008	0.2080	16.0668	0.2091	0.1211	0.0036
Upper Mud Creek-64	410	3.5	0.6094	0.0120	0.0757	0.0011	0.3357	13.1752	0.1909	0.0584	0.0012
Upper Mud Creek-65	952	2.6	0.6239	0.0380	0.0630	0.0015	0.0058	15.5280	0.3617	0.0719	0.0046
Upper Mud Creek-66	114	1.4	2.7860	0.0510	0.2332	0.0029	0.2893	4.2882	0.0533	0.0867	0.0017
Upper Mud Creek-67	336	1.9	0.3757	0.0080	0.0514	0.0006	0.2411	19.4364	0.2229	0.0530	0.0012
Upper Mud Creek-68	107	2.7	1.8522	0.0410	0.1814	0.0021	0.3018	5.5218	0.0640	0.0741	0.0016
Upper Mud Creek-69	89	1.1	1.6691	0.0410	0.1654	0.0021	0.2717	6.0350	0.0765	0.0732	0.0019
Upper Mud Creek-70	288	1.1	0.3848	0.0087	0.0492	0.0007	0.1760	20.2347	0.2743	0.0568	0.0014

Upper Mud Creek-71	169	1.2	0.7203	0.0200	0.0875	0.0014	0.3059	11.4025	0.1820	0.0597	0.0016
Upper Mud Creek-72	288	0.8	3.0861	0.0530	0.2413	0.0026	0.2830	4.1203	0.0441	0.0928	0.0016
Upper Mud Creek-73	168	1.5	0.6739	0.0200	0.0690	0.0010	0.1788	14.2106	0.1939	0.0709	0.0021
Upper Mud Creek-74	290	3.9	1.8934	0.0390	0.1775	0.0026	0.5642	5.6117	0.0819	0.0774	0.0013
Upper Mud Creek-75	30	0.6	1.5779	0.0490	0.1487	0.0028	0.2558	6.6534	0.1239	0.0770	0.0026
Upper Mud Creek-76	212	0.8	2.2853	0.0490	0.1926	0.0022	0.2705	5.1335	0.0580	0.0861	0.0018
Upper Mud Creek-77	39	2.5	1.8859	0.0460	0.1784	0.0027	0.2106	5.5897	0.0844	0.0767	0.0020
Upper Mud Creek-78	232	0.8	0.5780	0.0170	0.0675	0.0010	0.3969	14.6757	0.2111	0.0621	0.0018
Chickasaw Creek											
Chickasaw-1	581	1.1	0.3950	0.0079	0.0518	0.0005	0.2811	19.2382	0.1999	0.0553	0.0011
Chickasaw-2	638	1.5	0.4576	0.0230	0.0503	0.0007	0.1733	19.5389	0.2711	0.0660	0.0034
Chickasaw-3	384	1.2	0.3929	0.0120	0.0482	0.0007	0.3483	20.5846	0.2754	0.0592	0.0017
Chickasaw-4	1050	0.8	0.4373	0.0290	0.0531	0.0012	0.5269	18.6567	0.4177	0.0597	0.0029
Chickasaw-5	447	1.0	1.8692	0.0540	0.1654	0.0026	0.3210	5.9666	0.0926	0.0820	0.0023
Chickasaw-6	590	1.2	0.3807	0.0083	0.0514	0.0006	0.1812	19.4175	0.2187	0.0537	0.0013
Chickasaw-7	437	1.5	0.4321	0.0190	0.0547	0.0014	0.2358	18.1818	0.4628	0.0573	0.0025
Chickasaw-8	1038	0.8	0.3776	0.0120	0.0512	0.0009	0.6412	19.5084	0.3349	0.0535	0.0013
Chickasaw-9	509	1.3	0.3872	0.0100	0.0503	0.0005	0.0912	19.8177	0.2082	0.0559	0.0016
Chickasaw-10	410	1.5	0.3750	0.0110	0.0507	0.0009	0.1077	19.7122	0.3536	0.0537	0.0019
Chickasaw-11	665	1.4	0.3882	0.0075	0.0518	0.0006	0.0947	19.2753	0.2266	0.0544	0.0012
Chickasaw-12	679	1.1	0.3890	0.0130	0.0507	0.0009	0.4310	19.6618	0.3363	0.0557	0.0017
Chickasaw-13	482	0.8	0.4199	0.0140	0.0481	0.0010	0.0004	20.5170	0.4125	0.0634	0.0028
Chickasaw-14	532	0.9	0.4127	0.0097	0.0487	0.0006	0.1511	20.3005	0.2267	0.0615	0.0015
Chickasaw-15	691	1.0	0.3743	0.0080	0.0507	0.0005	0.0968	19.7161	0.1982	0.0536	0.0012

Chickasaw-16	63	1.4	3.4947	0.0940	0.2620	0.0041	0.2346	3.8008	0.0592	0.0968	0.0028
Chickasaw-17	711	1.1	0.3774	0.0092	0.0496	0.0006	0.2139	20.0924	0.2543	0.0552	0.0014
Chickasaw-18	866	1.2	0.4508	0.0290	0.0485	0.0009	0.0865	20.2388	0.3564	0.0675	0.0042
Chickasaw-19	776	1.2	0.3948	0.0090	0.0503	0.0005	0.2074	19.7902	0.1958	0.0570	0.0013
Chickasaw-20	455	1.9	0.5336	0.0110	0.0663	0.0009	0.3306	15.0195	0.1917	0.0584	0.0013
Chickasaw-21	617	1.3	0.4399	0.0110	0.0510	0.0005	0.1666	19.3648	0.1912	0.0626	0.0017
Chickasaw-22	1500	0.8	0.4045	0.0093	0.0525	0.0010	0.3329	18.9753	0.3601	0.0559	0.0014
Chickasaw-23	235	0.7	0.7948	0.0230	0.0854	0.0015	0.1188	11.5607	0.2005	0.0675	0.0020
Chickasaw-24	901	1.1	0.3785	0.0093	0.0515	0.0008	0.2468	19.3986	0.2935	0.0533	0.0014
Chickasaw-25	738	1.2	0.4091	0.0200	0.0498	0.0007	0.4960	19.9005	0.2891	0.0596	0.0024
Chickasaw-26	587	0.7	0.4191	0.0150	0.0500	0.0009	0.2806	19.7863	0.3367	0.0608	0.0022
Chickasaw-27	785	0.7	0.4364	0.0150	0.0523	0.0009	0.1523	18.9502	0.3160	0.0606	0.0022
Chickasaw-28	458	1.2	0.4688	0.0160	0.0511	0.0009	0.3269	19.2345	0.3404	0.0666	0.0021
Chickasaw-29	289	1.3	0.3970	0.0120	0.0503	0.0006	0.0738	19.7746	0.2268	0.0573	0.0018
Chickasaw-30	138	2.6	1.6589	0.0460	0.1660	0.0030	0.3554	6.0205	0.1087	0.0725	0.0020
Chickasaw-31	652	1.3	0.6003	0.0130	0.0750	0.0008	0.1798	13.3085	0.1382	0.0581	0.0013
Chickasaw-32	3107	0.7	0.3925	0.0110	0.0512	0.0009	0.2968	19.4553	0.3444	0.0556	0.0014
Chickasaw-33	790	0.7	0.4034	0.0084	0.0491	0.0006	0.2995	20.1776	0.2443	0.0596	0.0013
Chickasaw-34	408	1.0	0.3787	0.0100	0.0508	0.0007	0.4014	19.6541	0.2820	0.0541	0.0014
Chickasaw-35	1391	0.9	0.3827	0.0081	0.0515	0.0005	0.3010	19.3874	0.1842	0.0539	0.0011
Chickasaw-36	1144	1.1	0.4994	0.0160	0.0534	0.0012	0.3349	18.3824	0.4055	0.0679	0.0022
Chickasaw-37	617	1.2	0.3921	0.0081	0.0522	0.0005	0.2310	19.1205	0.1901	0.0545	0.0011
Chickasaw-38	297	1.3	0.3810	0.0093	0.0506	0.0005	0.0597	19.7044	0.2058	0.0546	0.0015
Chickasaw-39	625	0.8	0.4525	0.0150	0.0482	0.0008	0.4272	20.3252	0.3264	0.0681	0.0020
Chickasaw-40	1515	0.8	0.3848	0.0067	0.0519	0.0006	0.2591	19.2456	0.2371	0.0538	0.0010
Chickasaw-41	529	1.2	0.4004	0.0100	0.0508	0.0006	0.4629	19.5771	0.2300	0.0572	0.0014

Chickasaw-42	451	1.2	0.3873	0.0160	0.0515	0.0010	0.1973	19.3836	0.3607	0.0546	0.0023
Chickasaw-43	217	2.1	0.3819	0.0150	0.0506	0.0010	0.2122	19.7239	0.3696	0.0548	0.0021
Chickasaw-44	869	1.1	0.3951	0.0120	0.0512	0.0011	0.5923	19.4553	0.4164	0.0560	0.0016
Chickasaw-45	883	0.8	0.4122	0.0140	0.0494	0.0007	0.0083	20.0521	0.2895	0.0606	0.0022
Chickasaw-46	834	0.8	0.3897	0.0110	0.0510	0.0008	0.2186	19.5580	0.2907	0.0555	0.0016
Chickasaw-47	3031	0.5	0.4945	0.0130	0.0494	0.0008	0.3630	19.7394	0.2961	0.0727	0.0018
Chickasaw-48	357	0.9	0.4212	0.0120	0.0475	0.0006	0.0222	20.7168	0.2747	0.0643	0.0021
Chickasaw-49	222	1.4	0.3759	0.0140	0.0511	0.0007	0.2937	19.5618	0.2832	0.0534	0.0019
Chickasaw-50	453	1.0	0.5085	0.0160	0.0499	0.0006	0.2119	19.5046	0.2359	0.0740	0.0025
Chickasaw-51	598	1.0	0.3763	0.0092	0.0509	0.0006	0.1011	19.6425	0.2199	0.0537	0.0015
Chickasaw-52	557	0.8	0.4115	0.0240	0.0483	0.0006	0.1506	20.4499	0.2384	0.0618	0.0033
Chickasaw-53	1000	0.7	0.4732	0.0260	0.0554	0.0011	0.1606	17.8571	0.3508	0.0620	0.0034
Chickasaw-54	706	0.9	0.3840	0.0088	0.0502	0.0006	0.3405	19.8452	0.2205	0.0555	0.0012
Chickasaw-55	350	1.6	0.3793	0.0096	0.0510	0.0005	0.2746	19.5886	0.2072	0.0540	0.0013
Chickasaw-56	294	1.4	0.4002	0.0150	0.0519	0.0009	0.3047	19.2086	0.3247	0.0560	0.0020
Chickasaw-57	77	1.4	0.5081	0.0480	0.0570	0.0021	0.2120	17.3010	0.6286	0.0647	0.0062
Chickasaw-58	424	1.6	0.3824	0.0099	0.0518	0.0006	0.1531	19.3013	0.2123	0.0536	0.0015
Chickasaw-59	561	1.2	0.4153	0.0150	0.0503	0.0006	0.0500	19.6928	0.2172	0.0599	0.0023
Chickasaw-60	374	1.2	0.4825	0.0230	0.0486	0.0008	0.0339	20.0763	0.3224	0.0721	0.0034
Chickasaw-61	453	1.2	0.3744	0.0089	0.0509	0.0006	0.2178	19.6425	0.2122	0.0534	0.0013
Chickasaw-62	562	0.8	0.5397	0.0130	0.0652	0.0010	0.4152	15.2439	0.2324	0.0601	0.0014
Chickasaw-63	781	1.1	0.3807	0.0097	0.0507	0.0007	0.1868	19.6850	0.2558	0.0545	0.0014
Chickasaw-64	678	1.2	0.4010	0.0087	0.0527	0.0006	0.1829	18.9179	0.2112	0.0552	0.0013
Chickasaw-65	2700	0.5	0.4109	0.0055	0.0526	0.0005	0.2728	18.9107	0.1788	0.0566	0.0008
Chickasaw-66	648	3.3	2.0482	0.0870	0.1736	0.0064	0.8502	5.6689	0.2057	0.0856	0.0023
Chickasaw-67	1168	0.6	0.3898	0.0077	0.0511	0.0005	0.0471	19.5236	0.1906	0.0554	0.0012

Chickasaw-68	881	0.9	0.4846	0.0110	0.0537	0.0006	0.2851	18.3352	0.1983	0.0655	0.0014
Chickasaw-69	788	0.9	0.3972	0.0079	0.0500	0.0006	0.3090	19.8570	0.2405	0.0576	0.0012
Chickasaw-70	516	1.4	0.3759	0.0080	0.0511	0.0006	0.1788	19.5656	0.2182	0.0534	0.0012
Chickasaw-71	699	0.9	0.3823	0.0088	0.0509	0.0006	0.2744	19.6040	0.2306	0.0545	0.0012
Chickasaw-72	890	0.6	0.4072	0.0100	0.0498	0.0006	0.2571	19.8965	0.2534	0.0593	0.0015
Chickasaw-73	665	1.0	0.3880	0.0093	0.0505	0.0008	0.2803	19.7433	0.3040	0.0558	0.0013
Chickasaw-74	608	1.2	0.3813	0.0095	0.0509	0.0008	0.2596	19.6194	0.3079	0.0544	0.0014
Chickasaw-75	936	0.9	0.3899	0.0095	0.0516	0.0007	0.1455	19.3237	0.2464	0.0548	0.0013
Chickasaw-76	566	0.8	0.4107	0.0170	0.0515	0.0010	0.2588	19.3050	0.3652	0.0579	0.0023
Chickasaw-77	452	1.5	0.3961	0.0120	0.0519	0.0009	0.1778	19.2160	0.3176	0.0554	0.0017
Chickasaw-78	1609	0.8	0.3774	0.0110	0.0514	0.0008	0.4141	19.4515	0.3140	0.0533	0.0015
Chickasaw-79	901	0.6	0.6629	0.0280	0.0521	0.0008	0.0993	18.2382	0.2628	0.0924	0.0040
Chickasaw-80	515	0.8	0.4158	0.0110	0.0498	0.0009	0.4528	19.8807	0.3478	0.0606	0.0015
Chickasaw-81	868	1.0	0.3849	0.0120	0.0498	0.0008	0.1944	20.0000	0.3080	0.0561	0.0018
Barnett											
Barnett-1	658	1.0	0.2858	0.0100	0.0372	0.0008	0.5261	26.6951	0.5844	0.0557	0.0017
Barnett-2	2460	0.8	0.2886	0.0100	0.0390	0.0007	0.436	25.5624	0.4574	0.0537	0.0017
Barnett-3	545	0.2	0.3284	0.0110	0.0402	0.0006	0.4953	24.6305	0.3519	0.0593	0.0019
Barnett-4	97	0.7	0.3578	0.0120	0.0430	0.0008	0.4473	22.9727	0.4327	0.0603	0.0017
Barnett-5	103	0.3	0.38264	0.02654	0.04339	0.00194	0.730	22.6833	0.9993	0.0640	0.0030
Barnett-6	470	0.1	0.3180	0.0120	0.0435	0.0009	0.385	22.9885	0.4968	0.0544	0.0022
Barnett-7	308	1.0	0.3294	0.0080	0.0436	0.0005	0.3955	22.8415	0.2609	0.0548	0.0012
Barnett-8	169	1.5	0.3569	0.0140	0.0446	0.0013	0.7399	22.2222	0.6420	0.0580	0.0016
Barnett-9	297	0.3	0.3550	0.0120	0.0465	0.0007	0.022	21.5054	0.3191	0.0552	0.0017
Barnett-10	342	1.6	0.3532	0.0075	0.0466	0.0007	0.2597	21.3858	0.2973	0.0550	0.0012
Barnett-11	916	1.1	0.3597	0.0120	0.0467	0.0010	0.403	21.3174	0.4363	0.0559	0.0017

Barnett-12	258	0.6	0.4185	0.0130	0.0467	0.0007	0.1752	21.0526	0.3058	0.0650	0.0022
Barnett-13	173	0.5	0.3660	0.0110	0.0471	0.0009	0.174	21.2495	0.4154	0.0568	0.0015
Barnett-14	97	0.4	0.6540	0.0440	0.0471	0.0008	0.0001	19.9005	0.3287	0.1007	0.0068
Barnett-15	830	0.5	0.3969	0.0180	0.0472	0.0008	0.3702	20.9468	0.3510	0.0610	0.0026
Barnett-16	291	1.3	0.3583	0.0100	0.0477	0.0007	0.2995	20.9030	0.3102	0.0545	0.0016
Barnett-17	609	1.1	0.3761	0.0110	0.0479	0.0005	0.249	20.7641	0.2285	0.0570	0.0016
Barnett-18	480	1.5	0.4065	0.0140	0.0479	0.0006	0.192	20.6356	0.2640	0.0616	0.0021
Barnett-19	688	0.9	0.3476	0.0063	0.0480	0.0007	0.329	20.8290	0.2907	0.0527	0.0009
Barnett-20	406	1.4	0.3686	0.0130	0.0480	0.0009	0.4862	20.7383	0.4000	0.0557	0.0017
Barnett-21	232	0.7	0.4430	0.0120	0.0481	0.0007	0.172	20.7987	0.3158	0.0674	0.0019
Barnett-22	124	0.4	0.3982	0.0420	0.0482	0.0025	0.569	20.5339	1.0541	0.0599	0.0046
Barnett-23	860	1.1	0.3593	0.0080	0.0484	0.0005	0.1095	20.6356	0.2172	0.0539	0.0013
Barnett-24	892	1.5	0.3626	0.0087	0.0485	0.0006	0.288	20.5888	0.2543	0.0543	0.0013
Barnett-25	383	0.6	0.4690	0.0200	0.0485	0.0007	0.045	20.6186	0.3061	0.0712	0.0031
Barnett-26	200	1.8	0.3910	0.0110	0.0485	0.0006	0.3274	20.4583	0.2595	0.0585	0.0015
Barnett-27	958	0.7	0.3772	0.0130	0.0485	0.0009	0.406	20.5044	0.3952	0.0564	0.0018
Barnett-28	253	1.7	0.3673	0.0080	0.0488	0.0006	0.2777	20.4290	0.2295	0.0546	0.0012
Barnett-29	356	1.4	0.3556	0.0083	0.0490	0.0008	0.2486	20.4165	0.3251	0.0534	0.0011
Barnett-30	210	0.2	0.3850	0.0180	0.0491	0.0009	0.133	20.3583	0.3523	0.0577	0.0026
Barnett-31	272	2.1	0.3683	0.0180	0.0493	0.0008	0.3415	20.2388	0.3154	0.0542	0.0024
Barnett-32	785	0.4	0.4120	0.0100	0.0493	0.0005	0.2299	20.0642	0.2093	0.0606	0.0015
Barnett-33	119	1.0	0.3795	0.0097	0.0494	0.0007	0.3377	20.1450	0.2760	0.0557	0.0014
Barnett-34*	526	0.8	0.3750	0.0130	0.0496	0.0008	0.0344	20.1735	0.3215	0.0554	0.0019
Barnett-35	263	0.4	0.37640	0.02283	0.04957	0.00214	0.786	20.1080	0.8655	0.0551	0.0021
Barnett-36	372	1.7	0.3769	0.0082	0.0498	0.0005	0.1651	20.0160	0.2043	0.0549	0.0013
Barnett-37	310	0.4	0.4330	0.0130	0.0499	0.0007	0.078	20.0441	0.2732	0.0639	0.0019

Barnett-38	699	1.0	0.3722	0.0120	0.0499	0.0008	0.323	19.9960	0.3239	0.0541	0.0016
Barnett-39	229	2.0	0.3807	0.0120	0.0500	0.0006	0.2033	19.9203	0.2540	0.0552	0.0017
Barnett-40	216	1.9	0.3819	0.0120	0.0501	0.0007	0.2238	19.8886	0.2611	0.0553	0.0017
Barnett-41	369	0.5	0.36280	0.01809	0.05020	0.00174	0.788	19.9258	0.6928	0.0524	0.0016
Barnett-42	914	0.9	0.3926	0.0130	0.0502	0.0013	0.4182	19.8020	0.5098	0.0567	0.0020
Barnett-43	655	1.1	0.3761	0.0120	0.0503	0.0007	0.087	19.8570	0.2642	0.0543	0.0019
Barnett-44	191	2.0	0.3798	0.0120	0.0503	0.0006	0.1435	19.8334	0.2203	0.0548	0.0018
Barnett-45	272	3.8	0.3782	0.0110	0.0504	0.0006	0.1587	19.8138	0.2513	0.0545	0.0016
Barnett-46*	705	0.3	0.3620	0.0150	0.0504	0.0016	0.3678	19.8413	0.6299	0.0534	0.0023
Barnett-47	228	1.3	0.3669	0.0120	0.0505	0.0007	0.2517	19.7941	0.2782	0.0527	0.0017
Barnett-48	230	1.5	0.3789	0.0093	0.0505	0.0006	0.1244	19.7433	0.2222	0.0544	0.0014
Barnett-49	310	1.3	0.3747	0.0065	0.0506	0.0005	0.2571	19.7433	0.1910	0.0538	0.0010
Barnett-50	563	1.0	0.3787	0.0110	0.0506	0.0006	0.2120	19.7200	0.2178	0.0543	0.0015
Barnett-51	255	1.2	0.3797	0.0110	0.0506	0.0006	0.076	19.7044	0.2330	0.0544	0.0018
Barnett-52	628	1.9	0.3793	0.0088	0.0507	0.0005	0.1288	19.6928	0.1861	0.0543	0.0013
Barnett-53	270	1.3	0.3800	0.0140	0.0507	0.0008	0.0000	19.6889	0.2946	0.0544	0.0022
Barnett-54	314	0.5	0.36511	0.01738	0.05069	0.00152	0.744	19.7407	0.5917	0.0522	0.0017
Barnett-55	375	2.3	0.3781	0.0110	0.0507	0.0005	0.0307	19.6850	0.2093	0.0541	0.0017
Barnett-56*	99	1.8	0.3782	0.0110	0.0507	0.0006	0.1125	19.6812	0.2402	0.0541	0.0016
Barnett-57	122	1.3	0.3770	0.0100	0.0507	0.0008	0.3450	19.7083	0.2913	0.0543	0.0015
Barnett-58	387	1.3	0.3722	0.0084	0.0508	0.0007	0.168	19.6889	0.2830	0.0536	0.0011
Barnett-59	277	1.8	0.3752	0.0110	0.0508	0.0006	0.2192	19.6696	0.2244	0.0536	0.0015
Barnett-60	308	1.1	0.4120	0.0130	0.0508	0.0009	0.237	19.6812	0.3292	0.0604	0.0019
Barnett-61	623	0.7	0.3700	0.0130	0.0508	0.0007	0.153	19.6773	0.2672	0.0531	0.0018
Barnett-62	289	1.1	0.3779	0.0098	0.0509	0.0006	0.1758	19.6309	0.2197	0.0539	0.0015

Barnett-63	311	0.5	0.36717	0.01854	0.05087	0.00185	0.804	19.6683	0.7159	0.0523	0.0016
Barnett-64	189	3.0	0.3837	0.0120	0.0509	0.0008	0.2775	19.6002	0.3112	0.0547	0.0017
Barnett-65	641	1.0	0.3830	0.0130	0.0509	0.0011	0.317	19.6464	0.4246	0.0561	0.0019
Barnett-66	718	1.1	0.3806	0.0100	0.0510	0.0005	0.170	19.5886	0.2072	0.0542	0.0015
Barnett-67	728	1.2	0.3699	0.0097	0.0510	0.0007	0.314	19.6117	0.2769	0.0527	0.0013
Barnett-68	425	1.1	0.3809	0.0120	0.0510	0.0006	0.108	19.5733	0.2375	0.0542	0.0017
Barnett-69	521	2.1	0.3794	0.0091	0.0511	0.0006	0.2655	19.5503	0.2102	0.0539	0.0013
Barnett-70	189	1.8	0.3778	0.0120	0.0511	0.0006	0.1125	19.5313	0.2327	0.0536	0.0017
Barnett-71*	588	1.2	0.3755	0.0084	0.0512	0.0009	0.414	19.5427	0.3552	0.0532	0.0012
Barnett-72	151	2.1	0.3811	0.0120	0.0512	0.0006	0.2136	19.5008	0.2130	0.0540	0.0017
Barnett-73	182	1.6	0.3828	0.0100	0.0512	0.0007	0.2954	19.4818	0.2467	0.0542	0.0015
Barnett-74	374	0.7	0.3769	0.0083	0.0513	0.0004	0.203	19.5046	0.1674	0.0536	0.0012
Barnett-75	826	1.1	0.3851	0.0086	0.0513	0.0006	0.2617	19.4628	0.2235	0.0545	0.0012
Barnett-76	180	1.6	0.3842	0.0150	0.0513	0.0008	0.0660	19.4439	0.3062	0.0543	0.0023
Barnett-77	405	0.6	0.3789	0.0180	0.0514	0.0018	0.8298	19.4547	0.6890	0.0535	0.0014
Barnett-78	524	0.4	0.37780	0.01796	0.05136	0.00194	0.865	19.4581	0.7333	0.0533	0.0013
Barnett-79	370	1.0	0.3960	0.0160	0.0514	0.0012	0.4349	19.3798	0.4507	0.0559	0.0022
Barnett-80	1010	1.0	0.3861	0.0067	0.0514	0.0005	0.216	19.4137	0.1809	0.0545	0.0010
Barnett-81	141	0.7	0.3770	0.0140	0.0515	0.0011	0.2395	19.4175	0.4147	0.0543	0.0021
Barnett-82	643	1.1	0.3787	0.0089	0.0515	0.0005	0.1673	19.4213	0.1924	0.0534	0.0013
Barnett-83*	809	1.2	0.3694	0.0079	0.0515	0.0008	0.345	19.4213	0.2867	0.0523	0.0011
Barnett-84	473	0.6	0.3850	0.0084	0.0515	0.0007	0.253	19.4175	0.2677	0.0552	0.0011
Barnett-85	141	0.9	0.4741	0.0220	0.0515	0.0009	0.0586	19.0694	0.3346	0.0668	0.0032
Barnett-86	731	1.4	0.3954	0.0130	0.0515	0.0006	0.1685	19.3461	0.2246	0.0557	0.0018
Barnett-87	156	1.1	0.3664	0.0094	0.0516	0.0008	0.239	19.3986	0.3010	0.0518	0.0013

Barnett-88	589	1.1	0.3908	0.0100	0.0516	0.0006	0.0902	19.3424	0.2170	0.0550	0.0015
Barnett-89	847	0.6	0.3789	0.0081	0.0516	0.0008	0.357	19.3686	0.2964	0.0540	0.0012
Barnett-90	309	1.0	0.3821	0.0093	0.0516	0.0006	0.207	19.3499	0.2097	0.0537	0.0014
Barnett-91	799	1.5	0.3939	0.0089	0.0517	0.0007	0.5267	19.2901	0.2568	0.0553	0.0010
Barnett-92	333	2.0	0.3854	0.0110	0.0517	0.0006	0.2343	19.3162	0.2276	0.0541	0.0015
Barnett-93	528	1.0	0.3819	0.0098	0.0517	0.0006	0.3248	19.3274	0.2279	0.0536	0.0013
Barnett-94*	508	1.3	0.3750	0.0100	0.0517	0.0009	0.168	19.3349	0.3178	0.0538	0.0013
Barnett-95	532	0.9	0.3892	0.0120	0.0517	0.0008	0.528	19.2901	0.2977	0.0546	0.0015
Barnett-96	520	1.4	0.3892	0.0130	0.0517	0.0006	0.1905	19.2901	0.2307	0.0546	0.0018
Barnett-97*	353	1.0	0.3761	0.0098	0.0518	0.0008	0.3217	19.3125	0.2872	0.0536	0.0014
Barnett-98	228	1.5	0.3839	0.0095	0.0518	0.0006	0.2056	19.2901	0.2195	0.0538	0.0013
Barnett-99	81	2.3	0.3819	0.0140	0.0518	0.0007	0.1633	19.2901	0.2679	0.0535	0.0019
Barnett-100	305	1.3	0.3913	0.0110	0.0518	0.0007	0.2479	19.2530	0.2484	0.0548	0.0015
Barnett-101	518	1.0	0.3864	0.0110	0.0518	0.0008	0.0556	19.2678	0.2821	0.0541	0.0016
Barnett-102*	706	0.9	0.3770	0.0130	0.0518	0.0012	0.241	19.3050	0.4472	0.0533	0.0017
Barnett-103	218	1.2	0.3789	0.0089	0.0518	0.0009	0.382	19.2939	0.3387	0.0534	0.0013
Barnett-104	346	0.8	0.38113	0.02260	0.05183	0.00216	0.780	19.2824	0.8034	0.0533	0.0020
Barnett-105	722	1.2	0.3810	0.0085	0.0519	0.0005	0.176	19.2715	0.1746	0.0533	0.0012
Barnett-106	104	1.3	0.3775	0.0130	0.0519	0.0010	0.0971	19.2790	0.3605	0.0528	0.0020
Barnett-107*	478	1.2	0.3816	0.0090	0.0519	0.0008	0.2359	19.2715	0.2785	0.0535	0.0012
Barnett-108	521	0.8	0.3700	0.0094	0.0519	0.0009	0.153	19.2604	0.3190	0.0529	0.0012
Barnett-109	235	0.7	0.3845	0.0086	0.0519	0.0010	0.351	19.2567	0.3634	0.0539	0.0012
Barnett-110	569	1.0	0.3749	0.0070	0.0519	0.0008	0.344	19.2530	0.2780	0.0527	0.0010
Barnett-111	728	1.0	0.3873	0.0078	0.0519	0.0006	0.1765	19.2234	0.2106	0.0541	0.0012
Barnett-112	656	1.0	0.3832	0.0093	0.0520	0.0007	0.4046	19.2271	0.2662	0.0535	0.0012
Barnett-113	465	0.7	0.37672	0.01729	0.05198	0.00176	0.824	19.2464	0.6504	0.0526	0.0014

Barnett-114	436	1.2	0.3756	0.0076	0.0520	0.0008	0.371	19.2308	0.2885	0.0523	0.0010
Barnett-115	813	1.5	0.3837	0.0098	0.0520	0.0008	0.288	19.2308	0.2922	0.0539	0.0014
Barnett-116	441	1.3	0.3680	0.0100	0.0521	0.0008	0.217	19.2086	0.2767	0.0518	0.0014
Barnett-117	446	0.1	0.5170	0.0280	0.0521	0.0014	0.249	19.1939	0.5158	0.0723	0.0039
Barnett-118	332	0.7	0.37900	0.02029	0.05220	0.00195	0.782	19.1639	0.7149	0.0527	0.0018
Barnett-119	161	1.2	0.3774	0.0090	0.0523	0.0009	0.362	19.1278	0.3329	0.0531	0.0012
Barnett-120	686	1.3	0.3890	0.0073	0.0523	0.0005	0.252	19.1059	0.1862	0.0540	0.0010
Barnett-121	65	1.4	0.3716	0.0090	0.0523	0.0008	0.252	19.1241	0.2962	0.0523	0.0011
Barnett-122	367	1.2	0.3767	0.0085	0.0523	0.0008	0.290	19.1241	0.2853	0.0528	0.0012
Barnett-123	379	1.8	0.3761	0.0079	0.0523	0.0005	0.2311	19.1461	0.1906	0.0522	0.0011
Barnett-124	479	1.6	0.3862	0.0078	0.0524	0.0006	0.3294	19.0803	0.2257	0.0535	0.0011
Barnett-125	406	1.1	0.3901	0.0120	0.0524	0.0007	0.2187	19.0513	0.2359	0.0540	0.0017
Barnett-126	352	1.0	0.3822	0.0077	0.0524	0.0005	0.2500	19.0767	0.1820	0.0529	0.0010
Barnett-127	615	1.0	0.3920	0.0110	0.0525	0.0008	0.246	19.0440	0.3010	0.0549	0.0015
Barnett-128	808	1.3	0.3872	0.0089	0.0525	0.0008	0.225	19.0476	0.3011	0.0540	0.0011
Barnett-129*	328	1.2	0.3837	0.0097	0.0526	0.0008	0.129	19.0295	0.2788	0.0532	0.0012
Barnett-130	537	4.1	0.3873	0.0170	0.0526	0.0017	0.817	19.0117	0.6019	0.0534	0.0014
Barnett-131	1037	1.6	0.3936	0.0170	0.0526	0.0009	0.1309	18.9825	0.3099	0.0543	0.0022
Barnett-132*	684	0.9	0.3830	0.0110	0.0526	0.0009	0.1638	19.0006	0.3105	0.0538	0.0013
Barnett-133*	40	1.5	0.3858	0.0092	0.0526	0.0008	0.2400	18.9970	0.2923	0.0540	0.0013
Barnett-134	494	1.2	0.4433	0.0150	0.0526	0.0006	0.175	18.7970	0.1979	0.0611	0.0021
Barnett-135	494	1.3	0.3838	0.0100	0.0526	0.0007	0.1433	18.9970	0.2562	0.0529	0.0015
Barnett-136	1004	1.5	0.3770	0.0088	0.0527	0.0007	0.170	18.9861	0.2487	0.0526	0.0012
Barnett-137*	649	1.1	0.3840	0.0110	0.0527	0.0008	0.2507	18.9789	0.3026	0.0533	0.0014
Barnett-138	806	1.0	0.3984	0.0078	0.0527	0.0007	0.360	18.9681	0.2626	0.0561	0.0012
Barnett-139	423	1.4	0.3913	0.0096	0.0527	0.0008	0.297	18.9609	0.2948	0.0540	0.0013

Barnett-140	945	1.1	0.3880	0.0095	0.0527	0.0006	0.0681	18.9574	0.2048	0.0534	0.0014
Barnett-141	108	0.8	0.4658	0.0240	0.0527	0.0007	0.1946	18.6951	0.2342	0.0641	0.0032
Barnett-142	214	0.4	0.41412	0.02531	0.05280	0.00219	0.761	18.8476	0.7785	0.0569	0.0023
Barnett-143	331	1.1	0.3982	0.0094	0.0528	0.0005	0.0750	18.8929	0.1820	0.0547	0.0014
Barnett-144	771	1.0	0.3930	0.0100	0.0529	0.0013	0.540	18.9036	0.4645	0.0543	0.0015
Barnett-145*	286	0.5	0.3801	0.0217	0.0529	0.0020	0.7463	18.9278	0.7061	0.0521	0.0020
Barnett-146	523	0.6	0.4480	0.0120	0.0529	0.0010	0.336	18.9036	0.3573	0.0618	0.0015
Barnett-147	279	0.5	0.38823	0.02061	0.05293	0.00201	0.796	18.8886	0.7164	0.0532	0.0017
Barnett-148	474	1.4	0.4059	0.0160	0.0530	0.0007	0.243	18.8182	0.2514	0.0556	0.0021
Barnett-149	830	1.4	0.3845	0.0080	0.0530	0.0006	0.297	18.8679	0.2029	0.0526	0.0010
Barnett-150	864	1.0	0.4065	0.0098	0.0530	0.0008	0.320	18.8751	0.2921	0.0562	0.0013
Barnett-151*	736	1.3	0.3912	0.0097	0.0531	0.0008	0.2879	18.8253	0.2906	0.0538	0.0013
Barnett-152*	515	1.1	0.3930	0.0110	0.0531	0.0009	0.2335	18.8466	0.3090	0.0541	0.0015
Barnett-153	315	1.0	0.3816	0.0089	0.0532	0.0007	0.272	18.7864	0.2506	0.0525	0.0012
Barnett-154	309	0.6	0.4140	0.0120	0.0533	0.0008	0.217	18.7723	0.2819	0.0568	0.0015
Barnett-155	304	4.6	0.38203	0.01973	0.05334	0.00197	0.799	18.7754	0.6951	0.0519	0.0016
Barnett-156	362	1.1	0.3880	0.0110	0.0534	0.0009	0.263	18.7231	0.3155	0.0533	0.0016
Barnett-157	318	2.1	0.4350	0.0170	0.0535	0.0010	0.441	18.5529	0.3442	0.0590	0.0021
Barnett-158	308	4.6	0.37626	0.01873	0.05358	0.00198	0.823	18.7181	0.6951	0.0509	0.0015
Barnett-159	475	0.9	0.3959	0.0110	0.0536	0.0006	0.1751	18.6498	0.2226	0.0536	0.0015
Barnett-160	424	1.1	0.4056	0.0110	0.0536	0.0007	0.1764	18.6150	0.2460	0.0549	0.0016
Barnett-161	151	2.0	0.4045	0.0110	0.0537	0.0006	0.1896	18.6012	0.2180	0.0547	0.0016
Barnett-162*	621	4.1	0.39008	0.01616	0.05372	0.00152	0.798	18.6267	0.5286	0.0527	0.0013
Barnett-163*	485	3.7	0.4003	0.0181	0.0538	0.0018	0.830	18.5673	0.6221	0.0540	0.0014
Barnett-164*	560	1.1	0.3995	0.0099	0.0539	0.0007	0.309	18.5494	0.2374	0.0547	0.0013
Barnett-165	831	1.0	0.3910	0.0110	0.0539	0.0007	0.080	18.5460	0.2511	0.0534	0.0014

Barnett-166	447	0.5	0.38616	0.01867	0.05404	0.00184	0.796	18.5395	0.6329	0.0518	0.0015
Barnett-167*	268	0.4	0.4056	0.0202	0.0540	0.0017	0.754	18.4763	0.5974	0.0544	0.0018
Barnett-168	20	1.3	0.3920	0.0120	0.0541	0.0008	0.271	18.4945	0.2736	0.0536	0.0017
Barnett-169	952	1.0	0.3900	0.0110	0.0541	0.0009	0.275	18.4706	0.3173	0.0526	0.0014
Barnett-170*	990	1.3	0.4010	0.0110	0.0542	0.0007	0.1227	18.4638	0.2386	0.0545	0.0014
Barnett-171	758	0.6	0.3890	0.0110	0.0542	0.0009	0.221	18.4468	0.3029	0.0522	0.0013
Barnett-172	288	0.5	0.40251	0.02049	0.05449	0.00210	0.832	18.3457	0.7067	0.0536	0.0015
Barnett-173	370	0.5	0.39788	0.01850	0.05496	0.00196	0.847	18.2155	0.6508	0.0525	0.0013
Barnett-174	573	1.2	0.4232	0.0120	0.0551	0.0007	0.300	18.0865	0.2192	0.0557	0.0015
Barnett-175	361	0.9	0.4264	0.0150	0.0551	0.0010	0.307	18.0701	0.3135	0.0561	0.0019
Barnett-176	852	1.0	0.4081	0.0088	0.0553	0.0008	0.272	18.0799	0.2517	0.0542	0.0012
Barnett-177	532	1.6	0.4207	0.0210	0.0556	0.0011	0.2081	17.9533	0.3546	0.0549	0.0027
Barnett-178	499	1.0	0.4160	0.0110	0.0560	0.0007	0.2150	17.8476	0.2198	0.0539	0.0014
Barnett-179	304	2.6	0.4505	0.0120	0.0571	0.0011	0.5015	17.4216	0.3339	0.0572	0.0013
Barnett-180	472	3.7	0.4288	0.0186	0.0577	0.0018	0.829	17.3315	0.5516	0.0539	0.0013
Barnett-181	187	0.6	0.44873	0.02503	0.05800	0.00199	0.721	17.1892	0.5885	0.0561	0.0022
Barnett-182	108	0.4	0.51371	0.03544	0.05846	0.00259	0.727	16.8883	0.7387	0.0637	0.0030
Barnett-183	100	1.5	0.4480	0.0150	0.0591	0.0012	0.430	16.9205	0.3436	0.0557	0.0021
Barnett-184	29	0.2	0.5570	0.0270	0.0708	0.0015	0.249	14.1243	0.2992	0.0587	0.0029
Barnett-185	380	1.0	0.5340	0.0120	0.0717	0.0011	0.286	13.9470	0.2140	0.0545	0.0012
Barnett-186	96	2.9	0.6136	0.0240	0.0722	0.0013	0.3432	13.7552	0.2460	0.0617	0.0023
Barnett-187	253	0.7	0.7327	0.0210	0.0735	0.0011	0.4153	13.3156	0.1950	0.0723	0.0019
Barnett-188	1435	0.7	0.5772	0.0140	0.0737	0.0011	0.029	13.5501	0.2020	0.0568	0.0018
Barnett-189	549	1.9	0.5969	0.0170	0.0756	0.0010	0.271	13.2153	0.1677	0.0573	0.0016
Barnett-190	341	0.9	0.6001	0.0170	0.0756	0.0010	0.145	13.2083	0.1657	0.0576	0.0017
Barnett-191	220	1.9	0.7258	0.0190	0.0795	0.0017	0.4964	12.4224	0.2623	0.0662	0.0016

Barnett-192	188	0.7	0.65963	0.03391	0.08248	0.00288	0.772	12.1157	0.4227	0.0580	0.0019
Barnett-193	592	1.0	0.8701	0.0560	0.0846	0.0012	0.0906	11.5607	0.1604	0.0746	0.0047
Barnett-194	350	4.0	0.7617	0.0190	0.0908	0.0010	0.270	10.9890	0.1208	0.0609	0.0015
Barnett-195	240	0.9	1.0229	0.0360	0.0953	0.0020	0.7251	10.2459	0.2100	0.0779	0.0018
Barnett-196	302	1.7	0.8307	0.0530	0.0957	0.0030	0.2627	10.4058	0.3248	0.0630	0.0042
Barnett-197	672	3.4	0.7990	0.0200	0.0969	0.0017	0.214	10.3199	0.1811	0.0606	0.0014
Barnett-198	332	11.1	1.1702	0.0770	0.1029	0.0020	0.2356	9.4429	0.1783	0.0825	0.0049
Barnett-199	152	2.8	0.8971	0.0250	0.1043	0.0013	0.2196	9.5694	0.1190	0.0624	0.0017
Barnett-200	881	0.9	1.1688	0.0380	0.1071	0.0018	0.442	9.1241	0.1498	0.0792	0.0023
Barnett-201	769	4.0	1.1999	0.0500	0.1147	0.0033	0.6643	8.5690	0.2423	0.0759	0.0023
Barnett-202	107	5.6	1.0866	0.0270	0.1217	0.0015	0.0738	8.2102	0.1011	0.0648	0.0017
Barnett-203	566	0.4	1.4153	0.0220	0.1362	0.0013	0.367	7.2569	0.0685	0.0754	0.0012
Barnett-204	204	1.0	1.8195	0.0660	0.1403	0.0049	0.613	6.8776	0.2318	0.0941	0.0029
Barnett-205	939	2.9	1.4257	0.0350	0.1419	0.0020	0.3755	6.9979	0.0979	0.0729	0.0017
Barnett-206	76	2.7	1.4340	0.0430	0.1482	0.0019	0.1870	6.7340	0.0862	0.0702	0.0022
Barnett-207	450	0.8	1.4868	0.0430	0.1490	0.0018	0.2052	6.6800	0.0803	0.0724	0.0021
Barnett-208	343	0.9	1.6127	0.0510	0.1506	0.0021	0.4110	6.5660	0.0905	0.0777	0.0022
Barnett-209	397	1.8	1.5571	0.0220	0.1506	0.0015	0.3074	6.5876	0.0651	0.0750	0.0011
Barnett-210	139	14.7	1.5243	0.0380	0.1509	0.0016	0.2800	6.5920	0.0695	0.0733	0.0017
Barnett-211	140	5.9	1.5321	0.0360	0.1570	0.0016	0.2175	6.3654	0.0648	0.0708	0.0016
Barnett-212	183	2.5	1.6224	0.0350	0.1572	0.0020	0.2635	6.3251	0.0800	0.0749	0.0016
Barnett-213	176	3.6	1.5806	0.0700	0.1578	0.0032	0.4815	6.3211	0.1279	0.0727	0.0029
Barnett-214	370	0.6	1.5492	0.0580	0.1581	0.0028	0.288	6.3211	0.1119	0.0711	0.0024
Barnett-215	119	2.9	1.5720	0.0420	0.1584	0.0019	0.1432	6.3012	0.0754	0.0720	0.0020
Barnett-216	182	1.3	1.5593	0.0430	0.1589	0.0020	0.1239	6.2893	0.0791	0.0712	0.0021
Barnett-217	184	12.6	1.6728	0.0510	0.1595	0.0020	0.4370	6.2267	0.0775	0.0761	0.0021

Barnett-218	31	2.1	1.5815	0.0390	0.1600	0.0021	0.1516	6.2422	0.0818	0.0717	0.0019
Barnett-219	98	2.5	1.7501	0.0720	0.1609	0.0030	0.442	6.1501	0.1135	0.0789	0.0028
Barnett-220	166	2.5	1.6555	0.0360	0.1643	0.0016	0.0852	6.0753	0.0591	0.0731	0.0017
Barnett-221	74	11.2	1.6495	0.0390	0.1653	0.0019	0.2071	6.0459	0.0695	0.0724	0.0017
Barnett-222	263	6.2	1.7676	0.0520	0.1668	0.0020	0.2578	5.9595	0.0710	0.0769	0.0022
Barnett-223	323	7.0	1.8243	0.0440	0.1678	0.0018	0.0001	5.9102	0.0629	0.0789	0.0021
Barnett-224	513	1.5	1.8917	0.0470	0.1695	0.0025	0.5544	5.8377	0.0852	0.0810	0.0017
Barnett-225	81	0.9	1.74694	0.09495	0.17393	0.00677	0.796	5.7561	0.2242	0.0728	0.0024
Barnett-226	440	1.5	1.7260	0.0340	0.1689	0.0026	0.342	5.9207	0.0911	0.0742	0.0014
Barnett-227	375	3.0	1.8137	0.0370	0.1743	0.0017	0.210	5.7241	0.0557	0.0755	0.0016
Barnett-228	202	2.9	1.8842	0.0500	0.1757	0.0024	0.3425	5.6625	0.0770	0.0778	0.0020
Barnett-229	495	2.8	1.9260	0.0740	0.1881	0.0060	0.268	5.3163	0.1696	0.0746	0.0023
Barnett-230	794	3.0	1.9470	0.0350	0.1900	0.0026	0.242	5.2632	0.0720	0.0754	0.0012
Barnett-231	35	2.3	1.9660	0.0720	0.1813	0.0033	0.2876	5.4915	0.0995	0.0787	0.0029
Barnett-232	675	1.6	1.8910	0.0350	0.1813	0.0035	0.473	5.5157	0.1065	0.0760	0.0013
Barnett-233	983	1.8	2.1117	0.0600	0.1839	0.0037	0.747	5.3821	0.1072	0.0833	0.0016
Barnett-234	493	1.1	1.9920	0.0600	0.1889	0.0050	0.314	5.2938	0.1401	0.0768	0.0019
Barnett-235	1259	1.3	1.9210	0.0330	0.1791	0.0019	0.247	5.5835	0.0592	0.0779	0.0013
Barnett-236	331	0.7	1.9350	0.0480	0.1817	0.0035	0.128	5.5036	0.1060	0.0778	0.0015
Barnett-237	240	2.0	2.1542	0.0420	0.1966	0.0023	0.3354	5.0787	0.0593	0.0795	0.0015
Barnett-238	459	2.1	2.2380	0.0450	0.1968	0.0027	0.436	5.0531	0.0689	0.0825	0.0015
Barnett-239	388	3.9	2.1640	0.0490	0.2001	0.0046	0.188	4.9975	0.1149	0.0799	0.0010
Barnett-240	179	2.9	2.2065	0.0430	0.2032	0.0019	0.249	4.9285	0.0462	0.0788	0.0015
Barnett-241	422	4.4	2.3185	0.0680	0.2037	0.0027	0.454	4.8924	0.0646	0.0826	0.0022
Barnett-242	525	4.9	2.3620	0.0600	0.2098	0.0022	0.134	4.7642	0.0499	0.0817	0.0022
Barnett-243	81	2.3	2.4816	0.0670	0.2154	0.0024	0.2622	4.6361	0.0516	0.0836	0.0022

Sample ID											
Barnett-244	177	1.9	2.6768	0.0560	0.2261	0.0021	0.2809	4.4170	0.0410	0.0859	0.0017
Barnett-245	1053	2.8	2.5616	0.0850	0.2038	0.0033	0.3532	4.8333	0.0771	0.0912	0.0028
Barnett-246	259	1.6	2.3290	0.0640	0.1894	0.0039	0.281	5.2798	0.1087	0.0909	0.0019
Barnett-247	98	2.0	2.4883	0.1000	0.1861	0.0033	0.3823	5.2247	0.0901	0.0970	0.0035
Barnett-248	298	0.6	2.9753	0.0800	0.2192	0.0057	0.8122	4.4703	0.1139	0.0985	0.0016
Barnett-249	429	1.8	3.9504	0.1200	0.2821	0.0029	0.2672	3.5311	0.0362	0.1016	0.0029
Barnett-250	594	1.1	0.1710	0.0110	0.0114	0.0003	0.457	87.7963	2.2354	0.1115	0.0074
Barnett-251	258	0.4	2.6839	0.0940	0.1834	0.0052	0.3957	5.2329	0.1424	0.1062	0.0036
Barnett-252	251	1.2	4.4909	0.0960	0.3048	0.0045	0.6517	3.2723	0.0482	0.1069	0.0021

* U-Pb and Hf data simultaneously acquired by split-stream laser ablation (LASS)

*, grains not used for age calculation because of pb loss

Table S2-1 continues

Sample ID	U ppm	U/Th	$^{207}Pb/^{235}U$ Ma	2s Abs Error Ma	$^{206}Pb/^{238}U$ Ma	2s Abs Error Ma	$^{207}Pb/^{206}Pb$ Ma	2s Abs Error Ma	Best Date Ma	2s Abs Error Ma
Beavers Bend										
Beavers Bend-1	251	2.0	325.7	14.0	310.9	6.3	400.0	110.0	**310.9**	**6.3**
Beavers Bend-2	381	1.7	323.6	6.0	311.3	5.0	408.0	51.0	**311.3**	**5.0**
Beavers Bend-3	164	2.7	357.3	11.0	325.8	5.4	532.0	82.0	**325.8**	**5.4**
Beavers Bend-4	204	1.7	336.3	6.1	333.6	4.1	343.0	45.0	**333.6**	**4.1**
Beavers Bend-5	279	1.6	324.6	4.6	303.5	3.4	462.0	38.0	**303.5**	**3.4**
Beavers Bend-6	98	4.7	1059.5	13.0	1034.3	11.1	1088.0	40.0	**1088.0**	**40.0**
Beavers Bend-7	651	1.9	465.5	4.9	460.8	5.2	485.0	28.0	**460.8**	**5.2**
Beavers Bend-8	144	2.6	345.2	7.2	327.7	4.4	447.0	45.0	**327.7**	**4.4**

Beavers Bend-9	153	1.8	341.7	8.1	327.3	3.5	405.0	65.0	**327.3**	**3.5**
Beavers Bend-10	263	1.2	340.4	7.9	328.1	5.1	404.0	66.0	**328.1**	**5.1**
Beavers Bend-11	239	2.2	335.8	9.3	330.7	7.5	345.0	78.0	**330.7**	**7.5**
Beavers Bend-12	68	1.6	1050.6	14.0	1051.9	14.0	1028.0	42.0	**1028.0**	**42.0**
Beavers Bend-13	357	4.7	455.9	5.8	457.7	5.4	431.0	37.0	**457.7**	**5.4**
Beavers Bend-14	242	1.3	326.7	6.8	313.6	5.0	405.0	56.0	**313.6**	**5.0**
Beavers Bend-15	320	1.1	382.4	6.1	306.5	4.0	855.0	37.0	**306.5**	**4.0**
Beavers Bend-16	242	1.8	340.6	6.6	318.8	3.4	463.0	54.0	**318.8**	**3.4**
Beavers Bend-17	285	1.3	341.3	5.8	329.7	4.3	402.0	41.0	**329.7**	**4.3**
Beavers Bend-18	180	1.2	340.3	8.1	306.9	5.4	546.0	64.0	**306.9**	**5.4**
Beavers Bend-19	1108	0.6	342.3	6.1	326.3	3.5	435.0	47.0	**326.3**	**3.5**
Beavers Bend-20	476	1.1	323.7	4.7	314.8	2.9	374.0	38.0	**314.8**	**2.9**
Beavers Bend-21	535	1.0	337.7	9.5	301.8	5.7	552.0	81.0	**301.8**	**5.7**
Beavers Bend-22	657	5.5	996.3	9.2	990.4	15.6	1001.0	29.0	**1001.0**	**29.0**
Beavers Bend-23	337	1.3	327.2	5.2	322.9	3.2	343.0	41.0	**322.9**	**3.2**
Beavers Bend-24	434	1.2	341.1	6.6	328.3	4.7	415.0	54.0	**328.3**	**4.7**
Beavers Bend-25	489	0.8	322.7	8.5	313.1	4.3	374.0	71.0	**313.1**	**4.3**
Beavers Bend-26	453	1.2	330.1	7.9	321.9	4.5	373.0	69.0	**321.9**	**4.5**
Beavers Bend-27	273	1.0	366.4	10.0	306.1	5.4	738.0	66.0	**306.1**	**5.4**
Beavers Bend-28	831	0.8	330.4	4.9	312.5	3.7	445.0	37.0	**312.5**	**3.7**
Beavers Bend-29	375	1.5	324.4	6.7	316.7	3.6	354.0	58.0	**316.7**	**3.6**
Beavers Bend-30	2294	1.0	338.4	5.4	328.2	3.7	393.0	44.0	**328.2**	**3.7**
Beavers Bend-31	100	1.1	1164.7	16.0	1142.8	17.8	1188.0	47.0	**1188.0**	**47.0**
Beavers Bend-32	392	1.5	327.5	6.6	321.3	3.2	341.0	53.0	**321.3**	**3.2**
Beavers Bend-33	610	0.9	327.5	5.4	312.3	3.1	424.0	41.0	**312.3**	**3.1**
Beavers Bend-34	414	1.1	337.3	8.1	319.1	4.2	455.0	62.0	**319.1**	**4.2**

Beavers Bend-35	576	1.2	318.3	7.3	316.2	3.9	307.0	58.0	**316.2**	**3.9**
Beavers Bend-36	850	1.0	322.4	5.2	316.2	3.4	350.0	43.0	**316.2**	**3.4**
Beavers Bend-37	702	1.0	398.7	13.0	308.2	3.9	919.0	79.0	**308.2**	**3.9**
Beavers Bend-38	223	1.7	1090.1	19.0	1050.1	13.4	1168.0	51.0	**1168.0**	**51.0**
Beavers Bend-39	556	0.9	343.5	6.3	328.6	3.9	427.0	50.0	**328.6**	**3.9**
Beavers Bend-40	827	0.7	354.2	11.0	312.1	3.9	597.0	87.0	**312.1**	**3.9**
Beavers Bend-41	834	0.8	334.9	5.0	315.9	3.6	457.0	39.0	**315.9**	**3.6**
Beavers Bend-42	877	1.0	328.6	5.5	316.3	4.0	401.0	46.0	**316.3**	**4.0**
Beavers Bend-43	910	3.3	406.3	6.9	396.8	5.1	442.0	45.0	**396.8**	**5.1**
Beavers Bend-44	506	1.1	328.5	5.8	317.3	3.7	381.0	46.0	**317.3**	**3.7**
Beavers Bend-45	536	1.4	328.6	6.1	319.1	4.0	372.0	51.0	**319.1**	**4.0**
Beavers Bend-46	777	0.8	323.5	5.4	312.3	3.3	385.0	41.0	**312.3**	**3.3**
Beavers Bend-47	586	1.3	341.7	8.0	319.9	6.1	466.0	70.0	**319.9**	**6.1**
Beavers Bend-48	591	1.0	344.3	7.4	325.6	4.9	454.0	51.0	**325.6**	**4.9**
Beavers Bend-49	947	1.1	328.5	5.0	325.3	4.8	336.0	49.0	**325.3**	**4.8**
Beavers Bend-50	1240	1.1	389.6	21.0	379.0	17.8	420.0	110.0	**379.0**	**17.8**
Beavers Bend-51	556	6.0	453.5	7.7	438.5	6.1	504.0	54.0	**438.5**	**6.1**
Beavers Bend-52	403	1.4	323.2	6.2	315.3	3.5	357.0	50.0	**315.3**	**3.5**
Beavers Bend-53	595	1.2	328.3	7.0	317.0	5.2	388.0	57.0	**317.0**	**5.2**
Beavers Bend-54	169	0.9	574.8	10.0	562.0	7.3	586.0	55.0	**562.0**	**7.3**
Beavers Bend-55	584	1.1	339.1	5.8	325.6	3.5	414.0	45.0	**325.6**	**3.5**
Beavers Bend-56	399	0.7	326.8	7.8	314.9	4.7	384.0	61.0	**314.9**	**4.7**
Beavers Bend-57	620	1.1	336.2	5.1	329.9	3.7	363.0	43.0	**329.9**	**3.7**
Beavers Bend-58	567	1.2	325.3	6.1	315.5	5.8	386.0	52.0	**315.5**	**5.8**
Beavers Bend-59	539	1.1	321.0	5.4	316.4	3.1	340.0	44.0	**316.4**	**3.1**
Beavers Bend-60	725	0.9	338.7	9.9	325.7	4.7	408.0	71.0	**325.7**	**4.7**

Beavers Bend-61	568	1.1	339.5	4.9	330.1	3.4	387.0	38.0	**330.1**	**3.4**
Beavers Bend-62	473	1.2	321.1	6.5	320.5	4.8	311.0	51.0	**320.5**	**4.8**
Beavers Bend-63	545	1.0	327.9	5.6	317.8	3.7	385.0	50.0	**317.8**	**3.7**
Beavers Bend-64	532	1.0	323.6	6.5	321.0	3.3	318.0	55.0	**321.0**	**3.3**
Beavers Bend-65	342	1.2	324.3	5.1	321.8	3.5	338.0	43.0	**321.8**	**3.5**
Beavers Bend-66	427	1.2	341.0	5.7	324.3	3.0	434.0	46.0	**324.3**	**3.0**
Beavers Bend-67	423	1.1	346.8	6.0	326.6	3.3	462.0	49.0	**326.6**	**3.3**
Beavers Bend-68	787	0.6	386.5	14.0	317.7	3.7	733.0	87.0	**317.7**	**3.7**
Beavers Bend-69	549	0.7	349.2	7.1	308.6	5.7	616.0	46.0	**308.6**	**5.7**
Beavers Bend-70	420	1.3	323.9	5.3	316.2	3.3	360.0	44.0	**316.2**	**3.3**
Beavers Bend-71	443	1.1	334.8	6.1	330.1	4.3	342.0	49.0	**330.1**	**4.3**
Beavers Bend-72	563	1.2	328.0	5.0	319.0	3.5	375.0	41.0	**319.0**	**3.5**
Beavers Bend-73	705	1.0	328.9	5.8	319.4	3.7	387.0	44.0	**319.4**	**3.7**
Beavers Bend-74	349	1.3	336.3	5.8	324.7	3.7	396.0	46.0	**324.7**	**3.7**
Beavers Bend-75	327	1.6	340.8	6.7	331.5	4.0	382.0	55.0	**331.5**	**4.0**
Beavers Bend-76	344	1.6	338.6	9.4	328.5	6.8	376.0	80.0	**328.5**	**6.8**
Beavers Bend-77	669	1.1	337.7	7.1	328.0	4.0	379.0	51.0	**328.0**	**4.0**
Beavers Bend-78	596	1.1	340.9	7.9	324.7	4.0	435.0	53.0	**324.7**	**4.0**
Beavers Bend-79	392	1.4	344.1	9.2	323.1	5.2	448.0	68.0	**323.1**	**5.2**
Beavers Bend-80	260	1.6	344.1	8.7	328.2	4.6	428.0	68.0	**328.2**	**4.6**
Beavers Bend-81	677	0.8	348.7	13.0	303.6	6.8	636.0	76.0	**303.6**	**6.8**
Beavers Bend-82	490	1.5	329.8	8.1	322.7	4.6	350.0	64.0	**322.7**	**4.6**
Beavers Bend-83	149	1.7	471.0	9.5	455.9	6.0	518.0	53.0	**455.9**	**6.0**
Beavers Bend-84	378	1.8	453.6	8.5	409.8	4.4	645.0	51.0	**409.8**	**4.4**
Beavers Bend-85	298	1.2	341.6	7.8	327.2	4.4	428.0	59.0	**327.2**	**4.4**
Beavers Bend-86	811	1.1	341.5	7.9	308.6	4.9	569.0	63.0	**308.6**	**4.9**

Beavers Bend-87	515	1.1	349.3	12.0	314.2	6.2	544.0	87.0	**314.2**	**6.2**
Beavers Bend-88	971	1.2	344.0	7.5	323.6	4.6	466.0	52.0	**323.6**	**4.6**
Beavers Bend-89	385	1.3	349.6	8.1	326.8	7.4	470.0	69.0	**326.8**	**7.4**
Beavers Bend-90	546	1.1	322.1	5.4	315.3	3.2	352.0	42.0	**315.3**	**3.2**
Beavers Bend-91	229	1.1	976.9	22.0	929.3	16.5	1030.0	77.0	**1030.0**	**77.0**
Beavers Bend-92	399	1.5	321.0	6.7	318.6	4.8	320.0	56.0	**318.6**	**4.8**
Beavers Bend-93	162	1.9	325.2	7.3	321.0	3.9	321.0	60.0	**321.0**	**3.9**
Beavers Bend-94	312	1.6	338.6	7.7	327.9	4.7	388.0	55.0	**327.9**	**4.7**
Beavers Bend-95	501	1.0	353.1	5.5	338.2	4.3	434.0	35.0	**338.2**	**4.3**
Beavers Bend-96	178	0.9	366.6	7.4	329.1	5.6	588.0	53.0	**329.1**	**5.6**
Beavers Bend-97	385	1.2	322.3	5.2	318.5	3.4	338.0	43.0	**318.5**	**3.4**
Beavers Bend-98	446	1.1	325.7	5.1	318.1	4.0	360.0	42.0	**318.1**	**4.0**
Beavers Bend-99	587	0.9	318.9	4.1	316.3	3.2	328.0	34.0	**316.3**	**3.2**
Beavers Bend-100	488	1.0	351.2	8.2	324.1	3.9	503.0	56.0	**324.1**	**3.9**
Beavers Bend-101	394	1.7	324.2	6.0	322.9	4.4	319.0	55.0	**322.9**	**4.4**
Beavers Bend-102	355	1.3	316.4	6.8	318.8	4.6	285.0	57.0	**318.8**	**4.6**
Beavers Bend-103	166	2.2	1046.4	13.0	1037.9	17.9	1051.0	33.0	**1051.0**	**33.0**
Beavers Bend-104	289	1.4	342.1	8.4	328.8	6.2	413.0	59.0	**328.8**	**6.2**
Beavers Bend-105	61	2.7	1009.3	14.0	999.1	12.8	1015.0	45.0	**1015.0**	**45.0**
Beavers Bend-106	379	1.3	321.9	5.3	310.0	3.2	397.0	45.0	**310.0**	**3.2**
Beavers Bend-107	612	1.0	325.7	5.1	320.5	3.4	345.0	43.0	**320.5**	**3.4**
Beavers Bend-108	633	1.3	328.7	6.0	314.7	3.7	403.0	51.0	**314.7**	**3.7**
Beavers Bend-109	674	1.5	330.7	5.7	316.9	4.4	413.0	48.0	**316.9**	**4.4**
Beavers Bend-110	363	1.5	339.3	6.9	325.8	4.4	409.0	49.0	**325.8**	**4.4**
Beavers Bend-111	980	3.0	341.7	7.4	312.5	5.6	516.0	59.0	**312.5**	**5.6**
Beavers Bend-112	434	1.6	333.1	6.3	330.6	4.3	327.0	48.0	**330.6**	**4.3**

Hatton

Hatton Tuff_1	69	2.3	341.1	13.0	328.9	6.0	370.0	100.0	**328.9**	**6.0**
Hatton Tuff_2	152	2.5	327.0	6.7	315.7	3.5	377.0	54.0	**315.7**	**3.5**
Hatton Tuff_3	864	1.3	325.0	6.2	316.2	4.7	376.0	51.0	**316.2**	**4.7**
Hatton Tuff_4	202	1.8	327.7	5.3	315.8	3.0	396.0	42.0	**315.8**	**3.0**
Hatton Tuff_5	23	3.6	990.8	20.0	960.4	17.5	1038.0	65.0	**1038.0**	**65.0**
Hatton Tuff_6	91	2.5	335.4	9.1	316.0	5.4	457.0	74.0	**316.0**	**5.4**
Hatton Tuff_7	135	2.2	344.8	14.0	327.3	9.9	440.0	100.0	**327.3**	**9.9**
Hatton Tuff_8	144	2.4	321.4	6.0	317.3	3.4	326.0	54.0	**317.3**	**3.4**
Hatton Tuff_9	158	1.8	326.3	7.4	313.7	4.7	389.0	64.0	**313.7**	**4.7**
Hatton Tuff_10	288	1.7	331.7	5.5	302.5	3.5	523.0	47.0	**302.5**	**3.5**
Hatton Tuff_11	437	1.1	373.5	9.3	300.8	4.9	824.0	58.0	**300.8**	**4.9**
Hatton Tuff_12	167	2.3	326.2	6.3	307.2	3.6	452.0	55.0	**307.2**	**3.6**
Hatton Tuff_13	164	2.2	325.0	6.9	313.4	4.5	383.0	54.0	**313.4**	**4.5**
Hatton Tuff_14	117	1.9	332.7	7.5	309.8	4.1	458.0	59.0	**309.8**	**4.1**
Hatton Tuff_15	145	2.1	327.7	6.5	314.2	4.0	407.0	50.0	**314.2**	**4.0**
Hatton Tuff_16	184	2.6	321.3	7.2	318.5	4.8	325.0	57.0	**318.5**	**4.8**
Hatton Tuff_17	156	2.3	334.3	9.2	321.4	4.6	390.0	67.0	**321.4**	**4.6**
Hatton Tuff_18	334	1.3	326.6	4.5	315.6	3.4	389.0	37.0	**315.6**	**3.4**
Hatton Tuff_19	136	2.1	326.5	6.3	319.6	3.4	362.0	50.0	**319.6**	**3.4**
Hatton Tuff_20	165	1.9	326.0	6.1	314.5	3.2	387.0	47.0	**314.5**	**3.2**
Hatton Tuff_21	144	2.5	324.4	6.0	317.2	3.7	349.0	49.0	**317.2**	**3.7**
Hatton Tuff_22	140	2.4	321.9	6.8	315.6	3.3	347.0	57.0	**315.6**	**3.3**
Hatton Tuff_23	111	2.1	325.8	7.3	318.8	4.2	346.0	60.0	**318.8**	**4.2**
Hatton Tuff_24	253	1.4	323.0	6.2	312.3	3.9	380.0	51.0	**312.3**	**3.9**
Hatton Tuff_25	204	1.7	319.4	5.4	315.2	3.8	335.0	46.0	**315.2**	**3.8**

Hatton Tuff_26	49	2.6	920.9	13.0	900.6	14.0	965.0	41.0	**900.6**	**14.0**
Hatton Tuff_27	204	1.9	326.0	6.4	315.1	3.6	382.0	51.0	**315.1**	**3.6**
Hatton Tuff_28	169	2.1	323.9	6.1	315.5	4.8	363.0	51.0	**315.5**	**4.8**
Hatton Tuff_29	155	2.1	340.8	6.1	322.3	3.2	446.0	50.0	**322.3**	**3.2**
Hatton Tuff_30	187	1.8	325.5	5.4	314.0	3.8	394.0	42.0	**314.0**	**3.8**
Hatton Tuff_31	144	2.2	317.0	6.8	314.2	4.1	310.0	60.0	**314.2**	**4.1**
Hatton Tuff_32	135	2.4	341.8	6.2	328.0	4.2	407.0	48.0	**328.0**	**4.2**
Hatton Tuff_33	129	1.9	343.4	8.2	314.3	3.8	512.0	55.0	**314.3**	**3.8**
Hatton Tuff_34	104	2.9	322.9	8.7	315.0	4.5	364.0	75.0	**315.0**	**4.5**
Hatton Tuff_35	163	1.4	329.3	8.6	315.9	4.1	397.0	64.0	**315.9**	**4.1**
Hatton Tuff_36	179	1.9	319.3	4.5	313.7	3.0	342.0	38.0	**313.7**	**3.0**
Hatton Tuff_37	147	2.2	325.5	6.5	317.4	3.4	354.0	52.0	**317.4**	**3.4**
Hatton Tuff_38	119	2.4	327.2	6.4	319.8	3.4	349.0	54.0	**319.8**	**3.4**
Hatton Tuff_39	271	1.5	357.5	8.5	306.2	4.9	685.0	60.0	**306.2**	**4.9**
Hatton Tuff_40	235	1.3	321.5	7.1	312.3	3.8	356.0	61.0	**312.3**	**3.8**
Hatton Tuff_41	116	2.3	324.9	6.5	319.0	3.8	336.0	55.0	**319.0**	**3.8**
Hatton Tuff_42	179	1.6	368.0	8.2	311.9	3.5	708.0	59.0	**311.9**	**3.5**
Hatton Tuff_43	147	1.5	323.0	5.5	317.5	3.7	339.0	43.0	**317.5**	**3.7**
Hatton Tuff_44	121	2.1	344.5	6.5	339.2	3.9	358.0	46.0	**339.2**	**3.9**
Hatton Tuff_45	62	2.7	314.2	7.4	310.4	3.5	302.0	64.0	**310.4**	**3.5**
Hatton Tuff_46	202	1.5	320.3	8.9	312.7	4.6	345.0	70.0	**312.7**	**4.6**
Hatton Tuff_47	230	1.8	331.6	7.4	325.9	4.3	342.0	57.0	**325.9**	**4.3**
Hatton Tuff_48	113	3.1	330.2	13.0	315.2	8.1	431.0	96.0	**315.2**	**8.1**
Hatton Tuff_49	162	1.4	316.2	7.1	298.5	4.4	421.0	62.0	**298.5**	**4.4**
Hatton Tuff_50	70	1.4	865.6	19.0	861.7	17.7	852.0	73.0	**861.7**	**17.7**
Hatton Tuff_51	61	1.9	338.8	8.6	325.8	3.8	391.0	64.0	**325.8**	**3.8**

Hatton Tuff_52	380	1.8	362.9	8.6	312.1	4.7	684.0	64.0	**312.1**	**4.7**
Hatton Tuff_53	146	2.3	318.2	7.0	314.4	3.1	321.0	58.0	**314.4**	**3.1**
Hatton Tuff_54	226	2.1	325.6	7.1	316.9	4.5	377.0	55.0	**316.9**	**4.5**
Hatton Tuff_55	59	1.8	562.6	16.0	535.2	8.5	649.0	78.0	**535.2**	**8.5**
Hatton Tuff_56	148	2.4	317.5	6.9	300.4	3.8	412.0	58.0	**300.4**	**3.8**
Hatton Tuff_57	144	2.0	318.4	6.4	312.9	3.5	340.0	52.0	**312.9**	**3.5**
Hatton Tuff_58	143	1.5	335.4	6.9	324.9	3.9	373.0	58.0	**324.9**	**3.9**
Hatton Tuff_59	180	2.3	327.6	7.6	320.8	4.9	359.0	54.0	**320.8**	**4.9**
Hatton Tuff_60	164	2.3	321.2	5.8	317.7	2.9	330.0	48.0	**317.7**	**2.9**
Hatton Tuff_61	138	1.9	354.6	8.4	313.0	3.3	602.0	50.0	**313.0**	**3.3**
Hatton Tuff_62	271	1.8	334.2	13.0	308.2	6.9	469.0	95.0	**308.2**	**6.9**
Hatton Tuff_63	190	2.2	320.5	7.4	314.7	4.4	337.0	62.0	**314.7**	**4.4**
Hatton Tuff_64	175	2.6	321.3	7.7	312.2	4.2	370.0	54.0	**312.2**	**4.2**
Hatton Tuff_65	181	1.9	386.7	11.0	316.4	4.8	803.0	65.0	**316.4**	**4.8**
Hatton Tuff_66	24	2.1	1137.6	17.0	1121.6	14.0	1148.0	50.0	**1148.0**	**50.0**
Hatton Tuff_67	130	3.3	353.0	9.7	325.5	5.1	515.0	73.0	**325.5**	**5.1**
Hatton Tuff_68	157	1.6	329.7	8.0	314.7	4.1	406.0	67.0	**314.7**	**4.1**
Hatton Tuff_69	191	1.8	338.4	11.0	311.1	3.8	494.0	79.0	**311.1**	**3.8**
Hatton Tuff_70	216	2.4	324.6	7.1	319.2	4.6	337.0	60.0	**319.2**	**4.6**
Hatton Tuff_71	265	2.7	329.5	9.2	316.7	4.6	395.0	75.0	**316.7**	**4.6**
Hatton Tuff_72	454	1.3	321.1	4.2	316.2	2.9	341.0	36.0	**316.2**	**2.9**
Hatton Tuff_73	84	4.0	352.3	18.0	335.4	6.0	440.0	120.0	**335.4**	**6.0**
Hatton Tuff_74	157	2.7	323.4	6.7	317.9	3.4	330.0	58.0	**317.9**	**3.4**
Hatton Tuff_75	121	2.4	320.0	10.0	297.4	5.7	446.0	86.0	**297.4**	**5.7**
Hatton Tuff_76	212	2.2	330.3	6.0	325.0	3.5	341.0	51.0	**325.0**	**3.5**
Hatton Tuff_77	233	1.9	322.0	5.0	319.8	3.4	314.0	42.0	**319.8**	**3.4**

Hatton Tuff_78	126	2.1	324.4	6.7	317.8	4.1	336.0	56.0	**317.8**	**4.1**
Hatton Tuff_79	275	1.5	333.3	6.1	326.0	3.5	367.0	47.0	**326.0**	**3.5**
Hatton Tuff_80	219	2.3	323.3	5.1	320.3	3.1	328.0	42.0	**320.3**	**3.1**
Hatton Tuff_81	248	2.0	328.1	9.0	316.3	4.3	385.0	70.0	**316.3**	**4.3**
Hatton Tuff_82	184	2.1	323.5	7.1	311.2	4.9	378.0	63.0	**311.2**	**4.9**
Hatton Tuff_83	263	6.4	475.1	6.9	472.3	4.1	472.0	42.0	**472.3**	**4.1**
Hatton Tuff_84	162	2.3	322.0	9.6	319.8	4.0	308.0	76.0	**319.8**	**4.0**
Hatton Tuff_85	162	2.6	331.9	6.6	328.0	3.4	325.0	54.0	**328.0**	**3.4**
Hatton Tuff_86	206	2.1	329.7	5.7	325.0	3.0	346.0	45.0	**325.0**	**3.0**
Hatton Tuff_87	150	2.1	326.9	7.0	316.1	3.8	375.0	51.0	**316.1**	**3.8**
Hatton Tuff_88	147	1.6	328.0	9.2	321.3	3.8	349.0	79.0	**321.3**	**3.8**
Hatton Tuff_89	256	2.1	324.9	6.2	319.0	5.3	352.0	45.0	**319.0**	**5.3**
Hatton Tuff_90	88	2.8	355.9	7.2	340.6	4.7	419.0	57.0	**340.6**	**4.7**
Hatton Tuff_91	209	2.0	325.9	9.1	318.4	5.4	352.0	69.0	**318.4**	**5.4**
Hatton Tuff_92	84	2.0	332.7	10.0	304.1	6.0	499.0	81.0	**304.1**	**6.0**
Hatton Tuff_93	199	2.9	332.0	8.1	320.0	4.0	391.0	62.0	**320.0**	**4.0**
Hatton Tuff_94	166	1.6	333.1	5.7	316.7	3.1	422.0	43.0	**316.7**	**3.1**
Hatton Tuff_95	214	2.2	329.2	6.3	315.8	3.7	394.0	53.0	**315.8**	**3.7**
Hatton Tuff_96	114	4.6	904.2	11.0	901.2	7.7	897.0	37.0	**901.2**	**7.7**
Hatton Tuff_97	404	1.4	437.4	12.0	328.0	6.1	1040.0	76.0	**328.0**	**6.1**
Hatton Tuff_98	175	2.5	332.0	6.8	318.8	3.3	393.0	54.0	**318.8**	**3.3**
Hatton Tuff_99	210	2.9	337.6	12.0	308.2	4.7	499.0	82.0	**308.2**	**4.7**
Hatton Tuff_100	71	3.5	334.0	8.1	316.6	4.3	418.0	67.0	**316.6**	**4.3**
Hatton Tuff_101	205	2.0	324.6	6.2	321.6	3.3	327.0	49.0	**321.6**	**3.3**
Hatton Tuff_102	198	2.4	321.3	6.0	315.0	2.8	339.0	50.0	**315.0**	**2.8**
Hatton Tuff_103	183	1.7	330.4	7.4	321.0	4.4	364.0	60.0	**321.0**	**4.4**

L Mud Creek

Lower Mud Creek-1	495	1.0	362.9	14.0	325.3	4.6	532.0	99.0	**325.3**	**4.6**
Lower Mud Creek-2	739	1.8	340.1	10.0	323.8	4.3	396.0	83.0	**323.8**	**4.3**
Lower Mud Creek-3	301	1.7	326.3	9.8	317.7	3.9	323.0	79.0	**317.7**	**3.9**
Lower Mud Creek-4	208	1.4	348.2	11.0	341.0	4.9	339.0	73.0	**341.0**	**4.9**
Lower Mud Creek-5	446	1.1	320.9	8.5	316.3	4.8	321.0	71.0	**316.3**	**4.8**
Lower Mud Creek-6	176	1.5	323.3	9.6	313.3	4.0	342.0	75.0	**313.3**	**4.0**
Lower Mud Creek-7	364	1.6	365.6	11.0	314.8	4.3	625.0	80.0	**314.8**	**4.3**
Lower Mud Creek-8	51	2.0	346.9	15.0	338.4	7.5	350.0	100.0	**338.4**	**7.5**
Lower Mud Creek-9	176	1.6	325.5	10.0	325.0	4.1	272.0	82.0	**325.0**	**4.1**
Lower Mud Creek-10	437	1.0	348.3	12.0	321.0	4.1	469.0	92.0	**321.0**	**4.1**
Lower Mud Creek-11	186	1.3	391.4	18.0	318.6	5.0	770.0	110.0	**318.6**	**5.0**
Lower Mud Creek-12	208	1.5	327.2	10.0	323.4	4.1	318.0	76.0	**323.4**	**4.1**
Lower Mud Creek-13	507	2.5	363.2	9.4	333.6	7.4	547.0	74.0	**333.6**	**7.4**
Lower Mud Creek-14	384	1.1	332.2	8.3	329.5	5.2	312.0	60.0	**329.5**	**5.2**
Lower Mud Creek-15	672	1.1	332.7	11.0	322.5	5.1	357.0	77.0	**322.5**	**5.1**
Lower Mud Creek-16	172	1.6	326.2	8.3	314.7	3.6	364.0	65.0	**314.7**	**3.6**
Lower Mud Creek-17	257	1.9	331.4	9.9	319.3	4.0	369.0	74.0	**319.3**	**4.0**
Lower Mud Creek-18	233	1.5	336.5	9.8	325.0	3.4	369.0	76.0	**325.0**	**3.4**
Lower Mud Creek-19	383	1.2	351.4	9.9	318.4	4.5	528.0	67.0	**318.4**	**4.5**
Lower Mud Creek-20	239	1.6	339.0	13.0	307.6	5.1	485.0	96.0	**307.6**	**5.1**
Lower Mud Creek-21	490	1.0	336.8	8.7	327.7	4.3	376.0	71.0	**327.7**	**4.3**
Lower Mud Creek-22	344	1.0	333.3	9.7	310.4	4.7	443.0	70.0	**310.4**	**4.7**
Lower Mud Creek-23	303	1.3	333.1	8.5	324.1	4.5	349.0	66.0	**324.1**	**4.5**
Lower Mud Creek-24	341	1.2	335.7	9.0	324.7	7.4	375.0	70.0	**324.7**	**7.4**
Lower Mud Creek-25	196	1.6	340.5	9.7	316.0	3.7	446.0	76.0	**316.0**	**3.7**

Lower Mud Creek-26	461	1.1	350.2	9.2	309.5	5.0	583.0	67.0	**309.5**	**5.0**
Lower Mud Creek-27	209	1.5	339.5	7.2	320.4	3.6	440.0	54.0	**320.4**	**3.6**
Lower Mud Creek-28	319	0.9	335.2	9.5	318.4	4.3	406.0	74.0	**318.4**	**4.3**
Lower Mud Creek-29	186	1.8	325.7	11.0	320.4	4.8	313.0	84.0	**320.4**	**4.8**
Lower Mud Creek-30	390	1.2	337.4	8.5	326.0	4.4	373.0	66.0	**326.0**	**4.4**
Lower Mud Creek-31	890	0.6	336.6	8.1	320.0	3.3	412.0	66.0	**320.0**	**3.3**
Lower Mud Creek-32	227	1.4	332.1	8.8	328.8	4.7	341.0	68.0	**328.8**	**4.7**
Lower Mud Creek-33	527	1.9	324.1	8.2	310.2	4.1	380.0	68.0	**310.2**	**4.1**
Lower Mud Creek-34	181	1.6	323.7	8.9	322.3	3.8	288.0	71.0	**322.3**	**3.8**
Lower Mud Creek-35	260	1.6	333.0	9.8	322.3	4.6	357.0	77.0	**322.3**	**4.6**
Lower Mud Creek-36	184	1.7	341.4	10.0	324.6	4.3	412.0	74.0	**324.6**	**4.3**
Lower Mud Creek-37	186	1.7	330.3	9.4	322.2	3.4	349.0	69.0	**322.2**	**3.4**
Lower Mud Creek-38	155	2.0	364.0	16.0	322.7	5.4	570.0	110.0	**322.7**	**5.4**
Lower Mud Creek-39	428	1.3	327.4	6.5	326.5	3.3	301.0	54.0	**326.5**	**3.3**
Lower Mud Creek-40	180	1.2	327.7	12.0	318.1	5.8	364.0	96.0	**318.1**	**5.8**
Lower Mud Creek-41	312	1.4	338.7	8.0	332.8	4.6	361.0	59.0	**332.8**	**4.6**
Lower Mud Creek-42	210	1.6	322.4	7.2	317.9	4.0	328.0	60.0	**317.9**	**4.0**
Lower Mud Creek-43	861	1.0	342.7	7.9	319.4	4.1	488.0	60.0	**319.4**	**4.1**
Lower Mud Creek-44	274	1.5	347.5	9.3	324.6	4.4	457.0	70.0	**324.6**	**4.4**
Lower Mud Creek-45	216	1.5	325.1	7.6	323.9	3.7	310.0	60.0	**323.9**	**3.7**
Lower Mud Creek-46	168	1.6	326.1	10.0	321.5	7.5	321.0	80.0	**321.5**	**7.5**
Lower Mud Creek-47	398	1.3	328.9	7.0	327.6	4.1	305.0	56.0	**327.6**	**4.1**
Lower Mud Creek-48	359	1.1	333.1	8.4	316.8	3.9	418.0	65.0	**316.8**	**3.9**
Lower Mud Creek-49	204	1.7	328.7	10.0	322.6	4.5	329.0	72.0	**322.6**	**4.5**
Lower Mud Creek-50	282	1.2	331.9	7.0	316.0	4.5	413.0	59.0	**316.0**	**4.5**
Lower Mud Creek-51	164	1.8	323.2	8.7	321.7	4.3	305.0	74.0	**321.7**	**4.3**

Lower Mud Creek-52	373	1.6	326.8	7.7	310.4	5.3	436.0	52.0	**310.4**	**5.3**
Lower Mud Creek-53	291	1.4	342.6	8.9	315.1	4.4	494.0	64.0	**315.1**	**4.4**
Lower Mud Creek-54	454	1.3	335.6	8.1	309.7	4.9	483.0	67.0	**309.7**	**4.9**
Lower Mud Creek-55	399	0.9	329.9	5.1	321.7	3.5	374.0	44.0	**321.7**	**3.5**
Lower Mud Creek-56	230	1.4	332.1	9.0	328.2	4.9	321.0	74.0	**328.2**	**4.9**
Lower Mud Creek-57	225	1.5	328.3	7.4	324.6	3.5	314.0	59.0	**324.6**	**3.5**
Lower Mud Creek-58	328	1.1	330.2	8.1	319.2	5.9	386.0	77.0	**319.2**	**5.9**
Lower Mud Creek-59	170	1.8	340.2	8.7	326.7	4.4	388.0	73.0	**326.7**	**4.4**
Lower Mud Creek-60	184	1.7	333.4	9.6	321.5	6.0	401.0	78.0	**321.5**	**6.0**
Lower Mud Creek-61	324	0.9	320.1	11.0	314.7	5.2	322.0	78.0	**314.7**	**5.2**
Lower Mud Creek-62	178	1.4	342.3	7.6	323.9	4.3	431.0	62.0	**323.9**	**4.3**
Lower Mud Creek-63	210	1.7	330.8	9.2	318.1	4.3	389.0	65.0	**318.1**	**4.3**
Lower Mud Creek-64	151	1.8	329.4	9.6	324.6	4.5	303.0	78.0	**324.6**	**4.5**
Lower Mud Creek-65	197	1.6	324.1	8.4	321.0	4.8	299.0	67.0	**321.0**	**4.8**
Lower Mud Creek-66	225	1.5	334.9	8.7	327.9	4.1	345.0	66.0	**327.9**	**4.1**
Lower Mud Creek-67	351	1.4	333.9	14.0	314.4	6.5	400.0	160.0	**314.4**	**6.5**
Lower Mud Creek-68	354	1.3	335.1	11.0	320.0	5.6	419.0	77.0	**320.0**	**5.6**
Lower Mud Creek-69	371	1.5	327.5	12.0	326.1	7.5	321.0	86.0	**326.1**	**7.5**
Lower Mud Creek-70	335	1.5	329.2	8.1	321.5	3.7	341.0	65.0	**321.5**	**3.7**
Lower Mud Creek-71	198	1.4	364.1	14.0	295.8	5.5	778.0	82.0	**295.8**	**5.5**
Lower Mud Creek-72	309	2.0	321.6	8.7	315.9	4.9	328.0	71.0	**315.9**	**4.9**
Lower Mud Creek-73	251	1.6	332.7	7.7	329.5	4.1	327.0	62.0	**329.5**	**4.1**
Lower Mud Creek-74	195	1.8	336.1	8.7	323.4	4.0	372.0	70.0	**323.4**	**4.0**
Lower Mud Creek-75	200	1.5	333.4	8.5	314.9	4.3	419.0	69.0	**314.9**	**4.3**
Lower Mud Creek-76	214	1.6	323.8	9.0	318.9	3.9	317.0	70.0	**318.9**	**3.9**
Lower Mud Creek-77	184	2.1	953.7	23.0	911.0	15.9	1037.0	72.0	**911.0**	**15.9**

Lower Mud Creek-78	228	1.5	336.5	10.0	323.3	4.8	388.0	80.0	**323.3**	**4.8**
Lower Mud Creek-79	385	3.4	494.7	16.0	483.8	12.8	513.0	69.0	**483.8**	**12.8**
Lower Mud Creek-80	82	1.0	775.1	19.0	761.8	15.4	789.0	60.0	**761.8**	**15.4**
Lower Mud Creek-81	270	1.8	340.7	9.1	316.7	5.5	478.0	61.0	**316.7**	**5.5**
Lower Mud Creek-82	317	1.5	334.7	8.4	317.9	4.5	431.0	65.0	**317.9**	**4.5**
Lower Mud Creek-83	234	1.7	368.0	12.0	330.5	6.8	571.0	79.0	**330.5**	**6.8**
Lower Mud Creek-84	281	1.2	326.2	8.4	317.6	4.1	344.0	65.0	**317.6**	**4.1**
Lower Mud Creek-85	510	0.8	326.6	8.9	314.6	4.8	369.0	68.0	**314.6**	**4.8**
Lower Mud Creek-86	263	1.4	331.9	9.0	326.2	4.4	329.0	71.0	**326.2**	**4.4**
Lower Mud Creek-87	212	1.6	328.9	11.0	314.3	5.0	369.0	85.0	**314.3**	**5.0**
Lower Mud Creek-88	183	1.9	336.5	12.0	322.7	6.2	426.0	91.0	**322.7**	**6.2**
Lower Mud Creek-89	154	2.3	327.3	8.7	319.9	4.8	337.0	71.0	**319.9**	**4.8**
Lower Mud Creek-90	189	1.7	329.9	9.7	324.0	4.1	314.0	79.0	**324.0**	**4.1**
Lower Mud Creek-91	265	1.2	323.5	10.0	316.9	5.8	330.0	85.0	**316.9**	**5.8**
Lower Mud Creek-92	305	1.2	352.7	12.0	325.2	8.7	460.0	110.0	**325.2**	**8.7**
Lower Mud Creek-93	296	1.6	333.3	11.0	324.9	5.6	353.0	82.0	**324.9**	**5.6**
Lower Mud Creek-94	430	1.2	347.3	13.0	313.7	6.9	530.0	100.0	**313.7**	**6.9**
Lower Mud Creek-95	234	1.9	328.8	9.6	318.2	4.6	355.0	72.0	**318.2**	**4.6**
Lower Mud Creek-96	194	1.9	325.9	16.0	312.2	8.1	400.0	110.0	**312.2**	**8.1**
Lower Mud Creek-97	192	2.1	354.1	19.0	331.1	10.6	460.0	130.0	**331.1**	**10.6**
Lower Mud Creek-98	311	1.3	344.5	8.6	320.8	4.4	463.0	63.0	**320.8**	**4.4**
Lower Mud Creek-99	312	1.5	345.5	16.0	325.2	6.9	434.0	98.0	**325.2**	**6.9**
Lower Mud Creek-100	309	1.2	345.8	12.0	302.1	5.1	586.0	97.0	**302.1**	**5.1**
Lower Mud Creek-101	303	1.7	335.3	14.0	292.1	6.8	623.0	97.0	**292.1**	**6.8**
Lower Mud Creek-102	226	1.5	341.9	10.0	307.5	5.2	543.0	82.0	**307.5**	**5.2**
Lower Mud Creek-103	212	1.8	326.8	14.0	313.2	5.2	370.0	110.0	**313.2**	**5.2**

Lower Mud Creek-104	315	1.6	328.7	11.0	321.0	5.1	348.0	85.0	**321.0**	**5.1**
Lower Mud Creek-105	133	2.1	335.9	12.0	328.4	5.5	312.0	97.0	**328.4**	**5.5**
Lower Mud Creek-106	418	1.6	364.6	13.0	352.1	7.5	420.0	110.0	**352.1**	**7.5**
Lower Mud Creek-107	228	1.7	327.1	9.3	318.5	5.0	345.0	73.0	**318.5**	**5.0**
Lower Mud Creek-108	190	1.9	333.6	12.0	325.3	4.9	338.0	93.0	**325.3**	**4.9**
Lower Mud Creek-109	397	1.3	318.2	11.0	295.5	4.3	429.0	91.0	**295.5**	**4.3**
Lower Mud Creek-110	286	1.4	327.4	9.4	318.4	3.8	344.0	72.0	**318.4**	**3.8**
Lower Mud Creek-111	264	1.6	332.9	12.0	319.9	5.2	373.0	95.0	**319.9**	**5.2**
Lower Mud Creek-112	171	1.6	330.8	9.5	316.5	4.4	386.0	77.0	**316.5**	**4.4**
Lower Mud Creek-113	196	1.7	338.2	10.0	315.2	4.2	437.0	74.0	**315.2**	**4.2**
Lower Mud Creek-114	367	1.2	334.3	8.3	320.8	3.9	378.0	68.0	**320.8**	**3.9**
Lower Mud Creek-115	224	1.4	327.4	6.8	314.9	3.7	381.0	56.0	**314.9**	**3.7**
Upper Mud Creek										
Upper Mud Creek-1	94	2.6	963.1	11.0	955.2	8.8	966.0	39.0	**966.0**	**39.0**
Upper Mud Creek-2	138	1.6	1053.7	16.0	1029.6	14.0	1085.0	50.0	**1085.0**	**50.0**
Upper Mud Creek-3	43	1.2	1100.0	18.0	1070.8	15.1	1133.0	55.0	**1133.0**	**55.0**
Upper Mud Creek-4	285	1.2	471.8	8.9	456.8	5.9	523.0	54.0	**456.8**	**5.9**
Upper Mud Creek-5	714	3.9	439.2	6.1	416.4	5.3	538.0	43.0	**416.4**	**5.3**
Upper Mud Creek-6	54	1.8	1170.0	16.0	1165.5	15.6	1169.0	42.0	**1169.0**	**42.0**
Upper Mud Creek-7	377	1.6	496.5	11.0	471.1	7.9	603.0	61.0	**471.1**	**7.9**
Upper Mud Creek-8	917	5.6	413.4	11.0	394.1	8.6	506.0	65.0	**394.1**	**8.6**
Upper Mud Creek-9	561	1.5	377.2	5.0	377.0	3.8	366.0	35.0	**377.0**	**3.8**
Upper Mud Creek-10	90	0.7	636.9	12.0	615.8	8.5	685.0	57.0	**615.8**	**8.5**
Upper Mud Creek-11	90	1.8	991.8	15.0	978.9	11.2	997.0	51.0	**997.0**	**51.0**
Upper Mud Creek-12	151	0.9	1649.7	16.0	1609.2	21.5	1691.0	32.0	**1691.0**	**32.0**
Upper Mud Creek-13	168	1.3	1055.0	13.0	1051.8	11.6	1050.0	36.0	**1050.0**	**36.0**

171

Upper Mud Creek-14	151	2.7	1007.3	12.0	995.0	11.1	1023.0	34.0	**1023.0**	**34.0**
Upper Mud Creek-15	77	2.9	1399.4	20.0	1359.8	26.7	1444.0	49.0	**1444.0**	**49.0**
Upper Mud Creek-16	1110	5.2	428.8	8.7	386.9	4.7	630.0	50.0	**386.9**	**4.7**
Upper Mud Creek-17	119	1.6	474.4	9.7	474.0	6.1	460.0	56.0	**474.0**	**6.1**
Upper Mud Creek-18	144	3.3	1030.5	14.0	1007.2	13.4	1062.0	46.0	**1062.0**	**46.0**
Upper Mud Creek-19	63	3.1	1438.9	15.0	1397.0	17.6	1486.0	35.0	**1486.0**	**35.0**
Upper Mud Creek-20	459	7.8	362.6	5.9	359.2	5.1	379.0	43.0	**359.2**	**5.1**
Upper Mud Creek-21	292	1.2	477.7	9.9	415.0	6.1	785.0	49.0	**415.0**	**6.1**
Upper Mud Creek-22	377	0.8	452.3	6.9	447.5	4.1	452.0	43.0	**447.5**	**4.1**
Upper Mud Creek-23	115	1.9	1471.0	15.0	1462.6	17.2	1467.0	38.0	**1467.0**	**38.0**
Upper Mud Creek-24	495	1.9	435.1	7.3	422.2	4.7	486.0	41.0	**422.2**	**4.7**
Upper Mud Creek-25	177	3.6	1021.6	12.0	1013.2	9.9	1021.0	37.0	**1021.0**	**37.0**
Upper Mud Creek-26	939	1.8	468.1	9.3	448.7	5.4	561.0	57.0	**448.7**	**5.4**
Upper Mud Creek-27	523	0.9	476.7	7.2	370.2	5.2	1009.0	41.0	**370.2**	**5.2**
Upper Mud Creek-28	728	2.8	455.9	8.3	448.8	5.0	459.0	52.0	**448.8**	**5.0**
Upper Mud Creek-29	62	1.6	466.0	13.0	447.8	6.8	515.0	78.0	**447.8**	**6.8**
Upper Mud Creek-30	970	2.1	531.1	11.0	370.2	9.6	1241.0	77.0	**370.2**	**9.6**
Upper Mud Creek-31	407	2.1	1146.4	14.0	1132.2	18.3	1162.0	34.0	**1162.0**	**34.0**
Upper Mud Creek-32	639	1.6	450.3	6.9	441.4	4.8	483.0	43.0	**441.4**	**4.8**
Upper Mud Creek-33	928	5.3	414.7	11.0	365.5	7.4	677.0	83.0	**365.5**	**7.4**
Upper Mud Creek-34	286	1.6	460.0	9.3	452.8	5.4	453.0	60.0	**452.8**	**5.4**
Upper Mud Creek-35	74	2.9	995.2	16.0	975.1	13.5	1011.0	49.0	**1011.0**	**49.0**
Upper Mud Creek-36	509	6.1	436.5	8.5	421.8	4.7	477.0	56.0	**421.8**	**4.7**
Upper Mud Creek-37	122	2.5	1152.5	15.0	1152.2	13.3	1134.0	42.0	**1134.0**	**42.0**
Upper Mud Creek-38	344	6.6	434.1	6.4	426.7	5.0	454.0	39.0	**426.7**	**5.0**
Upper Mud Creek-39	323	1.1	333.3	6.6	312.1	3.6	452.0	52.0	**312.1**	**3.6**

Upper Mud Creek-40	178	1.7	474.4	9.3	466.8	5.7	473.0	54.0	**466.8**	**5.7**
Upper Mud Creek-41	601	4.6	1059.5	13.0	955.9	11.6	1261.0	40.0	**1261.0**	**40.0**
Upper Mud Creek-42	133	24.4	1488.1	29.0	1459.2	25.1	1500.0	72.0	**1500.0**	**72.0**
Upper Mud Creek-43	665	6.9	502.4	10.0	464.6	7.9	672.0	40.0	**464.6**	**7.9**
Upper Mud Creek-44	251	1.0	1087.6	14.0	1060.2	11.1	1118.0	41.0	**1118.0**	**41.0**
Upper Mud Creek-45	631	5.1	580.9	20.0	494.5	14.4	919.0	63.0	**494.5**	**14.4**
Upper Mud Creek-46	858	2.2	417.0	6.4	394.2	4.6	522.0	41.0	**394.2**	**4.6**
Upper Mud Creek-47	404	57.0	882.9	14.0	871.5	9.5	881.0	47.0	**871.5**	**9.5**
Upper Mud Creek-48	168	0.8	464.3	10.0	443.6	5.5	546.0	63.0	**443.6**	**5.5**
Upper Mud Creek-49	312	2.3	470.7	8.1	463.9	5.5	476.0	46.0	**463.9**	**5.5**
Upper Mud Creek-50	237	1.9	465.3	9.2	451.5	5.9	504.0	51.0	**451.5**	**5.9**
Upper Mud Creek-51	765	4.8	362.2	6.9	356.3	4.2	370.0	52.0	**356.3**	**4.2**
Upper Mud Creek-52	121	2.2	1468.7	17.0	1472.9	15.1	1438.0	42.0	**1438.0**	**42.0**
Upper Mud Creek-53	146	1.3	1479.1	13.0	1499.4	20.5	1437.0	35.0	**1437.0**	**35.0**
Upper Mud Creek-54	106	5.2	1011.0	11.0	1007.9	10.5	998.0	36.0	**998.0**	**36.0**
Upper Mud Creek-55	247	2.0	472.8	10.0	468.9	8.6	473.0	53.0	**468.9**	**8.6**
Upper Mud Creek-56	394	2.2	439.0	16.0	377.1	8.0	716.0	93.0	**377.1**	**8.0**
Upper Mud Creek-57	94	0.5	897.8	20.0	856.4	13.6	983.0	59.0	**856.4**	**13.6**
Upper Mud Creek-58	67	1.2	1014.9	25.0	970.6	19.3	1050.0	79.0	**1050.0**	**79.0**
Upper Mud Creek-59	483	1.1	467.6	8.1	461.9	5.9	466.0	48.0	**461.9**	**5.9**
Upper Mud Creek-60	153	1.0	1358.2	14.0	1342.0	16.0	1368.0	32.0	**1368.0**	**32.0**
Upper Mud Creek-61	141	2.4	1100.0	16.0	1109.9	12.8	1054.0	47.0	**1054.0**	**47.0**
Upper Mud Creek-62	466	9.7	370.9	6.1	368.8	3.8	363.0	46.0	**368.8**	**3.8**
Upper Mud Creek-63	809	0.6	677.8	15.0	356.4	4.9	1950.0	52.0	**356.4**	**4.9**
Upper Mud Creek-64	410	3.5	483.4	7.6	470.5	6.7	529.0	44.0	**470.5**	**6.7**
Upper Mud Creek-65	952	2.6	492.6	23.0	393.6	9.3	890.0	130.0	**393.6**	**9.3**

Upper Mud Creek-66	114	1.4	1352.6	14.0	1351.0	16.6	1339.0	38.0	**1339.0**	**38.0**
Upper Mud Creek-67	336	1.9	324.1	5.9	323.4	3.7	306.0	48.0	**323.4**	**3.7**
Upper Mud Creek-68	107	2.7	1064.9	15.0	1074.4	12.3	1017.0	44.0	**1017.0**	**44.0**
Upper Mud Creek-69	89	1.1	997.4	15.0	987.0	12.3	984.0	50.0	**984.0**	**50.0**
Upper Mud Creek-70	288	1.1	330.7	6.3	309.3	4.2	449.0	53.0	**309.3**	**4.2**
Upper Mud Creek-71	169	1.2	551.2	12.0	541.0	8.5	567.0	60.0	**541.0**	**8.5**
Upper Mud Creek-72	288	0.8	1430.1	13.0	1393.4	14.9	1474.0	33.0	**1474.0**	**33.0**
Upper Mud Creek-73	168	1.5	523.4	12.0	429.9	5.9	923.0	64.0	**429.9**	**5.9**
Upper Mud Creek-74	290	3.9	1079.4	14.0	1053.3	15.0	1134.0	36.0	**1134.0**	**36.0**
Upper Mud Creek-75	30	0.6	962.1	20.0	893.6	16.4	1079.0	72.0	**893.6**	**16.4**
Upper Mud Creek-76	212	0.8	1208.5	15.0	1135.4	12.7	1326.0	40.0	**1326.0**	**40.0**
Upper Mud Creek-77	39	2.5	1076.8	17.0	1058.3	15.7	1082.0	54.0	**1082.0**	**54.0**
Upper Mud Creek-78	232	0.8	463.5	11.0	421.3	6.0	652.0	61.0	**421.3**	**6.0**
Chickasaw Creek										
Chickasaw-1	581	1.1	338.2	5.8	325.7	3.4	404.0	42.0	**325.7**	**3.4**
Chickasaw-2	638	1.5	382.8	16.0	316.4	4.5	750.0	100.0	**316.4**	**4.5**
Chickasaw-3	384	1.2	336.7	9.0	303.2	4.1	549.0	63.0	**303.2**	**4.1**
Chickasaw-4	1050	0.8	368.6	20.0	333.8	7.5	580.0	100.0	**333.8**	**7.5**
Chickasaw-5	447	1.0	1070.9	19.0	986.7	15.1	1224.0	56.0	**1224.0**	**56.0**
Chickasaw-6	590	1.2	327.8	6.2	323.4	3.6	331.0	51.0	**323.4**	**3.6**
Chickasaw-7	437	1.5	364.9	14.0	343.4	8.7	500.0	110.0	**343.4**	**8.7**
Chickasaw-8	1038	0.8	325.5	8.7	322.0	5.5	337.0	56.0	**322.0**	**5.5**
Chickasaw-9	509	1.3	332.5	7.3	316.1	3.3	413.0	60.0	**316.1**	**3.3**
Chickasaw-10	410	1.5	323.5	8.4	318.6	5.7	325.0	76.0	**318.6**	**5.7**
Chickasaw-11	665	1.4	333.3	5.5	325.4	3.8	363.0	49.0	**325.4**	**3.8**
Chickasaw-12	679	1.1	333.8	9.6	318.6	5.4	426.0	68.0	**318.6**	**5.4**

174

Chickasaw-13	482	0.8	356.2	11.0	302.5	6.1	685.0	94.0	**302.5**	**6.1**
Chickasaw-14	532	0.9	351.0	6.9	306.5	3.4	626.0	52.0	**306.5**	**3.4**
Chickasaw-15	691	1.0	323.0	6.0	318.6	3.2	339.0	51.0	**318.6**	**3.2**
Chickasaw-16	63	1.4	1526.9	21.0	1499.8	23.6	1546.0	54.0	**1546.0**	**54.0**
Chickasaw-17	711	1.1	325.3	6.7	312.1	3.9	390.0	55.0	**312.1**	**3.9**
Chickasaw-18	866	1.2	378.0	19.0	305.0	5.5	810.0	130.0	**305.0**	**5.5**
Chickasaw-19	776	1.2	338.0	6.6	316.1	3.1	467.0	51.0	**316.1**	**3.1**
Chickasaw-20	455	1.9	434.4	7.7	413.8	5.2	525.0	48.0	**413.8**	**5.2**
Chickasaw-21	617	1.3	370.4	7.9	320.6	3.2	650.0	57.0	**320.6**	**3.2**
Chickasaw-22	1500	0.8	345.1	6.8	329.9	6.2	434.0	58.0	**329.9**	**6.2**
Chickasaw-23	235	0.7	594.2	13.0	528.5	9.1	838.0	63.0	**528.5**	**9.1**
Chickasaw-24	901	1.1	326.1	6.9	323.9	4.9	320.0	57.0	**323.9**	**4.9**
Chickasaw-25	738	1.2	348.4	14.0	313.3	4.6	551.0	85.0	**313.3**	**4.6**
Chickasaw-26	587	0.7	355.6	11.0	314.6	5.3	606.0	79.0	**314.6**	**5.3**
Chickasaw-27	785	0.7	367.9	12.0	328.3	5.5	585.0	79.0	**328.3**	**5.5**
Chickasaw-28	458	1.2	390.6	11.0	321.1	5.7	789.0	67.0	**321.1**	**5.7**
Chickasaw-29	289	1.3	339.7	8.4	316.2	3.6	448.0	67.0	**316.2**	**3.6**
Chickasaw-30	138	2.6	993.6	17.0	990.2	17.5	972.0	56.0	**972.0**	**56.0**
Chickasaw-31	652	1.3	477.7	8.3	466.0	4.8	502.0	49.0	**466.0**	**4.8**
Chickasaw-32	3107	0.7	336.4	7.9	322.0	5.6	423.0	56.0	**322.0**	**5.6**
Chickasaw-33	790	0.7	344.3	6.1	309.1	3.7	565.0	45.0	**309.1**	**3.7**
Chickasaw-34	408	1.0	326.3	7.5	319.4	4.5	348.0	56.0	**319.4**	**4.5**
Chickasaw-35	1391	0.9	329.2	6.0	323.8	3.1	343.0	47.0	**323.8**	**3.1**
Chickasaw-36	1144	1.1	411.6	11.0	335.2	7.3	846.0	69.0	**335.2**	**7.3**
Chickasaw-37	617	1.2	336.1	5.9	328.0	3.2	370.0	48.0	**328.0**	**3.2**
Chickasaw-38	297	1.3	328.0	7.0	318.4	3.3	365.0	59.0	**318.4**	**3.3**

175

Chickasaw-39	625	0.8	379.2	10.0	303.5	4.9	860.0	64.0	**303.5**	**4.9**
Chickasaw-40	1515	0.8	330.8	4.9	326.2	4.0	355.0	43.0	**326.2**	**4.0**
Chickasaw-41	529	1.2	342.1	7.5	319.4	3.7	472.0	53.0	**319.4**	**3.7**
Chickasaw-42	451	1.2	332.6	11.0	323.6	6.0	361.0	90.0	**323.6**	**6.0**
Chickasaw-43	217	2.1	328.6	11.0	318.0	5.9	375.0	86.0	**318.0**	**5.9**
Chickasaw-44	869	1.1	338.3	9.4	321.8	6.8	413.0	64.0	**321.8**	**6.8**
Chickasaw-45	883	0.8	350.7	9.7	310.6	4.5	593.0	80.0	**310.6**	**4.5**
Chickasaw-46	834	0.8	334.4	8.0	320.4	4.7	407.0	64.0	**320.4**	**4.7**
Chickasaw-47	3031	0.5	408.2	8.8	310.5	4.6	985.0	51.0	**310.5**	**4.6**
Chickasaw-48	357	0.9	357.1	8.9	299.3	4.0	709.0	70.0	**299.3**	**4.0**
Chickasaw-49	222	1.4	324.2	10.0	321.2	4.6	308.0	77.0	**321.2**	**4.6**
Chickasaw-50	453	1.0	417.7	11.0	313.7	3.9	989.0	69.0	**313.7**	**3.9**
Chickasaw-51	598	1.0	324.5	6.9	319.7	3.6	325.0	59.0	**319.7**	**3.6**
Chickasaw-52	557	0.8	350.2	16.0	304.1	3.7	640.0	110.0	**304.1**	**3.7**
Chickasaw-53	1000	0.7	393.7	18.0	347.5	6.9	630.0	110.0	**347.5**	**6.9**
Chickasaw-54	706	0.9	330.2	6.7	315.8	3.5	404.0	50.0	**315.8**	**3.5**
Chickasaw-55	350	1.6	326.8	7.1	320.5	3.4	339.0	55.0	**320.5**	**3.4**
Chickasaw-56	294	1.4	342.0	11.0	325.9	5.5	409.0	77.0	**325.9**	**5.5**
Chickasaw-57	77	1.4	417.4	32.0	357.2	13.1	680.0	200.0	**357.2**	**13.1**
Chickasaw-58	424	1.6	329.0	7.5	325.3	3.6	326.0	60.0	**325.3**	**3.6**
Chickasaw-59	561	1.2	352.9	11.0	316.4	3.6	548.0	81.0	**316.4**	**3.6**
Chickasaw-60	374	1.2	400.0	16.0	305.6	5.0	944.0	99.0	**305.6**	**5.0**
Chickasaw-61	453	1.2	323.1	6.6	319.9	3.4	319.0	54.0	**319.9**	**3.4**
Chickasaw-62	562	0.8	438.5	8.4	406.9	6.1	588.0	50.0	**406.9**	**6.1**
Chickasaw-63	781	1.1	327.8	7.1	318.7	4.1	381.0	61.0	**318.7**	**4.1**
Chickasaw-64	678	1.2	342.6	6.3	331.2	3.7	403.0	51.0	**331.2**	**3.7**

Chickasaw-65	2700	0.5	349.7	4.0	330.7	3.1	467.0	32.0	**330.7**	**3.1**
Chickasaw-66	648	3.3	1132.4	29.0	1032.0	36.4	1321.0	49.0	**1321.0**	**49.0**
Chickasaw-67	1168	0.6	334.4	5.6	321.0	3.1	407.0	48.0	**321.0**	**3.1**
Chickasaw-68	881	0.9	401.4	7.4	337.1	3.6	761.0	45.0	**337.1**	**3.6**
Chickasaw-69	788	0.9	339.9	5.9	314.8	3.8	490.0	45.0	**314.8**	**3.8**
Chickasaw-70	516	1.4	324.2	5.9	321.1	3.6	318.0	51.0	**321.1**	**3.6**
Chickasaw-71	699	0.9	328.9	6.5	320.0	3.7	378.0	49.0	**320.0**	**3.7**
Chickasaw-72	890	0.6	347.1	7.4	313.5	4.0	557.0	56.0	**313.5**	**4.0**
Chickasaw-73	665	1.0	333.1	6.8	317.3	4.8	420.0	52.0	**317.3**	**4.8**
Chickasaw-74	608	1.2	328.2	7.0	319.8	5.0	365.0	57.0	**319.8**	**5.0**
Chickasaw-75	936	0.9	334.5	6.9	324.5	4.1	389.0	56.0	**324.5**	**4.1**
Chickasaw-76	566	0.8	349.6	12.0	323.5	6.1	505.0	86.0	**323.5**	**6.1**
Chickasaw-77	452	1.5	339.0	8.6	326.0	5.4	419.0	71.0	**326.0**	**5.4**
Chickasaw-78	1609	0.8	325.3	8.4	323.0	5.2	319.0	61.0	**323.0**	**5.2**
Chickasaw-79	901	0.6	516.7	17.0	327.1	5.0	1412.0	81.0	**327.1**	**5.0**
Chickasaw-80	515	0.8	353.3	7.7	313.2	5.4	619.0	50.0	**313.2**	**5.4**
Chickasaw-81	868	1.0	330.8	8.5	313.2	4.8	418.0	66.0	**313.2**	**4.8**
Barnett										
Barnett-1	658	1.0	255.4	7.8	235.6	5.1	412.0	68.0	**235.6**	**5.1**
Barnett-2	2460	0.8	257.6	7.9	246.6	4.4	329.0	71.0	**246.6**	**4.4**
Barnett-3	545	0.2	288.5	8.4	254.0	3.6	546.0	65.0	**254.0**	**3.6**
Barnett-4	97	0.7	310.7	8.6	271.7	5.1	579.0	63.0	**271.7**	**5.1**
Barnett-5	103	0.3	329.0	19.3	273.8	12.0	740.0	49.0	**273.8**	**12.0**
Barnett-6	470	0.1	279.9	9.3	274.4	5.8	353.0	89.0	**274.4**	**5.8**
Barnett-7	308	1.0	289.3	6.1	275.2	3.1	391.0	50.0	**275.2**	**3.1**
Barnett-8	169	1.5	310.1	11.0	281.6	8.0	487.0	60.0	**281.6**	**8.0**

Barnett-9	297	0.3	306.9	9.0	292.9	4.3	382.0	68.0	**292.9**	**4.3**
Barnett-10	342	1.6	307.3	5.6	293.6	4.0	395.0	52.0	**293.6**	**4.0**
Barnett-11	916	1.1	312.2	8.9	294.2	6.0	426.0	69.0	**294.2**	**6.0**
Barnett-12	258	0.6	355.2	9.2	294.4	4.3	727.0	71.0	**294.4**	**4.3**
Barnett-13	173	0.5	315.0	8.2	296.4	5.7	453.0	56.0	**296.4**	**5.7**
Barnett-14	97	0.4	511.3	25.0	296.9	5.6	1520.0	120.0	**296.9**	**5.6**
Barnett-15	830	0.5	339.6	13.0	297.3	5.0	599.0	90.0	**297.3**	**5.0**
Barnett-16	291	1.3	311.2	7.7	300.4	4.4	358.0	63.0	**300.4**	**4.4**
Barnett-17	609	1.1	324.3	7.9	301.5	3.3	453.0	61.0	**301.5**	**3.3**
Barnett-18	480	1.5	346.6	9.9	301.5	3.9	599.0	73.0	**301.5**	**3.9**
Barnett-19	688	0.9	303.1	4.8	302.3	4.1	301.0	39.0	**302.3**	**4.1**
Barnett-20	406	1.4	318.8	9.7	302.3	5.8	411.0	68.0	**302.3**	**5.8**
Barnett-21	232	0.7	371.9	8.6	302.7	4.5	813.0	57.0	**302.7**	**4.5**
Barnett-22	124	0.4	340.5	30.0	303.7	15.5	570.0	160.0	**303.7**	**15.5**
Barnett-23	860	1.1	311.9	6.0	304.5	3.2	340.0	52.0	**304.5**	**3.2**
Barnett-24	892	1.5	314.4	6.5	305.0	3.7	352.0	51.0	**305.0**	**3.7**
Barnett-25	383	0.6	388.0	14.0	305.3	4.4	895.0	89.0	**305.3**	**4.4**
Barnett-26	200	1.8	335.3	7.9	305.3	3.9	516.0	58.0	**305.3**	**3.9**
Barnett-27	958	0.7	325.2	9.7	305.4	5.8	425.0	71.0	**305.4**	**5.8**
Barnett-28	253	1.7	317.9	5.9	307.3	3.4	369.0	48.0	**307.3**	**3.4**
Barnett-29	356	1.4	308.1	6.2	308.2	4.8	331.0	47.0	**308.2**	**4.8**
Barnett-30	210	0.2	329.0	13.0	309.1	5.2	460.0	97.0	**309.1**	**5.2**
Barnett-31	272	2.1	318.6	13.0	310.3	4.9	336.0	98.0	**310.3**	**4.9**
Barnett-32	785	0.4	350.5	7.5	310.4	3.2	585.0	55.0	**310.4**	**3.2**
Barnett-33	119	1.0	326.9	7.1	311.1	4.2	402.0	57.0	**311.1**	**4.2**
Barnett-34*	526	0.8	321.8	9.9	311.8	4.8	389.0	74.0	**311.8**	**4.8**

Barnett-35	263	0.4	324.4	16.8	311.9	13.3	414.9	41.5	**311.9**	**13.3**
Barnett-36	372	1.7	325.0	6.0	313.4	3.2	375.0	50.0	**313.4**	**3.2**
Barnett-37	310	0.4	363.3	9.5	313.8	4.2	697.0	61.0	**313.8**	**4.2**
Barnett-38	699	1.0	321.5	8.7	314.0	5.1	350.0	67.0	**314.0**	**5.1**
Barnett-39	229	2.0	327.7	8.5	314.7	4.0	373.0	65.0	**314.7**	**4.0**
Barnett-40	216	1.9	328.6	8.4	315.2	4.1	380.0	64.0	**315.2**	**4.1**
Barnett-41	369	0.5	314.3	13.4	315.8	10.8	303.4	35.0	**315.8**	**10.8**
Barnett-42	914	0.9	336.5	9.5	316.0	8.1	456.0	79.0	**316.0**	**8.1**
Barnett-43	655	1.1	324.4	9.2	316.1	4.2	342.0	76.0	**316.1**	**4.2**
Barnett-44	191	2.0	327.1	8.8	316.3	3.5	362.0	68.0	**316.3**	**3.5**
Barnett-45	272	3.8	325.9	8.2	316.7	4.0	350.0	65.0	**316.7**	**4.0**
Barnett-46*	705	0.3	312.0	11.0	317.0	9.6	307.0	95.0	**317.0**	**9.6**
Barnett-47	228	1.3	317.6	8.7	317.7	4.5	275.0	69.0	**317.7**	**4.5**
Barnett-48	230	1.5	326.5	6.9	317.9	3.6	350.0	56.0	**317.9**	**3.6**
Barnett-49	310	1.3	323.3	4.9	318.1	3.1	343.0	40.0	**318.1**	**3.1**
Barnett-50	563	1.0	326.3	7.9	318.3	3.5	358.0	62.0	**318.3**	**3.5**
Barnett-51	255	1.2	327.0	8.5	318.5	3.8	338.0	70.0	**318.5**	**3.8**
Barnett-52	628	1.9	326.7	6.4	318.7	3.0	353.0	52.0	**318.7**	**3.0**
Barnett-53	270	1.3	327.2	10.0	318.7	4.8	330.0	86.0	**318.7**	**4.8**
Barnett-54	314	0.5	316.0	12.9	318.8	9.4	295.9	36.5	**318.8**	**9.4**
Barnett-55	375	2.3	325.8	7.9	318.9	3.4	327.0	65.0	**318.9**	**3.4**
Barnett-56*	99	1.8	325.9	8.1	319.0	3.9	340.0	67.0	**319.0**	**3.9**
Barnett-57	122	1.3	323.5	7.3	319.0	4.6	348.0	60.0	**319.0**	**4.6**
Barnett-58	387	1.3	321.1	6.4	319.3	4.5	334.0	47.0	**319.3**	**4.5**
Barnett-59	277	1.8	323.7	8.0	319.3	3.6	317.0	62.0	**319.3**	**3.6**
Barnett-60	308	1.1	348.8	9.4	319.4	5.2	573.0	68.0	**319.4**	**5.2**

Barnett-61	623	0.7	317.7	9.6	319.5	4.2	305.0	73.0	**319.5**	**4.2**
Barnett-62	289	1.1	325.7	7.3	319.8	3.6	334.0	60.0	**319.8**	**3.6**
Barnett-63	311	0.5	317.6	13.7	319.9	11.5	300.6	34.2	**319.9**	**11.5**
Barnett-64	189	3.0	329.9	9.1	320.0	5.1	366.0	69.0	**320.0**	**5.1**
Barnett-65	641	1.0	328.8	9.6	320.3	6.8	428.0	74.0	**320.3**	**6.8**
Barnett-66	718	1.1	327.7	7.4	320.4	3.4	343.0	58.0	**320.4**	**3.4**
Barnett-67	728	1.2	318.8	7.1	320.5	4.4	296.0	56.0	**320.5**	**4.4**
Barnett-68	425	1.1	327.9	8.6	320.7	3.9	338.0	69.0	**320.7**	**3.9**
Barnett-69	521	2.1	326.8	6.6	321.1	3.4	338.0	51.0	**321.1**	**3.4**
Barnett-70	189	1.8	325.6	8.5	321.6	3.8	311.0	68.0	**321.6**	**3.8**
Barnett-71*	588	1.2	323.0	6.2	321.6	5.7	328.0	49.0	**321.6**	**5.7**
Barnett-72	151	2.1	328.0	8.7	321.9	3.5	329.0	67.0	**321.9**	**3.5**
Barnett-73	182	1.6	329.3	7.7	322.1	4.1	347.0	58.0	**322.1**	**4.1**
Barnett-74	374	0.7	324.9	6.3	322.3	2.7	332.0	50.0	**322.3**	**2.7**
Barnett-75	826	1.1	331.0	6.3	322.3	3.7	365.0	50.0	**322.3**	**3.7**
Barnett-76	180	1.6	330.3	11.0	322.7	5.1	337.0	90.0	**322.7**	**5.1**
Barnett-77	405	0.6	326.2	13.2	322.9	11.3	350.3	30.0	**322.9**	**11.3**
Barnett-78	524	0.4	325.4	13.2	322.9	12.0	343.7	27.0	**322.9**	**12.0**
Barnett-79	370	1.0	338.9	12.0	323.1	7.5	407.0	82.0	**323.1**	**7.5**
Barnett-80	1010	1.0	331.7	4.9	323.1	3.0	367.0	42.0	**323.1**	**3.0**
Barnett-81	141	0.7	324.0	11.0	323.4	6.6	348.0	83.0	**323.4**	**6.6**
Barnett-82	643	1.1	326.3	6.5	323.5	3.2	324.0	54.0	**323.5**	**3.2**
Barnett-83*	809	1.2	319.3	5.9	323.6	4.6	278.0	47.0	**323.6**	**4.6**
Barnett-84	473	0.6	329.9	6.1	323.7	4.3	393.0	46.0	**323.7**	**4.3**
Barnett-85	141	0.9	394.3	15.0	323.7	5.7	740.0	100.0	**323.7**	**5.7**

Barnett-86	731	1.4	338.5	9.4	323.7	3.8	385.0	70.0	**323.7**	**3.8**
Barnett-87	156	1.1	316.2	7.0	324.0	4.9	252.0	55.0	**324.0**	**4.9**
Barnett-88	589	1.1	335.2	7.3	324.1	3.6	383.0	59.0	**324.1**	**3.6**
Barnett-89	847	0.6	325.4	6.0	324.5	4.8	349.0	47.0	**324.5**	**4.8**
Barnett-90	309	1.0	328.8	7.0	324.5	3.5	335.0	55.0	**324.5**	**3.5**
Barnett-91	799	1.5	337.4	6.5	324.8	4.3	407.0	42.0	**324.8**	**4.3**
Barnett-92	333	2.0	331.2	8.2	324.9	3.8	359.0	62.0	**324.9**	**3.8**
Barnett-93	528	1.0	328.6	7.2	324.9	3.8	324.0	54.0	**324.9**	**3.8**
Barnett-94*	508	1.3	322.5	7.4	325.0	5.2	340.0	52.0	**325.0**	**5.2**
Barnett-95	532	0.9	334.0	8.7	325.1	5.0	374.0	61.0	**325.1**	**5.0**
Barnett-96	520	1.4	334.0	9.2	325.1	3.9	358.0	71.0	**325.1**	**3.9**
Barnett-97*	353	1.0	323.1	7.2	325.4	4.7	326.0	57.0	**325.4**	**4.7**
Barnett-98	228	1.5	330.1	6.8	325.5	3.7	339.0	54.0	**325.5**	**3.7**
Barnett-99	81	2.3	328.7	9.9	325.6	4.5	314.0	78.0	**325.6**	**4.5**
Barnett-100	305	1.3	335.5	7.8	325.7	4.2	361.0	60.0	**325.7**	**4.2**
Barnett-101	518	1.0	331.9	7.8	325.7	4.7	344.0	67.0	**325.7**	**4.7**
Barnett-102*	706	0.9	323.8	9.7	325.7	7.3	314.0	70.0	**325.7**	**7.3**
Barnett-103	218	1.2	325.4	6.5	325.7	5.6	332.0	55.0	**325.7**	**5.6**
Barnett-104	346	0.8	327.9	16.5	325.8	13.4	342.8	41.7	**325.8**	**13.4**
Barnett-105	722	1.2	328.0	6.3	326.0	2.9	318.0	50.0	**326.0**	**2.9**
Barnett-106	104	1.3	325.4	9.8	326.0	6.1	274.0	82.0	**326.0**	**6.1**
Barnett-107*	478	1.2	327.4	6.6	326.1	4.6	326.0	50.0	**326.1**	**4.6**
Barnett-108	521	0.8	319.5	7.1	326.2	5.3	299.0	52.0	**326.2**	**5.3**
Barnett-109	235	0.7	329.6	6.3	326.3	6.0	343.0	48.0	**326.3**	**6.0**
Barnett-110	569	1.0	323.5	5.0	326.4	4.6	299.0	43.0	**326.4**	**4.6**
Barnett-111	728	1.0	332.6	5.7	326.4	3.6	349.0	47.0	**326.4**	**3.6**

181

Barnett-112	656	1.0	329.6	6.8	326.6	4.5	325.0	50.0	**326.6**	**4.5**
Barnett-113	465	0.7	324.6	12.7	326.7	10.9	309.8	29.7	**326.7**	**10.9**
Barnett-114	436	1.2	323.8	5.7	326.7	4.8	277.0	43.0	**326.7**	**4.8**
Barnett-115	813	1.5	328.6	7.1	326.7	4.8	331.0	55.0	**326.7**	**4.8**
Barnett-116	441	1.3	318.2	7.6	327.1	4.6	254.0	57.0	**327.1**	**4.6**
Barnett-117	446	0.1	421.0	19.0	327.2	8.9	960.0	110.0	**327.2**	**8.9**
Barnett-118	332	0.7	326.3	14.9	328.0	12.1	314.0	37.9	**328.0**	**12.1**
Barnett-119	161	1.2	324.2	6.6	328.4	5.6	310.0	52.0	**328.4**	**5.6**
Barnett-120	686	1.3	333.9	5.3	328.5	3.2	352.0	43.0	**328.5**	**3.2**
Barnett-121	65	1.4	319.9	6.6	328.5	5.0	281.0	47.0	**328.5**	**5.0**
Barnett-122	367	1.2	323.7	6.3	328.5	4.8	293.0	49.0	**328.5**	**4.8**
Barnett-123	379	1.8	324.4	5.8	328.5	3.3	279.0	47.0	**328.5**	**3.3**
Barnett-124	479	1.6	331.8	5.9	329.1	3.9	331.0	46.0	**329.1**	**3.9**
Barnett-125	406	1.1	334.7	8.8	329.4	4.1	332.0	68.0	**329.4**	**4.1**
Barnett-126	352	1.0	328.9	5.6	329.4	3.1	308.0	44.0	**329.4**	**3.1**
Barnett-127	615	1.0	334.2	8.1	329.8	5.1	376.0	60.0	**329.8**	**5.1**
Barnett-128	808	1.3	331.4	6.5	329.8	5.1	346.0	46.0	**329.8**	**5.1**
Barnett-129*	328	1.2	328.8	7.1	330.1	4.7	314.0	49.0	**330.1**	**4.7**
Barnett-130	537	4.1	332.4	12.4	330.3	10.3	347.1	28.8	**330.3**	**10.3**
Barnett-131	1037	1.6	337.2	12.0	330.4	5.4	346.0	89.0	**330.4**	**5.4**
Barnett-132*	684	0.9	328.0	7.7	330.5	5.2	332.0	53.0	**330.5**	**5.2**
Barnett-133*	40	1.5	330.4	6.7	330.6	5.0	344.0	51.0	**330.6**	**5.0**
Barnett-134	494	1.2	372.8	11.0	330.8	3.5	587.0	71.0	**330.8**	**3.5**
Barnett-135	494	1.3	330.1	7.5	330.8	4.4	305.0	62.0	**330.8**	**4.4**
Barnett-136	1004	1.5	324.0	6.5	330.8	4.2	294.0	50.0	**330.8**	**4.2**
Barnett-137*	649	1.1	328.5	7.8	331.0	5.1	314.0	59.0	**331.0**	**5.1**

Barnett-138	806	1.0	339.7	5.7	331.1	4.4	432.0	45.0	**331.1**	**4.4**
Barnett-139	423	1.4	335.1	6.8	331.2	5.0	343.0	55.0	**331.2**	**5.0**
Barnett-140	945	1.1	333.1	6.9	331.2	3.6	314.0	57.0	**331.2**	**3.6**
Barnett-141	108	0.8	388.5	16.0	331.3	4.3	630.0	100.0	**331.3**	**4.3**
Barnett-142	214	0.4	351.8	18.1	331.7	13.5	487.2	43.3	**331.7**	**13.5**
Barnett-143	331	1.1	340.5	6.8	331.8	3.2	367.0	54.0	**331.8**	**3.2**
Barnett-144	771	1.0	335.9	7.4	332.2	7.9	369.0	64.0	**332.2**	**7.9**
Barnett-145*	286	0.5	327.1	15.9	332.3	12.2	290.7	43.2	**332.3**	**12.2**
Barnett-146	523	0.6	374.7	8.1	332.5	6.3	657.0	58.0	**332.5**	**6.3**
Barnett-147	279	0.5	333.1	15.0	332.5	12.4	337.0	36.3	**332.5**	**12.4**
Barnett-148	474	1.4	346.1	11.0	332.7	4.5	380.0	81.0	**332.7**	**4.5**
Barnett-149	830	1.4	330.5	5.9	333.1	3.6	304.0	44.0	**333.1**	**3.6**
Barnett-150	864	1.0	345.3	7.0	333.3	5.1	437.0	48.0	**333.3**	**5.1**
Barnett-151*	736	1.3	334.2	7.1	333.6	5.0	329.0	55.0	**333.6**	**5.0**
Barnett-152*	515	1.1	335.3	8.3	333.9	5.5	339.0	60.0	**333.9**	**5.5**
Barnett-153	315	1.0	327.4	6.5	334.2	4.3	279.0	50.0	**334.2**	**4.3**
Barnett-154	309	0.6	351.4	8.5	334.5	4.9	450.0	60.0	**334.5**	**4.9**
Barnett-155	304	4.6	328.5	14.5	335.0	12.2	282.8	35.5	**335.0**	**12.2**
Barnett-156	362	1.1	331.5	8.3	335.3	5.5	303.0	64.0	**335.3**	**5.5**
Barnett-157	318	2.1	366.9	12.0	336.0	6.2	529.0	77.0	**336.0**	**6.2**
Barnett-158	308	4.6	324.3	13.8	336.5	12.3	237.8	32.7	**336.5**	**12.3**
Barnett-159	475	0.9	338.9	7.9	336.5	4.0	319.0	61.0	**336.5**	**4.0**
Barnett-160	424	1.1	345.9	7.8	336.6	4.4	375.0	64.0	**336.6**	**4.4**
Barnett-161	151	2.0	345.1	8.2	336.9	3.9	365.0	62.0	**336.9**	**3.9**
Barnett-162*	621	4.1	334.4	11.8	337.3	9.4	314.2	28.7	**337.3**	**9.4**
Barnett-163*	485	3.7	341.8	13.1	337.9	11.2	369.0	28.5	**337.9**	**11.2**

Barnett-164*	560	1.1	340.2	7.1	338.4	4.2	374.0	55.0	**338.4**	**4.2**
Barnett-165	831	1.0	334.1	7.9	338.5	4.5	310.0	56.0	**338.5**	**4.5**
Barnett-166	447	0.5	331.6	13.6	339.3	11.4	277.9	33.6	**339.3**	**11.4**
Barnett-167*	268	0.4	345.7	14.5	339.3	10.8	389.0	36.7	**339.3**	**10.8**
Barnett-168	20	1.3	336.9	9.1	339.4	4.9	319.0	70.0	**339.4**	**4.9**
Barnett-169	952	1.0	333.2	8.1	339.8	5.7	287.0	60.0	**339.8**	**5.7**
Barnett-170*	990	1.3	341.4	7.8	339.9	4.3	370.0	54.0	**339.9**	**4.3**
Barnett-171	758	0.6	332.9	8.1	340.3	5.5	295.0	62.0	**340.3**	**5.5**
Barnett-172	288	0.5	343.5	14.8	342.0	13.0	353.2	31.9	**342.0**	**13.0**
Barnett-173	370	0.5	340.1	13.4	344.9	12.1	307.5	28.2	**344.9**	**12.1**
Barnett-174	573	1.2	358.5	8.6	345.9	4.2	409.0	60.0	**345.9**	**4.2**
Barnett-175	361	0.9	360.8	11.0	346.1	6.0	433.0	76.0	**346.1**	**6.0**
Barnett-176	852	1.0	346.6	6.3	346.9	4.7	364.0	49.0	**346.9**	**4.7**
Barnett-177	532	1.6	356.7	15.0	348.8	6.9	370.0	110.0	**348.8**	**6.9**
Barnett-178	499	1.0	353.4	7.8	351.3	4.3	331.0	58.0	**351.3**	**4.3**
Barnett-179	304	2.6	377.8	8.4	358.2	6.8	495.0	49.0	**358.2**	**6.8**
Barnett-180	472	3.7	362.3	13.2	361.6	11.3	367.0	27.5	**361.6**	**11.3**
Barnett-181	187	0.6	376.4	17.5	363.481	12.3	456.6	42.7	**363.5**	**12.3**
Barnett-182	108	0.4	420.9	23.5	366.3	15.8	732.7	49.1	**366.3**	**15.8**
Barnett-183	100	1.5	375.0	10.0	370.4	7.2	427.0	87.0	**370.4**	**7.2**
Barnett-184	29	0.2	448.0	17.0	440.6	9.3	510.0	110.0	**440.6**	**9.3**
Barnett-185	380	1.0	433.1	8.2	446.3	6.7	372.0	48.0	**446.3**	**6.7**
Barnett-186	96	2.9	486.1	15.0	449.1	8.0	602.0	79.0	**449.1**	**8.0**
Barnett-187	253	0.7	558.5	13.0	457.4	6.7	972.0	56.0	**457.4**	**6.7**
Barnett-188	1435	0.7	463.0	9.3	458.6	6.8	458.0	69.0	**458.6**	**6.8**
Barnett-189	549	1.9	475.6	11.0	469.7	5.9	463.0	63.0	**469.7**	**5.9**

Barnett-190	341	0.9	477.6	11.0	469.8	5.9	465.0	65.0	**469.8**	**5.9**
Barnett-191	220	1.9	554.4	11.0	493.4	10.2	799.0	52.0	**493.4**	**10.2**
Barnett-192	188	0.7	514.4	20.6	510.9	17.5	529.8	35.7	**510.9**	**17.5**
Barnett-193	592	1.0	636.0	30.0	523.7	7.8	1010.0	120.0	**523.7**	**7.8**
Barnett-194	350	4.0	575.3	11.0	560.0	6.1	603.0	52.0	**560.0**	**6.1**
Barnett-195	240	0.9	715.8	18.0	586.7	11.8	1128.0	48.0	**586.7**	**11.8**
Barnett-196	302	1.7	614.4	29.0	589.0	18.2	660.0	140.0	**589.0**	**18.2**
Barnett-197	672	3.4	594.0	11.0	596.0	10.0	600.0	49.0	**596.0**	**10.0**
Barnett-198	332	11.1	787.2	34.0	631.5	12.3	1200.0	120.0	**631.5**	**12.3**
Barnett-199	152	2.8	650.6	13.0	639.6	7.9	653.0	60.0	**639.6**	**7.9**
Barnett-200	881	0.9	786.5	18.0	655.7	10.7	1161.0	59.0	**655.7**	**10.7**
Barnett-201	769	4.0	801.0	23.0	700.0	19.4	1048.0	60.0	**700.0**	**19.4**
Barnett-202	107	5.6	747.3	13.0	740.1	9.0	739.0	56.0	**740.1**	**9.0**
Barnett-203	566	0.4	896.0	9.3	823.2	7.6	1066.0	30.0	**823.2**	**7.6**
Barnett-204	204	1.0	1053.1	24.0	846.3	27.8	1461.0	58.0	**846.3**	**27.8**
Barnett-205	939	2.9	900.3	15.0	855.4	11.8	1002.0	48.0	**855.4**	**11.8**
Barnett-206	76	2.7	903.8	18.0	891.0	11.3	897.0	64.0	**891.0**	**11.3**
Barnett-207	450	0.8	925.6	17.0	895.4	10.7	974.0	58.0	**895.4**	**10.7**
Barnett-208	343	0.9	975.7	19.0	904.3	12.4	1118.0	55.0	**1118.0**	**55.0**
Barnett-209	397	1.8	953.9	9.0	904.6	8.8	1061.0	31.0	**1061.0**	**31.0**
Barnett-210	139	14.7	940.8	15.0	906.0	9.5	1001.0	49.0	**1001.0**	**49.0**
Barnett-211	140	5.9	943.9	14.0	940.2	9.5	932.0	47.0	**932.0**	**47.0**
Barnett-212	183	2.5	979.5	13.0	941.0	11.7	1046.0	44.0	**1046.0**	**44.0**
Barnett-213	176	3.6	963.2	27.0	944.3	18.8	981.0	79.0	**981.0**	**79.0**
Barnett-214	370	0.6	950.7	28.0	946.2	16.5	965.0	85.0	**965.0**	**85.0**
Barnett-215	119	2.9	959.8	16.0	948.0	11.3	940.0	56.0	**940.0**	**56.0**

Barnett-216	182	1.3	954.8	17.0	950.7	11.9	916.0	60.0	**916.0**	**60.0**
Barnett-217	184	12.6	998.9	19.0	954.0	11.8	1065.0	54.0	**1065.0**	**54.0**
Barnett-218	31	2.1	963.6	16.0	957.1	12.4	957.0	54.0	**957.0**	**54.0**
Barnett-219	98	2.5	1027.8	27.0	962.0	17.5	1127.0	72.0	**1127.0**	**72.0**
Barnett-220	166	2.5	992.2	14.0	980.8	9.5	985.0	49.0	**985.0**	**49.0**
Barnett-221	74	11.2	990.0	15.0	986.2	11.2	973.0	48.0	**973.0**	**48.0**
Barnett-222	263	6.2	1034.3	19.0	994.4	11.8	1075.0	57.0	**1075.0**	**57.0**
Barnett-223	323	7.0	1054.9	16.0	999.8	10.7	1141.0	52.0	**1141.0**	**52.0**
Barnett-224	513	1.5	1078.8	16.0	1009.1	14.4	1203.0	40.0	**1203.0**	**40.0**
Barnett-225	81	0.9	1026.0	34.8	1033.7	39.1	1009.7	33.4	**1009.7**	**33.4**
Barnett-226	440	1.5	1015.0	13.0	1005.0	14.0	1029.0	38.0	**1029.0**	**38.0**
Barnett-227	375	3.0	1051.1	13.0	1035.8	10.0	1058.0	42.0	**1058.0**	**42.0**
Barnett-228	202	2.9	1076.2	18.0	1043.6	14.0	1117.0	50.0	**1117.0**	**50.0**
Barnett-229	495	2.8	1082.0	25.0	1109.0	32.0	1045.0	62.0	**1045.0**	**62.0**
Barnett-230	794	3.0	1095.0	12.0	1121.0	14.0	1069.0	31.0	**1069.0**	**31.0**
Barnett-231	35	2.3	1104.6	25.0	1073.8	19.3	1127.0	75.0	**1127.0**	**75.0**
Barnett-232	675	1.6	1076.0	12.0	1073.0	19.0	1087.0	32.0	**1087.0**	**32.0**
Barnett-233	983	1.8	1153.3	19.0	1088.5	21.1	1266.0	37.0	**1266.0**	**37.0**
Barnett-234	493	1.1	1110.0	20.0	1115.0	27.0	1113.0	50.0	**1113.0**	**50.0**
Barnett-235	1259	1.3	1087.0	11.0	1062.0	10.0	1129.0	33.0	**1129.0**	**33.0**
Barnett-236	331	0.7	1090.0	17.0	1076.0	19.0	1129.0	38.0	**1129.0**	**38.0**
Barnett-237	240	2.0	1167.1	13.0	1157.1	13.3	1167.0	38.0	**1167.0**	**38.0**
Barnett-238	459	2.1	1193.8	14.0	1158.3	15.5	1244.0	37.0	**1244.0**	**37.0**
Barnett-239	388	3.9	1166.0	16.0	1174.0	25.0	1187.0	24.0	**1187.0**	**24.0**
Barnett-240	179	2.9	1183.8	14.0	1192.3	11.1	1149.0	38.0	**1149.0**	**38.0**
Barnett-241	422	4.4	1218.7	21.0	1195.0	15.7	1237.0	52.0	**1237.0**	**52.0**

Barnett-242	525	4.9	1231.9	18.0	1227.6	13.0	1203.0	51.0	**1203.0**	**51.0**
Barnett-243	81	2.3	1267.4	19.0	1257.4	14.1	1244.0	51.0	**1244.0**	**51.0**
Barnett-244	177	1.9	1322.9	15.0	1314.1	12.2	1312.0	39.0	**1312.0**	**39.0**
Barnett-245	1053	2.8	1290.5	24.0	1195.7	19.0	1430.0	58.0	**1430.0**	**58.0**
Barnett-246	259	1.6	1218.0	19.0	1117.0	21.0	1433.0	41.0	**1433.0**	**41.0**
Barnett-247	98	2.0	1269.4	30.0	1100.4	19.1	1527.0	71.0	**1527.0**	**71.0**
Barnett-248	298	0.6	1402.2	21.0	1277.5	31.7	1589.0	31.0	**1589.0**	**31.0**
Barnett-249	429	1.8	1625.1	24.0	1602.1	17.4	1617.0	53.0	**1617.0**	**53.0**
Barnett-250	594	1.1	158.9	9.1	73.0	1.8	1660.0	130.0	**1660.0**	**130.0**
Barnett-251	258	0.4	1324.8	25.0	1085.4	29.1	1716.0	61.0	**1716.0**	**61.0**
Barnett-252	251	1.2	1730.3	18.0	1715.2	25.6	1732.0	36.0	**1732.0**	**36.0**

Table S2-2. Zircon Hf isotopic values

Samples ID	U-Pb date	Date Uncertainty	ƐHf(t)	Measured 176Hf/177Hf	Corrected 176Hf/177Hf	2SE	176Lu/177Hf	2SE	176Yb/177Hf	2SE
Hatton-1	328.9	6.0	4.21	0.28268	0.28271	0.00005	0.00210	0.00035	0.07200	0.01200
Hatton-32	328.0	4.2	1.42	0.28260	0.28263	0.00003	0.00100	0.00001	0.03170	0.00110
Hatton-76	325.0	3.5	0.66	0.28258	0.28261	0.00003	0.00115	0.00010	0.03560	0.00260
Hatton-79	326.0	3.5	1.48	0.28260	0.28263	0.00002	0.00103	0.00001	0.03270	0.00070
Lower Mud Creek-9	325.0	4.1	0.66	0.28259	0.28262	0.00004	0.00260	0.00062	0.08800	0.02100
Lower Mud Creek-14	329.5	5.2	0.75	0.28258	0.28261	0.00004	0.00165	0.00028	0.05450	0.00800
Lower Mud Creek-18	325.0	3.4	0.55	0.28258	0.28261	0.00004	0.00195	0.00044	0.06100	0.01300
Lower Mud Creek-21	327.7	4.3	3.13	0.28264	0.28267	0.00005	0.00092	0.00007	0.02990	0.00460

Lower Mud Creek-30	326.0	4.4	2.28	0.28263	0.28266	0.00005	0.00256	0.00090	0.08400	0.02900
Lower Mud Creek-32	328.8	4.7	1.84	0.28260	0.28264	0.00004	0.00114	0.00002	0.03830	0.00200
Lower Mud Creek-59	326.7	4.4	3.80	0.28266	0.28270	0.00004	0.00136	0.00007	0.04780	0.00540
Lower Mud Creek-66	327.9	4.1	0.99	0.28258	0.28261	0.00003	0.00122	0.00013	0.04020	0.00560
Lower Mud Creek-69	326.1	7.5	-4.89	0.28241	0.28245	0.00012	0.00137	0.00012	0.03970	0.00290
Lower Mud Creek-92	325.2	8.7	3.47	0.28266	0.28269	0.00004	0.00176	0.00028	0.05900	0.01000
Lower Mud Creek-93	324.9	5.6	2.47	0.28263	0.28266	0.00005	0.00157	0.00011	0.04910	0.00300
Beavers Bend-3	325.8	4.4	2.36	0.28263	0.28266	0.00004	0.00136	0.00012	0.04390	0.00300
Beavers Bend-9	327.3	3.5	1.37	0.28261	0.28263	0.00003	0.00197	0.00061	0.06500	0.02000
Beavers Bend-10	328.1	5.1	2.53	0.28264	0.28266	0.00004	0.00148	0.00026	0.04760	0.00940
Beavers Bend-17	329.7	4.3	8.76	0.28284	0.28286	0.00005	0.00582	0.00049	0.21700	0.01300
Beavers Bend-19	326.3	3.5	1.90	0.28262	0.28264	0.00003	0.00158	0.00015	0.04990	0.00450
Beavers Bend-24	328.3	4.7	4.48	0.28269	0.28271	0.00004	0.00145	0.00005	0.04450	0.00330
Beavers Bend-30	328.2	3.7	1.12	0.28260	0.28263	0.00004	0.00260	0.00011	0.08240	0.00560
Beavers Bend-39	328.6	3.9	2.28	0.28263	0.28265	0.00003	0.00185	0.00030	0.06000	0.01100
Beavers Bend-49	325.3	4.8	2.46	0.28263	0.28266	0.00006	0.00084	0.00004	0.02625	0.00067
Beavers Bend-55	325.6	3.5	2.60	0.28264	0.28267	0.00003	0.00270	0.00058	0.08700	0.01900
Beavers Bend-80	328.2	4.6	1.23	0.28259	0.28262	0.00003	0.00111	0.00018	0.03630	0.00750
Beavers Bend-94	327.9	4.7	0.76	0.28258	0.28261	0.00003	0.00080	0.00010	0.02510	0.00350
Barnett-29	308.2	4.8	1.69	0.28264	0.28265	0.00007	0.00153	0.00021	0.04940	0.00450
Barnett-34*	311.8	4.8	6.08	0.28277	0.28278	0.00004	0.00257	0.00021	0.10900	0.01000
Barnett-46*	317.0	9.6	2.27	0.28265	0.28266	0.00003	0.00133	0.00010	0.04850	0.00320

Barnett-56*	319.0	3.8	1.38	0.28245	0.28263	0.00003	0.00113	0.00002	0.02633	0.00073
Barnett-57*	319.0	4.6	1.02	0.28262	0.28262	0.00002	0.00108	0.00008	0.03800	0.00210
Barnett-58	319.3	4.5	1.09	0.28262	0.28262	0.00003	0.00128	0.00011	0.05120	0.00580
Barnett-71*	321.6	5.7	2.34	0.28266	0.28266	0.00004	0.00232	0.00012	0.08520	0.00440
Barnett-77*	322.9	11.3	2.20	0.28247	0.28265	0.00003	0.00102	0.00005	0.02410	0.00140
Barnett-79	323.1	7.5	4.39	0.28267	0.28272	0.00006	0.00152	0.00010	0.04450	0.00370
Barnett-83*	323.4	6.6	1.17	0.28262	0.28262	0.00003	0.00131	0.00004	0.04330	0.00110
Barnett-89	324.5	4.8	0.79	0.28261	0.28261	0.00002	0.00154	0.00005	0.05730	0.00380
Barnett-91	324.8	4.3	3.23	0.28264	0.28268	0.00005	0.00151	0.00006	0.04130	0.00370
Barnett-94*	325.0	5.2	1.68	0.28263	0.28264	0.00002	0.00126	0.00007	0.04660	0.00210
Barnett-95	325.1	5.0	1.82	0.28260	0.28264	0.00005	0.00117	0.00012	0.03240	0.00230
Barnett-96	325.1	3.9	2.94	0.28263	0.28267	0.00003	0.00121	0.00018	0.03710	0.00630
Barnett-97*	325.4	4.7	1.76	0.28263	0.28264	0.00003	0.00094	0.00005	0.03210	0.00160
Barnett-99	325.6	4.5	-2.69	0.28247	0.28251	0.00005	0.00113	0.00009	0.02930	0.00180
Barnett-102*	325.7	7.3	1.35	0.28262	0.28262	0.00003	0.00090	0.00003	0.03290	0.00190
Barnett-103	325.7	5.6	1.78	0.28263	0.28264	0.00003	0.00118	0.00009	0.04340	0.00310
Barnett-107*	326.1	4.6	2.35	0.28265	0.28265	0.00002	0.00136	0.00009	0.04830	0.00300
Barnett-111	326.4	3.6	4.35	0.28267	0.28271	0.00003	0.00090	0.00002	0.02594	0.00052
Barnett-112	326.6	4.5	3.82	0.28265	0.28269	0.00002	0.00108	0.00006	0.03050	0.00250
Barnett-120	328.5	3.2	2.90	0.28263	0.28267	0.00002	0.00128	0.00010	0.03700	0.00160
Barnett-125	329.4	4.1	3.15	0.28263	0.28267	0.00003	0.00102	0.00004	0.03110	0.00150
Barnett-129*	330.1	4.7	2.52	0.28265	0.28266	0.00003	0.00116	0.00006	0.04130	0.00150

Samples ID										
Barnett-132*	330.5	5.2	2.06	0.28264	0.28265	0.00002	0.00184	0.00018	0.06240	0.00490
Barnett-133*	330.6	5	2.04	0.28264	0.28264	0.00003	0.00143	0.00008	0.05180	0.00100
Barnett-137*	331.0	5.1	2.31	0.28265	0.28265	0.00003	0.00124	0.00004	0.04490	0.00140
Barnett-144	332.2	7.9	0.14	0.28259	0.28259	0.00007	0.00190	0.00015	0.06200	0.00280
Barnett-145*	332.3	7.9	1.79	0.28246	0.28264	0.00005	0.00133	0.00003	0.03140	0.00110
Barnett-151*	333.6	5	1.40	0.28262	0.28262	0.00004	0.00128	0.00007	0.04890	0.00250
Barnett-152*	333.9	5.5	7.19	0.28278	0.28279	0.00003	0.00153	0.00008	0.05843	0.00085
Barnett-160	336.6	4.4	3.13	0.28263	0.28267	0.00003	0.00115	0.00010	0.03310	0.00190
Barnett-162*	337.3	9.4	1.07	0.28244	0.28261	0.00003	0.00126	0.00007	0.03010	0.00180
Barnett-163*	337.9	11.2	2.31	0.28247	0.28265	0.00004	0.00108	0.00010	0.02410	0.00260
Barnett-164*	338.4	4.2	1.74	0.28262	0.28263	0.00002	0.00116	0.00007	0.04200	0.00340
Barnett-167*	339.3	10.8	2.87	0.28249	0.28266	0.00004	0.00131	0.00006	0.03100	0.00150
Barnett-170*	339.9	4.3	2.00	0.28263	0.28264	0.00003	0.00160	0.00006	0.05760	0.00230

* U-Pb and Hf data simultaneously acquired by split-stream laser ablation (LASS)

*Barnett-34 was not used for Hf interpretation because its TIMS date is 375Ma, check Table S3

Table s2 continues

Samples ID	U-Pb date	Date Uncertainty	ℰHf(t)	Measured 178Hf/177Hf	2SE	Corrected 180Hf/177Hf	2SE	176Hf/177Hfi	EHf0	2SE
Hatton-1	328.9	6.0	4.21	1.46725	0.00008	1.88693	0.00021	0.28270	-2.65219	1.69802
Hatton-32	328.0	4.2	1.42	1.46727	0.00005	1.88717	0.00016	0.28262	-5.65801	1.16774
Hatton-76	325.0	3.5	0.66	1.46722	0.00009	1.88712	0.00023	0.28260	-6.32990	1.02627

190

Hatton-79	326.0	3.5	1.48	1.46719	0.00007	1.88706	0.00019	0.28262	-5.55192	0.67233
Lower Mud Creek-9	325.0	4.1	0.66	1.46725	0.00006	1.88706	0.00017	0.28260	-6.01163	1.55705
Lower Mud Creek-14	329.5	5.2	0.75	1.46718	0.00009	1.88696	0.00020	0.28260	-6.22381	1.41554
Lower Mud Creek-18	325.0	3.4	0.55	1.46719	0.00010	1.88701	0.00019	0.28260	-6.25917	1.30938
Lower Mud Creek-21	327.7	4.3	3.13	1.46721	0.00012	1.88702	0.00025	0.28267	-3.96061	1.62750
Lower Mud Creek-30	326.0	4.4	2.28	1.46720	0.00008	1.88705	0.00018	0.28264	-4.42032	1.62758
Lower Mud Creek-32	328.8	4.7	1.84	1.46720	0.00008	1.88716	0.00020	0.28263	-5.23366	1.23848
Lower Mud Creek-59	326.7	4.4	3.80	1.46723	0.00020	1.88716	0.00030	0.28269	-3.18263	1.52125
Lower Mud Creek-66	327.9	4.1	0.99	1.46727	0.00008	1.88711	0.00021	0.28261	-6.04700	1.13242
Lower Mud Creek-69	326.1	7.5	-4.89	1.46727	0.00011	1.88732	0.00033	0.28244	-11.84646	4.24914
Lower Mud Creek-92	325.2	8.7	3.47	1.46726	0.00012	1.88709	0.00023	0.28268	-3.39481	1.37977
Lower Mud Creek-93	324.9	5.6	2.47	1.46722	0.00006	1.88705	0.00021	0.28265	-4.42032	1.62759
Beavers Bend-3	325.8	4.4	2.36	1.46721	0.00007	1.88705	0.00023	0.28265	-4.59713	1.37991
Beavers Bend-9	327.3	3.5	1.37	1.46721	0.00009	1.88703	0.00020	0.28262	-5.48120	1.09693
Beavers Bend-10	328.1	5.1	2.53	1.46713	0.00007	1.88680	0.00016	0.28265	-4.45568	1.48601
Beavers Bend-17	329.7	4.3	8.76	1.46721	0.00008	1.88687	0.00024	0.28283	2.68755	1.80315
Beavers Bend-19	326.3	3.5	1.90	1.46723	0.00006	1.88704	0.00024	0.28263	-5.02148	1.16765
Beavers Bend-24	328.3	4.7	4.48	1.46729	0.00013	1.88698	0.00023	0.28271	-2.51074	1.30885
Beavers Bend-30	328.2	3.7	1.12	1.46721	0.00009	1.88698	0.00022	0.28261	-5.62265	1.34465
Beavers Bend-39	328.6	3.9	2.28	1.46721	0.00006	1.88695	0.00023	0.28264	-4.63249	0.95532
Beavers Bend-49	325.3	4.8	2.46	1.46721	0.00008	1.88709	0.00015	0.28265	-4.59713	1.98139
Beavers Bend-55	325.6	3.5	2.60	1.46722	0.00006	1.88714	0.00021	0.28265	-4.06669	1.20293
Beavers Bend-80	328.2	4.6	1.23	1.46716	0.00009	1.88704	0.00017	0.28261	-5.83482	0.99082
Beavers Bend-94	327.9	4.7	0.76	1.46724	0.00009	1.88707	0.00019	0.28260	-6.36526	0.92010
Barnett-29	308.2	4.8	1.69	1.46715	0.00011	1.88663	0.00025	0.28264	-4.85784	2.29972
Barnett-34*	311.8	4.8	6.08	1.46723	0.00006	1.88661	0.00012	0.28276	-0.33135	1.52067

Barnett-46*	317.0	9.6	2.27	1.46714	0.00006	1.88655	0.00016	0.28265	-4.50420	1.02599
Barnett-56*	319.0	3.8	1.38	1.46694	0.00004	1.88630	0.00012	0.28262	-5.48088	1.02672
Barnett-57*	319.0	4.6	1.02	1.46722	0.00005	1.88669	0.00009	0.28261	-5.84800	0.74306
Barnett-58	319.3	4.5	1.09	1.46724	0.00006	1.88679	0.00013	0.28261	-5.74191	1.16765
Barnett-71*	321.6	5.7	2.34	1.46715	0.00005	1.88663	0.00013	0.28265	-4.32739	1.48589
Barnett-77*	322.9	11.3	2.20	1.46696	0.00004	1.88629	0.00012	0.28264	-4.77319	1.20365
Barnett-79	323.1	7.5	4.39	1.46704	0.00010	1.88683	0.00019	0.28271	-2.47538	1.94571
Barnett-83*	323.4	6.6	1.17	1.46719	0.00004	1.88672	0.00009	0.28261	-5.74191	0.91997
Barnett-89	324.5	4.8	0.79	1.46721	0.00004	1.88664	0.00012	0.28260	-6.09554	0.84923
Barnett-91	324.8	4.3	3.23	1.46712	0.00013	1.88704	0.00032	0.28267	-3.67771	1.80442
Barnett-94*	325.0	5.2	1.68	1.46722	0.00005	1.88673	0.00009	0.28263	-5.28219	0.84916
Barnett-95	325.1	5.0	1.82	1.46724	0.00007	1.88726	0.00018	0.28263	-5.16293	1.80468
Barnett-96	325.1	3.9	2.94	1.46721	0.00009	1.88726	0.00022	0.28266	-4.03133	1.13223
Barnett-97*	325.4	4.7	1.76	1.46722	0.00004	1.88675	0.00008	0.28263	-5.28219	1.02607
Barnett-99	325.6	4.5	-2.69	1.46714	0.00011	1.88692	0.00026	0.28250	-9.68934	1.69930
Barnett-102*	325.7	7.3	1.35	1.46721	0.00005	1.88670	0.00015	0.28262	-5.70655	0.99073
Barnett-103	325.7	5.6	1.78	1.46719	0.00004	1.88668	0.00011	0.28263	-5.21147	0.88454
Barnett-107*	326.1	4.6	2.35	1.46721	0.00004	1.88661	0.00010	0.28265	-4.61029	0.84911
Barnett-111	326.4	3.6	4.35	1.46721	0.00010	1.88717	0.00021	0.28270	-2.72292	1.06132
Barnett-112	326.6	4.5	3.82	1.46720	0.00009	1.88713	0.00019	0.28269	-3.21799	0.53069
Barnett-120	328.5	3.2	2.90	1.46717	0.00010	1.88725	0.00011	0.28266	-4.13742	0.63688
Barnett-125	329.4	4.1	3.15	1.46711	0.00007	1.88706	0.00027	0.28267	-3.96061	0.99069
Barnett-129*	330.1	4.7	2.52	1.46726	0.00005	1.88669	0.00013	0.28265	-4.57493	1.16752
Barnett-132*	330.5	5.2	2.06	1.46722	0.00005	1.88658	0.00013	0.28264	-4.89320	0.84913
Barnett-133*	330.6	5	2.04	1.46721	0.00005	1.88667	0.00013	0.28263	-4.99929	1.16757
Barnett-137*	331.0	5.1	2.31	1.46723	0.00005	1.88662	0.00011	0.28264	-4.78711	1.13216

Barnett-144	332.2	7.9	0.14	1.46722	0.00008	1.88667	0.00014	0.28258	-6.83817	2.37095
Barnett-145*	332.3	7.9	1.79	1.46694	0.00005	1.88617	0.00010	0.28263	-5.30396	1.59315
Barnett-151*	333.6	5	1.40	1.46723	0.00007	1.88682	0.00014	0.28261	-5.74191	1.30919
Barnett-152*	333.9	5.5	7.19	1.46716	0.00007	1.88667	0.00014	0.28278	0.09300	1.13161
Barnett-160	336.6	4.4	3.13	1.46725	0.00007	1.88724	0.00017	0.28266	-4.10206	0.91994
Barnett-162*	337.3	9.4	1.07	1.46693	0.00005	1.88626	0.00013	0.28260	-6.15319	1.20382
Barnett-163*	337.9	11.2	2.31	1.46697	0.00005	1.88633	0.00014	0.28264	-4.95011	1.34528
Barnett-164*	338.4	4.2	1.74	1.46721	0.00005	1.88671	0.00009	0.28262	-5.52973	0.74304
Barnett-167*	339.3	10.8	2.87	1.46700	0.00005	1.88627	0.00012	0.28265	-4.38396	1.48680
Barnett-170*	339.9	4.3	2.00	1.46718	0.00004	1.88668	0.00009	0.28263	-5.17610	1.06144

Table S2-3. U-Pb CA-IDTIMS zircon data

Sample	Weight (µg)	U (ppm)	sample Pb (ppm)	Pbc (pg)	Pb* (pg)	Pb*/Pbc	Th/U	206Pb/204Pb	208Pb/206Pb	206Pb/238UTh (rad.)	%err	207Pb/235U (rad.)	%err	207Pb/206PbTh (rad.)	%err	206/238Th Date (Ma)	err	207/235 Date (Ma)	207/206Th Date (Ma)	Rho	206/238 ICP date	err	206/207 ICP date	err	% Disc
Barnett Tuff										*327.78±0.79/0.80/0.87 Ma Weigthed mean 206Pb/238U date (±analytical/with tracer/with U-decay constant), 95% conf., MSWD 1.8, 5 of 7 analyses*															
Barnett-g19	0.11	1840	111.7	12.3	1.5		0.71	454	0.24	0.0522	(0.26)	0.3849	(1.38)	0.0535	(1.30)	**328.0**	**±0.8**	330.6	349.3	0.40	302.3	±4.1	301.0	±4.1	1.00
Barnett-g183	0.21	111	8.8	1.9	1.5	1.0	0.65	72	0.26	0.0523	(0.64)	0.3971	(10.49)	0.0551	(9.99)	**328.4**	**±2.1**	339.5	416.0	0.80	370.4	±7.2	427.0	±87.0	0.87
Barnett-g29*	0.09	717	43.1	3.8	1.2	3.0	0.61	194	0.20	0.0526	(0.64)	0.3879	(4.53)	0.0535	(4.29)	**330.2**	**±2.1**	332.8	351.4	0.43	308.2	±4.8	331.0	±4.7	0.93
Barnett-g180	0.11	404	22.5	2.5	0.6	4.1	1.49	260	0.20	0.0519	(0.31)	0.3492	(3.85)	0.0488	(3.69)	**326.0**	**±1.0**	304.1	139.1	0.56	361.6	±11.3	367.0	±27.5	0.99
Barnett-g41	0.14	1875	104.2	14.6	1.1	12.8	0.57	786	0.18	0.0521	(0.22)	0.3793	(1.07)	0.0528	(1.01)	**327.5**	**±0.7**	326.5	319.9	0.40	315.8	±10.8	303.4	±35.0	1.04
Barnett-g181	0.36	360	19.7	7.0	0.6	12.2	0.53	755	0.17	0.0521	(0.25)	0.3812	(1.32)	0.0530	(1.25)	**327.5**	**±0.8**	327.9	330.8	0.39	363.5	±12.3	456.6	±42.7	0.80
Barnett-g34*	0.35	166	10.8	3.8	0.7	5.5	0.50	341	0.20	0.0600	(0.29)	0.4692	(2.54)	0.0567	(2.42)	**375.8**	**±1.1**	390.6	479.3	0.49	311.8	±4.8	389.0	±4.8	0.80

Notes: sample: g_=single grain identifier from ICP mount, * excluded from date calculations

sample Pb: sample Pb (radiogenic + initial) corrected for laboratory blank

Pbc: total common Pb (blank plus sample initial Pb); 1 pg was assigned to blank, the remaining to initial Pb

Pb*/Pbc: radiogenic Pb to total common Pb (blank + initial)

Corrected atomic ratios: measured 206Pb/204Pb corrected for mass discrimination and tracer, all others corrected for blank, mass discrimination, tracer and initial Pb, values in parentheses are 2 sigma errors in percent.

Rho: 206Pb/238U vs 207Pb/235U error correlation coefficient

% disc.: percent discordant of LA-ICPMS 206Pb/238U vs. 206Pb/207Pb

_Th = 206Pb/238U, 207Pb/206Pb ratios and dates corrected for Th-disequilibrium after Schärer (1984) assuming a magma Th/U of 2.2.

Table S2-4. Zircon Rare Earth Element Compositions

Sample ID	U-Pb date	2σ error	Ti	Y	Nb	La	Ce	Pr	Nd	Sm	Eu	Gd	Tb	Dy	Ho	Er	Tm	Yb	Lu	Hf	U	Th
BB-3	325.8	4.4	5.4	1350.0	5.7	0.4	14.4	0.6	5.2	6.5	0.7	16.4	8.0	109.2	40.8	202.0	45.6	484.0	69.3	8610.0	468.0	360.0
BB-9	327.3	3.5	5.6	1230.0	3.3	1.1	10.9	1.0	7.2	6.4	0.9	16.3	7.6	96.5	34.7	175.0	37.5	376.0	60.1	7680.0	222.0	190.0
BB-10	328.1	5.1	5.0	2000.0	2.7	0.2	5.7	0.4	5.9	11.2	1.8	35.7	15.9	198.0	65.0	281.0	60.0	650.0	77.0	5890.0	203.0	155.0
BB-17	329.7	4.3	5.4	1220.0	3.5	0.2	11.0	0.4	2.7	5.5	0.7	15.4	8.3	114.6	35.7	196.0	48.4	472.0	60.2	9110.0	256.9	168.0
BB-19	326.3	3.5	5.7	2570.0	4.2	4.8	45.8	8.8	62.1	40.9	10.6	82.0	27.8	282.0	75.0	306.0	57.0	536.0	80.2	6900.0	273.0	500.0
BB-24	328.3	4.7	6.2	1810.0	4.8	1.0	18.0	1.7	13.8	11.7	1.6	27.1	11.9	159.0	56.0	270.0	58.6	584.0	90.5	8600.0	367.0	344.0
BB-30	328.2	3.7	5.2	2320.0	7.4	2.3	28.5	2.6	19.5	15.3	2.0	36.0	16.5	214.0	74.9	349.0	75.6	828.0	106.0	7460.0	699.0	629.0
BB-32	328.8	6.2	5.1	967.0	3.4	0.5	9.2	0.1	1.5	3.4	0.3	9.5	5.2	78.2	30.7	162.0	39.8	463.0	67.5	8990.0	336.0	117.0
BB-39	328.6	3.9	5.1	1369.0	2.3	0.2	9.7	0.2	2.3	5.6	0.6	18.7	9.0	115.0	43.5	208.4	44.7	512.0	69.4	7350.0	267.0	168.0
BB-49	325.3	4.8	5.2	2940.0	3.1	6.3	22.4	2.3	17.1	18.2	3.0	52.4	23.3	277.0	95.0	433.0	88.0	898.0	128.0	6000.0	336.0	269.0
BB-55	325.6	3.5	5.3	2020.0	3.9	0.3	16.0	0.4	4.5	8.6	0.8	25.3	12.9	169.0	60.0	311.0	68.0	700.0	102.0	8860.0	399.0	357.0
BB-80	328.2	4.6	5.1	1051.0	4.4	0.1	14.1	0.1	1.6	4.3	0.6	12.0	6.4	87.8	32.1	162.0	37.5	395.0	56.5	8140.0	323.0	288.0
BB-94	327.9	4.7	5.5	818.0	3.5	0.0	8.0	0.0	0.8	3.4	0.3	8.9	4.7	67.0	24.5	127.4	29.8	315.0	45.8	8590.0	242.2	128.5
Hatton-1	328.9	6.0	5.2	1560.0	4.0	8.3	31.1	3.3	20.0	15.5	3.2	33.0	13.6	157.0	50.0	229.0	48.0	480.0	69.0	8180.0	228.0	281.0
Hatton-32	328.0	4.2	5.5	1620.0	3.7	0.9	11.7	0.8	6.2	10.0	1.7	25.0	11.7	133.0	49.1	241.0	46.9	491.0	75.4	8500.0	316.0	180.0
Hatton-76	325.0	3.5	5.2	1030.0	2.8	0.4	8.4	0.5	5.6	7.3	1.6	19.2	8.2	102.0	39.7	166.0	37.8	488.0	56.5	7110.0	266.3	137.0
Hatton-79	326.0	3.5	4.9	1150.0	4.1	0.1	8.2	0.2	2.3	5.0	0.7	14.3	7.3	98.5	35.7	179.0	39.8	417.0	61.2	7630.0	286.0	182.0
LMC-9	325.0	4.1	4.8	730.0	1.8	0.0	3.7	0.0	0.8	3.0	0.3	8.0	4.2	57.7	21.7	111.0	24.3	259.0	39.8	8700.0	74.5	40.0
LMC-14	329.5	5.2	5.2	1350.0	3.0	0.1	10.9	0.2	3.3	7.0	1.3	19.4	9.2	127.0	43.7	208.0	47.4	486.0	66.8	8740.0	215.0	199.0
LMC-18	325.0	3.4	5.1	1090.0	4.0	0.3	13.8	0.3	3.0	5.6	1.5	14.4	7.3	112.0	38.2	177.0	45.0	518.0	57.8	8500.0	279.0	167.0
LMC-21	327.7	4.3	4.8	1900.0	5.2	1.0	19.9	0.5	4.5	7.5	0.6	25.2	12.6	172.0	61.0	297.0	64.4	652.0	92.4	8720.0	379.0	465.0
LMC-30	326.0	4.4	4.7	1600.0	3.8	1.1	24.1	1.2	10.7	12.8	4.8	30.9	13.2	164.0	56.0	245.0	54.6	617.0	71.0	8200.0	317.0	277.0

LMC-32	328.8	4.7	4.8	1240.0	2.6	0.8	9.1	0.2	1.9	4.6	0.5	14.5	7.7	112.0	40.2	197.0	46.7	516.0	65.9	8840.0	165.0	103.0
LMC-59	326.7	4.4	4.9	1450.0	2.9	0.7	11.5	0.3	2.7	5.5	1.0	16.9	8.6	121.0	45.0	226.0	51.9	550.0	80.2	8170.0	303.0	171.0
LMC-66	327.9	4.1	4.9	1100.0	3.6	0.4	11.8	0.3	3.1	5.1	1.4	14.0	7.2	99.0	35.2	175.0	39.0	410.0	58.5	9300.0	225.0	146.0
LMC-69	326.1	7.5	5.6	1310.0	3.3	0.5	14.5	0.5	4.8	6.5	2.4	16.4	8.0	105.0	37.4	196.0	43.5	439.0	71.0	9700.0	285.0	187.0
LMC-86	326.2	4.4	5.6	2040.0	2.9	3.6	20.7	1.5	9.9	9.4	2.3	27.1	13.4	178.0	62.6	311.0	64.4	627.0	100.0	10580.0	214.3	183.0
LMC-92	325.2	8.7	5.5	1330.0	3.2	0.2	9.4	0.2	2.7	5.6	0.8	16.1	8.4	113.0	39.9	206.0	48.4	485.0	67.0	10690.0	161.0	112.0
LMC-93	324.9	5.6	5.0	1480.0	2.8	0.3	14.7	0.4	4.0	6.9	1.7	20.8	10.7	151.0	48.0	240.0	58.0	614.0	67.0	8400.0	262.9	197.0
CS-11	325.4	3.8	5.4	1565.0	3.2	0.2	17.4	0.3	4.7	8.3	1.3	24.1	11.4	141.3	49.6	247.0	55.0	585.0	86.4	9290.0	361.0	277.0
CS-22	329.9	6.2	5.3	946.0	3.6	0.4	20.1	0.6	5.1	6.4	1.4	14.8	6.4	87.3	31.8	158.0	37.9	402.0	57.2	9960.0	338.0	209.0
CS-37	328.0	3.2	5.0	2680.0	5.5	0.5	26.0	0.6	8.2	15.7	2.9	49.9	22.1	273.0	92.8	434.0	91.9	948.0	131.0	7920.0	715.0	675.0
BNT-79	323.1	7.5	5.2	1313.0	4.1	0.1	22.7	0.2	2.3	4.1	1.5	13.1	6.7	91.1	35.1	194.0	46.0	491.0	88.9	8420.0	488.0	730.0
BNT-91	324.8	4.3	5.4	1520.0	4.1	0.3	14.6	0.2	3.4	6.5	2.1	21.2	10.0	131.0	48.0	245.0	55.2	616.0	98.2	9600.0	467.0	830.0
BNT-95	325.1	5.0	5.1	1170.0	4.0	0.1	19.5	0.1	1.6	3.2	1.2	11.2	6.0	82.0	32.4	190.0	45.3	507.0	97.0	9400.0	483.0	470.0
BNT-96	325.1	3.9	5.5	1110.0	3.6	0.1	16.6	0.2	3.1	5.0	2.2	13.5	6.2	92.0	30.0	170.0	42.2	439.0	75.0	10460.0	347.0	1640.0
BNT-99	325.6	4.5	4.9	800.0	2.6	0.1	15.8	0.1	1.3	2.3	1.5	7.8	4.0	54.0	21.0	113.0	26.8	326.0	66.0	8840.0	209.0	334.0
BNT-101	325.7	4.7	5.0	980.0	3.5	0.1	17.0	0.1	1.9	3.2	1.0	11.1	5.6	78.4	28.9	161.0	39.3	442.0	74.6	9450.0	352.0	430.0
BNT-105	326.0	2.9	5.5	1419.0	5.4	0.1	25.9	0.4	5.4	7.6	3.3	18.4	9.4	120.9	42.1	212.0	47.9	501.0	77.2	11290.0	452.0	459.0
BNT-111	326.4	3.6	5.9	1041.0	3.8	0.2	16.0	0.2	2.7	5.0	2.2	13.4	5.9	72.9	28.8	160.0	38.2	463.0	86.9	10040.0	404.0	1280.0
BNT-112	326.6	4.5	5.2	1329.0	3.8	6.8	35.2	1.8	9.7	6.7	1.4	18.9	8.6	114.1	41.6	216.0	52.2	607.0	93.8	9600.0	426.0	424.0
BNT-120	328.5	3.2	5.0	777.0	4.4	0.0	18.8	0.0	0.9	1.9	0.4	7.4	4.0	56.4	22.3	130.4	34.3	424.0	66.2	10000.0	379.0	256.0
BNT-125	329.4	4.1	5.2	718.0	3.1	0.1	13.1	0.1	1.7	2.9	1.1	8.7	4.2	61.1	21.3	113.4	28.9	322.0	51.8	9610.0	280.0	890.0
BNT-160	336.6	4.4	5.2	944.0	3.1	1.9	17.1	0.5	3.5	3.0	0.6	10.1	5.3	72.0	28.2	157.0	38.1	418.0	72.2	10100.0	241.0	190.0
BB-Beavers Bend, LMC-Lower Mud Creek, CS-Chicksaw, BNT-Barnett																						

Table S2-4 continues

Sample ID	∑REE	∑LREE (La-Sm)	∑HREE (Gd-Lu)	LaN/SmN	GdN/YbN	Eu/Eu*	Ce/Ce*	log (Ti, ppm)	T (K)	T (°C)
Beavers Bend-3	9687.7	27.0	982.5	0.02	0.02	0.6	4.7	0.74	963	690
Beavers Bend-9	8569.9	26.6	810.9	0.06	0.03	0.8	1.6	0.75	965	692
Beavers Bend-10	7355.7	23.3	1395.6	0.01	0.04	0.8	3.4	0.70	956	683
Beavers Bend-17	10167.6	19.8	956.8	0.01	0.02	0.7	6.2	0.73	962	689
Beavers Bend-19	8532.1	162.4	1497.5	0.05	0.10	1.7	1.1	0.76	967	694
Beavers Bend-24	9954.8	46.2	1270.4	0.03	0.03	0.8	2.1	0.79	973	700
Beavers Bend-30	9284.3	68.2	1717.3	0.06	0.03	0.8	1.8	0.71	959	686
Beavers Bend-32	9997.9	14.7	859.5	0.06	0.01	0.5	5.2	0.71	958	685
Beavers Bend-39	8480.7	17.9	1026.9	0.01	0.02	0.6	8.6	0.70	957	684
Beavers Bend-49	8113.3	66.3	2015.9	0.13	0.04	0.9	0.9	0.72	960	687
Beavers Bend-55	10420.2	29.8	1457.6	0.01	0.02	0.5	6.9	0.72	960	687
Beavers Bend-80	9042.1	20.2	794.1	0.01	0.02	0.7	17.7	0.71	958	685
Beavers Bend-94	9318.8	12.2	626.8	0.00	0.02	0.6	85.7	0.74	964	691
Hatton-1	9372.0	78.2	1098.3	0.21	0.05	1.3	0.9	0.72	960	687
Hatton-32	9653.4	29.5	1084.8	0.03	0.03	1.0	2.2	0.74	965	691
Hatton-76	8117.9	22.1	926.3	0.02	0.03	1.2	3.1	0.72	960	687
Hatton-79	8582.3	15.8	858.6	0.01	0.02	0.8	8.5	0.69	954	681
Lower Mud Creek-9	9320.7	7.5	528.9	0.00	0.02	0.5	18.7	0.68	953	680
Lower Mud Creek-14	9840.2	21.4	1015.8	0.01	0.03	1.0	11.0	0.71	959	686
Lower Mud Creek-18	9586.8	23.1	976.8	0.02	0.02	1.6	6.3	0.71	958	684
Lower Mud Creek-21	10217.4	33.5	1384.7	0.05	0.03	0.4	4.1	0.68	953	680
Lower Mud Creek-30	9554.6	49.9	1269.3	0.03	0.03	2.2	3.1	0.67	952	679
Lower Mud Creek-32	9970.5	16.5	1005.1	0.07	0.02	0.5	3.6	0.68	954	680
Lower Mud Creek-59	9391.1	20.6	1106.1	0.05	0.02	0.9	4.2	0.69	954	681

Lower Mud Creek-66	10240.4	20.7	844.4	0.03	0.02	1.5	5.2	0.69	955	682
Lower Mud Creek-69	10713.6	26.8	925.2	0.03	0.02	2.2	4.2	0.75	965	692
Lower Mud Creek-86	12077.8	45.1	1395.2	0.15	0.03	1.3	1.3	0.75	965	692
Lower Mud Creek-92	11779.7	18.1	990.2	0.01	0.02	0.8	7.0	0.74	964	691
Lower Mud Creek-93	9726.5	26.3	1218.1	0.02	0.02	1.3	6.2	0.70	956	683
Chickasaw-11	10592.8	30.9	1209.3	0.01	0.03	0.8	9.7	0.73	962	689
Chickasaw-22	10852.3	32.6	803.2	0.03	0.02	1.4	6.0	0.73	961	688
Chickasaw-37	10076.9	51.0	2061.3	0.01	0.03	0.9	6.8	0.70	956	683
Barnett-79	9537.4	29.4	971.5	0.01	0.02	1.9	21.5	0.72	960	686
Barnett-91	10945.9	25.1	1233.2	0.02	0.02	1.6	7.8	0.73	962	689
Barnett-95	10557.0	24.5	975.3	0.01	0.01	1.9	26.1	0.71	958	684
Barnett-96	11442.9	25.0	875.1	0.00	0.02	2.5	23.0	0.74	964	691
Barnett-99	9623.9	19.5	622.4	0.02	0.02	3.4	28.3	0.69	954	681
Barnett-101	10451.5	22.2	845.2	0.01	0.02	1.6	35.6	0.70	956	683
Barnett-105	12427.4	39.4	1039.8	0.00	0.02	2.6	24.4	0.74	963	690
Barnett-111	11027.9	24.1	876.3	0.01	0.02	2.4	12.9	0.77	969	696
Barnett-112	10904.6	60.1	1160.3	0.40	0.02	1.1	1.5	0.71	959	686
Barnett-120	10989.1	21.7	747.3	0.01	0.01	1.1	58.9	0.70	957	684
Barnett-125	10352.1	17.9	615.3	0.01	0.02	2.0	27.8	0.71	959	686
Barnett-160	11069.2	26.0	804.4	0.26	0.02	1.1	2.5	0.72	960	687

Table S2-5. Zircon U-Pb ages derived from LA-ICPMS dates of the Stanley and Barnett tuffs

Sample ID		N analyzed	Date (Ma)	±2σ	n	MSWD	PoF
Chickasaw Creek	this study	81	320.4	0.8	30	0.8	0.8
	Shaulis et al. (2012)	77	320.1	1.7	18	1.1	0.4
Upper Mud Creek	this study	78	N/A (not enough data)				
	Shaulis et al. (2012)	94	322.7	2.3	13	1	0.5
Lower Mud Creek	this study	115	320.7	0.6	50	1	0.4
	Shaulis et al. (2012)	70	322.3	1.7	22	0.6	0.9
Hatton	this study	103	317.4	0.5	48	1	0.5
	Shaulis et al. (2012)	88	324.8	2.5	9	1	0.4
Beaver Bend	this study	112	327.1	0.7	34	1	0.5
	Shaulis et al. (2012)	84	327.3	2.3	15	1	0.5
Barnett Tuff	this study	252	326.7	0.6	52	0.9	0.7
	CA-ID-TIMS	7	327.8	0.8	5	1.2	0.1

Appendix B

Supplemental materials for Chapter 3

SAMPLES
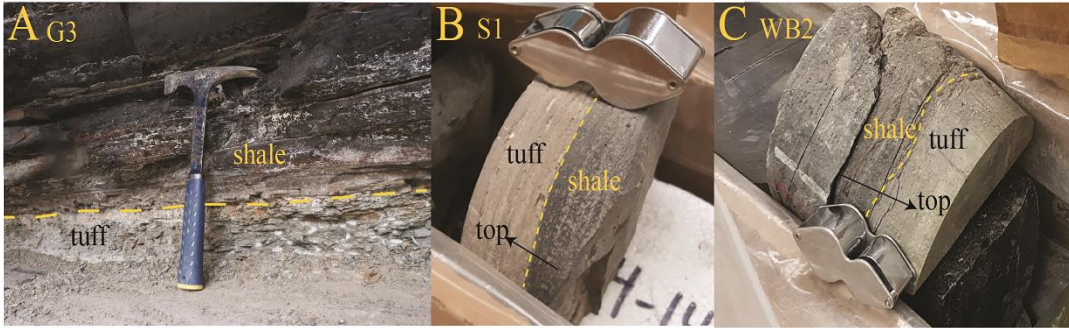
Figure S3-1. Representative images of the studied volcanic tuffs. The boundaries between tuff and the overlying or underlying shale are marked by yellow lines. G3 is from an exposure in the Guadalupe Mountains. S1 and WB2 are from subsurface of the Midland Basin. S1=Spraberry 1; WB2=Wolfcamp B 2.
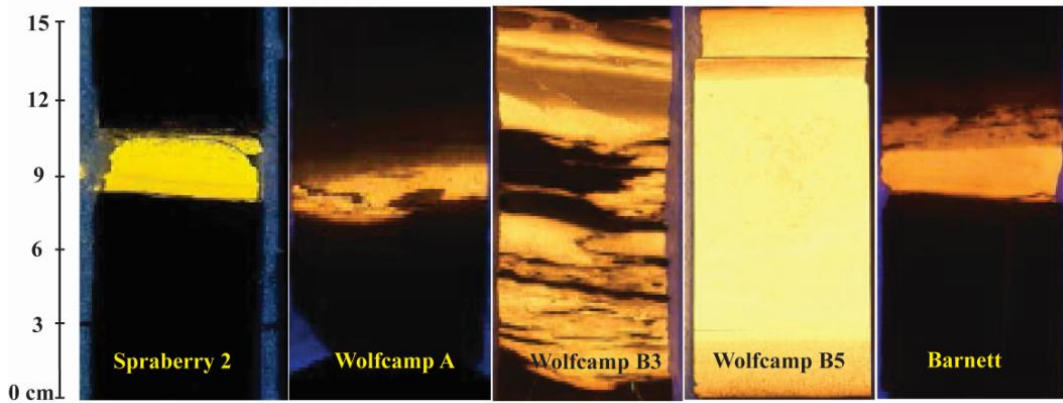
Figure S3-2. Representative images of the studied volcanic tuffs in the Midland Basin under ultraviolet light.
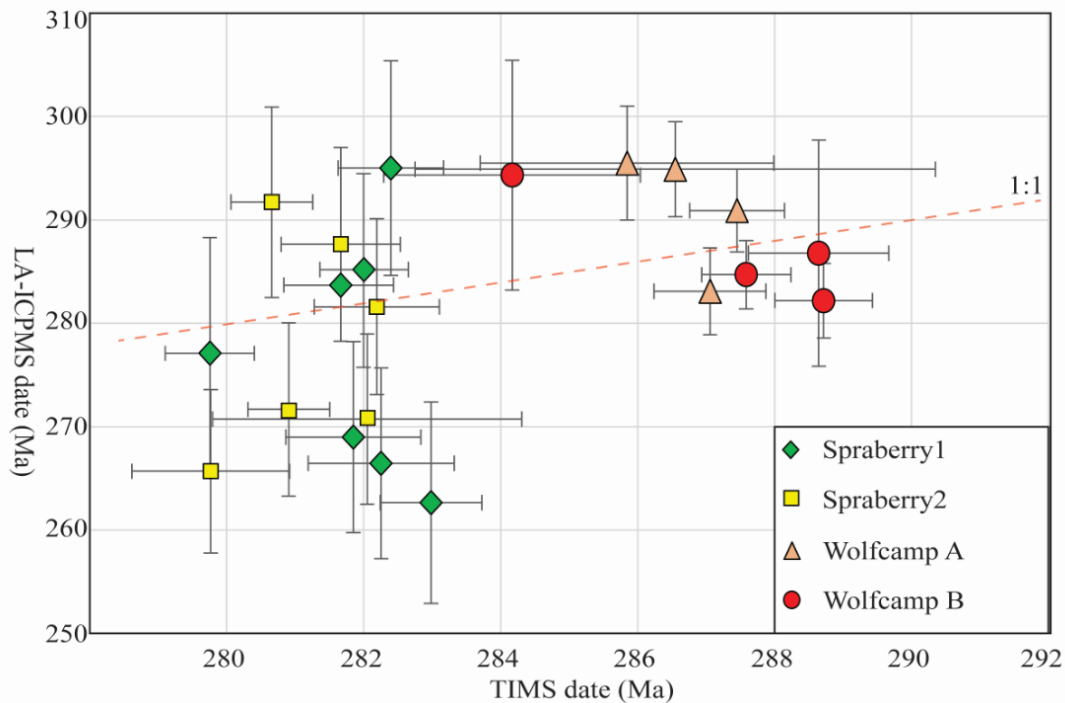
Figure S3-3. Comparison of individual LA-ICPMS dates and CA-ID-TIMS dates of the same zircons. The line of 1:1 means the two dates are equal.

ANALYTICAL METHODS

Bulk tuff and shale geochemistry

Bulk tuff and shale samples for major and trace element geochemistry were grounded in a molar and pestle and then transferred into a steel vial to be milled to a grain size of <75 μm using a SPEX SamplePrep 8000M Mixer/Mill. Approximately 2.00 ± 0.02g of powder from each sample was weighed and placed in a furnace at 900°C for 1.5 to 2 hrs. Upon removal from the furnace, the sample powders were re-weighed and their loss on ignition (LOI) was calculated. The major element geochemistry data were calibrated using eight international standards, including AGV-2, BHVO-2, JB-2, JGb-2, JSy-1, JR-3, JP-1, and GSP-2. The analytical error is generally less than 1%. Analytical results are listed in Table S1.

Trace element (Sc, Ti, V, Cr, Mn, Co, Ni, Cu, Zn, Ga, Rb, Sr, Y, Zr, Nb, Mo, Cd, Cs, Ba, REE, Hf, Ta, Pb, Th, U) compositions were measured. After major element geochemistry analyses, approximately 0.1 ± 0.001 g of each ignited sample was mixed with 0.6 ± 0.004 g of lithium borate in a platinum crucible. A few drops of lithium iodide wetting agent were added to each mixture and the mixture was then fused using the Claisse M4 Automated Fusion System. The mixture was then dissolved on a hotplate at 75°C in a mixed solution of 20 mL of 10% HNO_3 and 30 mL of 18.2 Ω deionized water obtained using a Milli-Q purification system. After the mixture was fully dissolved, 1 mL of 100 ppm Rh spike was added, and the solution was then made up to 100 mL by adding 18.2 Ω deionized water. An aliquot of 1 mL of each solution was added to a mixture with 1 mL of In and Tl and 8 mL of 2% HNO_3 for analysis. Rh, In and Tl were used as internal standards to monitor and correct for drift over the course of the analyses. Calibration was performed using natural rock standards, including W-2, BIR-1a, BHVO-2, AGV-2, BCR-2, and GSP-2 from the USGS and JR-3, JGb-2, JSy-1, JA-2, JB-2, and JG-3 from the Geological Survey of Japan. NCS certified reference material DC73305 and IGH black shale 85409-04 were used to check the accuracy of the calibration curves. Analytical precision and accuracy of all the elements are generally less than 5%. Analytical results are listed in Table S3-2 and S3-3.

Zircon LA-ICPMS U-Pb and Lu-Hf isotope analyses

Zircons were analyzed for U-Pb isotope compositions first, and all large grains (> 40 mm) were analyzed for Lu-Hf isotopes. The U-Pb analysis was conducted using an Analyte G2 193 excimer laser ablation system coupled with a Thermo-Finnigan Element 2 single-collector, inductively coupled plasma mass spectrometer. The analytical method mostly followed that of Chang et al. (2006), except for the use of the 193nm instead of the 213nm laser system. The laser parameters were 25-35 µm in diameter spot size (depending on the size of the zircon grains), 10 Hz repetition rate and ~5.5 J/cm^2. A 10-second blank measurement of the He and Ar carrier gasses (Laser off) before each analysis was

followed by 250 scans across masses ^{202}Hg, ^{204}Pb+Hg, ^{206}Pb, ^{207}Pb, ^{208}Pb, ^{232}Th, ^{235}U and ^{238}U during ~30 second laser ablation period. Analyses of zircon unknowns and quality control zircons were interspersed with analyses of external calibration standards, typically with 10-12 unknowns bracketed by multiple analyses of two different zircon standards (Plešovice and FC-1). The Plešovice standard (337 Ma; Sláma et al., 2008) was used to calibrate the ^{206}Pb/^{238}U and ^{207}Pb/^{235}U dates, and the FC-1 standard (1099 Ma; Paces and Miller, 1993) was used for calibrating ^{207}Pb/^{206}Pb dates owing to its high-count rate for ^{207}Pb (~2-4 times higher than that of Plešovice). Zircon 91500 (1065 Ma; Wiedenbeck et al., 1995) and Temora2 (417 Ma; Black et al., 2004) were used as quality control standards. Data were processed offline using the Iolite software (Paton et al., 2011). Common Pb correction was performed using the ^{207}Pb method (Williams, 1998). Plots were calculated using Isoplot (Ludwig, 2008). LA-ICP-MS zircon U-Pb data are reported in Table S3-4.

After the U-Pb analysis, Lu-Hf isotope compositions of selected zircons were analyzed using a Thermo-Finnigan Neptune multi-collector mass spectrometer coupled with an Analyte G2 193nm excimer laser ablation system. Because the laser beam used for this analysis was 35-40 μm in diameter, only larger zircon grains were selected. The laser system parameters used were laser fluence of ~5.5 J/cm2 and repetition rate of 10 Hz. This study used the same instrument configuration, operating parameters and data reduction methods discussed by Fisher et al. (2014), except that U-Pb dates were not simultaneously determined. In this "dedicated Hf" method, the output from the ablation cell was mixed with N_2 gas and delivered directly to the Neptune MC-ICPMS. To reduce inter-laboratory bias, the Plešovice zircon standard (^{176}Hf/^{177}Hf = 0.282482 ± 13, Sláma et al., 2008) was regularly analyzed between sample blocks and used to correct the measured ^{176}Hf/^{177}Hf of unknowns. Given the potentially large range of (Lu+Yb)/Hf in zircon samples, accurate correction for the isobaric interference of ^{176}Yb and ^{176}Lu on ^{176}Hf is imperative and should be assessed using quality control zircons interspersed with samples (Fisher et al., 2014). Over the course of analyses, five analyses of the FC-1 zircon (^{176}Hf/^{177}Hf = 0.282184 ± 16, Woodhead and Hergt, 2005) yielded a ^{176}Hf/^{177}Hf of 0.282186 ± 44 (2SD), ten

analyses of the Temora-2 zircon (^{176}Hf/^{177}Hf = 0.282686 ± 8, Woodhead and Hergt, 2005) yielded a ^{176}Hf/^{177}Hf of 0.282694 ± 38(2SD), and fourteen analyses of the 91500 zircon (S-MC-ICPMS ^{176}Hf/^{177}Hf = 0.282306 ± 8, Blichert-Toft, 2008) yielded a ^{176}Hf/^{177}Hf of 0.282305 ± 40 (2SD). Analyses of these quality control zircons agree well with published MC-ICPMS isotope compositions of purified Hf from these zircons, attesting to the accuracy of the interference correction methods employed. Zircon Lu-Hf data are reported in Table S3-5.

The U-Pb and Lu-Hf isotopic compositions of some zircons from the Wolfcamp A and B units were analyzed using a laser ablation split stream approach in which U-Pb dates and Lu-Hf isotopic compositions were determined simultaneously by coupling the single New Wave 213nm laser ablation system with two mass spectrometers. Ablated particles were evacuated from the sample cell in a single tube, which was then split downstream into two separate paths using a ''Y'' connection. Each tube was attached to an individual mass spectrometer and the separated components were analyzed for different compositions concurrently. Zircons with fractures or small grains (<40 μm) were excluded from analysis. The experimental procedures follow Fisher et al. (2014).

Present day εHf values were calculated using CHUR parameters reported by Bouvier et al. (2008). Errors of zircon U-Pb dates and εHf values are both reported as two standard deviations (2σ). Internal 2σ precision of the Lu-Hf isotope analysis was typically ~1.1 εHf. Analyses with less than 25 ratios, and/or internal 2σ uncertainty over 2 εHf units were discarded and not presented here. Depleted mantle model ages (T$_{DM2}$) were calculated using an average crustal value of ^{176}Lu/^{177}Hf = 0.015 following Griffin et al. (2002). ^{207}Pb/^{206}Pb dates were interpreted for grains older than 900 Ma and ^{206}Pb/^{238}U dates were interpreted for grains younger than 900 Ma. Filters of 10% discordance and a 5% reverse discordance were applied to zircons older than 500 Ma to exclude grains that may have been influenced by Pb loss or poor matrix match between samples and standards. Grains less than 500 Ma were not filtered by discordance because young ICPMS dates have large ^{207}Pb /^{235}U uncertainty. Age

plots were made using the Isoplot software (Ludwig, 2008) and the detritalPy toolset (Sharman et al., 2018).

Zircon CA-ID-TIMS geochronology

Three to five zircons in the youngest group of each of the Wolfcamp and Spraberry tuffs were analyzed by chemical abrasion, isotope dilution, thermal ionization mass spectrometry (CA-ID-TIMS). We mainly targeted youngest grains, but older grains were also included to test the matrix effect. Zircons were plucked from the epoxy mount after LA-ICPMS analysis and selected to test whether the range of dates from LA-ICPMS was robust or was an artifact of Pb loss and matrix mismatch. Zircon dissolution and chemistry were adapted from methods developed by Parrish et al. (1987) and Mattinson (2005). Zircons were chemically abraded by annealing for 50 hours at 850°C and partially dissolution in HF and HNO_3 for 12 hours at 180°C. Single zircon grains were then spiked with a mixed $^{205}Pb/^{233}U/^{235}U$ tracer (ET535), dissolved in HF and HNO_3 at 235 °C for 30 hours, and converted to chlorides at 180 °C for 16 hours. Dissolved zircons were loaded onto single rhenium filaments with silica gel and H_3PO_4 without further chemical processing. Isotopic compositions were measured on a Micromass Sector 54 mass spectrometer in single-collector, peak-switching mode using the Daly-photomultiplier collector for all isotopes. Mass discrimination of 0.25 ± 0.10 %/amu for Pb was determined by replicate analyses of NIST SRM 981. UO_2 fractionation was determined internally and corrected for oxide interference. Pb blank averaged <1 pg for zircons. Isotopic composition of the Pb blank was 18.572±0.39, 15.731±0.43, and 38.380±0.97 for $^{206}Pb/^{204}Pb$, $^{207}Pb/^{204}Pb$ and $^{208}Pb/^{204}Pb$, respectively. U blanks were < 0.01 pg. Concordia coordinates, intercepts, and uncertainties were calculated using PBMacDAT and ISOPLOT programs (based on Ludwig 1988, 1991); initial Pb isotopic compositions were estimated using Stacey and Kramers (1975). $^{206}Pb/^{238}U$ and $^{207}Pb/^{206}Pb$ ratios and dates were corrected for Th-disequilibrium after Schärer (1984) assuming a magma Th/U of 2.2. The decay constants used by PBMacDAT and ISOPLOT are those recommended by the I.U.G.S. Subcommission on Geochronology (Steiger and Jäger, 1977), including 0.155125 x 10^{-9}/yr for ^{238}U,

0.98485 x 10^{-9}/yr for ^{235}U and 137.88 for present-day ^{238}U/^{235}U ratio. Precision of the weighted mean ^{206}Pb/^{238}U date is reported in the ±X/Y/Z format of Schoene et al., (2006), with X as the analytical uncertainty (95% confidence), Y includes tracer calibration uncertainties for comparisons to other U-Pb dates, and Z includes U decay uncertainties for comparison to dates from other systems as long as the uncertainties of those dates have been fully propagated. Zircon U-Pb data of the CA-ID-TIMS analyses are reported in Table S3-6.

Zircon trace element (TE) analyses

Zircons large enough to accommodate another laser ablation spot were selected for trace element analysis at Washington State University using the same LA-ICPMS instrument used for Lu-Hf isotope analysis. New laser spots were placed within the same zone for U-Pb and Lu-Hf isotope analyses. Each analysis consists of two cleaning pulses followed by 10 seconds of washout, 18 seconds of gas blank, and 40 seconds ablation time followed by 15 seconds of waiting time before moving the stage. Three standards, including NIST610 and NIST612 synthetic glass standards and zircon reference 91500, were analyzed every 15 analyses. Correction and data reduction were carried out using the Iolite software (Woodhead et al, 2007). Eu/Eu* was calculated as $Eu_N/\sqrt{(Sm_N * Gd_N)}$ and Ce/Ce* was calculated as $Ce_N * Sm_N /Nd_N^2$ (Loader et al., 2017) where N denotes chondrite-normalized after McDonough and Sun (1995). Zircon trace element analytical data are reported in Table S3-7.

References

Black, L.P., Kamo, S.L., Allen, C.M., Davis, D.W., Aleinikoff, J.N., Valley, J.W., Mundil, R., Campbell, I.H., Korsch, R.J., Williams, I.S., and Foudoulis, C., 2004, Improved Pb-^{206}/U-^{218} microprobe geochronology by the monitoring of a trace-element-related matrix effect; SHRIMP, ID-TIMS, ELA-ICP-MS and oxygen isotope documentation for a series of zircon standards: Chemical Geology, v. 205, p. 115-140.

Blichert-Toft, J., 2008, The Hf isotopic composition of zircon reference material 91500: Chemical Geology, v. 253, p. 252-257.

Bouvier, A., Vervoort, J.D., Patchett, P.J., 2007, The Lu-Hf and Sm-Nd isotopic composition of

CHUR: constraints from unequilibrated chondrites and implications for the bulk composition of terrestrial planets: Earth and Planetary Science Letters, v 219, p. 311.

Chang, Z., Vervoort, J.D., McClelland, W.C., and Knaack, C., 2006, U-Pb dating of zircon by LA-ICP-MS: Geochemistry, Geophysics, Geosystems, v.7, p.1-14, doi: 10.1029/2005GC001100.

Fisher, C.M., Vervoort, J.D., and Dufrane, S.A., 2014, Accurate Hf isotope determinations of complex zircons using the "laser ablation split stream" method: Geochemistry, Geophysics, Geosystems, v. 15, p.121–139, doi: 10.1002/2013GC004962.

Loader, M.A., Wilkinson, J.J., and Armstrong, R.N., 2017, The effect of titanite crystallisation on Eu and Ce anomalies in zircon and its implications for the assessment of porphyry cu deposit fertility: Earth Planet Science Letter, v. 472, p. 107–119.

Ludwig, K.R., 1988, PBDAT for MS-DOS, a computer program for IBM-PC compatibles for processing raw Pb-U-Th isotope data, version 1.24: U.S. Geological Survey, Open-File Report 88-542, 32 pp.

Ludwig, K.R., 1991, ISOPLOT for MS-DOS, a plotting and regression program for radiogenic-isotope data, for IBM-PC compatible computers, version 2.75: U.S. Geological Survey, Open-File Report 91-445, 45 p.

Ludwig, K.R., 2008, User's Manual for Isoplot 3.70: Berkeley Geochronology Center Special Publication, p.76.

McDonough, W., and Sun, S.S.. 1995, The composition of the Earth: Chemical Geology,v.67, p.1050-1056.

Mattinson, J.M, 2005, Zircon U-Pb chemical abrasion ("CA-TIMS") method: combined annealing and multi-step partial dissolution analysis for improved precision and accuracy of zircon ages: Chemical Geology, v.220, p.47-66.

Paces, J.B., and Miller Jr, J.D., 1993, Precise U-Pb ages of Duluth Complex and related mafic intrusions, northeastern Minnesota: Geochronological insights to physical, petrogenetic, paleomagnetic, and tectonomagmatic processes associated with the 1.1 Ga Midcontinent Rift System: Journal of Geophysical Research, v. 98, p. 13997-14013.

Paton, C., Hellstrom, J., Paul, B., Woodhead, J., and Hergt, J., 2011, Iolite: Freeware for the visualization and processing of mass spectrometric data: Journal of Analytical Atomic Spectrometry, v.26, p. 2508-2518.

Parrish, R.R., Roddick, J.C., Loveridge, W.D., and Sullivan, R.D., l987, Uranium-lead analytical techniques at the geochronology laboratory, Geological Survey of Canada, in Radiogenic age and isotopic studies, Report 1: Geological Survey of Canada Paper 87-2, p.3–7.

Schoene, B., Crowley, J.L., Condon, D.J., Schmitz, M.D. and Bowring, S.A., 2006. Reassessing the uranium decay constants for geochronology using ID-TIMS U–Pb data: Geochimica et Cosmochimica Acta, v. 70, p.426-445.

Sláma, J., Košler, J., Condon, D.J., Crowley, J.L., Gerdes, A., Hanchar, J.M., Horstwood, M.S.A., Morris, G.A., Nasdala, L., Norberg, N., Schaltegger, U., Schoene, B., Tubrett, M.N., and Whitehouse, M.J., 2008, Plešovice zircon — A new natural reference material for U–Pb and Hf isotopic microanalysis: Chemical Geology v. 249, p. 1-35.

Stacey, J.S., and Kramers, J.D., 1975, Approximation of terrestrial lead isotope evolution by a two-stage model: Earth and Planetary Science Letters, v. 26, p.207–221.

Steiger, R.H., and Jäger, E., 1977, Subcommission on geochronology: convention on the use of decay constants in geo- and cosmochronology: Earth and Planetary Science Letters, v. 36, p.359-362.

Wiedenbeck, M., Allé, P., Corfu, F., Griffin, W.L., Meier, M., Oberli, F., Von Quadt, A., Roddick, J.C., and Spiegel, W., 1995, Three natural zircon standards for U-Th-Pb, Lu-Hf, trace element and REE analyses: Geostandards Newsletters, v. 19, p. 1-23.

Williams, I.S., 1998, U-Th-Pb geochronology by ion microprobe: M.A. McKibben, W.C. Shanks III, W.I. Ridley (Eds.), Applications of Microanalytical Techniques to Understanding Mineralizing Processes: Reviews in Economic Geology, v. 7, p. 1-35.

Woodhead, J. and Hergt, J., 2007, A Preliminary Appraisal of Seven Natural Zircon Reference Materials   for In Situ Hf Isotope Determination: Geostandards and Geoanalytical Research, v.29, p.183-195.

Table S3-1. Sample ID, location, stratigraphic interval, dates and description of all the tuffs

Sample ID	Location	Formation/Unit	CA-ID-TIMS date (Ma)	Descriptions
G1	104°46'56.58"W 31°49'28.11"N	Bell Canyon	262.1 ± 0.1 (Wu et al., 2020)	Sample ID BR040915-1B in Wu et al. (2020)
G2	104°52'32.95"W 31°54'31.91"N	Cherry Canyon	265.5 ± 0.3 (Wu et al., 2020)	Sample ID NippleHill-2 in Wu et al. (2020)
G3	104°47'20.08"W 31°54'44.37"N	Cherry Canyon	266.5 ± 0.1 (Wu et al., 2020)	Sample ID MC053117-3 in Wu et al. (2020)
Spraberry1 (S1)	Martin County	Spraberry	282.0 ±0.4 Ma (This study)	At 2469 m of core S1, ~3 cm thick
Spraberry2 (S2)	Midland County	Spraberry	280.7 ±1.1 Ma (This study)	At 2672 m of core S2, ~3 cm thick
WA	Midland County	Wolfcamp A	287.2 ±0.5 Ma (This study)	At 2885 m of core A, ~2.5 cm thick
WB1	Upton County	Wolfcamp B		At 2689 m of core B1, ~8 cm thick
WB2	Upton County	Wolfcamp B		At 2694 m of core B1, ~3 cm thick
WB3	Upton County	Wolfcamp B	288.2 ±1.7 Ma (This study)	At 2701 m of core B2, ~12 cm thick
WB4	Upton County	Wolfcamp B		At 2710 m of core B2, ~ 3 cm thick
WB5	Upton County	Wolfcamp B		At 2789 m of core B2, ~14 cm thick
WB6	Upton County	Wolfcamp B		At 2400 m of core B3, ~12 cm thick

Table S3-2. Whole rock major and trace element compositions of the Midland Basin tuffs

Sample ID	S2	S1	WA	WB1	WB2	WB3	WB4	WB5	WB6
SiO_2	57.8	58.8	64.8	60.6	69.8	62.6	66.5	66.3	66.9
Al_2O_3	30.9	29.1	23.4	27.5	20.8	25.0	21.1	21.9	23.5
TiO_2	0.3	0.3	0.5	0.3	0.4	0.4	0.5	0.5	0.5
Fe_2O_3	2.2	2.3	2.8	3.9	2.5	3.5	2.8	3.6	2.5
MgO	2.0	2.4	2.0	1.1	1.1	1.1	1.2	1.2	1.2
CaO	1.1	0.6	1.2	0.7	0.8	1.4	1.9	1.4	0.6
Na_2O	0.4	1.4	0.8	1.7	1.1	1.2	1.2	1.3	0.8
K_2O	5.1	5.2	4.5	4.0	3.4	4.1	3.7	3.8	3.9
P_2O_5	0.1	0.1	0.0	0.3	0.1	0.8	1.2	0.1	0.1
CIA	0.8	0.8	0.8	0.8	0.8	0.8	0.8	0.7	0.8
LOI	12.0	11.1	10.5	11.8	10.5	10.8	11.5	11.4	10.9
Total	100.0	100.0	100.0	100.0	100.0	100.0	100.0	100.0	100.0
Sc	16.6	25.2	43.9	27.0	29.1	26.0	33.0	33.9	33.6
V	17.6	14.3	86.0	24.5	67.0	72.9	61.0	62.1	136.7
Cr	b.d.l.	b.d.l.	178.1	19.0	156.1	71.3	99.9	99.2	101.1
Mn	55.2	54.9	53.6	27.5	63.6	64.5	81.3	102.6	120.0
Co	3.7	3.8	8.7	6.4	8.7	10.0	8.7	12.4	9.2
Ni	11.1	4.8	72.2	21.1	61.9	23.4	40.2	99.9	99.4
Ga	39.7	25.4	39.0	34.9	26.7	27.6	26.7	17.5	27.5
Rb	171.7	144.8	252.9	170.6	186.9	208.2	183.6	91.5	234.5
Sr	415.7	265.6	216.3	450.5	365.8	338.0	414.6	1467.4	339.8
Y	34.8	34.2	40.2	53.2	52.2	34.5	18.0	24.5	12.2
Zr	381.7	335.1	326.0	296.1	234.7	189.8	218.2	153.1	175.6

Nb	22.4	16.8	30.5	32.3	19.3	14.6	19.3	11.0	18.7
Mo	4.0	4.1	8.2	10.4	16.4	15.6	8.2	17.5	7.9
Ba	234.1	232.5	424.6	458.0	439.9	416.4	1114.3	435.2	367.4
La	12.6	5.4	43.7	39.2	41.5	31.8	32.7	34.7	23.8
Ce	28.8	10.6	85.1	87.1	80.2	60.5	59.3	54.0	40.4
Pr	3.7	1.3	9.0	10.3	10.8	7.8	5.9	6.7	4.5
Nd	14.0	5.5	28.6	36.0	39.8	27.7	18.0	22.8	14.2
Sm	3.3	1.4	5.4	9.3	8.9	6.1	2.6	3.4	2.1
Eu	0.8	0.6	0.8	1.0	1.4	1.1	0.7	0.8	0.5
Gd	3.4	1.9	5.0	8.8	8.2	5.5	2.2	2.9	1.6
Tb	0.6	0.5	1.0	1.7	1.4	0.9	0.4	0.5	0.3
Dy	4.3	3.9	6.6	10.4	7.9	5.3	2.8	3.2	1.8
Ho	0.9	0.9	1.5	2.2	1.6	1.1	0.7	0.7	0.4
Er	3.8	3.9	4.8	6.5	4.1	2.8	2.0	2.6	1.1
Tm	0.6	0.6	1.0	1.3	0.7	0.5	0.4	0.4	0.2
Yb	3.3	3.8	7.1	8.1	4.6	3.1	3.3	2.8	1.8
Lu	0.5	0.6	1.2	1.2	0.7	0.5	0.5	0.5	0.3
Hf	16.2	14.5	15.5	17.7	10.7	9.4	10.2	6.0	11.0
Ta	4.2	3.6	6.1	7.7	3.8	5.0	3.9	2.3	8.3
Pb	16.9	13.8	67.3	86.0	41.0	44.3	55.5	72.2	56.4
Th	174.5	155.0	197.2	252.2	124.2	113.6	127.1	139.2	230.7
U	45.1	35.1	48.0	92.4	48.0	28.7	31.8	22.5	14.6
Zr/Nb	17.0	20.0	10.7	9.2	12.2	13.0	11.3	13.9	9.4
Eu/Eu*	0.7	1.0	0.5	0.3	0.5	0.6	0.9	0.7	0.8
Ce/Lu$_N$	2.2	0.7	2.9	3.0	4.5	4.9	4.7	4.6	5.4
Rb/Ba$_N$	0.8	0.7	0.6	0.4	0.5	0.5	0.2	0.2	0.7

Table S3-3. Major and trace element compositions of shale samples near the associated tuffs

Sample ID	S1	WA	WB1	WB3
SiO$_2$	72.6	54.8	73.4	74.5
Al$_2$O$_3$	13.9	5.2	9.2	15.5
TiO$_2$	0.8	0.2	0.1	0.6
Fe$_2$O$_3$	4.3	3.4	2.7	3.3
MnO	0.0	0.0	0.0	0.0
MgO	2.1	1.6	1.2	1.3
CaO	1.7	32.8	10.3	0.6
Na$_2$O	1.4	0.7	0.9	1.0
K$_2$O	3.1	1.0	1.7	3.1
P$_2$O$_5$	0.1	0.4	0.5	0.0
LOI	7.4	21.7	11.6	12.0
Total	100.0	100.0	100.0	100.0
CIA	0.6	0.6	0.7	0.7
Sc	29.2	b.d.l.	18.2	18.9
Ti	4433.2	1336.5	2244.1	3458.4
V	196.5	72.5	87.0	145.1
Cr	202.6	156.3	177.0	329.5
Mn	255.4	194.0	160.8	158.2
Co	15.0	6.0	9.7	12.0
Ni	109.9	52.0	64.9	123.3
Cu	71.5	55.1	60.2	77.6
Zn	133.9	144.4	332.0	1887.4
Ga	22.1	6.8	14.9	25.0

As	12.6	9.9	9.2	9.4
Rb	189.1	45.5	115.1	180.0
Sr	214.9	2403.6	11070.3	148.4
Y	28.2	30.0	57.7	12.5
Zr	350.0	70.7	112.7	165.8
Nb	22.1	6.9	11.9	17.9
Mo	6.1	10.4	4.6	4.1
Cd	0.9	0.3	0.7	3.8
Sn	2.4	1.0	1.7	3.2
Sb	2.0	1.3	1.1	1.7
Cs	10.6	2.5	6.1	12.5
Ba	438.4	145.5	11914.8	302.2
La	29.0	29.2	30.8	25.2
Ce	52.6	33.6	50.0	43.9
Pr	6.1	5.4	7.3	4.5
Nd	21.5	19.8	28.5	13.4
Sm	4.0	3.5	6.4	1.8
Eu	0.8	0.7	2.9	0.4
Gd	3.5	3.7	6.4	1.3
Tb	0.6	0.6	1.1	0.3
Dy	3.7	3.6	6.8	1.8
Ho	0.8	0.8	1.4	0.4
Er	2.8	2.8	4.5	2.0
Tm	0.5	0.4	0.7	0.4
Yb	3.7	2.6	4.5	2.5
Lu	0.6	0.4	0.7	0.4

Hf	11.0	2.2	3.9	7.0
Ta	1.9	0.7	1.1	2.1
Pb	47.2	17.2	31.2	31.2
Th	36.2	7.9	18.9	25.0
U	10.1	6.9	12.4	5.8

Table S3-4. Zircon U-Pb geochronologic analyses by Laser-Ablation Multicollector Inductively Coupled Plasma Mass Spectrometry

	Isotopic Ratios				Dates							
Sample ID	Non Corrected $^{238}U/^{206}Pb$	2s Abs Error	$^{207}Pb/^{206}Pb$	2s Abs Error	$^{207}Pb/^{235}U$ Ma	2s Abs Error Ma	$^{206}Pb/^{238}U$ Ma	2s Abs Error Ma	$^{207}Pb/^{206}Pb$ Ma	2s Abs Error Ma	Best Date Ma	2s Abs Error Ma
G1-1	72.6744	1.0563	0.0752	0.0055	131.0	8.7	85.0	1.4	890.0	140.0	85	1
G1-2	42.4809	0.7399	0.0522	0.0020	158.4	5.3	149.4	2.6	256.0	81.0	149	3
G1-3	26.0078	0.3314	0.0563	0.0015	263.7	6.1	241.6	3.1	432.0	57.0	242	3
G1-4	25.8198	0.3267	0.0555	0.0015	262.3	6.0	243.6	3.1	407.0	59.0	244	3
G1-5	24.4618	0.5385	0.0932	0.0048	409.8	18.0	244.6	5.6	1471.0	91.0	245	6
G1-6	24.5098	0.6007	0.0813	0.0043	370.1	13.0	248.0	6.2	1170.0	110.0	248	6
G1-7	22.7273	0.5682	0.1240	0.0100	528.2	43.0	252.2	7.2	1830.0	160.0	252	7
G1-8	24.4798	0.3356	0.0522	0.0018	261.5	8.3	257.8	3.5	286.0	77.0	258	4
G1-9	24.1488	0.3382	0.0581	0.0023	288.8	9.5	259.4	3.7	499.0	84.0	259	4
G1-10	23.9234	0.2747	0.0548	0.0014	277.7	6.8	262.9	3.0	376.0	56.0	263	3
G1-11	19.9720	0.2712	0.0554	0.0013	327.9	6.2	313.9	4.2	403.0	50.0	314	4
G1-12	19.5542	0.2562	0.0586	0.0016	349.0	8.4	319.2	4.2	523.0	62.0	319	4
G1-13	16.8067	0.2457	0.1280	0.0035	677.9	14.0	337.7	5.2	2040.0	49.0	338	5
G1-14	15.9236	0.1876	0.0679	0.0015	463.1	8.1	386.0	4.5	848.0	44.0	386	5

G1-15	14.9321	0.2118	0.0701	0.0025	499.1	13.0	410.0	5.9	901.0	78.0	410	6
G1-16	14.9254	0.2450	0.0565	0.0017	425.9	10.0	417.3	6.8	446.0	65.0	417	7
G1-17	14.2857	0.2041	0.0603	0.0015	463.6	9.1	433.6	6.1	593.0	54.0	434	6
G1-18	13.9256	0.1532	0.0614	0.0015	479.6	8.7	443.9	4.9	628.0	54.0	444	5
G1-19	13.4048	0.2156	0.0583	0.0013	476.1	8.4	462.6	7.3	532.0	48.0	463	7
G1-20	11.7509	0.2209	0.0806	0.0031	661.2	20.0	511.4	9.6	1179.0	75.0	511	10
G1-21	11.6550	0.1902	0.0651	0.0012	575.9	9.4	525.9	8.4	771.0	39.0	526	8
G1-22	6.8446	0.1359	0.0798	0.0022	963.7	17.0	866.3	16.9	1174.0	56.0	866	17
G1-23	5.7637	0.0764	0.0753	0.0015	1044.8	14.0	1029.2	13.4	1061.0	39.0	1029	13
G1-24	5.2056	0.0488	0.0783	0.0018	1139.8	15.0	1131.5	10.6	1127.0	46.0	1132	11
G1-25	5.0378	0.0812	0.0865	0.0022	1225.5	18.0	1155.7	18.4	1335.0	49.0	1335	18
G1-26	4.6620	0.0717	0.0851	0.0019	1274.5	18.0	1248.2	18.9	1303.0	41.0	1303	19
G1-27	4.1220	0.0391	0.0909	0.0019	1416.1	17.0	1396.4	13.4	1422.0	40.0	1422	40
G1-28	4.6555	0.1257	0.1011	0.0035	1386.2	30.0	1223.9	32.6	1625.0	66.0	1625	66
G1-29	3.4578	0.0418	0.1031	0.0016	1654.2	12.0	1632.3	19.9	1673.0	28.0	1673	28
G1-30	3.3727	0.0398	0.1045	0.0024	1686.4	19.0	1669.9	20.3	1679.0	42.0	1679	42
G1-31	4.1911	0.0615	0.1039	0.0020	1490.7	15.0	1350.4	19.6	1683.0	36.0	1683	36
G1-32	3.4904	0.0451	0.1069	0.0016	1670.4	14.0	1608.9	20.8	1741.0	27.0	1741	27
G1-33	3.1736	0.0524	0.1123	0.0030	1793.6	25.0	1755.2	29.9	1824.0	49.0	1824	49
G1-34	5.2329	0.1342	0.1216	0.0051	1409.6	25.0	1063.0	27.4	1956.0	75.0	1956	75
G1-35	2.9155	0.0603	0.1415	0.0039	2035.6	32.0	1833.4	39.7	2231.0	48.0	2231	48
G1-36	142.0455	5.8513	0.2290	0.0180	160.0	16.0	34.7	1.8	2980.0	130.0	2980	130
G1-37	78.0640	4.0220	0.4260	0.0270	333.6	39.0	42.5	3.6	3910.0	110.0	3910	110
G2-1	100.9082	1.2219	0.0512	0.0018	68.3	2.1	63.3	0.8	212.0	73.0	63	1
G2-2	29.4551	0.5379	0.0719	0.0029	287.5	8.9	209.4	3.9	914.0	84.0	209	4

G2-3	27.7008	0.8441	0.0683	0.0024	291.4	8.5	223.5	6.8	843.0	75.0	224	7
G2-4	25.7666	0.3452	0.06870	0.0026	311.7	9.6	240.0	3.3	835.0	83	240	3
G2-5	25.0878	0.3839	0.0618	0.0023	293.5	8.9	248.6	3.8	612.0	78.0	249	4
G2-6	25.2398	0.4714	0.0524	0.0029	255.3	13.0	250.1	4.7	260.0	120.0	250	5
G2-7	24.5700	0.6641	0.0569	0.0043	279.7	16.0	255.4	7.0	420.0	160.0	255	7
G2-8	24.3962	0.3988	0.0614	0.0017	299.2	7.5	255.7	4.2	636.0	60.0	256	4
G2-9	24.6305	0.3519	0.0528	0.0017	262.6	7.1	256.1	3.7	279.0	66.0	256	4
G2-10	24.3368	0.3258	0.0543	0.0016	271.5	6.9	258.6	3.5	343.0	64.0	259	3
G2-11	24.0732	0.3419	0.0538	0.0016	272.1	6.8	261.6	3.7	341.0	65.0	262	4
G2-12	24.1138	0.2617	0.0524	0.0010	265.8	4.6	261.6	2.8	295.0	42.0	262	3
G2-13	23.4247	0.3512	0.0592	0.0022	301.1	9.5	266.9	4.0	512.0	83.0	267	4
G2-14	21.9491	0.2650	0.1073	0.0055	493.7	23.0	267.1	3.8	1630.0	110.0	267	4
G2-15	20.2470	0.3853	0.0736	0.0049	403.3	24.0	302.5	6.0	970.0	140.0	303	6
G2-16	20.3046	0.2268	0.0599	0.0015	343.8	7.0	307.0	3.4	568.0	53.0	307	3
G2-17	19.7746	0.1994	0.0653	0.0018	375.9	7.6	313.0	3.2	741.0	58.0	313	3
G2-18	18.1159	0.3938	0.1026	0.0063	557.3	31.0	324.8	7.5	1610.0	110.0	325	7
G2-19	18.4196	0.2477	0.0702	0.0016	421.2	8.3	333.5	4.5	916.0	46.0	334	4
G2-20	17.3611	0.3315	0.0772	0.0031	473.8	16.0	350.3	6.7	1101.0	80.0	350	7
G2-21	17.3370	0.2284	0.0732	0.0014	456.5	6.5	352.6	4.6	1011.0	40.0	353	5
G2-22	16.1760	0.1989	0.0850	0.0013	536.3	6.8	371.7	4.5	1305.0	31.0	372	5
G2-23	16.2602	0.2644	0.0741	0.0015	485.1	9.9	375.1	6.0	1035.0	43.0	375	6
G2-24	16.2787	0.1881	0.0554	0.0013	390.3	6.9	383.8	4.4	402.0	53.0	384	4
G2-25	15.9490	0.1679	0.0583	0.0011	412.8	6.2	390.1	4.1	519.0	42.0	390	4
G2-26	15.5763	0.2669	0.0646	0.0034	454.5	16.0	396.1	6.9	707.0	98.0	396	7
G2-27	15.1976	0.3003	0.0728	0.0028	505.6	12.0	401.5	7.9	987.0	77.0	402	8
G2-28	15.3516	0.1720	0.0627	0.0016	449.9	8.8	402.8	4.5	665.0	55.0	403	5

G2-29	15.0376	0.1877	0.0556	0.0014	418.2	7.8	414.8	5.1	402.0	53.0	415	5
G2-30	14.4300	0.2082	0.0548	0.0018	428.0	11.0	432.3	6.2	356.0	71.0	432	6
G2-31	13.7363	0.1887	0.0561	0.0010	453.6	6.4	453.0	6.1	445.0	42.0	453	6
G2-32	13.6968	0.1501	0.0570	0.0011	460.1	7.0	453.7	4.9	471.0	41.0	454	5
G2-33	13.4481	0.1573	0.0566	0.0009	464.4	6.4	462.2	5.3	469.0	36.0	462	5
G2-34	12.3305	0.2433	0.0678	0.0016	567.0	12.0	496.0	9.6	849.0	48.0	496	10
G2-35	12.0846	0.1198	0.0586	0.0007	519.2	5.3	511.9	5.0	541.0	27.0	512	5
G2-36	12.0250	0.1374	0.0591	0.0010	524.7	7.4	514.0	5.8	557.0	38.0	514	6
G2-37	11.2867	0.1656	0.0606	0.0020	561.5	14.0	545.8	7.9	588.0	72.0	546	8
G2-38	11.1857	0.1376	0.0622	0.0019	575.9	12.0	549.5	6.7	630.0	66.0	549	7
G2-39	10.8342	0.1643	0.0665	0.0021	618.2	14.0	563.8	8.5	763.0	70.0	564	8
G2-40	10.8578	0.1650	0.0615	0.0020	584.7	14.0	566.2	8.5	606.0	73.0	566	9
G2-41	10.4603	0.1094	0.0662	0.0012	633.0	8.5	583.7	6.0	795.0	38.0	584	6
G2-42	10.3413	0.1497	0.0659	0.0016	636.6	14.0	590.4	8.4	795.0	55.0	590	8
G2-43	10.4058	0.1191	0.0608	0.0012	599.5	8.3	590.7	6.7	608.0	44.0	591	7
G2-44	9.8912	0.1272	0.0600	0.0014	617.6	12.0	621.2	7.9	592.0	51.0	621	8
G2-45	8.9606	0.1847	0.0657	0.0027	707.2	18.0	679.0	13.8	778.0	89.0	679	14
G2-46	7.0671	0.0799	0.0710	0.0018	880.1	14.0	849.3	9.5	921.0	52.0	849	10
G2-47	7.0522	0.0895	0.0677	0.0015	856.2	12.0	854.7	10.6	832.0	46.0	855	11
G2-48	6.9061	0.0811	0.0781	0.0018	946.1	14.0	860.7	10.0	1131.0	47.0	861	10
G2-49	6.7522	0.1094	0.0716	0.0021	912.8	19.0	887.0	14.1	952.0	62.0	887	14
G2-50	6.2344	0.0738	0.0725	0.0018	970.6	14.0	957.2	11.2	971.0	51.0	957	11
G2-51	6.1652	0.0798	0.0732	0.0015	983.3	14.0	966.8	12.3	1006.0	46.0	967	12
G2-52	6.1237	0.1012	0.0767	0.0027	1014.5	21.0	968.8	15.9	1093.0	67.0	969	16
G2-53	6.1425	0.0566	0.0740	0.0010	992.2	8.0	969.2	8.7	1032.0	27.0	969	9
G2-54	6.1125	0.0710	0.0743	0.0010	997.5	8.4	973.5	11.0	1042.0	27.0	973	11

216

G2-55	6.0827	0.1147	0.0745	0.0020	1002.3	20.0	977.8	18.0	1042.0	54.0	978	18
G2-56	6.0386	0.0839	0.0732	0.0009	997.4	9.3	986.3	13.3	1020.0	23.0	986	13
G2-57	5.9701	0.0820	0.0772	0.0013	1035.3	12.0	992.3	13.3	1117.0	33.0	992	13
G2-58	5.9737	0.0678	0.0756	0.0012	1022.8	11.0	993.7	11.0	1074.0	34.0	994	11
G2-59	5.8445	0.0956	0.0810	0.0026	1078.0	23.0	1008.0	16.3	1208.0	65.0	1008	16
G2-60	5.8617	0.0584	0.0735	0.0015	1019.3	12.0	1014.8	10.0	1004.0	42.0	1015	10
G2-61	5.6689	0.0996	0.0819	0.0019	1105.9	17.0	1037.0	17.8	1227.0	45.0	1037	18
G2-62	5.5710	0.1366	0.0768	0.0020	1079.9	20.0	1061.6	25.3	1113.0	49.0	1062	25
G2-63	5.5617	0.0804	0.0768	0.0019	1081.1	14.0	1063.3	15.1	1102.0	47.0	1063	15
G2-64	5.5157	0.0700	0.0757	0.0015	1078.3	14.0	1073.4	13.3	1064.0	42.0	1073	13
G2-65	5.4975	0.0967	0.0781	0.0022	1099.2	20.0	1073.5	18.5	1125.0	55.0	1074	19
G2-66	5.4705	0.0599	0.0798	0.0011	1115.7	10.0	1076.3	11.5	1189.0	27.0	1076	12
G2-67	5.4142	0.0762	0.0756	0.0017	1090.5	13.0	1093.0	15.1	1059.0	46.0	1093	15
G2-68	5.3533	0.0487	0.0787	0.0013	1122.7	10.0	1100.7	9.9	1149.0	32.0	1101	10
G2-69	5.3763	0.0578	0.0749	0.0010	1089.9	9.6	1101.5	11.6	1053.0	28.0	1101	12
G2-70	5.3135	0.0706	0.0713	0.0012	1068.7	13.0	1119.2	14.5	958.0	34.0	1119	15
G2-71	5.2549	0.0911	0.0782	0.0023	1132.2	22.0	1121.4	19.1	1138.0	59.0	1121	19
G2-72	5.1626	0.0746	0.0900	0.0019	1231.8	16.0	1123.5	16.0	1415.0	40.0	1415	16
G2-73	5.2356	0.0576	0.0778	0.0015	1131.7	13.0	1125.9	12.2	1127.0	38.0	1126	12
G2-74	5.0607	0.0563	0.0801	0.0011	1174.4	10.0	1160.2	12.6	1194.0	27.0	1160	13
G2-75	4.9776	0.0619	0.0824	0.0017	1204.2	15.0	1175.5	14.4	1235.0	40.0	1175	14
G2-76	4.9628	0.0419	0.0794	0.0012	1183.4	9.5	1183.4	9.9	1170.0	29.0	1183	10
G2-77	4.9140	0.0821	0.0800	0.0022	1195.4	20.0	1193.9	19.6	1190.0	58.0	1194	20
G2-78	4.7939	0.0620	0.0814	0.0011	1224.9	9.5	1220.7	15.4	1220.0	27.0	1221	15
G2-79	4.7506	0.0519	0.0843	0.0016	1253.9	14.0	1226.9	13.3	1287.0	37.0	1227	13
G2-80	4.6970	0.0507	0.0828	0.0018	1251.3	17.0	1242.9	13.4	1246.0	44.0	1243	13

G2-81	4.6773	0.0503	0.0833	0.0010	1257.9	9.1	1247.2	13.1	1268.0	22.0	1247	13
G2-82	4.6751	0.0612	0.0831	0.0014	1257.2	12.0	1248.1	16.0	1259.0	34.0	1248	16
G2-83	4.5872	0.0463	0.0849	0.0015	1285.5	13.0	1268.3	12.7	1302.0	33.0	1302	13
G2-84	4.3898	0.0482	0.0878	0.0013	1342.0	13.0	1318.7	14.3	1372.0	30.0	1372	30
G2-85	4.4111	0.0584	0.0877	0.0014	1337.4	13.0	1312.7	17.1	1373.0	31.0	1373	31
G2-86	4.1806	0.0489	0.0919	0.0017	1411.6	16.0	1375.5	16.0	1449.0	33.0	1449	33
G2-87	3.7994	0.0491	0.0936	0.0021	1504.6	18.0	1506.8	19.5	1483.0	44.0	1483	44
G2-88	3.8850	0.0709	0.0946	0.0013	1492.6	16.0	1472.3	26.4	1517.0	25.0	1517	25
G2-89	3.7850	0.0401	0.0981	0.0016	1539.6	13.0	1503.4	15.9	1575.0	31.0	1575	31
G2-90	3.5791	0.0384	0.1005	0.0022	1605.5	17.0	1583.2	17.4	1614.0	42.0	1614	42
G2-91	3.3434	0.0313	0.1028	0.0014	1683.2	11.0	1688.3	16.0	1668.0	25.0	1668	25
G2-92	4.9554	0.1031	0.1096	0.0024	1387.7	19.0	1139.0	23.3	1786.0	39.0	1786	39
G2-93	3.1075	0.0280	0.1116	0.0018	1809.6	14.0	1794.4	16.9	1818.0	30.0	1818	30
G2-94	3.0294	0.0863	0.1130	0.0027	1843.2	31.0	1837.4	53.3	1837.0	44.0	1837	44
G2-95	3.5211	0.0558	0.1195	0.0023	1738.3	16.0	1567.7	25.0	1941.0	35.0	1941	35
G2-96	1.8498	0.0195	0.1882	0.0024	2771.0	13.0	2829.6	46.2	2723.0	21.0	2723	21
G2-97	1.9153	0.0172	0.1894	0.0023	2718.1	12.0	2689.8	34.3	2732.0	20.0	2732	20
G3-22	28.0426	0.6999	0.0661	0.0044	280.8	15.0	221.5	5.6	700.0	130.0	221	6
G3-4	24.9314	0.5532	0.1074	0.0067	445.7	26.0	235.5	5.6	1630.0	120.0	235	6
G3-58	26.1986	0.4461	0.0699	0.0028	311.5	11.0	235.7	4.1	893.0	85.0	236	4
G3-77	25.9000	0.4629	0.0738	0.0036	328.1	13.0	237.2	4.3	950.0	100.0	237	4
G3-81	26.2330	0.5712	0.0577	0.0029	267.0	9.4	239.1	5.2	490.0	110.0	239	5
G3-61	25.7599	0.4313	0.0716	0.0028	322.0	11.0	239.1	4.1	894.0	76.0	239	4
G3-3	24.1371	0.5593	0.1133	0.0055	474.5	21.0	241.2	5.8	1817.0	92.0	241	6
G3-76	24.8633	0.5625	0.0768	0.0037	350.3	15.0	246.0	5.6	1072.0	98.0	246	6

G3-20	24.7647	0.5152	0.0686	0.0031	322.3	12.0	249.6	5.2	835.0	92.0	250	5
G3-14	24.4439	0.3406	0.0695	0.0023	329.2	9.7	252.5	3.6	853.0	70.0	253	4
G3-34	24.6792	0.3411	0.0591	0.0022	287.2	8.8	253.5	3.5	514.0	79.0	254	4
G3-64	24.5942	0.3085	0.0614	0.0016	297.1	7.6	253.7	3.2	616.0	57.0	254	3
G3-51	24.8324	0.5981	0.0537	0.0027	264.3	11.0	253.7	6.1	340.0	110.0	254	6
G3-78	24.8324	0.4193	0.0533	0.0015	262.7	6.4	253.9	4.3	317.0	62.0	254	4
G3-43	24.7709	0.3497	0.0542	0.0016	266.9	7.2	254.2	3.6	336.0	63.0	254	4
G3-46	24.7280	0.3119	0.0535	0.0014	264.5	5.9	254.9	3.2	325.0	57.0	255	3
G3-48	24.6853	0.3656	0.0538	0.0017	266.1	7.2	255.2	3.8	353.0	75.0	255	4
G3-55	24.5459	0.4941	0.0576	0.0031	282.7	13.0	255.4	5.2	470.0	120.0	255	5
G3-63	24.6548	0.3404	0.0536	0.0017	265.6	6.7	255.6	3.5	315.0	69.0	256	4
G3-28	24.6975	0.2562	0.0522	0.0011	259.5	4.6	255.6	2.6	282.0	47.0	256	3
G3-9	24.5761	0.3262	0.0535	0.0016	265.9	6.7	256.4	3.4	324.0	66.0	256	3
G3-42	24.5700	0.2898	0.0532	0.0014	264.8	6.4	256.6	3.0	313.0	60.0	257	3
G3-79	24.2131	0.3928	0.0635	0.0022	309.3	9.2	256.9	4.2	678.0	77.0	257	4
G3-35	24.5339	0.3070	0.0521	0.0013	260.6	5.2	257.3	3.2	273.0	55.0	257	3
G3-72	24.5218	0.3488	0.0524	0.0020	261.9	8.5	257.3	3.7	263.0	79.0	257	4
G3-69	24.3962	0.3273	0.0522	0.0014	262.3	6.5	258.7	3.5	267.0	60.0	259	3
G3-2	24.2954	0.3365	0.0544	0.0019	272.3	8.3	259.0	3.6	351.0	75.0	259	4
G3-17	24.3605	0.3086	0.0523	0.0013	263.1	5.7	259.0	3.3	272.0	52.0	259	3
G3-15	24.3072	0.3013	0.0535	0.0019	268.5	7.9	259.2	3.2	301.0	76.0	259	3
G3-80	24.2836	0.4128	0.0532	0.0021	267.5	9.5	259.6	4.4	300.0	89.0	260	4
G3-11	24.2424	0.2527	0.0539	0.0014	270.8	6.3	259.8	2.7	338.0	56.0	260	3
G3-54	24.2718	0.5891	0.0527	0.0024	265.6	10.0	259.8	6.3	280.0	100.0	260	6
G3-38	24.2366	0.4934	0.0533	0.0025	268.4	10.0	260.0	5.3	300.0	100.0	260	5
G3-67	24.0500	0.4338	0.0592	0.0030	294.2	12.0	260.1	4.7	540.0	110.0	260	5

G3-57	24.2660	0.3003	0.0514	0.0014	260.2	5.9	260.3	3.2	239.0	59.0	260	3
G3-41	24.2131	0.3342	0.0530	0.0017	267.4	7.3	260.4	3.6	297.0	72.0	260	4
G3-60	24.1022	0.4473	0.0557	0.0019	279.6	7.8	260.7	4.8	400.0	75.0	261	5
G3-31	24.2072	0.3633	0.0520	0.0015	263.3	6.6	260.8	3.9	265.0	63.0	261	4
G3-74	24.2189	0.2640	0.0513	0.0014	260.3	6.5	260.9	2.8	237.0	60.0	261	3
G3-62	24.1429	0.2740	0.0529	0.0012	267.7	5.3	261.2	3.0	299.0	51.0	261	3
G3-6	24.1546	0.3209	0.0525	0.0015	265.9	6.2	261.2	3.5	286.0	62.0	261	3
G3-10	24.1313	0.4950	0.0529	0.0023	267.8	9.6	261.3	5.3	287.0	91.0	261	5
G3-75	24.0848	0.4061	0.0544	0.0018	274.4	7.6	261.3	4.4	344.0	70.0	261	4
G3-52	24.0096	0.3286	0.0539	0.0015	273.1	6.5	262.3	3.6	335.0	58.0	262	4
G3-53	23.9751	0.4771	0.0540	0.0021	273.9	9.6	262.6	5.2	342.0	83.0	263	5
G3-50	23.9006	0.4684	0.0550	0.0028	278.8	13.0	263.1	5.2	360.0	100.0	263	5
G3-5	23.9751	0.2702	0.0522	0.0013	266.4	5.7	263.2	3.0	273.0	54.0	263	3
G3-65	23.9177	0.4119	0.0527	0.0024	269.1	9.8	263.6	4.6	264.0	95.0	264	5
G3-25	23.8835	0.3365	0.0534	0.0018	272.3	8.2	263.8	3.7	303.0	72.0	264	4
G3-39	23.8607	0.3985	0.0541	0.0012	275.5	5.3	263.8	4.4	354.0	51.0	264	4
G3-29	23.6407	0.5142	0.0603	0.0031	303.1	13.0	264.1	5.8	570.0	110.0	264	6
G3-71	23.8493	0.4607	0.0527	0.0023	269.7	10.0	264.4	5.1	275.0	90.0	264	5
G3-36	23.8152	0.4991	0.0538	0.0016	274.7	7.1	264.4	5.5	328.0	64.0	264	5
G3-82	23.7473	0.3271	0.0555	0.0015	282.4	7.1	264.6	3.6	416.0	60.0	265	4
G3-1	23.5960	0.3619	0.0605	0.0032	304.4	14.0	264.6	4.1	510.0	110.0	265	4
G3-37	23.8152	0.4254	0.0532	0.0016	272.2	7.4	264.6	4.7	297.0	65.0	265	5
G3-49	23.7869	0.4809	0.0534	0.0022	273.3	9.5	264.8	5.3	305.0	90.0	265	5
G3-33	23.7643	0.2541	0.0532	0.0015	272.7	6.4	265.2	2.8	304.0	61.0	265	3
G3-47	23.7473	0.4230	0.0525	0.0021	269.9	9.7	265.6	4.7	271.0	85.0	266	5
G3-21	23.3100	0.4130	0.0662	0.0030	330.2	11.0	265.8	4.8	757.0	90.0	266	5

G3-32	23.7023	0.2865	0.0517	0.0014	267.0	6.0	266.3	3.2	244.0	57.0	266	3
G3-12	23.6295	0.3797	0.0530	0.0016	273.2	6.9	266.7	4.3	307.0	68.0	267	4
G3-56	23.5128	0.4920	0.0567	0.0035	289.9	15.0	266.8	5.6	410.0	130.0	267	6
G3-8	23.4852	0.3585	0.0552	0.0021	283.9	8.2	267.6	4.1	378.0	82.0	268	4
G3-23	23.5682	0.3611	0.0522	0.0017	270.5	7.9	267.7	4.1	273.0	72.0	268	4
G3-40	23.5183	0.2876	0.0529	0.0012	273.9	5.3	268.0	3.3	301.0	50.0	268	3
G3-44	23.4907	0.3973	0.0534	0.0018	276.3	8.2	268.1	4.5	296.0	71.0	268	5
G3-16	23.4797	0.5072	0.0537	0.0021	277.7	10.0	268.2	5.8	320.0	84.0	268	6
G3-24	23.5183	0.3263	0.0520	0.0016	270.1	7.4	268.3	3.7	258.0	69.0	268	4
G3-26	23.0947	0.5867	0.0647	0.0041	327.0	16.0	268.8	6.9	670.0	140.0	269	7
G3-66	23.4082	0.3890	0.0542	0.0026	280.6	11.0	268.8	4.5	316.0	98.0	269	4
G3-59	23.4028	0.2738	0.0525	0.0017	273.4	7.6	269.4	3.2	264.0	69.0	269	3
G3-7	23.3918	0.3721	0.0525	0.0019	273.6	8.6	269.6	4.3	278.0	78.0	270	4
G3-70	23.3918	0.3994	0.0523	0.0023	272.7	10.0	269.6	4.6	271.0	96.0	270	5
G3-18	23.3590	0.3274	0.0523	0.0017	273.0	7.3	270.0	3.8	268.0	71.0	270	4
G3-45	23.2883	0.4718	0.0537	0.0031	279.7	14.0	270.3	5.5	310.0	120.0	270	6
G3-30	23.3263	0.2993	0.0505	0.0014	265.6	6.8	271.0	3.5	197.0	61.0	271	3
G3-73	23.0627	0.2766	0.0529	0.0013	278.7	5.5	273.2	3.3	303.0	53.0	273	3
G3-68	22.3864	0.3859	0.0527	0.0025	285.2	11.0	281.4	4.9	265.0	97.0	281	5
G3-19	20.9644	0.4395	0.0536	0.0024	306.3	11.0	299.9	6.3	294.0	92.0	300	6
G3-27	13.6986	0.2252	0.0576	0.0015	463.7	11.0	453.3	7.4	497.0	53.0	453	7
G3-13	3.0120	0.0272	0.1132	0.0024	1850.1	18.0	1847.5	18.0	1830.0	39.0	1830	39
S1-1	50.4598	1.7602	0.0554	0.0022	141.9	7.6	125.4	4.4	427.8	44.1	125	4
S1-2	32.7791	1.0544	0.0536	0.0019	205.6	9.6	192.8	6.2	354.4	39.3	193	6
S1-3	28.9948	1.0347	0.0527	0.0011	226.4	9.0	218.0	7.7	315.3	24.0	218	8

221

S1-4	26.7868	1.1229	0.0563	0.0024	256.9	14.5	234.7	9.7	464.9	46.8	235	10
S1-5	23.9993	0.9001	0.0530	0.0020	269.6	13.2	262.7	9.7	329.9	41.3	263	10
S1-6	23.7739	0.8021	0.0543	0.0013	277.1	10.8	264.7	8.8	383.3	27.3	265	9
S1-7	23.7361	0.9975	0.0524	0.0013	269.7	12.0	265.7	11.0	304.5	27.0	266	11
S1-8	23.6774	0.8292	0.0522	0.0016	269.3	11.9	266.5	9.2	294.0	35.6	266	9
S1-9	23.5187	0.8738	0.0519	0.0017	269.6	12.3	268.3	9.9	280.1	36.1	268	10
S1-10	23.4248	0.8127	0.0531	0.0018	275.7	12.6	269.0	9.2	332.9	38.6	269	9
S1-11	23.0571	0.8297	0.0520	0.0013	274.7	11.3	273.6	9.7	283.5	28.6	274	10
S1-12	22.7842	0.7476	0.0522	0.0013	278.6	10.7	276.8	9.0	294.2	28.0	277	9
S1-13	22.7950	0.9310	0.0508	0.0022	272.6	15.1	277.1	11.2	233.6	49.6	277	11
S1-14	22.5533	0.8782	0.0542	0.0021	289.9	14.7	278.8	10.7	380.3	43.0	279	11
S1-15	22.5148	0.7933	0.0534	0.0011	286.7	10.8	279.6	9.7	345.2	22.3	280	10
S1-16	22.2382	0.8772	0.0530	0.0014	288.3	12.6	283.2	11.0	329.9	29.8	283	11
S1-17	22.2725	0.8015	0.0513	0.0014	280.3	11.8	283.3	10.1	255.3	31.1	283	10
S1-18	22.2485	0.9742	0.0512	0.0030	280.3	18.9	283.7	12.3	251.9	65.8	284	12
S1-19	22.2094	0.7353	0.0525	0.0022	286.3	14.3	283.7	9.3	307.4	47.0	284	9
S1-20	22.2029	0.7572	0.0514	0.0019	281.7	13.3	284.2	9.6	260.7	42.3	284	10
S1-21	22.1266	0.7179	0.0513	0.0012	282.0	10.5	285.2	9.1	256.0	26.4	285	9
S1-22	22.1302	0.6599	0.0510	0.0021	280.7	13.3	285.2	8.4	242.6	46.2	285	8
S1-23	22.0461	0.7160	0.0532	0.0017	291.1	12.5	285.6	9.2	335.9	36.8	286	9
S1-24	22.0541	0.9732	0.0514	0.0025	283.2	17.1	286.1	12.5	259.5	54.7	286	12
S1-25	21.9982	0.6919	0.0525	0.0011	288.8	10.3	286.4	8.9	308.0	24.0	286	9
S1-26	21.8709	0.7409	0.0521	0.0015	288.4	11.8	288.2	9.6	290.3	31.6	288	10
S1-27	21.8565	0.6576	0.0516	0.0016	286.1	11.7	288.6	8.6	265.8	35.9	289	9
S1-28	21.7888	0.6851	0.0522	0.0013	289.6	11.0	289.2	9.0	292.6	29.3	289	9
S1-29	21.7362	0.7074	0.0535	0.0022	296.4	14.6	289.4	9.3	352.0	46.3	289	9

S1-30	21.5832	0.7607	0.0528	0.0019	294.8	13.9	291.7	10.2	318.8	41.4	292	10
S1-31	21.4693	0.6696	0.0514	0.0015	289.7	11.7	293.8	9.1	256.7	34.0	294	9
S1-32	21.3097	0.7595	0.0539	0.0017	303.0	13.4	295.0	10.4	364.9	35.5	295	10
S1-33	21.1488	0.7100	0.0538	0.0016	304.8	12.8	297.2	9.9	363.3	34.2	297	10
S1-34	21.0848	0.7687	0.0527	0.0016	300.7	13.1	298.5	10.7	317.6	34.2	299	11
S1-35	20.9518	0.6689	0.0516	0.0015	297.0	12.0	300.9	9.5	266.5	33.7	301	9
S1-36	20.6013	0.7463	0.0558	0.0020	321.2	15.1	304.2	10.9	446.3	40.1	304	11
S1-37	20.4357	0.7631	0.0534	0.0017	312.3	13.8	307.6	11.3	347.0	34.6	308	11
S1-38	20.4145	0.5726	0.0515	0.0014	303.3	11.0	308.7	8.5	261.9	30.0	309	9
S1-39	19.8245	0.8567	0.0526	0.0012	316.8	14.0	317.3	13.5	313.7	26.0	317	14
S1-40	19.6911	0.7234	0.0534	0.0019	322.2	14.8	319.1	11.6	344.4	38.8	319	12
S1-41	16.8830	0.6420	0.0535	0.0023	368.1	18.7	371.2	13.9	348.5	47.5	371	14
S2-1	25.3705	1.2499	0.0518	0.0012	251.7	12.6	249.0	12.1	276.4	25.7	249	12
S2-2	23.7956	0.9469	0.0519	0.0014	267.0	11.8	265.2	10.4	282.8	29.6	265	10
S2-3	23.7268	0.7155	0.0528	0.0010	271.5	9.1	265.7	7.9	322.0	20.8	266	8
S2-4	23.5068	0.6591	0.0521	0.0011	270.5	9.1	268.4	7.4	289.1	24.0	268	7
S2-5	23.4885	0.7694	0.0518	0.0011	269.5	9.8	268.7	8.7	276.2	23.3	269	9
S2-6	23.2732	0.7158	0.0530	0.0011	277.0	9.7	270.7	8.2	330.5	22.8	271	8
S2-7	23.2322	0.6996	0.0529	0.0019	277.0	12.4	271.2	8.1	325.4	40.7	271	8
S2-8	23.1966	0.7220	0.0529	0.0015	277.2	10.9	271.7	8.4	323.7	30.9	272	8
S2-9	23.1725	0.7013	0.0519	0.0014	273.3	10.4	272.3	8.1	282.0	29.9	272	8
S2-10	23.0752	0.7082	0.0526	0.0012	277.1	10.1	273.2	8.3	310.5	26.1	273	8
S2-11	23.0599	0.6794	0.0522	0.0011	275.8	9.6	273.5	8.0	295.9	24.2	273	8
S2-12	22.8821	0.7631	0.0528	0.0014	280.1	11.3	275.4	9.1	319.1	30.3	275	9
S2-13	22.8736	0.6930	0.0521	0.0013	277.0	10.5	275.7	8.3	288.1	29.2	276	8

S2-14	22.7929	0.7584	0.0524	0.0014	279.2	11.2	276.6	9.1	300.8	30.4	277	9
S2-15	22.6346	0.6854	0.0524	0.0011	281.0	9.9	278.5	8.3	301.7	24.4	279	8
S2-16	22.5537	0.7131	0.0521	0.0014	280.8	10.9	279.6	8.7	290.5	29.5	280	9
S2-17	22.5420	0.7926	0.0522	0.0011	281.5	10.9	279.7	9.7	296.3	24.9	280	10
S2-18	22.4908	0.7164	0.0523	0.0017	282.3	12.0	280.3	8.8	298.9	36.4	280	9
S2-19	22.4654	0.8343	0.0525	0.0013	283.2	11.6	280.5	10.3	305.2	27.2	281	10
S2-20	22.4792	0.6772	0.0519	0.0012	280.5	10.1	280.6	8.3	280.1	26.2	281	8
S2-21	22.4213	0.6660	0.0520	0.0014	281.6	10.6	281.3	8.3	284.1	30.0	281	8
S2-22	22.3812	0.6833	0.0524	0.0012	284.0	10.2	281.6	8.5	303.6	25.9	282	8
S2-23	22.2689	0.8802	0.0536	0.0015	290.3	13.0	282.6	11.0	352.4	31.7	283	11
S2-24	22.3154	0.7067	0.0517	0.0016	281.6	11.8	282.7	8.8	273.2	35.1	283	9
S2-25	22.2123	0.8988	0.0530	0.0015	288.6	13.0	283.5	11.3	330.0	30.8	283	11
S2-26	22.1457	0.6644	0.0532	0.0014	290.1	10.9	284.3	8.4	337.7	29.1	284	8
S2-27	22.0106	0.6517	0.0505	0.0012	279.8	10.1	287.0	8.4	220.0	27.6	287	8
S2-28	21.9099	0.6059	0.0535	0.0012	294.4	10.1	287.2	7.8	352.1	26.0	287	8
S2-29	21.9237	0.7185	0.0524	0.0011	289.3	10.6	287.4	9.3	304.8	24.5	287	9
S2-30	21.8999	0.7221	0.0526	0.0013	290.3	11.1	287.6	9.4	312.0	27.5	288	9
S2-31	21.8974	0.6517	0.0518	0.0016	286.9	11.6	287.9	8.5	278.0	34.7	288	8
S2-32	21.7665	0.6205	0.0526	0.0012	292.0	10.2	289.4	8.1	313.2	26.2	289	8
S2-33	21.5752	0.6895	0.0531	0.0015	296.4	11.8	291.7	9.2	333.0	31.4	292	9
S2-34	21.5179	0.6794	0.0526	0.0016	294.9	12.0	292.7	9.1	313.1	33.9	293	9
WA-1	25.5624	0.4378	0.0563	0.0013	267.7	5.5	245.8	4.2	443.0	51.0	246	4
WA-2	24.6792	0.5055	0.0528	0.0009	262.2	5.3	255.6	5.2	313.0	40.0	256	5
WA-3	24.6670	0.4381	0.0529	0.0017	262.6	7.7	255.7	4.5	306.0	70.0	256	5
WA-4	24.5882	0.4111	0.0529	0.0013	263.4	5.7	256.5	4.3	304.0	54.0	256	4

WA-5	24.3784	0.3863	0.0527	0.0008	264.3	4.2	258.7	4.1	301.0	34.0	259	4
WA-6	24.1313	0.5532	0.0555	0.0020	278.5	9.8	260.4	5.9	384.0	79.0	260	6
WA-7	23.0947	0.5334	0.0523	0.0010	275.0	6.7	273.4	6.2	283.0	41.0	273	6
WA-8	23.0521	0.2444	0.0527	0.0008	277.9	3.5	273.4	2.9	303.0	34.0	273	3
WA-9	23.0150	0.3337	0.0534	0.0014	281.4	5.7	273.6	3.9	319.0	56.0	274	4
WA-10	22.9568	0.2740	0.0524	0.0006	277.7	3.4	274.6	3.2	294.0	26.0	275	3
WA-11	22.9305	0.3470	0.0523	0.0008	277.7	3.4	275.0	4.1	289.0	36.0	275	4
WA-12	22.8938	0.2935	0.0522	0.0007	277.5	3.9	275.5	3.5	282.0	31.0	275	3
WA-13	22.8624	0.2352	0.0527	0.0009	280.0	3.8	275.7	2.8	309.0	39.0	276	3
WA-14	22.8676	0.3347	0.0523	0.0007	278.4	4.1	275.7	4.0	289.0	31.0	276	4
WA-15	22.7428	0.3103	0.0524	0.0008	280.1	4.3	277.2	3.7	291.0	35.0	277	4
WA-16	22.7635	0.4715	0.0517	0.0010	276.7	5.1	277.2	5.7	264.0	42.0	277	6
WA-17	22.6706	0.2467	0.0534	0.0011	285.1	4.8	277.7	3.0	325.0	45.0	278	3
WA-18	22.6809	0.3601	0.0516	0.0007	277.2	4.0	278.2	4.4	263.0	32.0	278	4
WA-19	22.6809	0.3807	0.0514	0.0010	276.3	5.2	278.3	4.6	249.0	44.0	278	5
WA-20	22.6091	0.2454	0.0523	0.0009	281.0	4.1	278.8	3.0	287.0	39.0	279	3
WA-21	22.5887	0.2500	0.0521	0.0010	280.4	4.7	279.2	3.1	274.0	45.0	279	3
WA-22	22.5276	0.3349	0.0523	0.0019	281.9	8.7	279.8	4.2	258.0	76.0	280	4
WA-23	22.4921	0.1922	0.0524	0.0008	282.6	3.4	280.2	2.4	292.0	34.0	280	2
WA-24	22.4770	0.3536	0.0524	0.0013	282.9	6.3	280.4	4.4	284.0	54.0	280	4
WA-25	22.4517	0.2873	0.0528	0.0010	284.3	4.9	280.9	3.5	301.0	41.0	281	4
WA-26	22.3964	0.3060	0.0533	0.0011	287.9	5.5	281.6	3.7	322.0	47.0	282	4
WA-27	22.3364	0.2046	0.0522	0.0007	283.7	3.0	282.2	2.6	285.0	29.0	282	3
WA-28	22.2717	0.3323	0.0531	0.0008	288.7	4.1	283.1	4.2	323.0	33.0	283	4
WA-29	22.2173	0.3208	0.0529	0.0008	288.7	4.1	283.8	4.0	308.0	35.0	284	4
WA-30	22.0751	0.2242	0.0521	0.0009	286.6	4.6	285.6	2.8	274.0	41.0	286	3

WA-31	21.9829	0.2561	0.0529	0.0008	290.5	3.3	286.5	3.3	311.0	33.0	286	3
WA-32	21.9202	0.2643	0.0526	0.0009	290.2	4.3	287.4	3.4	297.0	36.0	287	3
WA-33	21.8771	0.2632	0.0528	0.0008	291.7	3.7	287.8	3.4	314.0	34.0	288	3
WA-34	21.8675	0.2630	0.0527	0.0009	291.0	4.6	288.2	3.4	301.0	37.0	288	3
WA-35	21.8150	0.3093	0.0522	0.0009	289.6	4.5	288.9	4.1	282.0	40.0	289	4
WA-36	21.8150	0.2379	0.0524	0.0007	290.2	3.7	288.9	3.1	291.0	30.0	289	3
WA-37	21.7675	0.3459	0.0531	0.0009	294.0	3.6	289.2	4.5	321.0	38.0	289	5
WA-38	21.7061	0.2403	0.0525	0.0009	292.1	4.0	290.2	3.2	295.0	37.0	290	3
WA-39	21.6591	0.3049	0.0523	0.0009	290.5	4.3	290.9	4.0	284.0	37.0	291	4
WA-40	21.6591	0.2721	0.0521	0.0008	289.7	3.9	290.9	3.6	281.0	34.0	291	4
WA-41	21.5610	0.3301	0.0528	0.0009	294.6	4.6	292.2	4.4	305.0	38.0	292	4
WA-42	21.3220	0.6365	0.0526	0.0019	297.2	10.0	295.3	8.7	297.0	80.0	295	9
WA-43	21.3174	0.4044	0.0523	0.0009	296.2	5.7	295.5	5.5	292.0	39.0	296	6
WA-44	21.3083	0.2270	0.0527	0.0008	298.3	4.2	295.6	3.1	304.0	36.0	296	3
WA-45	21.3129	0.2362	0.0527	0.0010	295.7	4.8	295.6	3.2	294.0	42.0	296	3
WA-46	21.2314	0.4508	0.0530	0.0009	297.4	5.1	296.7	6.1	316.0	39.0	297	6
WA-47	21.0926	0.2625	0.0530	0.0008	300.2	4.8	298.6	3.6	318.0	34.0	299	4
WA-48	20.6228	0.2722	0.0525	0.0006	305.3	3.7	305.2	3.9	298.0	26.0	305	4
WA-49	19.8059	0.3609	0.0528	0.0009	315.3	5.7	317.4	5.6	305.0	40.0	317	6
WA-50	17.9212	0.2184	0.0851	0.0014	494.9	6.9	336.0	4.1	1308.0	33.0	336	4
WA-51	12.6904	0.2899	0.0708	0.0016	571.4	12.0	480.4	10.8	926.0	45.0	480	11
WA-52	12.0279	0.1273	0.0599	0.0010	529.5	6.8	513.4	5.3	587.0	35.0	513	5
WA-53	11.6713	0.1280	0.0581	0.0008	530.4	5.4	529.9	5.7	519.0	30.0	530	6
WA-54	11.2360	0.2399	0.0595	0.0012	556.2	11.0	548.9	11.5	561.0	45.0	549	11
WA-55	11.1857	0.1376	0.0589	0.0009	554.0	6.4	551.8	6.7	554.0	33.0	552	7
WA-56	11.0497	0.1709	0.0598	0.0013	565.6	10.0	557.8	8.5	577.0	47.0	558	8

WA-57	10.0402	0.1109	0.0612	0.0011	619.0	7.6	611.3	6.6	632.0	40.0	611	7
WA-58	6.3980	0.1146	0.0806	0.0017	1013.5	15.0	923.9	16.2	1202.0	40.0	924	16
WA-59	5.9988	0.0864	0.0735	0.0016	1003.8	15.0	992.4	14.0	1019.0	45.0	992	14
WA-60	5.7937	0.0873	0.0778	0.0017	1060.3	14.0	1020.7	15.1	1125.0	43.0	1021	15
WA-61	5.3079	0.0789	0.0755	0.0017	1103.8	17.0	1114.4	16.2	1053.0	47.0	1114	16
WA-62	3.1270	0.0792	0.1290	0.0036	1903.2	33.0	1740.1	44.9	2077.0	53.0	2077	53
WA-63	3.8314	0.1204	0.1663	0.0047	1876.7	37.0	1350.5	42.4	2513.0	49.0	2513	49
WB1-1	42.7533	1.2429	0.0553	0.0010	165.4	4.7	147.9	4.3	409.0	42.0	148	4
WB1-2	33.6022	1.1065	0.0633	0.0015	230.9	9.3	185.8	6.1	694.0	50.0	186	6
WB1-3	29.4811	0.7475	0.0592	0.0013	245.7	4.5	212.6	5.3	552.0	47.0	213	5
WB1-4	26.5887	0.5373	0.0602	0.0019	273.0	8.1	235.2	4.7	582.0	69.0	235	5
WB1-5	26.1029	0.4088	0.0635	0.0009	289.6	4.6	238.5	3.7	715.0	29.0	239	4
WB1-6	25.3872	0.5672	0.0580	0.0017	276.0	7.6	246.9	5.5	511.0	65.0	247	5
WB1-7	24.9004	0.5704	0.0556	0.0013	271.3	6.5	252.4	5.7	420.0	52.0	252	6
WB1-8	22.7790	0.5708	0.0706	0.0024	354.0	12.0	270.4	6.7	932.0	69.0	270	7
WB1-9	22.9358	0.5787	0.0560	0.0025	293.3	12.0	273.6	6.9	402.0	96.0	274	7
WB1-10	22.5175	0.2130	0.0532	0.0008	285.8	4.1	279.7	2.6	329.0	35.0	280	3
WB1-11	22.3764	0.2353	0.0528	0.0012	285.8	5.3	281.5	3.0	302.0	49.0	282	3
WB1-12	21.9877	0.2562	0.0526	0.0010	290.1	4.9	286.7	3.2	297.0	41.0	287	3
WB1-13	20.6016	0.4032	0.0611	0.0011	344.9	5.9	302.2	5.8	640.0	43.0	302	6
WB1-14	20.6612	0.4269	0.0577	0.0022	328.9	11.0	302.7	6.2	474.0	84.0	303	6
WB1-15	20.4082	0.4581	0.0575	0.0012	331.5	7.7	306.4	6.8	501.0	44.0	306	7
WB1-16	20.4499	0.9200	0.0555	0.0022	321.8	12.0	306.6	13.6	414.0	93.0	307	14
WB1-17	20.1613	0.4065	0.0563	0.0013	329.5	8.5	310.6	6.2	447.0	53.0	311	6
WB1-18	20.0401	0.4819	0.0549	0.0011	324.6	7.6	313.0	7.4	392.0	44.0	313	7

WB1-19	19.4553	0.3331	0.0549	0.0011	333.4	7.5	323.0	5.4	396.0	44.0	323	5
WB1-20	18.5908	0.2039	0.0540	0.0010	341.7	5.9	337.4	3.7	356.0	42.0	337	4
WB1-21	18.0278	0.2373	0.0545	0.0013	353.5	6.3	347.6	4.5	383.0	53.0	348	5
WB1-22	18.0083	0.3146	0.0553	0.0014	357.8	7.9	347.6	6.0	410.0	57.0	348	6
WB1-23	17.8699	0.2140	0.0575	0.0013	371.3	7.9	349.2	4.2	486.0	50.0	349	4
WB1-24	17.7525	0.2395	0.0544	0.0012	357.6	6.6	352.9	4.7	370.0	48.0	353	5
WB1-25	17.7336	0.2422	0.0551	0.0012	361.5	5.8	353.0	4.8	395.0	46.0	353	5
WB1-26	17.4004	0.1635	0.0550	0.0009	366.7	5.0	359.7	3.3	394.0	37.0	360	3
WB1-27	17.3671	0.1629	0.0562	0.0010	373.6	5.4	359.8	3.3	443.0	38.0	360	3
WB1-28	17.3581	0.2682	0.0552	0.0012	368.7	7.3	360.4	5.5	409.0	51.0	360	6
WB1-29	16.6667	0.3611	0.0790	0.0030	497.7	15.0	363.8	7.9	1134.0	75.0	364	8
WB1-30	16.7785	0.3941	0.0599	0.0017	404.0	8.7	370.4	8.6	580.0	60.0	370	9
WB1-31	16.8748	0.2449	0.0548	0.0011	374.2	6.9	371.0	5.2	385.0	43.0	371	5
WB1-32	16.8379	0.1956	0.0559	0.0015	382.0	7.9	371.0	4.3	416.0	58.0	371	4
WB1-33	16.8634	0.2844	0.0549	0.0011	373.9	6.2	371.2	6.2	385.0	43.0	371	6
WB1-34	16.8294	0.2011	0.0559	0.0012	382.2	7.5	371.2	4.4	424.0	46.0	371	4
WB1-35	16.8294	0.2351	0.0548	0.0011	376.3	5.8	371.7	5.1	387.0	43.0	372	5
WB1-36	16.7504	0.3367	0.0561	0.0012	384.7	8.2	372.8	7.4	437.0	46.0	373	7
WB1-37	16.6667	0.1944	0.0552	0.0010	381.6	6.0	375.1	4.3	404.0	42.0	375	4
WB1-38	16.5508	0.2274	0.0571	0.0012	394.0	7.8	376.8	5.1	481.0	49.0	377	5
WB1-39	16.5563	0.1754	0.0557	0.0010	386.4	5.3	377.3	4.0	436.0	42.0	377	4
WB1-40	16.3399	0.3204	0.0643	0.0009	435.4	7.3	378.1	7.3	743.0	30.0	378	7
WB1-41	15.8228	0.3004	0.0730	0.0016	490.5	6.8	385.9	7.2	991.0	44.0	386	7
WB1-42	15.9744	0.3573	0.0635	0.0010	439.6	8.8	387.0	8.5	713.0	35.0	387	9
WB1-43	15.5280	0.2893	0.0625	0.0009	444.8	8.0	398.4	7.3	696.0	31.0	398	7
WB1-44	15.5691	0.2400	0.0552	0.0012	402.3	7.6	401.2	6.0	404.0	49.0	401	6

WB1-45	15.0150	0.4284	0.0695	0.0017	493.9	15.0	408.1	11.5	876.0	52.0	408	11
WB1-46	14.4509	0.2715	0.0615	0.0016	466.0	11.0	428.0	7.9	624.0	59.0	428	8
WB1-47	14.2450	0.2232	0.0678	0.0017	506.0	9.6	430.6	6.7	850.0	51.0	431	7
WB1-48	14.0647	0.2769	0.0617	0.0012	477.5	9.2	439.5	8.5	657.0	40.0	439	9
WB1-49	13.7741	0.2846	0.0585	0.0014	466.9	9.8	450.4	9.2	524.0	55.0	450	9
WB1-50	13.6743	0.1645	0.0567	0.0013	458.9	8.0	454.6	5.4	453.0	49.0	455	5
WB1-51	13.4048	0.1725	0.0698	0.0018	542.1	11.0	455.9	5.8	890.0	57.0	456	6
WB1-52	13.0839	0.1524	0.0586	0.0013	487.4	8.7	473.6	5.5	527.0	50.0	474	5
WB1-53	12.0627	0.1746	0.0684	0.0012	580.3	11.0	506.4	7.2	868.0	37.0	506	7
WB1-54	12.1507	0.1476	0.0587	0.0012	517.8	8.7	509.0	6.1	533.0	45.0	509	6
WB1-55	11.8203	0.2096	0.0614	0.0019	546.6	13.0	521.2	9.1	632.0	67.0	521	9
WB1-56	11.7509	0.4281	0.0617	0.0014	547.0	18.0	525.0	19.0	636.0	50.0	525	19
WB1-57	10.6610	0.1478	0.0616	0.0014	593.7	9.9	576.3	7.9	630.0	51.0	576	8
WB1-58	10.5042	0.1434	0.0621	0.0015	603.9	11.0	584.3	7.9	645.0	51.0	584	8
WB1-59	10.5263	0.1440	0.0604	0.0012	591.4	8.9	584.4	7.8	600.0	42.0	584	8
WB1-60	10.4932	0.1101	0.0611	0.0011	597.7	8.4	585.6	6.0	625.0	38.0	586	6
WB1-61	10.2354	0.1362	0.0610	0.0011	606.1	8.4	600.6	7.9	623.0	38.0	601	8
WB1-62	9.6061	0.1569	0.0653	0.0013	668.8	10.0	634.9	10.2	773.0	42.0	635	10
WB1-63	9.6061	0.1384	0.0670	0.0014	683.0	12.0	639.2	8.9	810.0	44.0	639	9
WB1-64	8.8339	0.3356	0.0801	0.0024	810.4	28.0	675.9	25.1	1175.0	60.0	676	25
WB1-65	9.0171	0.1382	0.0642	0.0013	693.3	11.0	676.2	10.1	739.0	44.0	676	10
WB1-66	9.0009	0.2430	0.0604	0.0034	666.4	29.0	680.6	18.1	550.0	120.0	681	18
WB1-67	8.3822	0.1546	0.0906	0.0022	904.5	16.0	701.6	12.7	1415.0	47.0	702	13
WB1-68	8.2102	0.0944	0.0670	0.0015	763.5	12.0	738.1	8.4	810.0	48.0	738	8
WB1-69	7.4129	0.1319	0.0733	0.0015	868.0	13.0	808.5	14.0	1012.0	40.0	809	14
WB1-70	7.2359	0.0733	0.0723	0.0016	875.4	12.0	828.8	8.3	976.0	44.0	829	8

WB1-71	6.9109	0.1528	0.0777	0.0021	942.8	18.0	860.5	18.6	1114.0	53.0	861	19
WB1-72	6.7522	0.0957	0.0721	0.0013	916.6	11.0	886.5	12.3	974.0	36.0	886	12
WB1-73	6.5232	0.0723	0.0748	0.0013	958.7	11.0	913.5	9.9	1049.0	35.0	913	10
WB1-74	6.4020	0.0943	0.0728	0.0015	955.7	13.0	932.6	13.4	999.0	42.0	933	13
WB1-75	6.3654	0.1540	0.0742	0.0016	970.1	20.0	936.1	22.0	1036.0	44.0	936	22
WB1-76	6.3573	0.1374	0.0744	0.0017	972.4	17.0	937.0	19.7	1052.0	46.0	937	20
WB1-77	6.3654	0.0770	0.0728	0.0010	959.4	9.1	937.8	11.1	1005.0	27.0	938	11
WB1-78	6.1350	0.1618	0.0970	0.0019	1150.5	20.0	941.8	24.2	1555.0	37.0	942	24
WB1-79	6.2344	0.0738	0.0729	0.0011	973.7	10.0	956.7	11.1	998.0	30.0	957	11
WB1-80	6.1996	0.0922	0.0734	0.0017	981.2	13.0	961.3	14.0	1012.0	46.0	961	14
WB1-81	6.0496	0.0659	0.0739	0.0014	1001.3	13.0	983.8	10.5	1021.0	40.0	984	11
WB1-82	5.8754	0.0587	0.0753	0.0013	1031.7	12.0	1010.2	9.9	1064.0	36.0	1010	10
WB1-83	5.4526	0.0832	0.0757	0.0020	1086.4	16.0	1085.4	16.3	1066.0	53.0	1085	16
WB1-84	5.2798	0.0781	0.0793	0.0019	1137.3	16.0	1114.7	16.2	1153.0	50.0	1115	16
WB1-85	5.1467	0.0477	0.0793	0.0009	1156.1	8.2	1142.5	10.3	1173.0	23.0	1143	10
WB1-86	5.1414	0.0634	0.0800	0.0016	1162.0	12.0	1142.7	13.9	1183.0	39.0	1143	14
WB1-87	4.2790	0.0421	0.0876	0.0013	1361.1	11.0	1352.3	13.2	1365.0	29.0	1365	29
WB1-88	4.1288	0.1688	0.1036	0.0015	1501.4	34.0	1370.8	54.7	1680.0	26.0	1680	26
WB1-89	3.2873	0.0497	0.1085	0.0021	1736.3	17.0	1703.6	26.1	1767.0	36.0	1767	36
WB1-90	5.3163	0.1413	0.1120	0.0022	1345.7	22.0	1060.6	27.5	1822.0	37.0	1822	37
WB1-91	3.1230	0.0419	0.1141	0.0018	1820.1	13.0	1779.2	24.4	1857.0	29.0	1857	29
WB1-92	8.0192	0.1994	0.1538	0.0034	1221.5	27.0	671.7	16.6	2376.0	39.0	2376	39
WB1-93	3.4819	0.0740	0.1534	0.0027	1914.8	27.0	1510.9	32.1	2379.0	30.0	2379	30
WB1-94	5.0736	0.1313	0.1623	0.0039	1613.3	30.0	1034.5	26.6	2469.0	40.0	2469	40
WB1-95	2.3425	0.0307	0.1673	0.0024	2382.9	16.0	2211.8	32.5	2528.0	24.0	2528	24
WB1-96	2.1959	0.0338	0.2207	0.0034	2617.7	18.0	2166.7	38.1	2984.0	26.0	2984	26

WB1-97	6.5189	0.1317	0.2239	0.0096	1582.5	33.0	738.8	18.6	2985.0	67.0	2985	67
WB2-1	21.3122	0.6176	0.0523	0.0014	296.0	10.8	295.6	8.5	299.0	29.9	296	8
WB2-2	20.0242	0.5931	0.0536	0.0010	318.6	10.3	313.8	9.2	354.1	20.2	314	9
WB2-3	20.0094	0.7253	0.0532	0.0012	316.9	12.5	314.2	11.2	336.9	26.3	314	11
WB2-4	19.7403	0.5231	0.0533	0.0014	321.2	11.1	318.3	8.3	342.2	28.8	318	8
WB2-5	19.6541	0.8203	0.0533	0.0014	322.4	14.3	319.7	13.2	341.4	29.3	320	13
WB2-6	19.4009	0.6468	0.0542	0.0015	330.3	13.2	323.5	10.6	378.3	31.3	323	11
WB2-7	19.3178	0.6278	0.0543	0.0015	331.9	12.9	324.8	10.4	381.8	30.5	325	10
WB2-8	19.1103	0.6914	0.0527	0.0017	327.4	14.6	328.9	11.7	316.7	37.3	329	12
WB2-9	19.0777	0.6111	0.0532	0.0017	330.1	13.7	329.3	10.4	335.6	36.0	329	10
WB2-10	18.9551	0.7123	0.0542	0.0015	337.0	14.3	330.9	12.3	379.0	31.2	331	12
WB2-11	18.9612	0.5671	0.0532	0.0012	331.8	11.3	331.3	9.8	335.5	24.6	331	10
WB2-12	18.8910	0.5875	0.0533	0.0019	333.7	14.3	332.4	10.2	343.0	38.9	332	10
WB2-13	18.8692	0.5569	0.0534	0.0016	334.6	13.0	332.7	9.7	347.6	33.9	333	10
WB2-14	18.6350	0.4734	0.0545	0.0009	343.3	9.7	336.4	8.4	390.2	19.1	336	8
WB2-15	18.6295	0.6258	0.0544	0.0019	343.2	15.1	336.5	11.2	388.5	38.8	337	11
WB2-16	18.6935	0.6366	0.0508	0.0015	323.8	13.3	337.0	11.3	230.2	33.4	337	11
WB2-17	18.6303	0.6098	0.0531	0.0018	336.3	14.4	337.1	10.9	330.9	37.7	337	11
WB2-18	18.4345	0.6293	0.0550	0.0018	349.2	14.9	339.8	11.4	412.6	35.9	340	11
WB2-19	18.1187	0.5719	0.0531	0.0020	344.7	15.6	346.5	10.8	333.2	43.0	346	11
WB2-20	18.0823	0.5778	0.0546	0.0019	353.0	15.3	346.5	10.9	395.9	39.5	346	11
WB2-21	18.0399	0.5843	0.0552	0.0016	356.8	13.9	347.0	11.1	420.6	32.0	347	11
WB2-22	18.0320	0.5662	0.0547	0.0015	354.2	13.3	347.4	10.7	399.2	29.8	347	11
WB2-23	17.8914	0.4738	0.0548	0.0010	357.4	10.6	350.0	9.1	405.7	21.2	350	9
WB2-24	17.7088	0.5881	0.0543	0.0014	357.9	13.6	353.8	11.6	384.3	28.8	354	12

WB2-25	17.5938	0.4481	0.0546	0.0013	361.1	11.3	356.0	8.9	394.0	25.6	356	9
WB2-26	17.4571	0.6791	0.0554	0.0012	367.8	14.3	358.3	13.7	427.7	23.2	358	14
WB2-27	17.1088	0.5090	0.0548	0.0011	371.3	11.8	365.7	10.7	405.9	21.3	366	11
WB2-28	16.9897	0.6007	0.0543	0.0011	370.4	13.3	368.5	12.8	382.0	22.2	369	13
WB2-29	16.9253	0.5357	0.0546	0.0011	373.6	12.5	369.7	11.5	397.4	22.4	370	12
WB2-30	16.7360	0.5080	0.0547	0.0015	377.5	13.6	373.8	11.2	400.0	29.8	374	11
WB2-31	16.5709	0.4845	0.0546	0.0018	380.0	15.0	377.5	10.9	395.3	37.0	378	11
WB2-32	16.4804	0.5348	0.0547	0.0012	382.7	13.3	379.5	12.1	402.0	24.6	379	12
WB2-33	16.2677	0.5440	0.0551	0.0016	389.1	15.5	384.2	12.6	418.3	32.9	384	13
WB2-34	16.1273	0.4654	0.0556	0.0013	394.5	13.0	387.2	11.0	437.1	25.7	387	11
WB2-35	16.1196	0.5345	0.0550	0.0016	391.0	15.0	387.7	12.6	410.7	31.4	388	13
WB2-36	16.0406	0.5282	0.0549	0.0017	392.2	15.6	389.6	12.6	407.0	33.7	390	13
WB2-37	16.0527	0.5340	0.0542	0.0013	388.2	13.9	389.7	12.7	379.7	26.3	390	13
WB2-38	15.9694	0.4533	0.0548	0.0011	393.2	12.2	391.4	10.9	404.2	22.6	391	11
WB2-39	15.7156	0.5279	0.0552	0.0015	401.0	15.2	397.4	13.1	422.2	30.6	397	13
WB2-40	15.5287	0.5995	0.0554	0.0014	406.2	16.2	402.0	15.2	430.1	28.1	402	15
WB2-41	13.6617	0.4011	0.0570	0.0009	460.8	13.3	454.9	13.1	490.2	17.8	455	13
WB2-42	9.8994	0.3095	0.0624	0.0011	633.9	18.4	618.8	18.9	688.1	19.5	619	19
WB2-43	6.9048	0.2837	0.0672	0.0022	864.8	31.6	872.9	34.8	844.0	33.1	844	33
WB2-44	5.9677	0.2112	0.0714	0.0011	990.1	25.8	1000.1	34.3	968.1	16.3	968	16
WB2-45	5.8452	0.2103	0.0727	0.0013	1014.7	26.9	1018.6	35.5	1006.1	17.6	1006	18
WB2-46	5.7776	0.1722	0.0728	0.0016	1023.3	25.9	1030.0	29.8	1009.0	22.6	1009	23
WB2-47	6.4179	0.2025	0.0731	0.0014	955.9	24.7	930.0	28.5	1016.1	19.6	1016	20
WB2-48	7.0801	0.3355	0.0733	0.0024	896.1	35.4	845.3	38.9	1023.6	32.4	1024	32
WB2-49	5.6290	0.1757	0.0741	0.0014	1051.5	25.2	1054.6	31.9	1045.0	18.5	1045	18
WB2-50	4.8041	0.1314	0.0799	0.0014	1210.8	24.7	1220.6	32.5	1193.4	17.2	1193	17

WB2-51	4.6579	0.1383	0.0822	0.0022	1252.8	30.5	1253.9	36.3	1250.8	25.8	1251	26
WB2-52	4.4391	0.1196	0.0823	0.0020	1290.8	28.1	1313.8	34.6	1252.6	23.1	1253	23
WB2-53	5.2442	0.1754	0.0870	0.0017	1198.6	29.0	1110.9	36.1	1360.3	18.4	1360	18
WB2-54	3.9261	0.1244	0.0888	0.0015	1440.7	29.4	1468.4	45.6	1400.1	15.8	1400	16
WB2-55	2.9256	0.0740	0.1131	0.0016	1877.7	27.1	1903.2	49.2	1849.5	13.1	1850	13
WB2-56	2.6658	0.0697	0.1214	0.0018	2023.4	28.3	2069.9	56.8	1976.3	12.9	1976	13
WB4-1	34.9528	0.9407	0.0616	0.0013	217.9	6.2	179.1	4.8	639.0	43.0	179	5
WB4-2	35.0140	1.0298	0.0567	0.0018	203.0	6.9	179.9	5.3	462.0	72.0	180	5
WB4-3	22.7324	0.2791	0.0524	0.0010	280.1	4.5	277.3	3.4	292.0	43.0	277	3
WB4-4	22.6655	0.2723	0.0524	0.0009	280.8	4.7	278.1	3.3	300.0	40.0	278	3
WB4-5	22.2124	0.2516	0.0521	0.0011	284.5	5.2	283.8	3.2	269.0	47.0	284	3
WB4-6	21.2811	0.3351	0.0555	0.0012	310.8	5.3	294.8	4.6	421.0	48.0	295	5
WB4-7	19.5695	0.2872	0.0574	0.0011	343.2	6.1	319.4	4.6	480.0	42.0	319	5
WB4-8	18.8501	0.3233	0.0750	0.0030	433.9	15.0	324.0	5.6	1033.0	79.0	324	6
WB4-9	19.1571	0.3670	0.0542	0.0009	334.2	6.1	327.5	6.2	371.0	39.0	328	6
WB4-10	19.0949	0.2042	0.0533	0.0008	330.6	4.1	328.9	3.5	331.0	36.0	329	3
WB4-11	18.9036	0.4288	0.0548	0.0016	340.9	9.2	331.6	7.4	381.0	67.0	332	7
WB4-12	18.5151	0.2400	0.0548	0.0010	347.0	6.0	338.4	4.3	389.0	41.0	338	4
WB4-13	17.7211	0.2512	0.0559	0.0010	365.8	5.0	352.8	4.9	432.0	40.0	353	5
WB4-14	17.6460	0.2429	0.0547	0.0009	360.7	5.7	354.9	4.8	379.0	39.0	355	5
WB4-15	17.6243	0.2299	0.0546	0.0009	360.9	5.6	355.3	4.6	384.0	37.0	355	5
WB4-16	17.5593	0.2713	0.0560	0.0015	369.2	8.0	356.0	5.5	412.0	61.0	356	5
WB4-17	17.4825	0.3973	0.0541	0.0013	360.7	8.3	358.4	8.0	352.0	55.0	358	8
WB4-18	17.4338	0.1945	0.0550	0.0011	366.3	6.1	359.0	4.0	390.0	44.0	359	4
WB4-19	17.4186	0.2397	0.0554	0.0011	368.6	6.0	359.1	4.9	417.0	44.0	359	5

WB4-20	17.4186	0.2700	0.0548	0.0009	365.7	6.7	359.4	5.5	391.0	37.0	359	5
WB4-21	17.3641	0.2774	0.0553	0.0012	369.1	6.6	360.2	5.7	401.0	50.0	360	6
WB4-22	16.7029	0.2232	0.0555	0.0011	382.5	6.7	374.2	4.9	411.0	45.0	374	5
WB4-23	16.7112	0.1731	0.0547	0.0009	378.1	4.9	374.4	3.8	386.0	36.0	374	4
WB4-24	16.6362	0.1799	0.0547	0.0010	379.3	5.8	376.0	4.0	385.0	38.0	376	4
WB4-25	16.5810	0.2667	0.0559	0.0014	387.0	7.6	376.7	6.0	430.0	52.0	377	6
WB4-26	16.5755	0.1648	0.0551	0.0008	382.7	4.6	377.2	3.7	403.0	31.0	377	4
WB4-27	16.5563	0.3015	0.0548	0.0010	381.6	7.2	377.8	6.8	386.0	42.0	378	7
WB4-28	16.3399	0.1869	0.0550	0.0010	386.9	6.2	382.6	4.3	393.0	42.0	383	4
WB4-29	14.3761	0.1922	0.0628	0.0017	475.2	9.7	429.5	5.7	674.0	60.0	430	6
WB4-30	13.9860	0.3521	0.0581	0.0039	458.8	23.0	443.9	11.2	480.0	140.0	444	11
WB4-31	13.7893	0.1616	0.0567	0.0014	455.8	9.0	450.9	5.2	456.0	57.0	451	5
WB4-32	13.6426	0.2047	0.0590	0.0012	473.6	7.7	454.3	6.7	557.0	43.0	454	7
WB4-33	13.5685	0.1841	0.0589	0.0011	475.1	7.3	456.8	6.1	544.0	40.0	457	6
WB4-34	13.6054	0.1777	0.0566	0.0013	460.2	8.7	456.9	5.9	444.0	51.0	457	6
WB4-35	12.2234	0.1404	0.0579	0.0012	510.3	8.1	506.597	5.7	497.0	46.0	507	6
WB4-36	11.6822	0.1638	0.0597	0.0011	540.7	7.7	528.3	7.3	576.0	38.0	528	7
WB4-37	11.5741	0.1474	0.0597	0.0011	544.7	7.8	533.1	6.7	584.0	41.0	533	7
WB4-38	11.1857	0.2377	0.0593	0.0014	556.9	12.0	551.5	11.5	562.0	54.0	551	11
WB4-39	10.6045	0.1687	0.0599	0.0013	584.7	11.0	580.5	9.1	583.0	46.0	581	9
WB4-40	9.5057	0.4156	0.0853	0.0028	799.7	26.0	625.1	26.7	1306.0	62.0	625	27
WB4-41	8.5470	0.1096	0.0700	0.0014	762.7	11.0	707.1	8.9	913.0	42.0	707	9
WB4-42	8.3822	0.1546	0.0743	0.0016	802.9	13.0	716.6	12.9	1034.0	45.0	717	13
WB4-43	8.3893	0.1126	0.0655	0.0017	740.8	13.0	724.1	9.6	754.0	53.0	724	10
WB4-44	7.7882	0.1880	0.0695	0.0014	811.5	14.0	774.4	18.2	901.0	42.0	774	18
WB4-45	7.7761	0.1149	0.0671	0.0015	794.7	12.0	778.0	11.3	826.0	47.0	778	11

WB4-46	7.5472	0.0911	0.0712	0.0010	842.2	9.1	796.7	9.4	950.0	29.0	797	9
WB4-47	7.1994	0.1140	0.0690	0.0016	853.9	15.0	836.3	13.0	883.0	49.0	836	13
WB4-48	7.0522	0.0945	0.0726	0.0010	893.3	10.0	849.4	11.1	990.0	28.0	849	11
WB4-49	6.7797	0.1885	0.0723	0.0017	915.5	20.0	882.8	23.9	979.0	49.0	883	24
WB4-50	6.6225	0.1053	0.0878	0.0026	1039.2	21.0	885.2	14.0	1355.0	58.0	885	14
WB4-51	6.5317	0.0811	0.0706	0.0014	926.0	12.0	917.2	11.1	931.0	41.0	917	11
WB4-52	6.4641	0.1045	0.0741	0.0023	959.4	20.0	922.4	14.7	1003.0	65.0	922	15
WB4-53	6.2972	0.1784	0.0744	0.0022	978.6	23.0	945.7	26.1	1023.0	60.0	946	26
WB4-54	6.2854	0.0711	0.0732	0.0012	970.7	9.9	948.9	10.5	1006.0	34.0	949	11
WB4-55	6.2657	0.0667	0.0723	0.0011	965.8	9.5	952.9	9.9	983.0	31.0	953	10
WB4-56	5.7670	0.0665	0.0751	0.0013	1042.8	12.0	1028.9	11.6	1055.0	36.0	1029	12
WB4-57	5.6980	0.0584	0.0775	0.0021	1069.6	16.0	1037.7	10.7	1099.0	53.0	1038	11
WB4-58	5.6465	0.0701	0.0778	0.0014	1078.2	11.0	1046.5	12.7	1130.0	35.0	1046	13
WB4-59	5.5310	0.0520	0.0778	0.0012	1092.7	11.0	1067.6	9.9	1131.0	31.0	1068	10
WB4-60	5.5340	0.0704	0.0764	0.0013	1081.5	13.0	1069.0	13.3	1089.0	34.0	1069	13
WB4-61	5.4855	0.0512	0.0756	0.0010	1081.1	8.9	1079.3	9.8	1077.0	26.0	1079	10
WB4-62	5.3591	0.0804	0.0794	0.0013	1127.3	13.0	1098.5	16.1	1172.0	33.0	1099	16
WB4-63	5.3191	0.0821	0.0770	0.0021	1114.1	18.0	1109.9	16.9	1087.0	56.0	1110	17
WB4-64	5.2219	0.1145	0.0874	0.0012	1205.0	16.0	1114.9	23.8	1361.0	27.0	1115	24
WB4-65	4.8780	0.0666	0.0813	0.0013	1211.0	11.0	1200.4	16.0	1218.0	32.0	1200	16
WB4-66	4.8123	0.0556	0.0823	0.0010	1228.9	9.9	1214.8	13.7	1245.0	25.0	1215	14
WB4-67	4.7916	0.0758	0.0840	0.0013	1245.1	12.0	1217.2	18.8	1282.0	30.0	1217	19
WB4-68	4.5372	0.1009	0.0839	0.0016	1286.5	22.0	1283.5	27.9	1282.0	36.0	1284	28
WB4-69	4.4903	0.0605	0.0859	0.0016	1309.8	13.0	1293.2	17.1	1329.0	36.0	1329	36
WB4-70	3.9032	0.0548	0.0907	0.0016	1460.3	15.0	1473.2	20.5	1438.0	35.0	1438	35
WB4-71	4.9652	0.0690	0.0916	0.0019	1272.5	15.0	1164.3	16.0	1447.0	40.0	1447	40

WB4-72	4.0700	0.0414	0.0922	0.0013	1436.0	11.0	1411.4	14.2	1463.0	26.0	1463	26
WB4-73	4.4248	0.0861	0.0931	0.0024	1373.8	21.0	1299.5	24.9	1474.0	50.0	1474	50
WB4-74	2.9630	0.0351	0.1199	0.0014	1906.4	12.0	1860.8	22.6	1950.0	22.0	1950	22
WB4-75	3.3979	0.0473	0.1263	0.0014	1809.0	14.0	1608.4	22.4	2040.0	20.0	2040	20
WB4-76	3.0184	0.0501	0.1317	0.0024	1952.2	17.0	1795.8	30.6	2115.0	32.0	2115	32
WB4-77	2.7012	0.0306	0.1323	0.0018	2069.5	12.0	2008.9	24.2	2120.0	24.0	2120	24
WB4-78	2.0325	0.0454	0.1832	0.0044	2615.2	27.0	2527.1	71.1	2673.0	39.0	2673	39
WB5-1	26.5957	0.3961	0.0569	0.0011	260.8	4.6	236.1	3.5	468.0	44.0	236	3
WB5-2	25.2908	0.6076	0.0601	0.0021	285.0	7.5	247.2	5.9	591.0	75.0	247	6
WB5-3	23.3100	0.2880	0.0526	0.0015	274.8	5.9	270.5	3.3	290.0	62.0	270	3
WB5-4	23.2504	0.3081	0.0530	0.0009	277.0	4.5	271.0	3.6	312.0	36.0	271	4
WB5-5	23.0415	0.2601	0.0543	0.0010	285.1	4.6	273.0	3.1	370.0	40.0	273	3
WB5-6	22.2965	0.2834	0.0546	0.0012	294.6	5.8	281.9	3.6	383.0	51.0	282	4
WB5-7	22.3414	0.2945	0.0522	0.0013	280.9	6.1	282.2	3.6	270.0	54.0	282	4
WB5-8	22.2965	0.2883	0.0525	0.0013	285.4	6.2	282.6	3.6	302.0	59.0	283	4
WB5-9	22.2767	0.1935	0.0527	0.0010	286.5	4.8	282.8	2.4	295.0	44.0	283	2
WB5-10	22.2519	0.2030	0.0523	0.0010	285.0	4.5	283.3	2.6	280.0	44.0	283	3
WB5-11	22.1926	0.2758	0.0532	0.0017	289.6	6.9	283.7	3.5	303.0	69.0	284	4
WB5-12	22.1484	0.2649	0.0521	0.0010	281.1	4.9	284.7	3.3	276.0	44.0	285	3
WB5-13	22.0702	0.2630	0.0522	0.0012	286.6	5.8	285.6	3.4	277.0	51.0	286	3
WB5-14	21.9346	0.2021	0.0523	0.0010	288.5	4.2	287.3	2.6	279.0	42.0	287	3
WB5-15	21.5193	0.3658	0.0593	0.0021	324.5	11.0	290.2	4.9	551.0	81.0	290	5
WB5-16	21.6638	0.2581	0.0534	0.0011	296.7	5.2	290.4	3.4	333.0	47.0	290	3
WB5-17	21.5796	0.3493	0.0541	0.0017	300.9	7.6	291.3	4.7	350.0	70.0	291	5
WB5-18	21.3973	0.8171	0.0525	0.0024	295.8	16.2	294.3	11.1	307.5	50.9	294	11

WB5-19	20.9987	0.6270	0.0530	0.0012	303.1	10.5	299.6	8.8	329.3	24.4	300	9
WB5-20	20.7039	0.4072	0.0610	0.0019	343.0	7.4	300.8	5.9	603.0	68.0	301	6
WB5-21	19.6850	0.4263	0.0649	0.0028	375.6	11.0	314.5	6.8	743.0	90.0	315	7
WB5-22	19.6464	0.5790	0.0619	0.0044	362.8	20.0	316.4	9.4	600.0	150.0	316	9
WB5-23	19.3424	0.7108	0.0665	0.0043	388.3	20.0	319.4	11.7	780.0	130.0	319	12
WB5-24	18.1620	0.2474	0.0576	0.0016	366.7	7.9	343.7	4.7	486.0	60.0	344	5
WB5-25	18.1291	0.2662	0.0555	0.0015	356.8	8.2	345.2	5.0	430.0	66.0	345	5
WB5-26	18.1159	0.2757	0.0548	0.0011	353.5	6.5	345.8	5.2	390.0	47.0	346	5
WB5-27	17.9598	0.1968	0.0558	0.0014	361.2	7.7	348.3	3.8	414.0	53.0	348	4
WB5-28	17.9614	0.6415	0.0545	0.0013	354.4	13.6	348.8	12.3	391.1	26.3	349	12
WB5-29	17.8827	0.2590	0.0556	0.0015	361.5	8.8	349.8	5.0	410.0	61.0	350	5
WB5-30	17.6367	0.3422	0.0586	0.0021	381.0	10.0	353.3	6.8	527.0	83.0	353	7
WB5-31	17.6678	0.3434	0.0563	0.0017	368.8	8.9	353.7	6.8	447.0	67.0	354	7
WB5-32	17.3611	0.3617	0.0649	0.0022	417.2	9.7	355.9	7.4	748.0	71.0	356	7
WB5-33	17.3010	0.2185	0.0552	0.0015	363.9	8.7	362.2	4.5	382.0	61.0	362	5
WB5-34	17.2622	0.2414	0.0550	0.0012	364.8	7.2	362.9	4.9	390.0	50.0	363	5
WB5-35	17.2236	0.1750	0.0553	0.0010	371.5	5.0	363.1	3.7	413.0	40.0	363	4
WB5-36	17.1380	0.1997	0.0565	0.0014	379.5	8.4	364.4	4.2	437.0	54.0	364	4
WB5-37	17.1321	0.1732	0.0564	0.0014	379.1	8.3	364.5	3.7	428.0	54.0	365	4
WB5-38	17.1204	0.1641	0.0562	0.0009	378.1	5.4	364.9	3.5	442.0	37.0	365	3
WB5-39	17.1561	0.7834	0.0543	0.0016	367.6	17.7	365.0	16.4	383.9	33.6	365	16
WB5-40	17.1233	0.2492	0.0561	0.0015	371.3	7.9	365.9	5.2	426.0	58.0	366	5
WB5-41	16.9492	0.2356	0.0570	0.0015	385.6	9.0	368.1	5.1	478.0	60.0	368	5
WB5-42	16.9205	0.2348	0.0578	0.0017	390.4	9.1	368.4	5.1	498.0	65.0	368	5
WB5-43	16.9751	0.2449	0.0559	0.0010	374.4	6.0	368.9	5.2	429.0	39.0	369	5
WB5-44	16.9291	0.2321	0.0553	0.0011	377.1	5.9	369.3	5.0	397.0	44.0	369	5

WB5-45	16.8039	0.1948	0.0597	0.0018	402.4	9.7	370.0	4.3	556.0	61.0	370	4
WB5-46	16.8937	0.6450	0.0554	0.0019	378.3	17.3	370.0	13.9	429.3	38.1	370	14
WB5-47	16.8663	0.1764	0.0560	0.0013	382.0	6.7	370.4	3.9	424.0	49.0	370	4
WB5-48	16.9005	0.2028	0.0549	0.0011	374.2	6.3	370.5	4.3	387.0	43.0	371	4
WB5-49	16.8152	0.1951	0.0570	0.0017	388.2	9.5	371.0	4.3	455.0	64.0	371	4
WB5-50	16.7977	0.6972	0.0554	0.0017	380.1	17.4	372.1	15.2	429.1	34.5	372	15
WB5-51	16.7870	0.1747	0.0553	0.0010	379.6	5.2	372.4	3.8	408.0	41.0	372	4
WB5-52	16.7757	0.2251	0.0544	0.0013	375.2	7.4	373.1	5.0	363.0	54.0	373	5
WB5-53	16.7333	0.6145	0.0557	0.0014	383.0	15.2	373.4	13.5	441.6	28.5	373	13
WB5-54	16.7424	0.6495	0.0549	0.0016	378.5	16.3	373.6	14.3	408.6	32.5	374	14
WB5-55	16.7308	0.2155	0.0554	0.0013	376.6	7.7	374.2	4.7	411.0	49.0	374	5
WB5-56	16.6973	0.1673	0.0548	0.0011	378.8	5.9	374.6	3.7	381.0	44.0	375	4
WB5-57	16.6834	0.2728	0.0545	0.0017	377.5	9.6	375.1	6.1	363.0	68.0	375	6
WB5-58	16.6500	0.1996	0.0565	0.0009	385.3	6.0	375.9	4.4	453.0	36.0	376	4
WB5-59	16.6334	0.2130	0.0548	0.0013	380.1	7.8	376.0	4.8	379.0	53.0	376	5
WB5-60	16.5948	0.2396	0.0561	0.0018	387.8	11.0	376.3	5.4	421.0	69.0	376	5
WB5-61	16.5838	0.1815	0.0553	0.0010	383.7	5.4	376.9	4.1	410.0	40.0	377	4
WB5-62	16.5590	0.1947	0.0569	0.0013	389.3	7.7	377.9	4.3	461.0	50.0	378	4
WB5-63	16.5123	0.5442	0.0562	0.0015	390.0	14.5	378.1	12.3	461.7	28.3	378	12
WB5-64	16.4935	0.1741	0.0563	0.0015	390.8	8.5	378.4	4.0	423.0	59.0	378	4
WB5-65	16.3666	0.3214	0.0618	0.0022	422.3	14.0	378.7	7.4	643.0	82.0	379	7
WB5-66	16.4177	0.2372	0.0585	0.0021	404.0	9.7	379.1	5.5	524.0	76.0	379	5
WB5-67	16.4842	0.6764	0.0538	0.0018	377.3	17.5	379.9	15.3	361.5	36.7	380	15
WB5-68	16.4528	0.2003	0.0549	0.0013	384.1	7.2	380.0	4.6	401.0	54.0	380	5
WB5-69	16.4042	0.2395	0.0567	0.0012	394.8	8.4	380.3	5.5	467.0	47.0	380	5
WB5-70	16.4282	0.6004	0.0539	0.0014	379.3	15.1	381.1	13.7	368.7	29.5	381	14

WB5-71	16.3466	0.4875	0.0539	0.0014	380.6	13.4	383.0	11.2	366.7	28.2	383	11
WB5-72	16.2698	0.6375	0.0561	0.0013	394.2	15.6	383.7	14.8	456.2	24.7	384	15
WB5-73	16.2628	0.2142	0.0573	0.0014	390.3	7.5	384.6	4.9	478.0	54.0	385	5
WB5-74	16.2522	0.1664	0.0549	0.0012	388.1	7.4	384.6	3.9	393.0	50.0	385	4
WB5-75	16.1031	0.3112	0.0547	0.0014	380.0	7.6	388.4	7.5	375.0	56.0	388	8
WB5-76	16.0270	0.5087	0.0551	0.0017	393.8	15.5	389.8	12.2	417.3	34.0	390	12
WB5-77	15.9871	0.5460	0.0541	0.0015	389.0	15.4	391.3	13.1	375.4	31.9	391	13
WB5-78	15.9490	0.2010	0.0554	0.0013	397.1	8.4	391.6	4.9	430.0	56.0	392	5
WB5-79	15.9447	0.5684	0.0542	0.0015	390.3	15.7	392.3	13.8	378.3	31.6	392	14
WB5-80	15.7978	0.3244	0.0561	0.0018	404.1	9.8	394.9	8.0	429.0	70.0	395	8
WB5-81	15.8225	0.4771	0.0543	0.0021	393.5	17.0	395.2	11.7	383.4	42.3	395	12
WB5-82	15.6193	0.6900	0.0545	0.0016	398.9	18.4	400.2	17.4	391.3	33.1	400	17
WB5-83	15.5645	0.5299	0.0542	0.0014	398.6	15.2	401.7	13.4	381.1	29.6	402	13
WB5-84	14.7929	0.2188	0.0574	0.0015	428.0	10.0	421.3	6.0	473.0	59.0	421	6
WB5-85	13.7880	0.5938	0.0584	0.0023	465.9	22.9	450.0	19.0	545.0	42.0	450	19
WB5-86	13.7552	0.2081	0.0582	0.0013	465.7	7.8	451.1	6.7	516.0	50.0	451	7
WB5-87	13.3433	0.4419	0.0565	0.0012	466.9	15.7	465.8	15.1	472.4	23.3	466	15
WB5-88	12.2699	0.2710	0.0615	0.0018	531.3	13.0	502.4	10.9	647.0	61.0	502	11
WB5-89	12.1212	0.1616	0.0583	0.0014	516.3	9.2	510.5	6.7	507.0	54.0	511	7
WB5-90	12.0890	0.1388	0.0588	0.0016	520.6	11.0	511.5	5.8	519.0	58.0	512	6
WB5-91	12.0773	0.2188	0.0586	0.0013	519.7	11.0	512.1	9.1	541.0	50.0	512	9
WB5-92	11.6959	0.2189	0.0595	0.0014	538.9	8.5	527.9	9.7	561.0	50.0	528	10
WB5-93	11.2486	0.1898	0.0707	0.0014	626.3	11.0	540.6	9.0	942.0	40.0	541	9
WB5-94	11.2002	0.4453	0.0601	0.0027	561.4	27.6	550.2	21.4	606.9	48.5	550	21
WB5-95	10.3199	0.1385	0.0613	0.0014	606.7	11.0	595.1	7.9	631.0	50.0	595	8
WB5-96	10.2250	0.1568	0.0627	0.0019	620.6	13.0	599.4	9.1	666.0	64.0	599	9

WB5-97	10.1833	0.1659	0.0643	0.0015	627.0	12.0	603.4	9.6	730.0	48.0	603	10
WB5-98	9.5420	0.1639	0.0649	0.0022	669.4	18.0	639.4	10.8	756.0	73.0	639	11
WB5-99	9.4073	0.1239	0.0624	0.0011	648.5	8.9	650.8	8.4	671.0	39.0	651	8
WB5-100	9.0744	0.1812	0.0831	0.0030	813.3	19.0	655.9	13.0	1235.0	73.0	656	13
WB5-101	8.7796	0.1310	0.0650	0.0017	712.9	14.0	693.3	10.2	743.0	52.0	693	10
WB5-102	7.0972	0.1159	0.0693	0.0020	864.7	18.0	847.7	13.6	887.0	61.0	848	14
WB5-103	6.8776	0.1324	0.0802	0.0018	963.3	17.0	861.8	16.2	1172.0	45.0	862	16
WB5-104	6.7843	0.0921	0.0809	0.0016	977.0	15.0	872.5	11.6	1202.0	36.0	873	12
WB5-105	6.4599	0.3088	0.0776	0.0024	985.7	33.0	918.8	42.7	1110.0	64.0	919	43
WB5-106	5.9630	0.0711	0.0829	0.0021	1077.7	16.0	986.1	11.7	1235.0	49.0	986	12
WB5-107	5.9916	0.0574	0.0741	0.0012	1009.2	9.8	992.8	9.3	1032.0	34.0	993	9
WB5-108	5.9137	0.0734	0.0736	0.0013	1014.1	12.0	1006.1	12.2	1019.0	36.0	1006	12
WB5-109	5.5586	0.0680	0.0766	0.0014	1079.9	12.0	1064.1	12.7	1096.0	37.0	1064	13
WB5-110	5.2938	0.0532	0.0827	0.0018	1161.0	16.0	1106.9	11.1	1235.0	43.0	1107	11
WB5-111	5.2632	0.0499	0.0786	0.0014	1134.2	11.0	1119.1	10.5	1146.0	35.0	1119	10
WB5-112	5.2632	0.0693	0.0785	0.0018	1133.4	14.0	1119.2	14.5	1140.0	45.0	1119	15
WB5-113	5.6123	0.1866	0.0782	0.0017	1084.9	28.5	1052.1	34.0	1151.3	21.9	1052	22
WB5-114	4.9334	0.0828	0.0852	0.0020	1231.8	19.0	1181.4	19.5	1304.0	45.0	1304	19
WB5-115	5.1404	0.1737	0.0805	0.0016	1165.4	28.8	1142.2	37.5	1208.7	19.1	1142	19
WB5-116	4.7619	0.0544	0.0819	0.0015	1233.8	13.0	1227.9	13.8	1225.0	36.0	1228	14
WB5-117	3.7750	0.0485	0.0955	0.0018	1523.7	16.0	1512.5	19.4	1525.0	36.0	1525	36
WB5-118	4.2337	0.0538	0.0961	0.0021	1430.7	18.0	1351.2	17.1	1526.0	42.0	1526	42
WB5-119	4.3630	0.0628	0.1028	0.0023	1450.0	19.0	1300.6	18.6	1660.0	41.0	1660	41
WB5-120	3.3416	0.1151	0.1031	0.0021	1684.9	34.9	1688.6	57.9	1680.3	18.7	1680	19
WB5-121	2.6274	0.0283	0.1307	0.0020	2091.0	13.0	2072.6	24.2	2108.0	27.0	2108	27
WB5-122	12.1507	0.2805	0.2587	0.0075	1169.8	21.0	379.6	10.0	3227.0	45.0	3227	45

WB5-123	11.8906	0.2121	0.2978	0.0073	1234.0	18.0	361.7	8.3	3445.0	37.0	3445	37
WB6-1	21.9621	0.8468	0.0527	0.0021	290.1	15.0	286.8	10.9	317.2	45.5	287	11
WB6-2	17.7448	0.5941	0.0557	0.0018	364.1	15.3	352.5	11.6	438.5	35.6	352	12
WB6-3	16.6546	0.6040	0.0556	0.0025	383.7	19.9	375.2	13.4	435.4	50.2	375	13
WB6-4	15.7752	0.5635	0.0553	0.0028	400.1	21.6	395.9	13.9	424.6	54.8	396	14
WB6-5	15.1766	0.4899	0.0553	0.0016	413.4	15.7	411.2	13.0	426.0	31.8	411	13
WB6-6	14.9635	0.4808	0.0567	0.0014	426.2	15.0	416.2	13.1	480.4	26.2	416	13
WB6-7	11.2271	0.3439	0.0601	0.0014	560.5	18.1	548.9	16.4	607.7	25.8	549	16

Note: * not used for statistical calculation because of lead loss or matrix effect, * excluded by applyina a filter (15% discordance and 5% reverse discordance)

Table S3-5. Zircon Hf isotopic values.

Samples ID	U-Pb date	Date Uncertainty	$\varepsilon Hf(t)$	Measured 176Hf/177Hf	Corrected 176Hf/177Hf	2SE	176Lu/177Hf	2SE	176Yb/177Hf	2SE
G3-1	263.1	5.2	-0.78	0.282560	0.282606	0.000027	0.00170	0.00013	0.0577	0.0043
G3-2	263.2	3.0	-2.52	0.282511	0.282560	0.000044	0.00237	0.00084	0.0810	0.0320
G3-3	263.6	4.6	0.24	0.282587	0.282633	0.000028	0.00144	0.00018	0.0456	0.0066
G3-4	263.8	3.7	1.00	0.282606	0.282655	0.000051	0.00156	0.00037	0.0510	0.0130
G3-5	263.8	4.4	0.67	0.282599	0.282647	0.000033	0.00182	0.00022	0.0626	0.0087
G3-6	264.1	5.8	0.63	0.282597	0.282645	0.000037	0.00170	0.00027	0.0548	0.0087
G3-7	264.4	5.1	0.83	0.282606	0.282650	0.000026	0.00156	0.00014	0.0525	0.0064
G3-8	264.6	4.1	-0.79	0.282558	0.282601	0.000048	0.00095	0.00018	0.0310	0.0068
G3-9	264.6	3.6	-0.28	0.282574	0.282619	0.000017	0.00167	0.00026	0.0556	0.0088
G3-10	264.6	4.7	-0.23	0.282573	0.282621	0.000031	0.00178	0.00033	0.0580	0.0098
G3-11	264.8	5.3	1.29	0.282617	0.282663	0.00004	0.00166	0.00047	0.0580	0.0190

G3-12	265.2	2.8	1.49	0.282628	0.282675	0.000055	0.00295	0.00075	0.0870	0.0220
G3-13	265.6	4.7	-1.83	0.282526	0.282572	0.000034	0.00117	0.00013	0.0376	0.0042
G3-14	266.7	4.3	1.91	0.282638	0.282681	0.000035	0.00194	0.00018	0.0652	0.0070
G3-15	267.6	4.1	-0.56	0.282561	0.282610	0.000059	0.00182	0.00011	0.0593	0.0035
G3-16	268.0	3.3	-0.33	0.282567	0.282614	0.000035	0.00135	0.00019	0.0453	0.0053
G3-17	268.1	4.5	0.65	0.282596	0.282643	0.000057	0.00167	0.00022	0.0526	0.0049
G3-18	268.2	5.8	-0.26	0.282567	0.282616	0.000034	0.00140	0.00048	0.0480	0.0190
G3-19	268.3	3.7	1.76	0.282624	0.282673	0.000063	0.00141	0.00016	0.0501	0.0074
G3-20	268.8	4.5	0.32	0.282587	0.282632	0.000021	0.00138	0.00015	0.0455	0.0050
G3-21	269.4	3.2	-1.05	0.282549	0.282594	0.000048	0.00163	0.00017	0.0522	0.0057
G3-22	269.6	4.3	-1.04	0.282543	0.282593	0.000038	0.00140	0.00008	0.0470	0.0045
G3-23	270.0	3.8	-0.55	0.282558	0.282607	0.000054	0.00148	0.00034	0.0500	0.0130
G3-24	270.3	5.5	-2.76	0.282500	0.282544	0.000037	0.00137	0.00013	0.0442	0.0039
S1-1	262.7	9.7	-2.23	0.282393	0.282569	0.00004	0.00246	0.00008	0.0639	0.0019
S1-2	268.0	9.9	-4.56	0.282317	0.282493	0.000038	0.00107	0.00013	0.0267	0.0039
S1-3	272.9	5.6	0.48	0.282630	0.282635	0.000029	0.00148	0.00007	0.0532	0.0018
S1-4	273.2	5	-5.99	0.282447	0.282452	0.000035	0.00151	0.00003	0.0612	0.0028
S1-5	274.0	5.3	-2.49	0.282542	0.282547	0.000023	0.00084	0.00011	0.0320	0.0048
S1-6	276.8	9	-2.64	0.282376	0.282552	0.000047	0.00301	0.00017	0.0757	0.0039
S1-7	278.7	5.2	-0.76	0.282594	0.282599	0.000036	0.00200	0.00008	0.0741	0.0033
S1-8	278.7	5.2	-0.76	0.282594	0.282599	0.000036	0.00200	0.00008	0.0741	0.0033
S1-9	283.0	12.3	-2.58	0.282365	0.282541	0.000075	0.00130	0.00002	0.0322	0.0004
S1-10	288.0	9.6	-2.93	0.282352	0.282528	0.000037	0.00130	0.00008	0.0308	0.0018
S1-11	288.0	8.6	-3.12	0.282351	0.282527	0.000037	0.00211	0.00005	0.0528	0.0014
S1-12	300.0	9.5	-6.33	0.282250	0.282426	0.000051	0.00152	0.00019	0.0387	0.0051
S1-13	305.9	5.9	0.46	0.282617	0.282622	0.000063	0.00280	0.00022	0.1150	0.0099

S1-14	307.0	11.3	-3.48	0.282318	0.282494	0.000038	0.00005	0.00000	0.0020	0.0001
S1-15	317.3	13.5	-5.12	0.282276	0.282452	0.000045	0.00189	0.00012	0.0462	0.0031
S1-16	330.1	5.3	-2.04	0.282526	0.282531	0.000032	0.00179	0.00007	0.0708	0.0026
S2-1	271.2	8.1	-0.38	0.282438	0.282614	0.000049	0.00198	0.00025	0.0475	0.0060
S2-2	273.2	8.3	-4.50	0.282321	0.282497	0.000049	0.00211	0.00010	0.0541	0.0032
S2-3	274.4	8.9	-1.52	0.282403	0.282579	0.00005	0.00178	0.00018	0.0458	0.0052
S2-4	280.5	10.3	-2.54	0.282380	0.282556	0.000072	0.00364	0.00023	0.1006	0.0065
S2-5	281.6	8.5	-3.32	0.282349	0.282525	0.000036	0.00210	0.00008	0.0521	0.0022
S2-6	282.7	8.8	-4.86	0.282305	0.282481	0.000049	0.00209	0.00012	0.0560	0.0050
S2-7	287.2	7.8	-4.23	0.282318	0.282494	0.000075	0.00171	0.00005	0.0434	0.0017
S2-8	291.7	9.2	-4.86	0.282297	0.282473	0.000042	0.00164	0.00016	0.0424	0.0047
S2-9	297.9	9.1	-5.08	0.282289	0.282465	0.000065	0.00197	0.00014	0.0499	0.0035
S2-10	302.1	8.3	-5.94	0.282257	0.282433	0.000039	0.00104	0.00006	0.0251	0.0013
WA-1	257.8	4.1	-4.98	0.282486	0.282491	0.000033	0.00178	0.00007	0.0783	0.0050
WA-2	264.6	4.8	-5.10	0.282477	0.282482	0.000039	0.00147	0.00015	0.0539	0.0032
WA-3	267.9	4.9	-5.35	0.282472	0.282477	0.000045	0.00226	0.00007	0.1028	0.0076
WA-4	273.4	6.2	-4.70	0.282484	0.282489	0.000036	0.00162	0.00007	0.0685	0.0028
WA-5	280.9	3.5	-5.87	0.282446	0.282451	0.000023	0.00153	0.00004	0.0677	0.0028
WA-6	281.6	3.7	-5.10	0.282469	0.282474	0.000029	0.00185	0.00012	0.0757	0.0080
WA-7	283.1	4.2	-5.70	0.282450	0.282455	0.00003	0.00164	0.00009	0.0709	0.0032
WA-8	283.8	4	-5.98	0.282442	0.282447	0.000032	0.00174	0.00013	0.0743	0.0072
WA-9	285.6	2.8	-2.82	0.282543	0.282548	0.000035	0.00412	0.00011	0.1558	0.0034
WA-10	287.4	3.4	-2.34	0.282510	0.282545	0.00007	0.00128	0.00019	0.0398	0.0046
WA-11	287.8	3.4	-2.24	0.282516	0.282552	0.000049	0.00210	0.00018	0.0693	0.0063
WA-12	288.2	3.4	-4.98	0.282470	0.282475	0.000044	0.00218	0.00007	0.0970	0.0034
WA-13	288.9	3.1	-4.77	0.282471	0.282476	0.000038	0.00132	0.00005	0.0602	0.0018

WA-14	289.2	4.5	-3.22	0.282483	0.282518	0.000044	0.00108	0.00006	0.0347	0.0027
WA-15	290.2	3.2	-4.91	0.282430	0.282470	0.000057	0.00117	0.00004	0.0353	0.0008
WA-16	290.9	4	-4.25	0.282490	0.282495	0.000057	0.00235	0.00015	0.1170	0.0110
WA-17	290.9	3.6	-5.68	0.282446	0.282451	0.000032	0.00166	0.00005	0.0690	0.0023
WA-18	292.2	4.4	-5.10	0.282461	0.282466	0.000029	0.00156	0.00008	0.0649	0.0021
WA-19	295.5	5.5	-4.30	0.282483	0.282488	0.000031	0.00183	0.00006	0.0762	0.0046
WA-20	295.6	3.1	-3.96	0.282491	0.282496	0.000037	0.00151	0.00010	0.0553	0.0032
WA-21	295.6	3.2	-3.88	0.282500	0.282505	0.000043	0.00276	0.00016	0.1275	0.0033
WA-22	296.7	6.1	-5.35	0.282454	0.282459	0.000031	0.00208	0.00014	0.0896	0.0051
WA-23	298.6	3.6	-5.46	0.282448	0.282453	0.000034	0.00176	0.00005	0.0727	0.0037
WA-24	305.2	3.9	-5.05	0.282456	0.282461	0.000026	0.00179	0.00005	0.0758	0.0027
WA-25	317.4	5.6	-4.38	0.282467	0.282472	0.000032	0.00172	0.00005	0.0734	0.0015
WA-26	322.0	9.2	-3.70	0.282483	0.282488	0.000039	0.00163	0.00009	0.0702	0.0025
WB-1	290.2	4.9	0.53	0.282586	0.282624	0.000059	0.00122	0.00015	0.0369	0.0050
WB-2	290.4	3.4	8.49	0.282823	0.282861	0.000044	0.00343	0.00018	0.1220	0.0100
WB-3	287.3	2.6	8.81	0.282833	0.282872	0.000052	0.00346	0.00038	0.1120	0.0140
WB-4	291.3	4.7	7.37	0.282782	0.282821	0.000064	0.00203	0.00079	0.0710	0.0360
WB-5	285.6	3.4	7.02	0.282780	0.282820	0.000038	0.00302	0.00008	0.0985	0.0052
WB-6	284.7	3.3	4.49	0.282743	0.282748	0.000041	0.00278	0.00009	0.1115	0.0034
WB-7	286.7	3.2	1.49	0.282654	0.282659	0.00004	0.00223	0.00024	0.0916	0.0096
WB-8	553.1	6.7	12.70	0.282780	0.282817	0.000029	0.00201	0.00016	0.0632	0.0049
WB-Detrital-1	1976.7	17.2	-1.55	0.281361	0.281536	0.000043	0.00155	0.00004	0.0389	0.0017
WB-Detrital-2	454	13.1	5.25	0.282483	0.282659	0.000032	0.00138	0.00002	0.0325	0.0012
WB-Detrital-3	384.2	12.6	3.28	0.282470	0.282646	0.000034	0.00142	0.00009	0.0321	0.0019
WB-Detrital-4	377.5	10.9	2.64	0.282453	0.282629	0.000048	0.00099	0.00002	0.0240	0.0008
WB-Detrital-5	373.8	11.2	2.43	0.282460	0.282636	0.000055	0.00251	0.00010	0.0596	0.0022

WB-Detrital-6	465.8	15.1	0.34	0.282339	0.282515	0.000034	0.00158	0.00006	0.0382	0.0013
WB-Detrital-7	1640	17.9	7.40	0.281822	0.281998	0.000044	0.00157	0.00004	0.0394	0.0016
WB-Detrital-8	919	32	5.18	0.282195	0.282371	0.000051	0.00122	0.00007	0.0314	0.0019
WB-Detrital-9	389.8	12.7	3.74	0.282477	0.282653	0.000033	0.00105	0.00007	0.0233	0.0016
WB-Detrital-10	395.2	11.7	2.94	0.282452	0.282628	0.000039	0.00118	0.00006	0.0277	0.0014
WB-Detrital-11	378	12.3	2.69	0.282455	0.282631	0.000042	0.00112	0.00007	0.0249	0.0014
WB-Detrital-12	390.7	14.1	2.22	0.282436	0.282612	0.000034	0.00140	0.00004	0.0314	0.0007
WB-Detrital-13	391.3	13.1	2.23	0.282443	0.282619	0.000055	0.00238	0.00007	0.0579	0.0019
WB-Detrital-14	381	13.7	3.08	0.282469	0.282645	0.000036	0.00179	0.00003	0.0433	0.0012
WB-Detrital-15	401.7	14.2	4.72	0.282500	0.282676	0.000035	0.00141	0.00009	0.0325	0.0023
WB-Detrital-16	377.9	4.3	2.00	0.282606	0.282611	0.00003	0.00101	0.00004	0.0378	0.0027
WB-Detrital-17	375.9	4.4	3.88	0.282662	0.282667	0.000025	0.00124	0.00009	0.0444	0.0027
WB-Detrital-18	362.2	4.5	3.99	0.282675	0.282680	0.00003	0.00147	0.00006	0.0531	0.0029
WB-Detrital-19	365.9	5.2	3.25	0.282650	0.282655	0.000022	0.00117	0.00005	0.0435	0.0021
WB-Detrital-20	374.2	4.7	3.57	0.282663	0.282668	0.000063	0.00247	0.00008	0.0771	0.0021
WB-Detrital-21	388.4	7.5	6.33	0.282733	0.282738	0.000043	0.00253	0.00022	0.0896	0.0055
WB-Detrital-22	384.6	4.9	4.57	0.282678	0.282683	0.000032	0.00147	0.00006	0.0558	0.0021
WB-Detrital-23	398.3	3.9	-5.23	0.282386	0.282391	0.000025	0.00055	0.00002	0.0180	0.0008
WB-Detrital-24	345.3	3.7	3.67	0.282675	0.282680	0.000028	0.00128	0.00009	0.0450	0.0023
WB-Detrital-25	371	5.2	2.38	0.282624	0.282629	0.000034	0.00141	0.00016	0.0526	0.0065
WB-Detrital-26	639.2	8.9	7.76	0.282620	0.282625	0.000035	0.00200	0.00015	0.0755	0.0058
WB-Detrital-27	525	19	10.91	0.282784	0.282789	0.000039	0.00270	0.00003	0.1068	0.0053
WB-Detrital-28	401.2	6	-1.25	0.282504	0.282509	0.0000079	0.00152	0.00004	0.0611	0.0018
WB-Detrital-29	600.6	7.9	-2.71	0.282331	0.282336	0.000026	0.00054	0.00006	0.0238	0.0029
WB-Detrital-30	371.2	5.2	3.37	0.282654	0.282659	0.000037	0.00172	0.00030	0.0710	0.0170

Table S3-5 continues

Samples ID	U-Pb date	Date Uncertainty	ƐHf(t)	178Hf/177Hf	2SE	180Hf/177Hf	2SE	176Hf/177Hfi	EHf0	2SE
G3-1	263.1	5.2	-0.78	1.467186	0.00008	1.88712	0.00013	14.1	-6.33	0.955549
G3-2	263.2	3.0	-2.52	1.467227	0.000073	1.88726	0.00016	17.2	-7.96	1.557461
G3-3	263.6	4.6	0.24	1.467143	0.000094	1.88716	0.00015	15.5	-5.38	0.990845
G3-4	263.8	3.7	1.00	1.467191	0.000061	1.88710	0.00024	17.9	-4.60	1.804633
G3-5	263.8	4.4	0.67	1.467148	0.000087	1.88707	0.00017	15.9	-4.88	1.167732
G3-6	264.1	5.8	0.63	1.467140	0.00011	1.88715	0.00025	12.2	-4.95	1.309285
G3-7	264.4	5.1	0.83	1.467070	0.000062	1.88723	0.00023	15.5	-4.77	0.920009
G3-8	264.6	4.1	-0.79	1.467096	0.000048	1.88712	0.00021	16.2	-6.51	1.698766
G3-9	264.6	3.6	-0.28	1.467170	0.00013	1.88720	0.00021	16.3	-5.87	0.601612
G3-10	264.6	4.7	-0.23	1.467197	0.000067	1.88709	0.00022	13.1	-5.80	1.097062
G3-11	264.8	5.3	1.29	1.467195	0.000074	1.88709	0.00013	14.1	-4.31	1.415343
G3-12	265.2	2.8	1.49	1.467154	0.00004	1.88726	0.00017	15.8	-3.89	1.946021
G3-13	265.6	4.7	-1.83	1.467156	0.000093	1.88714	0.00026	14.1	-7.53	1.203429
G3-14	266.7	4.3	1.91	1.467157	0.000075	1.88710	0.00020	14.4	-3.68	1.238333
G3-15	267.6	4.1	-0.56	1.467135	0.000098	1.88688	0.00039	12.3	-6.19	2.088045
G3-16	268.0	3.3	-0.33	1.467270	0.000069	1.88722	0.00022	12.2	-6.05	1.238644
G3-17	268.1	4.5	0.65	1.467183	0.000071	1.88719	0.00040	9.3	-5.02	2.017014
G3-18	268.2	5.8	-0.26	1.467131	0.000073	1.88711	0.00020	16.8	-5.98	1.203254
G3-19	268.3	3.7	1.76	1.467232	0.000088	1.88721	0.00023	14.74	-3.96	2.229110
G3-20	268.8	4.5	0.32	1.467170	0.000047	1.88716	0.00014	15.3	-5.41	0.743134
G3-21	269.4	3.2	-1.05	1.467141	0.000049	1.88705	0.00014	13.2	-6.75	1.698820
G3-22	269.6	4.3	-1.04	1.467150	0.00014	1.88724	0.00039	17.5	-6.79	1.344928
G3-23	270.0	3.8	-0.55	1.467193	0.000082	1.88726	0.00031	15.9	-6.29	1.911112

G3-24	270.3	5.5	-2.76	1.467240	0.00012	1.88723	0.00026	13.5	-8.52	1.309735
S1-1	262.7	9.7	-2.23	1.466902	0.000039	1.88626	0.00015	9.52	-7.64	1.416466
S1-2	268.0	9.9	-4.56	1.466886	0.000044	1.88611	0.00013	12.44	-10.33	1.346005
S1-3	272.9	5.6	0.48	1.467201	0.00005	1.88661	0.00012	14	-5.32	1.026076
S1-4	273.2	5	-5.99	1.467267	0.00005	1.88687	0.00013	12.8	-11.79	1.239171
S1-5	274.0	5.3	-2.49	1.467175	0.000046	1.88661	0.00009	10.23	-8.43	0.814038
S1-6	276.8	9	-2.64	1.466944	0.000056	1.88631	0.00013	9.21	-8.24	1.664447
S1-7	278.7	5.2	-0.76	1.467157	0.000087	1.88663	0.00015	12.6	-6.59	1.273912
S1-8	278.7	5.2	-0.76	1.467157	0.000087	1.88663	0.00015	12.6	-6.59	1.273912
S1-9	283.0	12.3	-2.58	1.466834	0.000062	1.88660	0.00024	9.0	-8.63	2.656137
S1-10	288.0	9.6	-2.93	1.466935	0.000056	1.88632	0.00016	10.76	-9.09	1.310421
S1-11	288.0	8.6	-3.12	1.466958	0.000046	1.88634	0.00012	7.04	-9.13	1.310426
S1-12	300.0	9.5	-6.33	1.466915	0.000045	1.88634	0.00016	11.21	-12.70	1.806909
S1-13	305.9	5.9	0.46	1.467198	0.000066	1.88653	0.00023	11	-5.78	2.229165
S1-14	307.0	11.3	-3.48	1.466933	0.000035	1.88627	0.00013	10.29	-10.29	1.346000
S1-15	317.3	13.5	-5.12	1.466849	0.000069	1.88641	0.00022	9.48	-11.78	1.594184
S1-16	330.1	5.3	-2.04	1.467191	0.000053	1.88673	0.00015	13.76	-9.00	1.132639
S2-1	271.2	8.1	-0.38	1.466909	0.000049	1.88644	0.00013	8.89	-6.05	1.734894
S2-2	273.2	8.3	-4.50	1.466901	0.000062	1.88634	0.00015	7.76	-10.19	1.735613
S2-3	274.4	8.9	-1.52	1.466984	0.000058	1.88636	0.00016	9.48	-7.29	1.770519
S2-4	280.5	10.3	-2.54	1.466928	0.000067	1.88620	0.00021	7.83	-8.10	2.549756
S2-5	281.6	8.5	-3.32	1.466954	0.000057	1.88631	0.00016	7.52	-9.20	1.275018
S2-6	282.7	8.8	-4.86	1.466947	0.000045	1.88643	0.00020	10.37	-10.75	1.735711
S2-7	287.2	7.8	-4.23	1.466921	0.000049	1.88642	0.00023	10.61	-10.29	2.656579
S2-8	291.7	9.2	-4.86	1.466927	0.00004	1.88624	0.00015	8.86	-11.04	1.487795
S2-9	297.9	9.1	-5.08	1.466954	0.000048	1.88640	0.00020	10.3	-11.32	2.302605

S2-10	302.1	8.3	-5.94	1.466909	0.000062	1.88631	0.00014	6.58	-12.45	1.381719
WA-1	257.8	4.1	-4.98	1.467179	0.000063	1.88665	0.00011	14.2	-10.41	1.168199
WA-2	264.6	4.8	-5.10	1.467209	0.000054	1.88672	0.00013	10.8	-10.73	1.380643
WA-3	267.9	4.9	-5.35	1.467142	0.000087	1.88663	0.00021	13.37	-10.90	1.593078
WA-4	273.4	6.2	-4.70	1.467217	0.000055	1.88682	0.00015	13.48	-10.48	1.274408
WA-5	280.9	3.5	-5.87	1.467260	0.000047	1.88686	0.00008	15.87	-11.82	0.814315
WA-6	281.6	3.7	-5.10	1.467231	0.000047	1.88664	0.00010	15.5	-11.01	1.026661
WA-7	283.1	4.2	-5.70	1.467205	0.000048	1.88681	0.00008	16.2	-11.68	1.062135
WA-8	283.8	4	-5.98	1.467190	0.000044	1.88669	0.00011	13.8	-11.97	1.132976
WA-9	285.6	2.8	-2.82	1.467158	0.000057	1.88664	0.00014	11.5	-8.39	1.238750
WA-10	287.4	3.4	-2.34	1.467104	0.000038	1.88710	0.00018	22.4	-8.49	2.477788
WA-11	287.8	3.4	-2.24	1.467082	0.000096	1.88707	0.00037	14.4	-8.24	1.734415
WA-12	288.2	3.4	-4.98	1.467208	0.000083	1.88674	0.00017	12.6	-10.98	1.557688
WA-13	288.9	3.1	-4.77	1.467271	0.000092	1.88678	0.00018	16.68	-10.94	1.345271
WA-14	289.2	4.5	-3.22	1.467210	0.00012	1.88722	0.00019	18.9	-9.44	1.557616
WA-15	290.2	3.2	-4.91	1.467150	0.00011	1.88711	0.00035	16	-11.14	2.018199
WA-16	290.9	4	-4.25	1.467229	0.000084	1.88670	0.00019	14.03	-10.27	2.017771
WA-17	290.9	3.6	-5.68	1.467213	0.000044	1.88668	0.00011	15.1	-11.82	1.132960
WA-18	292.2	4.4	-5.10	1.467200	0.000056	1.88673	0.00016	16.5	-11.29	1.026690
WA-19	295.5	5.5	-4.30	1.467205	0.000044	1.88668	0.00012	15.1	-10.52	1.097411
WA-20	295.6	3.1	-3.96	1.467199	0.000051	1.88658	0.00013	11.1	-10.23	1.309776
WA-21	295.6	3.2	-3.88	1.467164	0.000066	1.88668	0.00014	11.26	-9.91	1.522124
WA-22	296.7	6.1	-5.35	1.467235	0.000056	1.88684	0.00011	11.6	-11.54	1.097524
WA-23	298.6	3.6	-5.46	1.467181	0.000057	1.88679	0.00012	13	-11.75	1.203761
WA-24	305.2	3.9	-5.05	1.467205	0.000038	1.88671	0.00010	12.9	-11.47	0.920497
WA-25	317.4	5.6	-4.38	1.467253	0.000045	1.88674	0.00012	15.9	-11.08	1.132876

WA-26	322.0	9.2	-3.70	1.467239	0.000054	1.88680	0.00012	15.56	-10.52	1.380614
WB-1	290.2	4.9	0.53	1.467130	0.00011	1.88707	0.00021	14.3	-5.69	2.087860
WB-2	290.4	3.4	8.49	1.467200	0.00012	1.88710	0.00026	11.7	2.69	1.555743
WB-3	287.3	2.6	8.81	1.467220	0.00014	1.88733	0.00031	13.8	3.08	1.838541
WB-4	291.3	4.7	7.37	1.467130	0.00011	1.88690	0.00040	16.7	1.27	2.263228
WB-5	285.6	3.4	7.02	1.467325	0.000061	1.88744	0.00020	13	1.24	1.343801
WB-6	284.7	3.3	4.49	1.467172	0.000057	1.88677	0.00012	9.45	-1.32	1.450080
WB-7	286.7	3.2	1.49	1.467199	0.000057	1.88674	0.00014	13.5	-4.47	1.415158
WB-8	553.1	6.7	12.70	1.467180	0.00011	1.88703	0.00022	12.3	1.13	1.025532
WB-Detrital-1	1976.7	17.2	-1.55	1.466931	0.000051	1.88635	0.00018	9.78	-44.16	1.528286
WB-Detrital-2	454	13.1	5.25	1.466950	0.000062	1.88625	0.00016	10.89	-4.45	1.132812
WB-Detrital-3	384.2	12.6	3.28	1.466971	0.000045	1.88629	0.00012	8.87	-4.91	1.203668
WB-Detrital-4	377.5	10.9	2.64	1.466896	0.00005	1.88629	0.00016	10.18	-5.52	1.699398
WB-Detrital-5	373.8	11.2	2.43	1.466866	0.000057	1.88626	0.00016	7.51	-5.27	1.947178
WB-Detrital-6	465.8	15.1	0.34	1.466926	0.000047	1.88631	0.00011	10.73	-9.55	1.204226
WB-Detrital-7	1640	17.9	7.40	1.466950	0.000049	1.88634	0.00012	8.01	-27.84	1.561269
WB-Detrital-8	919	32	5.18	1.466847	0.00005	1.88646	0.00020	9.16	-14.65	1.807261
WB-Detrital-9	389.8	12.7	3.74	1.466912	0.000041	1.88620	0.00013	10.27	-4.67	1.168237
WB-Detrital-10	395.2	11.7	2.94	1.466868	0.000051	1.88622	0.00012	11.09	-5.55	1.380766
WB-Detrital-11	378	12.3	2.69	1.466910	0.000056	1.88622	0.00012	9.71	-5.45	1.486963
WB-Detrital-12	390.7	14.1	2.22	1.466876	0.000044	1.88620	0.00012	9.91	-6.12	1.203813
WB-Detrital-13	391.3	13.1	2.23	1.466875	0.000062	1.88631	0.00022	12.5	-5.87	1.947296
WB-Detrital-14	381	13.7	3.08	1.466893	0.000043	1.88619	0.00011	9.66	-4.95	1.274476
WB-Detrital-15	401.7	14.2	4.72	1.466851	0.000042	1.88606	0.00014	12.01	-3.85	1.238938
WB-Detrital-16	377.9	4.3	2.00	1.467153	0.000044	1.88662	0.00016	13.86	-6.17	1.061549
WB-Detrital-17	375.9	4.4	3.88	1.467280	0.000041	1.88675	0.00009	12.53	-4.19	0.884449

WB-Detrital-18	362.2	4.5	3.99	1.467223	0.000042	1.88673	0.00012	13.71	-3.73	1.061289
WB-Detrital-19	365.9	5.2	3.25	1.467246	0.000037	1.88676	0.00009	13.3	-4.61	0.778348
WB-Detrital-20	374.2	4.7	3.57	1.467245	0.000067	1.88672	0.00024	9	-4.15	2.228802
WB-Detrital-21	388.4	7.5	6.33	1.467172	0.000058	1.88671	0.00015	10.2	-1.68	1.520870
WB-Detrital-22	384.6	4.9	4.57	1.467237	0.000039	1.88680	0.00011	11.62	-3.62	1.132030
WB-Detrital-23	398.3	3.9	-5.23	1.467246	0.000041	1.88677	0.00010	12.41	-13.95	0.885313
WB-Detrital-24	345.3	3.7	3.67	1.467166	0.000056	1.88664	0.00012	11.5	-3.73	0.990537
WB-Detrital-25	371	5.2	2.38	1.467194	0.000043	1.88675	0.00011	12.6	-5.53	1.203012
WB-Detrital-26	639.2	8.9	7.76	1.467219	0.000055	1.88666	0.00012	13.1	-5.67	1.238412
WB-Detrital-27	525	19	10.91	1.467203	0.000051	1.88671	0.00013	10.52	0.13	1.379145
WB-Detrital-28	401.2	6	-1.25	1.467200	0.0000096	1.88672	0.00002	5.31	-9.78	0.279642
WB-Detrital-29	600.6	7.9	-2.71	1.467234	0.000055	1.88678	0.00013	16.25	-15.89	0.920905
WB-Detrital-30	371.2	5.2	3.37	1.467289	0.000054	1.88703	0.00021	15.81	-4.47	1.309021

Table S3-6. U-Pb CAIDTIMS zircon data

	University of Wyoming							Corrected atomic ratios														
	Weight	U	sample Pb	Pbc	Pb*	Th	206Pb	208Pb	206Pb/238UTh		207Pb/235U		207Pb/206P		206/238Th		207/235	207/206Th	Rho	206/238	
Sample	(µg)	(ppm)	(ppm)	(pg)	Pbc	U	204Pb	206Pb	(rad.)	%err	(rad.)	%err	(rad.)	%err	Date (Ma	err	Date (Ma	Date (Ma		ICP date	err
S1	*282.02±0.36/0.37/0.47 Ma Weigthed mean 206Pb/238U date (±analytical/with tracer/with U-decay constant), 95% conf., MSWD 0.55, 5 of 7 analyses*																				
g12	0.28	639	30.1	8.5	1.5	5.3	0.36	354	0.11	0.0444	(0.23)	0.3170	(1.83)	0.0518	(1.73)	279.8	±0.7	279.6	277.9	0.45	277.1	±11.2
g6*	2.04	62	3.5	7.1	2.3	2.4	0.34	172	0.12	0.0447	(0.28)	0.3244	(2.54)	0.0527	(2.42)	281.6	±0.8	285.3	315.2	0.48	283.7	±12.3
g10*	0.65	233	22.4	14.6	8.7	0.8	0.26	67	0.12	0.0447	(0.35)	0.3375	(3.48)	0.0548	(3.30)	281.8	±1.0	295.3	402.8	0.54	269.0	±9.2
g4*	1.27	161	7.1	9.1	0.9	9.6	0.32	636	0.10	0.0447	(0.23)	0.3202	(1.43)	0.0519	(1.35)	282.0	±0.6	282.1	282.5	0.40	285.2	±8.4
g35*	0.45	704	31.1	14.0	0.9	15.1	0.29	993	0.10	0.0448	(0.38)	0.3220	(1.02)	0.0522	(0.91)	282.3	±1.1	283.4	293.0	0.46	266.5	±9.2
g32*	0.80	179	9.0	7.3	1.7	3.8	0.39	255	0.13	0.0448	(0.27)	0.3225	(2.38)	0.0522	(2.26)	282.4	±0.8	283.8	295.3	0.49	295.0	±10.4
g9	0.41	493	23.1	9.3	1.3	7.2	0.36	469	0.13	0.0449	(0.26)	0.3257	(1.80)	0.0526	(1.70)	283.0	±0.7	286.3	313.5	0.44	262.7	±9.7
g8	0.65	64	14.6	9.5	5.9	0.8	0.73	59	0.33	0.0912	(0.56)	0.8386	(5.72)	0.0667	(5.35)	562.7	±3.2	618.4	827.7	0.69	268.3	±9.9
S2	*280.66±1.06/1.06/1.10 Ma Weigthed mean 206Pb/238U date (±analytical/with tracer/with U-decay constant), 95% conf., MSWD 1.5, 3 of 8 analyses*																				
g50*	0.23	250	17.2	3.9	2.3	1.1	0.44	88	0.16	0.0444	(0.41)	0.3220	(5.87)	0.0526	(5.60)	279.8	±1.2	283.4	313.5	0.69	265.7	±7.9
g5*	2.47	234	10.4	25.8	1.4	17.6	0.29	1149	0.09	0.0445	(0.21)	0.3199	(0.65)	0.0521	(0.59)	280.7	±0.6	281.8	291.7	0.43	291.7	±9.2
g4*	2.13	127	5.6	12.0	0.5	24.1	0.32	1558	0.11	0.0445	(0.21)	0.3204	(0.64)	0.0522	(0.59)	280.9	±0.6	282.2	292.9	0.42	271.7	±8.4
g33	0.76	130	8.6	6.5	3.1	1.5	0.26	110	0.12	0.0447	(0.31)	0.3365	(3.44)	0.0546	(3.27)	281.7	±0.9	294.5	397.7	0.58	287.6	±9.4
g14	1.18	15	0.7	0.8	1.0	0.8	0.32	70	0.14	0.0447	(0.80)	0.3377	(15.47)	0.0548	(14.78)	282.1	±2.3	295.4	402.3	0.87	270.7	±8.2
g27	0.53	393	18.1	9.7	1.0	10.1	0.41	643	0.14	0.0447	(0.32)	0.3241	(1.41)	0.0525	(1.32)	282.2	±0.9	285.0	308.3	0.39	281.6	±8.5
g32	0.58	216	13.8	8.0	3.0	2.0	0.43	137	0.18	0.0452	(0.26)	0.3376	(2.86)	0.0541	(2.71)	285.1	±0.8	295.3	377.2	0.57	292.7	±9.1
s37	0.23	60	20.5	4.8	4.3	0.4	0.27	41	0.13	0.1071	(0.73)	1.0954	(8.13)	0.0742	(7.60)	655.7	±4.8	751.1	1047.1	0.74	268.4	±7.4
WA	*287.19±0.50/0.50/0.59 Ma Weigthed mean 206Pb/238U date (±analytical/with tracer/with U-decay constant), 95% conf., MSWD 0.8, 4 of 6 analyses*																				
g17*	0.18	131	8.0	1.4	1.3	0.8	0.24	69	0.13	0.0453	(0.75)	0.3575	(12.25)	0.0572	(11.64)	285.8	±2.1	310.3	498.7	0.82	295.5	±5.5
g15*	0.14	99	17.5	2.5	2.8	0.2	0.25	33	0.16	0.0455	(1.33)	0.3745	(20.43)	0.0598	(19.36)	286.6	±3.8	323.0	594.8	0.82	294.9	±4.6
g8*	0.36	123	5.7	2.1	0.4	4.6	0.41	305	0.14	0.0455	(0.28)	0.3310	(2.96)	0.0527	(2.82)	287.1	±0.8	290.3	316.5	0.51	283.1	±4.2
g28*	0.46	214	9.8	4.5	0.6	7.9	0.34	517	0.12	0.0456	(0.24)	0.3319	(1.73)	0.0528	(1.64)	287.5	±0.7	291.0	320.0	0.42	290.9	±4.0
g1	0.09	35	1.8	0.2	1.0	0.1	0.14	27	0.16	0.0460	(5.37)	0.4571	(73.70)	0.0721	(69.07)	290.0	±15.6	382.2	987.4	0.87	305.2	±3.9
g16	0.56	108	6.5	3.7	1.4	2.3	0.79	146	0.26	0.0472	(0.36)	0.3427	(4.89)	0.0526	(4.66)	297.6	±1.1	299.2	312.1	0.66	280.9	±3.5
WB	*288.2 ±1.7 Ma Weighted mean 206Pb/238U date (±analytical/with tracer/with U-decay constant), 95% conf., MSWD 3.2, 3 of 4 analyses*																				
WBU8910 g31	0.46	174	29.5	13.5	10.5	0.4	0.48	40	0.25	0.0451	(0.66)	0.3506	(8.14)	0.0564	(7.71)	284.2	±1.9	305.2	469.1	0.67	294.3	±11.1
g27	0.14	956	48.9	6.9	0.6	10.9	0.81	638	0.25	0.0456	(0.23)	0.3268	(1.47)	0.0520	(1.39)	287.6	±0.7	287.1	283.5	0.40	284.7	±3.3
WBR7874 g8	0.27	215	11.2	3.0	1.0	2.9	0.73	185	0.26	0.0458	(0.36)	0.3339	(5.09)	0.0529	(4.86)	288.6	±1.0	292.5	323.7	0.68	286.8	±10.9
g13	0.55	191	9.7	5.3	1.0	5.5	0.62	338	0.23	0.0458	(0.25)	0.3354	(2.64)	0.0531	(2.52)	288.7	±0.7	293.7	333.6	0.52	282.2	±3.6
g20	0.83	118	8.7	7.2	1.4	4.9	0.92	290	0.28	0.0609	(0.32)	0.4524	(2.41)	0.0538	(2.28)	381.4	±1.2	378.9	364.0	0.45	377.9	±4.3
g30	1.00	255	17.5	17.4	0.5	34.1	0.81	1947	0.25	0.0610	(0.25)	0.4552	(0.60)	0.0542	(0.53)	381.4	±1.0	380.9	377.7	0.48	362.2	±4.5
g2	0.26	78	5.3	1.4	0.6	2.3	0.53	150	0.23	0.0612	(0.41)	0.4873	(6.04)	0.0577	(5.76)	382.9	±1.6	403.0	519.9	0.73	370.5	±4.3

Notes: sample: g_=single grain identifier from ICP mount, * excluded from date calculations

sample Pb: sample Pb (radiogenic + initial) corrected for laboratory blank

Pbc: total common Pb (blank plus sample initial Pb); 1 pg was assigned to blank, the remaining to initial Pb

Pb*/Pbc: radiogenic Pb to total common Pb (blank + initial)

Corrected atomic ratios: measured ^{206}Pb/^{204}Pb corrected for mass discrimination and tracer, all others corrected for blank, mass discrimination, tracer and initial Pb, values in parentheses are 2 sigma errors in percent.

Rho: ^{206}Pb/^{238}U vs ^{207}Pb/^{235}U error correlation coefficient

% disc.: percent discordant

Th = 206Pb/238U, 207Pb/206Pb ratios and dates corrected for Th-disequilibrium after Schärer (1984) assuming a magma Th/U of 2.2.

Table S3-7. Zircon Rare Earth Element Compositions.

Sample ID	U-Pb date	2σ error	Ti	Y	Nb	La	Ce	Pr	Nd	Sm	Eu	Gd	Tb	Dy	Ho	Er	Tm	Yb	Lu	Hf	U	Th
G3-1	264.6	4.1	5.09	1340	3.72	0.14	16.6	0.288	3.7	5.8	1.4	20.1	9.7	125	43.9	211	46.7	490	69	9170	162	146
G3-2	266.7	4.3	5.65	2860	5.15	0.57	18.5	1.07	11.7	17.8	5.16	51.6	23.8	288	93.1	445	93.1	896	130.4	9270	251	289
G3-3	270.3	5.5	4.96	1390	2.89	0.07	11.4	0.196	3.7	6.7	1.78	23.3	10.7	140	47	224	49	490	71	8720	139	105
G3-4	268.8	4.5	4.97	2010	3.15	0.2	17.2	0.244	4.6	9.2	3.17	34	15.9	207	71	330	70.1	708	100	9030	150	126
G3-5	264.6	3.6	5.15	1370	3.36	0.06	12.57	0.169	3.1	6.2	1.66	22.2	11	144	48	236	52	530	72	9660	173	112
G3-6	264.4	5.1	5.07	1630	2.57	0.01	9.7	0.196	3.66	7.4	2.29	25.6	12.3	162	54.8	271	59.5	603	85.5	8360	110	91
G3-7	261.3	4.4	5.03	1810	2.62	0.07	10.9	0.309	4.79	9.12	2.9	32.4	15.1	191	65.4	298	64.4	670	88.1	8150	119	105
G3-8	260.7	4.8	5.32	1840	3.66	0.20	13.4	0.387	4.66	8	2.35	28.6	13.9	187	65.6	307	68.8	739	96	8720	227	170
G3-9	269.4	3.2	5.11	1570	4.04	0.03	9.7	0.173	3.38	6.7	1.31	24	11.9	155	54.1	269	59	616	85.6	9370	292	151
G3-10	260.1	4.7	5.1	1550	3.32	0.26	13.4	0.255	3.44	6.02	1.69	22.3	10.95	146	51.3	255	57.2	587	86	9250	163	124
G3-11	263.6	4.6	5.01	676	3.7	0.23	11.2	0.23	1.72	2.01	0.55	7.54	4.15	58.4	21.6	113.2	28.6	331	46.3	9810	130	70
G3-12	263.1	5.2	5.29	1550	4.9	0.43	19.8	0.91	7.3	9.35	2.42	27.4	12.61	162	56.1	258	56.1	641	77.7	8040	245	200
G3-13	264.8	5.3	5.05	1780	2.58	0.03	9.4	0.256	4.8	9.4	3.43	30.8	14.4	180	59	287	62	640	91	7730	101	93
G3-14	265.6	4.7	5.08	1550	3.22	0.85	15.8	0.37	3.9	6.06	1.27	23.8	11.3	149	53.2	251	53.9	567	79.7	9300	191.8	137
G3-15	268.1	4.5	5.7	2220	15	2.27	27.5	1.52	9.9	8.91	1.87	28.8	14.66	203.6	74.9	371	78.7	800	125	10780	557	517
G3-16	268.0	3.3	5.28	1480	2.79	0.49	13	0.335	3.72	6	1.49	22.6	11.1	140	50.4	243	52	529	79	8400	151	120
G3-17	260.4	3.6	5.18	1200	3.57	0.16	12.3	0.31	3.2	4.7	1.33	16.7	8.2	105	38.4	193	40.9	418	68.4	9360	149	140
G3-18	263.8	4.4	5.25	2380	4.53	0.06	13.1	0.33	5.07	10.1	3.33	37.6	18.7	250	84.4	399	86.1	855	114	8500	179	162
G3-19	264.6	4.7	5.21	1168	6.54	0.09	14.2	0.136	1.69	3.26	0.689	13.95	7.55	107.8	40.2	205	47.3	501	73.2	10540	336	159.7
G3-20	265.2	2.8	5.7	2760	4.88	0.21	15.1	0.484	4.65	7.1	2.02	29.7	15.7	223	84	439	94	930	156	10210	298	261
G3-21	271.0	3.5	5.09	2160	6.39	0.09	18.35	0.206	4	7.97	1.41	30.6	15.2	201	73.8	361	75.7	776	115.3	8810	389	244
G3-22	264.1	5.8	5.28	1177	2.71	0.18	8.8	0.193	2.48	4.36	1.66	17.39	8.83	119	42.6	205	46.1	476	68.4	8650	91.2	56.1

G3-23	263.8	3.7	5.24	1330	4.03	0.26	15.2	0.41	3.85	5.19	1.38	18.5	9.1	122	44.4	221	49.8	517	75.9	9550	181	157
G3-24	249.6	5.2	5.18	1610	2.35	0.01	9.19	0.16	3.28	6.5	1.89	24.5	11.9	159	56.1	268	59.3	616	88.5	9070	150	106
G3-25	268.3	3.7	5.22	1950	4.74	0.36	15.01	0.77	7.52	10	2.61	31.9	15.04	195	66.4	310	64.5	603	94.2	9210	174	233
G3-26	270.0	3.8	4.96	1490	4.28	0.19	19.1	0.42	4.8	8.9	2	27	12.8	155	54	281	60	690	89	8770	320	250
G3-27	268.2	5.8	5.33	930	2.88	0.03	9.9	0.09	1.9	2.9	1.01	11.5	5.9	81	29	147	34.8	380	55	10620	112	62
G3-28	269.6	4.3	5.33	3410	5.79	0.35	15	0.51	8.1	15.4	2.49	60.2	28	341	117.7	543	104	1034	148	9000	472	334
G3-29	267.6	4.1	5.4	1810	3.22	0.22	6.92	0.29	4.93	10.27	2.14	33.7	15.6	192	63.6	297	61.9	615	85.5	8340	221	138
G3-30	263.2	3.0	5.08	1124	7.94	0.22	12.53	0.14	1.42	2.43	0.307	11.62	6.71	97.1	36.9	193.4	45	485	70	11580	410	170
WA-1	287.8	3.4	5.63	3340	14.5	0.22	22.7	1.11	11.5	16.1	2.01	47.8	22.6	278	97.8	461	89.9	846	143.4	11650	1600	1270
WA-2	277.2	3.7	5.73	3120	18.68	0.30	46.2	2.92	25.8	24.3	5.8	50.8	23.9	287	92.8	443	86.8	799	133.4	12130	1503	1660
WA-3	290.2	3.2	5.34	2290	13.4	0.46	25.7	3.54	28.4	22.6	4.71	38.1	17.6	209	66.5	304	59.2	543	89.8	10700	1180	1192
WA-4	280.4	4.4	5.92	1090	3.63	0.08	6.67	0.84	7.63	8.5	2.1	14.7	6.92	90	29.5	150	32.7	314	53.2	9870	290	680
WA-5	289.2	4.5	5.57	2380	15.8	0.27	19.3	1.92	16.4	16.6	3.73	37.5	17.9	235	72	327	68	620	97	10500	1140	1640
WA-6	275.0	4.1	5.05	2890	11.1	0.49	24.7	4	36	31.5	7.3	54.7	24	277	90	398	77	678	119	10400	1350	2310
WA-7	280.2	2.4	4.79	1890	9.3	0.82	18.6	2.61	21.4	19.2	3.95	31.7	14.2	161	50.6	244	45	421	73	10200	654	1140
WA-8	278.8	3.0	5.66	2370	16.6	0.194	24	1.34	12.5	14.9	2.44	35.5	17.3	215	71	333	67.7	637	100.1	11800	1390	1680
WA-9	275.7	2.8	5.4	3100	12.8	1.28	41.2	7.53	64	44.9	9	69.6	27.8	297	91.8	403	75.5	689	113.2	9920	1300	4460
WA-10	287.4	3.4	5.35	2870	11.1	0.37	46	3.2	30	29	5.9	59	25.1	276	90	401	77	760	110	11100	1080	4000
WA-11	277.2	5.7	5.38	2100	7.6	0.267	23.1	1.03	9.4	12.5	2.1	31.5	14.6	179	59.8	273	54.2	501	83.1	9200	732	810
WA-12	282.2	2.6	5.26	2360	13.2	0.55	19.1	1.62	15.7	15.9	3.39	40.4	18.2	227	74	328	66	620	97	10260	1180	1270
WA-13	275.5	3.5	5.84	3490	20.8	0.82	39.5	3.87	32.8	25.5	5.3	57	25.8	316	108	476	94	910	143	11400	2080	2710
WB-1	283.8	3.2	4.9	3050	3.86	0.0448	16.8	0.391	6.41	12.57	2.43	45	22.4	291	100.2	485	103.7	1059	147.6	7120	608	682
WB-2	294.8	4.6	5.52	2440	8.14	1.214	34	6.88	51.5	32.1	11.35	38.1	18.71	228	67.9	320	73.3	793	137	15300	1269	1114
WB-3	279.7	2.6	5.75	1310	3.22	1.12	29.7	4.25	33	21.4	5.09	27.5	12.2	139	41.6	188	40.5	451	91.8	13300	914	920
WB-4	281.5	3.0	6.1	11200	38.2	5.98	194	43.6	352	306	69.5	353	155	16200	402	14900	330	2640	356	11800	1920	4520

253

WB-5	281.9	3.6	5.577	1940	4.28	0.167	21.2	0.8	9	12.3	2.73	31.6	15.2	190	63.3	301	63	610	93	7730	283	463
WB-6	283.3	2.6	5.19	3370	3.98	0.061	20.4	0.52	6.6	12.6	2.76	45.8	23.9	327	114.9	541	117	1197	160.6	7710	805	980
WB-7	290.2	4.9	5.59	1700	6.02	1.49	45.4	1.18	10.8	10.8	2.14	24	11.7	150	53.8	280	63.3	699	110.6	11080	545	677
WB-8	283.7	3.5	5.67	1260	2.97	0.076	8.43	0.423	4.6	6.14	1.231	15.22	7.9	105	38.52	204	45.8	484	84.7	7740	226.3	201
WB-9	290.4	3.4	5.25	5470	5.05	0.5	41.5	1.44	20.1	31.4	9	99.7	43.8	533	188	832	158	1610	237	6690	520	761
WB-10	287.3	2.6	5.75	2960	6.74	0.421	19.7	1.31	12.3	15.7	2.51	36.9	20	261	90.5	466	95	884	147	7620	614	1073
WB-11	282.8	2.4	5.83	1200	4.72	0.36	25.8	1.29	11.9	12.4	1.83	18.4	8.8	103	37.3	172	40	415	78.3	9290	357	437
WB-12	270.5	3.3	5.54	2070	3.83	0.118	13.08	0.85	9.2	10.9	1.8	27.3	13.62	185	67.2	334	71.3	707	127.7	7990	436	479
WB-13	291.3	4.7	5.96	3170	5	0.209	14	1.46	16.7	21.4	3.56	55	25.7	316	107	490	96	980	153	8220	475	850
WB-14	285.6	3.4	5.9	3860	5.78	0.156	20.51	1.011	12.8	20.3	3.83	61	29.1	382	130	606	127.1	1273	187	8170	772	1141
WB-15	273.0	3.1	4.6	850	4.2	1.36	16.6	1.6	19.2	43	5.6	22	12.7	160	28.1	135	25	260	24.4	8800	500	550

Table S3-7 continues

Sample ID	U-Pb date	2σ error	∑REE	∑LREE (La-Sm)	∑HREE (Gd-Lu)	LaN/SmN	GdN/YbN	Eu/Eu*	Ce/Ce*	log (Ti, ppm)	T (K)	T (°C)
G3-1	264.6	4.1	10297.8	26.5	1022.6	0.01	0.03	0.4	22.0	0.7	957.9	684.7
G3-2	266.7	4.3	11396.1	49.6	2044.0	0.01	0.04	0.5	5.0	0.8	966.2	693.0
G3-3	270.3	5.5	9872.0	22.1	1063.5	0.00	0.03	0.4	11.0	0.7	955.9	682.7
G3-4	268.8	4.5	10677.6	31.4	1548.4	0.01	0.03	0.5	29.9	0.7	956.1	682.9
G3-5	264.6	3.6	10884.4	22.1	1123.1	0.00	0.03	0.4	6.4	0.7	958.8	685.7
G3-6	264.4	5.1	9738.4	21.0	1283.4	0.00	0.03	0.5	19.4	0.7	957.6	684.4
G3-7	261.3	4.4	9676.0	25.2	1436.4	0.00	0.03	0.5	25.3	0.7	957.0	683.8
G3-8	260.7	4.8	10347.3	26.7	1516.3	0.01	0.03	0.5	4.9	0.7	961.4	688.2
G3-9	269.4	3.2	10757.8	20.0	1282.6	0.00	0.03	0.3	11.5	0.7	958.3	685.1
G3-10	260.1	4.7	10588.3	23.4	1223.5	0.02	0.02	0.4	29.2	0.7	958.1	684.9
G3-11	263.6	4.6	10601.4	15.4	613.4	0.04	0.01	0.4	16.9	0.7	956.7	683.5
G3-12	263.1	5.2	9439.7	37.8	1302.7	0.02	0.03	0.5	7.4	0.7	960.9	687.8

254

G3-13	264.8	5.3	9189.6	23.9	1377.0	0.00	0.03	0.6	64.6	0.7	957.3	684.1
G3-14	265.6	4.7	10610.7	27.0	1196.2	0.05	0.03	0.3	22.0	0.7	957.7	684.6
G3-15	268.1	4.5	12618.4	50.1	1707.4	0.10	0.02	0.4	5.0	0.8	966.9	693.7
G3-16	268.0	3.3	9640.3	23.5	1134.6	0.03	0.03	0.4	11.0	0.7	960.8	687.6
G3-17	260.4	3.6	10359.5	20.7	894.6	0.01	0.03	0.5	29.9	0.7	959.3	686.1
G3-18	263.8	4.4	10461.4	28.7	1858.2	0.00	0.03	0.5	6.4	0.7	960.3	687.2
G3-19	264.6	4.7	11709.7	19.4	999.9	0.01	0.02	0.3	19.4	0.7	959.7	686.6
G3-20	265.2	2.8	12341.9	27.5	1980.5	0.01	0.02	0.4	25.3	0.8	966.9	693.7
G3-21	271.0	3.5	10588.0	30.6	1658.0	0.00	0.03	0.3	4.9	0.7	957.9	684.7
G3-22	264.1	5.8	9760.2	16.0	989.3	0.02	0.02	0.6	11.5	0.7	960.8	687.6
G3-23	263.8	3.7	10733.6	24.9	1064.3	0.02	0.02	0.4	29.2	0.7	960.2	687.0
G3-24	249.6	5.2	10469.1	19.1	1291.7	0.00	0.03	0.5	16.9	0.7	959.3	686.1
G3-25	268.3	3.7	10686.6	33.7	1392.7	0.01	0.03	0.4	7.4	0.7	959.9	686.7
G3-26	270.0	3.8	10251.7	33.4	1379.7	0.01	0.03	0.4	64.6	0.7	955.8	682.7
G3-27	268.2	5.8	11511.1	14.8	748.1	0.00	0.02	0.5	22.0	0.7	961.5	688.3
G3-28	269.6	4.3	11484.9	39.4	2393.8	0.01	0.04	0.2	5.0	0.7	961.5	688.4
G3-29	267.6	4.1	9789.0	22.6	1376.7	0.01	0.04	0.4	11.0	0.7	962.6	689.4
G3-30	263.2	3.0	12742.4	16.7	948.5	0.04	0.02	0.2	29.9	0.7	957.8	684.6
WA-1	287.8	3.4	13742.7	51.6	2004.6	0.01	0.04	0.2	6.4	0.8	965.9	692.7
WA-2	277.2	3.7	14184.9	99.5	1946.8	0.00	0.04	0.5	19.4	0.8	967.3	694.1
WA-3	290.2	3.2	12136.6	80.7	1354.5	0.01	0.05	0.5	25.3	0.7	961.7	688.5
WA-4	280.4	4.4	10623.8	23.7	701.6	0.00	0.03	0.6	4.9	0.8	969.9	696.7
WA-5	289.2	4.5	12070.0	54.5	1494.7	0.01	0.04	0.5	11.5	0.7	965.0	691.9
WA-6	275.0	4.1	12243.2	96.7	1756.5	0.01	0.05	0.5	29.2	0.7	957.3	684.1
WA-7	280.2	2.4	11329.0	62.6	1063.7	0.02	0.05	0.5	16.9	0.7	953.2	680.0
WA-8	278.8	3.0	13374.7	52.9	1493.9	0.01	0.04	0.3	7.4	0.8	966.3	693.1
WA-9	275.7	2.8	11870.2	158.9	1820.8	0.01	0.07	0.5	64.6	0.7	962.6	689.4
WA-10	287.4	3.4	13038.8	108.6	1833.0	0.00	0.05	0.4	22.0	0.7	961.8	688.7

WA-11	277.2	5.7	10484.7	46.3	1210.8	0.01	0.04	0.3	5.0	0.7	962.3	689.1
WA-12	282.2	2.6	11825.9	52.9	1489.9	0.01	0.04	0.4	11.0	0.7	960.5	687.3
WA-13	275.5	3.5	13673.3	102.5	2160.6	0.01	0.04	0.4	29.9	0.8	968.8	695.7
WB-1	283.8	3.2	9496.8	36.2	2268.9	0.00	0.03	0.3	19.4	0.7	954.9	681.8
WB-2	294.8	4.6	17137.8	125.7	1719.5	0.01	0.03	1.0	25.3	0.7	964.3	691.2
WB-3	279.7	2.6	14407.2	89.5	1018.1	0.02	0.04	0.6	29.2	0.8	967.6	694.4
WB-4	281.5	3.0	20125.7	901.6	7721.5	0.01	0.09	0.6	16.9	0.8	972.3	699.2
WB-5	281.9	3.6	9192.9	43.5	1382.1	0.01	0.03	0.4	64.6	0.7	965.1	692.0
WB-6	283.3	2.6	10375.1	40.2	2542.6	0.00	0.03	0.4	5.0	0.7	959.4	686.3
WB-7	290.2	4.9	12608.9	69.7	1405.3	0.05	0.02	0.4	11.0	0.7	965.3	692.2
WB-8	283.7	3.5	8824.9	19.7	992.5	0.00	0.02	0.4	29.9	0.8	966.4	693.3
WB-9	290.4	3.4	10546.7	94.9	3741.9	0.01	0.04	0.5	6.4	0.7	960.3	687.2
WB-10	287.3	2.6	9728.6	49.4	2018.6	0.01	0.03	0.3	19.4	0.8	967.6	694.4
WB-11	282.8	2.4	10249.8	51.8	887.0	0.01	0.03	0.4	25.3	0.8	968.7	695.5
WB-12	270.5	3.3	9623.9	34.1	1545.8	0.00	0.03	0.3	4.9	0.7	964.6	691.4
WB-13	291.3	4.7	10545.8	53.8	2247.7	0.00	0.04	0.3	11.5	0.8	970.4	697.3
WB-14	285.6	3.4	11086.5	54.8	2819.3	0.00	0.03	0.3	29.2	0.8	969.6	696.5
WB-15	273.0	3.1	9560.61	81.8	715.8	0.01	0.06	0.6	16.9	0.7	950.0	676.9

Biographical Information

Hepeng Tian was born on September 26, 1990, in HeBei Province, China. He joined the Department of Earth Sciences and Resources, China University of Geosciences (Beijing), in 2009 to start his undergraduate study. He received his Bachelor of Science majoring in geochemistry in 2013.

Hepeng participated in a national science project in China during his sophomore year. The reseach was funded by the China University of Geosciences (Beijing) and Hepeng's research achievement stand out among his peers. His outstanding performance led to an internship from China Academy of Science in Hepeng's junior year, inspiring him to pursue a Master's degree in geosciences. Hepeng graduated with honor in 2013 and became a geologist engineer intern in west China.

In 2014, Hepeng was awarded full scholarship from the Texas Tech University, Lubbock, Texas, to work on his Master's degree. He conducted field work in the Yosemite National Park, California, in the summer of 2015 and conducted lab work at the University of Oklahoma, Norman, Oklahoma, in fall 2015 to analyze major and trace element compositions of hornblende to decipher the emplacement of magmatic structures. He was also a teaching assistant during his tenure at Texas Tech University. Hepeng earned his Master of Science degree in 2016 and was admitted by the PhD program in the Department of Earth and Environmental Sciences at the University of Texas at Arlington.

Hepeng joined the University of Texas at Arlington in the fall of 2017. In addition to maintaining a 4.0/4.0 GPA, Hepeng has served as the president of the AAPG student organization and interned with the Pioneer Natural Resources in the summer of 2020. Two of the three chapters of his dissertation has been published in high-impact, peer-reviewed geology journals. Hepeng also taught himself basics of data science and machine learning algorithms through online courses and applied these techniques into his research. With this experience, he was admitted by the Computer Science Master program at the Georgia Institute of Technology. Hepeng aims to become a software engineer/research scientist in the tech industry upon finishing his PhD. He has always been dedicated

and determined to achieve his ambitions. He is an active, energetic, sociable, and pleasant person to work with. His future is bright as long as he keeps his strong faith in himself.